SECONDARY ION TIME-OF-FLIGHT MASS SPECTROMETRY: PEPTIDES AND LANGMUIR BLODGETT FILMS

BY

NANCY POPPE-SCHRIEMER

A Thesis
Submitted to the Faculty of Graduate Studies
in partial Fulfillment of the Requirements
for the Degree of

DOCTOR OF PHILOSOPHY

Department of Physics and Department of Chemistry
University of Manitoba
Winnipeg, Manitoba, Canada

ISBN 0-612-13455-5

Name _____

Dissertation Abstracts International is arranged by broad, general subject categories. Please select the one subject which most nearly describes the content of your dissertation. Enter the corresponding four-digit code in the spaces provided.

ANALYTICAL CHEMISTRY — SUBJECT TERM

0486 — SUBJECT CODE

U·M·I

Subject Categories

THE HUMANITIES AND SOCIAL SCIENCES

COMMUNICATIONS AND THE ARTS
Architecture 0729
Art History 0377
Cinema 0900
Dance 0378
Fine Arts 0357
Information Science 0723
Journalism 0391
Library Science 0399
Mass Communications 0708
Music 0413
Speech Communication 0459
Theater 0465

EDUCATION
General 0515
Administration 0514
Adult and Continuing 0516
Agricultural 0517
Art 0273
Bilingual and Multicultural 0282
Business 0688
Community College 0275
Curriculum and Instruction 0727
Early Childhood 0518
Elementary 0524
Finance 0277
Guidance and Counseling 0519
Health 0680
Higher 0745
History of 0520
Home Economics 0278
Industrial 0521
Language and Literature 0279
Mathematics 0280
Music 0522
Philosophy of 0998
Physical 0523
Psychology 0525
Reading 0535
Religious 0527
Sciences 0714
Secondary 0533
Social Sciences 0534
Sociology of 0340
Special 0529
Teacher Training 0530
Technology 0710
Tests and Measurements 0288
Vocational 0747

LANGUAGE, LITERATURE AND LINGUISTICS
Language
- General 0679
- Ancient 0289
- Linguistics 0290
- Modern 0291

Literature
- General 0401
- Classical 0294
- Comparative 0295
- Medieval 0297
- Modern 0298
- African 0316
- American 0591
- Asian 0305
- Canadian (English) 0352
- Canadian (French) 0355
- English 0593
- Germanic 0311
- Latin American 0312
- Middle Eastern 0315
- Romance 0313
- Slavic and East European 0314

PHILOSOPHY, RELIGION AND THEOLOGY
Philosophy 0422
Religion
- General 0318
- Biblical Studies 0321
- Clergy 0319
- History of 0320
- Philosophy of 0322

Theology 0469

SOCIAL SCIENCES
American Studies 0323
Anthropology
- Archaeology 0324
- Cultural 0326
- Physical 0327

Business Administration
- General 0310
- Accounting 0272
- Banking 0770
- Management 0454
- Marketing 0338

Canadian Studies 0385
Economics
- General 0501
- Agricultural 0503
- Commerce-Business 0505
- Finance 0508
- History 0509
- Labor 0510
- Theory 0511

Folklore 0358
Geography 0366
Gerontology 0351
History
- General 0578
- Ancient 0579
- Medieval 0581
- Modern 0582
- Black 0328
- African 0331
- Asia, Australia and Oceania 0332
- Canadian 0334
- European 0335
- Latin American 0336
- Middle Eastern 0333
- United States 0337

History of Science 0585
Law 0398
Political Science
- General 0615
- International Law and Relations 0616
- Public Administration 0617

Recreation 0814
Social Work 0452
Sociology
- General 0626
- Criminology and Penology 0627
- Demography 0938
- Ethnic and Racial Studies 0631
- Individual and Family Studies 0628
- Industrial and Labor Relations 0629
- Public and Social Welfare 0630
- Social Structure and Development 0700
- Theory and Methods 0344

Transportation 0709
Urban and Regional Planning 0999
Women's Studies 0453

THE SCIENCES AND ENGINEERING

BIOLOGICAL SCIENCES
Agriculture
- General 0473
- Agronomy 0285
- Animal Culture and Nutrition 0475
- Animal Pathology 0476
- Food Science and Technology 0359
- Forestry and Wildlife 0478
- Plant Culture 0479
- Plant Pathology 0480
- Plant Physiology 0817
- Range Management 0777
- Wood Technology 0746

Biology
- General 0306
- Anatomy 0287
- Biostatistics 0308
- Botany 0309
- Cell 0379
- Ecology 0329
- Entomology 0353
- Genetics 0369
- Limnology 0793
- Microbiology 0410
- Molecular 0307
- Neuroscience 0317
- Oceanography 0416
- Physiology 0433
- Radiation 0821
- Veterinary Science 0778
- Zoology 0472

Biophysics
- General 0786
- Medical 0760

EARTH SCIENCES
Biogeochemistry 0425
Geochemistry 0996
Geodesy 0370
Geology 0372
Geophysics 0373
Hydrology 0388
Mineralogy 0411
Paleobotany 0345
Paleoecology 0426
Paleontology 0418
Paleozoology 0985
Palynology 0427
Physical Geography 0368
Physical Oceanography 0415

HEALTH AND ENVIRONMENTAL SCIENCES
Environmental Sciences 0768
Health Sciences
- General 0566
- Audiology 0300
- Chemotherapy 0992
- Dentistry 0567
- Education 0350
- Hospital Management 0769
- Human Development 0758
- Immunology 0982
- Medicine and Surgery 0564
- Mental Health 0347
- Nursing 0569
- Nutrition 0570
- Obstetrics and Gynecology 0380
- Occupational Health and Therapy 0354
- Ophthalmology 0381
- Pathology 0571
- Pharmacology 0419
- Pharmacy 0572
- Physical Therapy 0382
- Public Health 0573
- Radiology 0574
- Recreation 0575
- Speech Pathology 0460
- Toxicology 0383

Home Economics 0386

PHYSICAL SCIENCES
Pure Sciences
Chemistry
- General 0485
- Agricultural 0749
- Analytical 0486
- Biochemistry 0487
- Inorganic 0488
- Nuclear 0738
- Organic 0490
- Pharmaceutical 0491
- Physical 0494
- Polymer 0495
- Radiation 0754

Mathematics 0405
Physics
- General 0605
- Acoustics 0986
- Astronomy and Astrophysics 0606
- Atmospheric Science 0608
- Atomic 0748
- Electronics and Electricity 0607
- Elementary Particles and High Energy 0798
- Fluid and Plasma 0759
- Molecular 0609
- Nuclear 0610
- Optics 0752
- Radiation 0756
- Solid State 0611

Statistics 0463

Applied Sciences
Applied Mechanics 0346
Computer Science 0984
Engineering
- General 0537
- Aerospace 0538
- Agricultural 0539
- Automotive 0540
- Biomedical 0541
- Chemical 0542
- Civil 0543
- Electronics and Electrical 0544
- Heat and Thermodynamics 0348
- Hydraulic 0545
- Industrial 0546
- Marine 0547
- Materials Science 0794
- Mechanical 0548
- Metallurgy 0743
- Mining 0551
- Nuclear 0552
- Packaging 0549
- Petroleum 0765
- Sanitary and Municipal 0554
- System Science 0790

Geotechnology 0428
Operations Research 0796
Plastics Technology 0795
Textile Technology 0994

PSYCHOLOGY
General 0621
Behavioral 0384
Clinical 0622
Developmental 0620
Experimental 0623
Industrial 0624
Personality 0625
Physiological 0989
Psychobiology 0349
Psychometrics 0632
Social 0451

Nom _____

Dissertation Abstracts International est organisé en catégories de sujets. Veuillez s.v.p. choisir le sujet qui décrit le mieux votre thèse et inscrivez le code numérique approprié dans l'espace réservé ci-dessous.

_____ ☐☐☐ U·M·I

SUJET — CODE DE SUJET

Catégories par sujets

HUMANITÉS ET SCIENCES SOCIALES

COMMUNICATIONS ET LES ARTS
Architecture 0729
Beaux-arts 0357
Bibliothéconomie 0399
Cinéma 0900
Communication verbale 0459
Communications 0708
Danse 0378
Histoire de l'art 0377
Journalisme 0391
Musique 0413
Sciences de l'information 0723
Théâtre 0465

ÉDUCATION
Généralités 515
Administration 0514
Art 0273
Collèges communautaires 0275
Commerce 0688
Économie domestique 0278
Éducation permanente 0516
Éducation préscolaire 0518
Éducation sanitaire 0680
Enseignement agricole 0517
Enseignement bilingue et multiculturel 0282
Enseignement industriel 0521
Enseignement primaire. 0524
Enseignement professionnel 0747
Enseignement religieux 0527
Enseignement secondaire 0533
Enseignement spécial 0529
Enseignement supérieur 0745
Évaluation 0288
Finances 0277
Formation des enseignants 0530
Histoire de l'éducation 0520
Langues et littérature 0279
Lecture 0535
Mathématiques 0280
Musique 0522
Orientation et consultation 0519
Philosophie de l'éducation 0998
Physique 0523
Programmes d'études et enseignement 0727
Psychologie 0525
Sciences 0714
Sciences sociales 0534
Sociologie de l'éducation 0340
Technologie 0710

LANGUE, LITTÉRATURE ET LINGUISTIQUE
Langues
- Généralités 0679
- Anciennes 0289
- Linguistique 0290
- Modernes 0291

Littérature
- Généralités 0401
- Anciennes 0294
- Comparée 0295
- Médiévale 0297
- Moderne 0298
- Africaine 0316
- Américaine 0591
- Anglaise 0593
- Asiatique 0305
- Canadienne (Anglaise) 0352
- Canadienne (Française) 0355
- Germanique 0311
- Latino-américaine 0312
- Moyen-orientale 0315
- Romane 0313
- Slave et est-européenne 0314

PHILOSOPHIE, RELIGION ET THÉOLOGIE
Philosophie 0422
Religion
- Généralités 0318
- Clergé 0319
- Études bibliques 0321
- Histoire des religions 0320
- Philosophie de la religion 0322

Théologie 0469

SCIENCES SOCIALES
Anthropologie
- Archéologie 0324
- Culturelle 0326
- Physique 0327

Droit 0398
Économie
- Généralités 0501
- Commerce-Affaires 0505
- Économie agricole 0503
- Économie du travail 0510
- Finances 0508
- Histoire 0509
- Théorie 0511

Études américaines 0323
Études canadiennes 0385
Études féministes 0453
Folklore 0358
Géographie 0366
Gérontologie 0351
Gestion des affaires
- Généralités 0310
- Administration 0454
- Banques 0770
- Comptabilité 0272
- Marketing 0338

Histoire
- Histoire générale 0578
- Ancienne 0579
- Médiévale 0581
- Moderne 0582
- Histoire des noirs 0328
- Africaine 0331
- Canadienne 0334
- États-Unis 0337
- Européenne 0335
- Moyen-orientale 0333
- Latino-américaine 0336
- Asie, Australie et Océanie 0332

Histoire des sciences 0585
Loisirs 0814
Planification urbaine et régionale 0999
Science politique
- Généralités 0615
- Administration publique 0617
- Droit et relations internationales 0616

Sociologie
- Généralités 0626
- Aide et bien-être social 0630
- Criminologie et établissements pénitentiaires 0627
- Démographie 0938
- Études de l' individu et de la famille 0628
- Études des relations interethniques et des relations raciales 0631
- Structure et développement social 0700
- Théorie et méthodes. 0344
- Travail et relations industrielles 0629

Transports 0709
Travail social 0452

SCIENCES ET INGÉNIERIE

SCIENCES BIOLOGIQUES
Agriculture
- Généralités 0473
- Agronomie. 0285
- Alimentation et technologie alimentaire 0359
- Culture 0479
- Élevage et alimentation 0475
- Exploitation des pâturages 0777
- Pathologie animale 0476
- Pathologie végétale 0480
- Physiologie végétale 0817
- Sylviculture et faune 0478
- Technologie du bois 0746

Biologie
- Généralités 0306
- Anatomie 0287
- Biologie (Statistiques) 0308
- Biologie moléculaire 0307
- Botanique 0309
- Cellule 0379
- Écologie 0329
- Entomologie 0353
- Génétique 0369
- Limnologie 0793
- Microbiologie 0410
- Neurologie 0317
- Océanographie 0416
- Physiologie 0433
- Radiation 0821
- Science vétérinaire 0778
- Zoologie 0472

Biophysique
- Généralités 0786
- Medicale 0760

SCIENCES DE LA TERRE
Biogéochimie 0425
Géochimie 0996
Géodésie 0370
Géographie physique 0368
Géologie 0372
Géophysique 0373
Hydrologie 0388
Minéralogie 0411
Océanographie physique 0415
Paléobotanique 0345
Paléoécologie 0426
Paléontologie 0418
Paléozoologie 0985
Palynologie 0427

SCIENCES DE LA SANTÉ ET DE L'ENVIRONNEMENT
Économie domestique 0386
Sciences de l'environnement 0768
Sciences de la santé
- Généralités 0566
- Administration des hôpitaux 0769
- Alimentation et nutrition 0570
- Audiologie 0300
- Chimiothérapie 0992
- Dentisterie 0567
- Développement humain 0758
- Enseignement 0350
- Immunologie 0982
- Loisirs 0575
- Médecine du travail et thérapie 0354
- Médecine et chirurgie 0564
- Obstétrique et gynécologie 0380
- Ophtalmologie 0381
- Orthophonie 0460
- Pathologie 0571
- Pharmacie 0572
- Pharmacologie 0419
- Physiothérapie 0382
- Radiologie 0574
- Santé mentale 0347
- Santé publique 0573
- Soins infirmiers 0569
- Toxicologie 0383

SCIENCES PHYSIQUES
Sciences Pures
Chimie
- Généralités 0485
- Biochimie 487
- Chimie agricole 0749
- Chimie analytique 0486
- Chimie minérale 0488
- Chimie nucléaire 0738
- Chimie organique 0490
- Chimie pharmaceutique 0491
- Physique 0494
- PolymÈres 0495
- Radiation 0754

Mathématiques 0405
Physique
- Généralités 0605
- Acoustique 0986
- Astronomie et astrophysique 0606
- Électronique et électricité 0607
- Fluides et plasma 0759
- Météorologie 0608
- Optique 0752
- Particules (Physique nucléaire) 0798
- Physique atomique 0748
- Physique de l'état solide 0611
- Physique moléculaire 0609
- Physique nucléaire 0610
- Radiation 0756

Statistiques 0463

Sciences Appliqués Et Technologie
Informatique 0984
Ingénierie
- Généralités 0537
- Agricole 0539
- Automobile 0540
- Biomédicale 0541
- Chaleur et thermodynamique 0348
- Conditionnement (Emballage) 0549
- Génie aérospatial 0538
- Génie chimique 0542
- Génie civil 0543
- Génie électronique et électrique 0544
- Génie industriel 0546
- Génie mécanique 0548
- Génie nucléaire 0552
- Ingénierie des systèmes 0790
- Mécanique navale 0547
- Métallurgie 0743
- Science des matériaux 0794
- Technique du pétrole 0765
- Technique minière 0551
- Techniques sanitaires et municipales 0554
- Technologie hydraulique 0545

Mécanique appliquée 0346
Géotechnologie 0428
Matières plastiques (Technologie) 0795
Recherche opérationnelle 0796
Textiles et tissus (Technologie) 0794

PSYCHOLOGIE
Généralités 0621
Personnalité 0625
Psychobiologie 0349
Psychologie clinique 0622
Psychologie du comportement 0384
Psychologie du développement 0620
Psychologie expérimentale 0623
Psychologie industrielle 0624
Psychologie physiologique 0989
Psychologie sociale 0451
Psychométrie 0632

SECONDARY ION TIME-OF-FLIGHT MASS SPECTROMETRY: PEPTIDES AND LANGMUIR BLODGETT FILMS

BY

NANCY POPPE-SCHRIEMER

A Thesis submitted to the Faculty of Graduate Studies of the University of Manitoba in partial fulfillment of the requirements of the degree of

DOCTOR OF PHILOSOPHY

ACKNOWLEDGMENTS

I would like to thank Dr. Ken Standing, my advisor, for his guidance, encouragement, support and example throughout the years. He and everyone else in the lab have been very understanding and accommodating the last two years when I worked in a somewhat untraditional fashion. Dr. Werner Ens has also contributed significantly and has often allowed me to benefit from his special ability to fix electronics and computer systems by simply walking into the room. He and his wife have helped immeasurably by sharing their incomparable nanny. Dr. Westmore has spent many long hours helping me interpret the chemistry of my results and giving me a feel for how chemists approach problems.

I am grateful to Dr. Standing, to my advisory committee and to the departments of Physics and Chemistry for allowing me to switch to an interdisciplinary program near the end of a physics program so that I would have a more formal educational basis for some of my research work. I am also grateful to Dr. C. Bigelow, Dr J.O'Neil and especially Dr. H. Duckworth for patiently answering my many physicist-type questions about biochemistry.

My coworkers through the years have added to the educational experience and to the enjoyment of a long study period, and I thank each one of them: Dennis Main, Ron Beavis, X-J. Tang, Franz Mayer, John Martens, J. Zhou, Anatoli Verenchikov, Victor Spicer, Garrett Westmacott, and Igor Chernushevich, as well as Joe O'Neil, Adelinda Yee and Linda Donald of the Chemistry Department.

Dr. Standing also kindly provided summer student assistants for three summers. Alan Hyland assisted in the monolayer work; he also made some of the equipment improvements mentioned in chapter 3. He and Dāvid Binding assisted in the alamethicin and dynorphin work, respectively.

I am grateful for the generous support of the Natural Sciences and Engineering Research Council of Canada (four years), the Manitoba Health Research Council (two years), Abiotics Systems (a consultantship), and Dr. Standing's research grants, which filled in the gaps.

Dr. A. Chow gave me the free use of his nanopure water, Dr. Morrish the free use

of his vacuum evaporator, and Gilles Roy the free use of his equipment, time and brains. Gilles, the one person in the physics department who knows where everything is, how everything works, and how to fix almost anything, was very helpful in setting up the monolayer work apparatus.

I also wish to thank my parents for their encouragement, confidence, love and prayers throughout the years. My five siblings have also encouraged me, each in their own way.

The greatest support and encouragement came from my dear husband, Henry Schriemer, who couriered things to school and back, printed innumerable versions of the thesis, photocopied figures and did thousands of other big and little things while very busy with his own research. Most importantly, he prayed. Our daughter Lydia contributed many hugs and much happiness; she also spent many hours doing work for "Dokker Danning" while I was at my desk.

Finally, thanks to God who made it all possible.

ABSTRACT

The procedure used in sequencing the peptide Dynorphin 1-17 (mass 2146.20 u) as an unknown using a reflecting time-of-flight mass spectrometer is reported. Samples (1.5 μg) of the peptide were distributed as unknowns to participating laboratories in preparation for a workshop at the 1990 meeting of the American Society for Mass Spectrometry. At the time of the workshop about half the sequence had been determined correctly from the secondary ion spectrum with the aid of enzymatic digestions carried out on the target. Subsequent measurements have defined the remainder, apart from a couple of uncertainties.

Time-of-flight correlation methods have been used to determine the primary structure of the major component in a nonstandard preparation of alamethicins, and to give some sequence information about minor components. The peptide (mw~2000 u) is blocked at the N terminus with an acetyl group and has a primary alcohol rather than a carboxyl group at the C terminus, so the usual wet chemical sequencing methods cannot be applied. Upon bombardment with 25 keV I^- ions, the peptide, deposited on the surface of a solid target, produces both molecular ions and prompt fragment ions (*i.e.* ions formed at or very near the surface of the target). After acceleration, these ions may undergo metastable decay as they pass along the flight tube of a reflecting time-of-flight mass spectrometer. Measurement of the correlations between the neutral and charged daughters from these decompositions determines the decay pattern of each ion, which, in turn, yields definitive information about the sequence of the original peptide. All events are recorded on magnetic tape and analyzed off-line, so a single run on the spectrometer provides information on the decay of every ion produced at the target, *i.e.* information similar to that obtainable from a complete set of daughter ion scans on a multiple sector or triple quadrupole instrument.

Langmuir-Blodgett films of deuterated and undeuterated cadmium stearate have

been prepared and examined using the TOF SIMS correlation technique. Fragmentation occurring on different time scales (*i.e.* both prompt and metastable fragmentation) is reported. Two distinct patterns of ion yield with respect to film thickness were noted: metal-containing ions and $[M+H]^-$ ions have a maximum yield at ~ 1 monolayer and ions involving only the fatty acid have a maximum yield at ~ 5 to 7 monolayers. The effect of the I^- ion source on the spectra was noted as a function of time; adducts were formed in the negative mode whereas a Cs^+ ion source produces no adducts in the positive mode.

TABLE OF CONTENTS

LIST OF FIGURES

LIST OF TABLES

CHAPTER 1

INTRODUCTION

Mass spectrometry (MS) has been used since the early 1900's to separate ions of different mass to charge (m/z) values. These ions are produced in an ion source, mass analyzed by the spectrometer, and detected. Each of these processes will be discussed. Then their specific applications in our time-of-flight secondary ion mass spectrometer will be described. Finally the thesis will be outlined.

1.1 ION SOURCES

To be mass analyzed, ions must leave the ion source and enter a mass analyzer intact. Ion sources have been reviewed recently [Tang '91, Harrision '90]. Gaseous atoms and molecules can simply be ionized by an electron beam. Larger molecules, however, such as peptides and proteins are difficult to volatilize and need a more gentle ionization technique to remain intact after ionization. Ionization techniques gentle enough to study such large molecules have been developed within the last two decades. Ions may be produced so gently that even noncovalently-bound complexes remain intact, or they may be desorbed as fragments which give extensive structural information. In some cases energy is deposited into the ions so that they undergo metastable decay after leaving the ion source; in other cases ions must pass through a collision chamber before characteristic fragmentations are produced.

The most successful ionization techniques will be discussed in some detail with an emphasis on their use in peptide sequencing. In one family of desorption and ionization

techniques, particle induced desorption (PID), the sample ions are formed when a beam of particles (ions, atoms, or photons) strike a surface (liquid or solid) coated with the sample. Recently two other techniques applicable to very large ions have been developed. Although collisionally activated dissociation and metastable decay are not ion sources, they are a source of fragment ions and will also be discussed in this section.

1.1.1 PDMS

Historically the first of the PID techniques, plasma desorption mass spectrometry (PDMS), was discovered by Macfarlane and Torgerson in 1974 [Torgerson '74, Macfarlane '76]. ^{252}Cf fission fragments (masses ~110 or ~145 u [Sundqvist '85]) with 60 - 100 MeV energies strike a target on which a thin layer of sample is deposited and desorb large intact molecules as well as their fragments. In a related technique, heavy ion beams with similar energies from particle accelerators have also been used to study organic samples. Metallic surfaces such as etched silver, aluminum and gold can be used as supports for thick samples. For larger molecules, deposition on a nitrocellulose surface produces less fragmentation under particle bombardment and allows higher masses to be observed [Chait '87, Roepstorff '87, Jonsson '86]. In some cases anthroic acid has been shown to be more effective as a sample substrate [Wolf '91], but it has not become widely used.

Although PDMS has not been widely used for peptide sequencing, molecular weight determination is possible even for small proteins; in fact, masses as high as ~45000 u have been observed [Jonsson '89]. Peptide mixtures can be examined but their analysis may be complicated by fragmentation and it may be necessary to examine both positive and negative ion spectra to see all the components [Nielsen '89a]. Because of the energy deposited into the ions, many fragment at the target so that sequence information is available [*eg.* Bunk '92, Chait '82]. Examples of peptides and proteins examined range from alamethicin I (1964 u) [Chait '82] to ribonuclease A (13,682 u) and proteinase K (28,665 u) [Bunk '92]; Although PDMS has not become very popular in sequencing, it has been demonstrated to be powerful [Texas '92, Sundqvist '85]. Metastable decay occurs in PDMS [Chait '81], but is not routinely utilized in peptide sequencing,and its effects may sometimes not be recognized [Bunk '92].

1.1.2 SIMS

In another PID technique, secondary ion mass spectrometry (SIMS), a beam of keV ions is used to bombard a solid sample target. SIMS with such high beam currents that the entire target surface is affected (dynamic SIMS) had been used for years to examine inorganic surfaces [Benninghoven '87], but because the intense incident beam destroys the target surface, this method is not applicable to large biomolecules. The much lower total beam current (*i.e.* integrated flux) used in static SIMS (10^{12} - 10^{13} ions/cm^2 or 10^{-9} A/cm^2 for ~1000 s) [Benninghoven '76] gives spectra similar to those in PDMS. Unlike in PDMS, thin samples on metal backings are effective. Nitrocellulose reduces fragmentation [Lafortune '87], but anthroic acid does not have a significant effect in enhancing the molecular ion yield [Poppe-Schriemer '91a].

The mass range for molecular weight determination is usually limited to about 5000 u, although masses over 10,000 u have been observed [Ens '88a]. SIMS produces many fragment ions and metastable ions, very similar to those in PDMS. Even though peptide mixtures can be examined, overlap of the molecular ions with the fragment ions is likely [Poppe-Schriemer '94, '93]. Although the secondary ion current is too low for conventional MS/MS, mixtures can be sequenced using a TOF correlation technique (§1.2.4.3) if the components are suitably metastable. Procedures such as off- and on-target enzymatic digestions and various derivatizations, can be applied to SIMS [Poppe-Schriemer '91, Tang '91]. Few SIMS sequencing studies have been published on unknown sequences but this thesis presents two such studies (§ 2.2 and §2.3).

Recent work has shown that, whereas TOF SIMS has been used to sequence a highly basic peptide (§2.2) [Poppe-Schriemer, '91], neither LSIMS (§1.1.3) with high energy collisionally activated dissociation (CAD, §1.1.6) in a four-sector instrument with an array detector, nor electrospray mass spectrometry (ESMS, §1.1.5) with low energy collisions in a quadrupole instrument, provided adequate sequence information [Curtis '93]. Similarly for a wide range of dynorphins and other endorphins (all of which are very basic), coherent fragment ion series permitting sequence identification, were rarely observed.

1.1.3 FAB MS

In 1981 fast atom bombardment (FAB) was developed[Barber '81a, '81b, Surman '81]. It uses a high flux keV atom or ion beam to strike a *liquid* target in which sample ions are dissolved and produces a particle beam intense enough that FAB sources can be interfaced with conventional (*i.e.* sector or quadrupole) mass spectrometers. The breakthrough in this technique which allowed interfacing with conventional instruments was the use of the liquid matrix; the beam's charge state was not as important. If the primary particles are ions, the technique is generally called liquid SIMS (LSIMS). Because the nature of the target affects the experimental results more than the charge of the impinging particle, LSIMS is grouped with FAB, not with solid SIMS (§1.1.3). Peptide and protein samples are often dissolved in a matrix of glycerol, but other solvents and solvent mixtures are also common [DePauw '86].

FAB's potential for peptide sequencing was recognized almost immediately [Williams '82]. Because the fragment ions are generally of much lower intensity than molecular ions, sequence information is often not easy to obtain [1] (although it is possible with suitable matrices [*eg.* Przybylski '84]), but peptide mixtures such as the products of a chemical or enzymatic digestion are often examined. The molecular weights of the components of such a digest may be matched to amino acid fragments of expected sequences, a technique called FAB mapping. Due to suppression of the hydrophilic peptides by the hydrophobic ones, not all components in a mixture can always be observed so that a complex mixture may need to be separated according to hydrophobicity before FAB analysis (e.g. by reverse phase HPLC)[2]. Also, since basic peptides tend to give positively charged ions and acidic peptides tend to give negatively charged ones, it may sometimes be necessary to examine a mixture by recording spectra of both polarities [Harrison '90].

Selecting and fragmenting each of the peptides in a mixture by using collisionally activated dissociation (CAD) (§1.1.6) and tandem mass spectrometry (MS/MS) (§1.2)

[1] *eg.*, In an evaluation of FAB peptide sequencing, 14 peptides containing 3-13 residues (with an average of 7) were examined. No sequence information was obtained for 8 of the peptides and none of the peptides was completely sequenced (although one was determined to within a Leu/Ile ambiguity). [Roepstorff '85].

[2] Although the result may still be a mixture, it will generally not be composed of hydrophobic and hydrophilic peptides of a similar mass [Biemann '92].

often allows one to sequence peptide mixtures successfully [Biemann '92]. FAB has also been combined with liquid chromatography to analyze mixtures, to study enzyme reaction kinetics, and to obtain peptide sequence ladders by identifying the products of digestion with various enzymes [Caprioli '88]. Continuous flow (CF) FAB, in which the sample is continuously refreshed in a more aqueous matrix than is possible for ordinary FAB, exhibits much better sensitivity, less chemical noise, less ion suppression and better salt tolerance than standard FAB [Caprioli '92]. CF-FAB can be interfaced with on-line HPLC or capillary electrophoresis and with MS/MS to enhance its sequencing ability. Thioredoxin (11750 u, >100 amino acid residues) was the first protein sequenced using only MS/MS and enzymatic digestions; though 100 nmol of the protein were available, much less was used [Johnson '87].

1.1.4 MALDI

Although photon beams have long been used to desorb ions from bulk samples [Harrison '90, Hillenkamp '86], this technique is not very gentle; thus only small ions can be desorbed intact. By mixing the high mass molecules in a metal powder and glycerol matrix, Tanaka obtained ions as large as 34,000 u [Tanaka '88]. An even more gentle technique, matrix assisted laser desorption/ionization (MALDI), which can be applied to biomolecules as large as 10^5 u , was later developed by Karsas and Hillenkamp [Karas '88, '87]. In MALDI, a UV laser pulse is used to desorb and ionize large molecules, such as proteins, that have been incorporated into a crystal of an ultraviolet-sensitive matrix acid. When a laser pulse of the appropriate wavelength is used, a volume of the matrix sublimes, forming a gas jet that entrains the protein molecules [Zhou '92, Beavis '91]. Various matrices have been used, all of them forming crystals composed of flat, weakly interacting planes.

This soft ionization technique is useful in obtaining molecular weights of components of mixtures, such as the digestion products of a protein whose sequence is being confirmed. Often [Beavis '90], but not always [Roepstorff '91, Zhao '91], all of the peptides in a mixture appear in a spectrum. It is generally unnecessary to examine a mixture by recording

both positive and negative ion spectra, because the positive and negative ion spectra of peptide mixtures almost always show the same components [Beavis] (see §2.3 for a rare exception). Although, in general, MALDI produces no prompt fragment ions (recently some prompt fragmentation dependent on laser irradiance has been observed [Talbo '93]), it does produce ions that are 'metastable' [Spengler '91]. The decay is induced by collisions, either with matrix molecules in the gas jet or with residual gas molecules in the flight tube. Peptide fragmentation occurs with either low or high energy collision conditions depending on the acceleration voltage and the flight tube pressure. The fragmentations, which include abundant a-17 and b-17 ions (see §2.1, Figure 2.1 for an explanation of the nomenclature) [Kaufmann], are reminiscent of those observed by SIMS [Tang '89]. Using a two stage mirror, sequence information has been observed for peptides as large as melittin [Kaufmann '93, Spengler '92].

Other recent studies have shown new applications of MALDI to peptide and protein work. In one technique, if the surface is specific to the desired protein (as in affinity chromatography), then picomol amounts of this protein can be detected in complex mixtures [Hutchins '93]. In ladder sequencing [Chait '93], a new application of MALDI to peptide and protein sequencing, chemical means, such as the subtractive Edman technique in the presence of a terminating agent, are used to generate a mixture of polypeptides. MALDI is used to examine the resulting peptide mixture; the amino acid sequence can be deduced from the mass differences between peaks. As well, MALDI may be useful in assigning interchain disulfide bonds directly, without any chemical treatment, although assigning intrachain bridges requires very good resolution [Zhou '93a].

1.1.5 ESMS

In electrospray mass spectrometry (ESMS), the sample molecules are entrained in a liquid spray across a high electric potential difference [Fenn '90, JASMS '93]. Some of the spray enters a vacuum chamber, often through an orifice and sometimes through a capillary tube. The spray droplets are multiply charged by the electric field. When the droplets evaporate, sometimes with the aid of an air flow or a heated capillary tube, the isolated protein molecules retain a number of charges related to their sequence and

conformation [Katta '91]. The mass spectrum shows several peaks corresponding to ions of different charge. These multiple peaks decrease both the mass uncertainty and the necessary mass range of the spectrometer used, although they do complicate deconvolution of the spectrum of a mixture.

ESMS is such a gentle desorption technique that even noncovalently bound complexes may remain intact. It can also be used for molecular weight determination of components of mixtures although suppression of some components may occur depending on the volatility [Hiraoka '93], nature [Chait '92] or mass [Perkins '93] of the proteins. The multiply charged peptides can be sequenced using fragmentation produced by CAD in the source (by increasing pressure in the skimmer region), or by analyzing parent ions by traditional MS/MS techniques. Note that, because more than one charge is involved, these fragmentations may differ from the less-complex fragmentations of singly charged species [Fabris '93, Tang '93]. Reactions, such as carboxypeptidase digestions, can also be studied as an aid for sequencing [Rosnak '92]. Because ES is compatible with both on-line chromatography and tandem MS, very complex peptide mixtures can be separated and sequenced. In one of the most spectacular examples in biological MS, ~200 ion species (masses ranging from 737 u to 1370 u) were observed from a ~300 pmol sample mixture. Eight peptides were completely sequenced and another eleven were partially sequenced using microcapillary high-performance liquid chromatography electrospray ionization tandem mass spectrometry [Hunt '92]. However, in general it seems that ESMS and MALDI-MS are most informative when used together [Chernushevich , Perkins '93], because they yield complementary information.

1.1.6 Prompt Fragmentation, CAD and Metastable Decay

Collisionally activated dissociation (CAD) helps to determine the identity or structure of parent ions: the daughter ions produced are examined by tandem mass spectrometry (MS/MS) (§1.2) [Busch '88, McLafferty '83]. In this technique, parent ions are selected and passed through a collision cell filled with an inert gas, and then the corresponding daughter ions are mass analyzed. The nature of the gas, its pressure, and the energy of the parent ions can all be adjusted. Different fragmentation patterns of peptides are produced

depending on the energy of the parent ions and the number of collisions they undergo. In both high (keV) and low (eV) energy collisions the peptide backbone is susceptible to cleavage, but in high energy collisions the amino acid side chains may also be fragmented. Many peptide mixtures have been sequenced by FAB MS/MS. An extension of CAD is surface induced dissociation (SID) which gives similar spectra [Despeyroux '93] and allows greater control over the energy deposited into the ions. Amino acid side chain fragmentations can be produced in SID using a high enough collision energy [McCormack '93].

Bombardment of a *solid* target by primary ions at keV energies (SIMS) yields a variety of secondary ions at the target surface very similar to those produced by CAD of ions from a *liquid* matrix (FAB, LSIMS) or from an ESMS source; in some cases SIMS is the more informative technique (even surpassing ESMS-CAD) [Curtis '93, Poppe-Schriemer '91]. The usual difference between a spectrum produced from a solid target and that produced by FAB is presumably caused by a larger energy transfer to the molecules in a solid target, although the difference in spectrometers also plays a role [Ens '93a]. Because they often contain continuous (or semicontinuous) sequences of one or two series of fragment ions, and are relatively free from background, SIMS and CAD spectra are more easily interpreted than the spectra produced by FAB and LSIMS.

In TOF SIMS metastable decay, the parent ion decomposes in the flight tube due to the internal energy resulting from the desorption / ionization process, with fragmentation similar to that observed in CAD and, at very small time scales, in SIMS itself. Metastable decay cannot be controlled as easily as CAD; it depends largely on the nature of the peptide involved, as will be discussed later (§2.3). Mixtures can be analyzed very well if their components exhibit enough metastable decay (§1.2.4.3). Because the decay occurs at an exponentially decreasing rate [Cooks '73], spectrometers with only a narrow observation time window have poor sensitivity for metastable decay.

1.2 MASS SPECTROMETERS

Once the sample is ionized and volatilized, the ions are separated in a mass

spectrometer according to their m/z ratios (since most of the ions discussed in this thesis are singly charged, "m/z ratio" and "mass" are used interchangeably). Various kinds of mass spectrometers have been used in conjunction with the above sources. Because of their low beam current, PDMS and static SIMS are ideally suited to time-of-flight (TOF) spectrometers, although they have also been used with Fourier transform mass spectrometry (FTMS) [Wilkins '89, Laude '86] and SIMS with quadrupole instruments [Benninghoven '87]. Because of their high beam current, FAB and LSIMS can be interfaced with sector field instruments and are therefore the most commercialized of the particle induced desorption sources. MALDI has generally been interfaced with TOF machines although it is also used with quadrupole ion traps [Jonscher '93, J. Schwartz '93], magnetic spectrometers [Annan '93] and FTMS [Koster '92]. ES sources have routinely been used with quadrupole spectrometers and are also being interfaced with TOF spectrometers [Chernushevich '94, Verentchikov '94], magnetic sector instruments [Larsen '91, Allen '89], and FTMS machines [Beu '93, Winger '93]. Many variants and improvements in these techniques are being developed.

The four main kinds of mass spectrometers, sector field, quadrupole, FTMS and TOF are based on distinct physical principles and therefore have different characteristics. These spectrometers will be described and their advantages and disadvantages for mass spectrometry of large biomolecules will be noted. All of these spectrometers can be used for tandem mass spectrometry in which ion dissociations of various kinds, including dissociations of peptides in mixtures, can be studied. The first MS stage selects the parent ion and the second stage analyzes the daughter ion. These two stages may or may not be similar. Tandem mass spectrometry using each of these various machines will also be outlined. Special emphasis will be placed on TOF systems.

1.2.1 SECTOR FIELD

Sector field instruments use specific electric and magnetic fields to examine ions of a given mass and have been described in great detail [Duckworth '86]. The ions are deflected through a curved flight tube and only those of the appropriate mass follow the

correct path in the vacuum; the others have different radii of curvature and are lost to the spectrometer walls. Thus the field must usually be scanned to examine the entire mass range. If an ion decays, its fragments will follow an incorrect flight path and will be lost to the spectrometer walls. Very high resolution is possible if the ion beam collimating slits at the entrance and exit of the spectrometer are very small. For these three reasons, *i.e.* the mass scanning, the collimating slits, and the loss of metastable ions, the sensitivity of these instruments is low. The mass range is generally limited to several thousand u by the maximum electric and magnetic field values [Jennings '90], although much higher masses are attainable. Such instruments are suited to high current ion beams of relatively low mass such as those produced by FAB.

The possibilities for tandem mass spectrometry range from two sector machines, *i.e.* magnetic sector / electrostatic sector (B/E), with a collision cell between sectors, or electrostatic sector / magnetic sector machines (E/B) with a collision cell at the source slit [Jennings '83], to four-sector spectrometers [Todd '83] in which both the parent and daughter ions are selected using double-focussing spectrometers. For MS/MS it is essential to increase sensitivity with the use of an array detector (§1.3), which is position sensitive and therefore allows the exit slit to be widened. If the collision cells contain no collision gas, any metastable decays occurring in them can be analyzed as well [Fraefel '85]. All such systems are complicated to scan [Jennings '83], produce artifact peaks due to decay before the analyzing fields [Busch '88], have low transmission and sensitivity, and are expensive. The two sector machines produce low resolutions in MS/MS but are much cheaper. In sector field MS/MS machines, the ions have high kinetic energies and undergo one collision, on average [*e.g.* Beimann '82], as they pass through the cell.

1.2.2 QUADRUPOLE

Quadrupole mass spectrometers use both RF and DC voltages between opposing quadrupole electrodes in the spectrometer [Dawson '86, Duckworth '86, Dawson '76]. The quadrupole fields allow only ions of a chosen mass to have stable oscillations on their way through the spectrometer to the detector, while the others are lost to the electrodes.

The two voltages (RF and DC) must be scanned to obtain a complete mass spectrum. The resolution and transmission depend on the size of the spectrometer, and the mass range is usually limited to about 2000 u [Katta '91]. Such instruments have been used with FAB sources and are standard for use with electrospray sources.

Quadrupole MS/MS is usually done using triple quadrupole instruments [Yost '78]. The first quadrupole selects the parent ion; the second one, an RF only quadrupole, is the collision chamber which focuses ions scattered by the collision process, and contains all masses [Dawson '83, Yost '83a]. The third quadrupole is used to analyze the daughter ions. Such machines are relatively small and simple [Yost '83b], and have a high CAD efficiency and adequate resolution. The limited mass range hampers them somewhat, but they are commonly used to study low m/z ions, in peptide sequencing for example [*eg.* Hunt '92, Henderson '92]. CAD collision energies used are usually 10-100eV in the laboratory frame, for which the collision cross sections are high, and parent ions usually undergo many collisions in the cell. Of course, if no collision gas is present in the collision chamber, any metastable decay occurring in this region can be observed. Hybrid instruments may involve sector machines in place of the first quadrupole, or a FT spectrometer in place of the third.

A special example of a quadrupole machine is the three dimensional ion trap which has also become a popular spectrometer [Doroshenko '93, Mann '92, Dawson '86, '76].

1.2.3 FOURIER TRANSFORM ION CYCLOTRON RESONANCE

The Fourier transform ion cyclotron resonance mass spectrometer (FTMS) [Koster '92, Wilkins '89, Laude '86, Johlman '83] combines a homogeneous magnetic field with an electric ion trap [Duckworth '86]. Ions are excited using a sweep of their cyclotron frequencies on the plates of the trap. As they follow a circular path in the cell, they induce an image current in electrode plates adjacent to the cell. The entire mass spectrum can be derived from this image current at one time, without mass scanning. (Mass scanning may be used in high mass, high resolution experiments [Ijames '88] but this is technically not FTMS) . Resolution varies inversely with ion mass and total pressure [Russell '86] but if the magnet used is strong, and the pressure is low, very good resolutions have been

attained [3]. Sensitivity degrades with increasing residual gas.

Because the ions remain in the machine, the FTMS spectrometer itself can be used to perform MS/MS experiments. All ions present in the cell, except the selected parent ions, are ejected. If a collision gas is present in the cell, collisionally induced dissociation may occur when the parent ions are excited. If no collision gas is present, metastable decay may be observed. All daughter ions can be examined as described above for the parents. Repeated MS experiments can be performed by ejecting all but one kind of daughter ion and causing it to undergo CAD [Johlman '83]. The main purpose of a quadrupole FTMS instrument is to use the RF-only quadrupole ion guide to allow ions produced outside the FTMS cell to be injected into the cell, thus preserving the high vacuum required for the ion cyclotron resonance cell [Li '94, Koster '92, Laude '86]. For this same reason, laser dissociation has been used instead of a collision gas in a tandem quadrupole FTMS machine [Hunt '87].

1.2.4 TIME-OF-FLIGHT

Most modern TOF machines use static electric fields to accelerate packets of ions produced by a pulsed source; the whole mass range is examined for each ion pulse and no mass scanning is needed. Usually the mass is measured by determining an ion's flight time through a field-free linear tube from the source to the detector. If an ion, of charge q and mass m, is accelerated across a potential difference, V, all of the ions achieve the same kinetic energy, $(mv^2)/2 = qV$. The transit time, t, of an ion of velocity v, through a flight tube of length L is given by

$$t = L/v = L\sqrt{(m/2qV)}. \qquad (1.1)$$

If metastable decay occurs in the field free region, the daughter ions and neutrals will have almost the same velocity as the parent had, except for small variations due to energy release in the decay. Thus, they are observed as a broad base at the bottom of the parent ion peak. Tandem TOF machines with collision cells have been constructed [Cornish

[3] *eg.* 160,000 resolution at 3200 u and 60,000 at 5900 u for nonpeptide organic molecules, [Ijames '88].

'92]. Laser induced dissociation after ion acceleration has also been studied, but the experiments were not continued because of technical difficulties and poor preliminary results [Standing '89]. Metastable decay products, formed in the field-free region, can be separated from their parents and analyzed by deflecting them in various ways [Chait '81, Haddon '69], but an electrostatic ion mirror (§1.2.4.2) is especially well-suited to such studies.

1.2.4.1 Electrostatic Ion Mirror

An ion mirror compensates for the initial velocity spread of the ions and so improves the resolution. It also improves the signal to noise ratio [Tang '91]. Although it does reduce the spectrometer sensitivity somewhat by doubling the ion flight path and so reducing the solid angle acceptance of the detection system, this can be corrected using an ion lens to focus the ion beam onto the detector [Tang '91].

The theory of resolution enhancement by electrostatic ion mirrors was developed by Mamyrin [Mamyrin '73]. The ions that have a higher velocity will penetrate farther into the mirror than the slower ones, so that the faster ions compensate for their shorter time in free flight by their longer time in the mirror. If the mirror voltage is chosen correctly, the initial velocity spread is compensated to first order. One and two stage mirror fields have been used[Spengler '91, Tang '88, '88a, Della-Negra '86, '85, '84, Mamyrin '73]. Most single stage mirror fields are linear, but curved fields have also been used [Cornish '93], although they may reduce sensitivity by focussing or defocussing the beam.

For a simple single stage plane mirror with a linear field, the theory has been described in detail [Tang '91, Tang '88]. Very simply, the desorbed ion of mass m and charge q is accelerated across a potential difference V so that its kinetic energy is

$$mv^2/2 = qV. \qquad (1.2)$$

In figure 1.1 the distances from the target to the mirror, L_1 and from the mirror to the detector, L_2, are the total free flight distance L. The speed of the ion is the same after reflection as before, so that the total time spent in free flight is

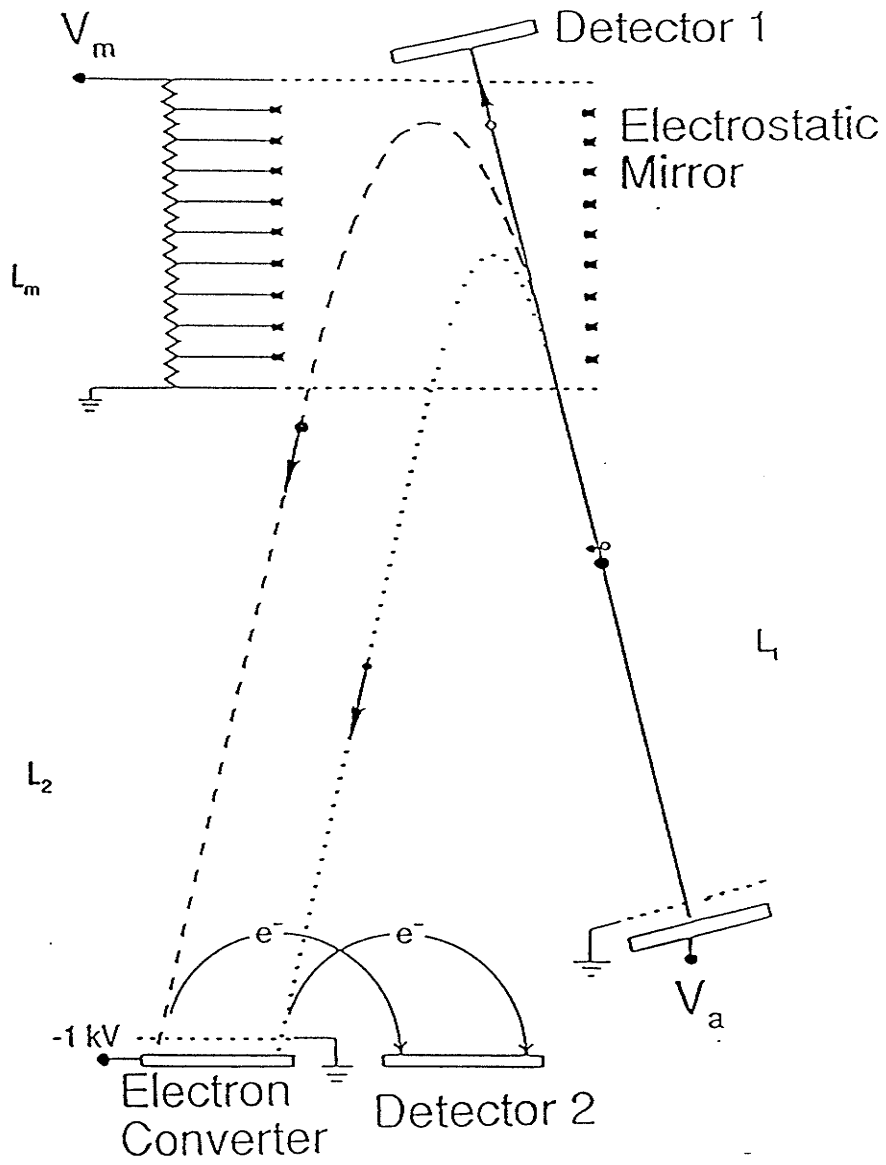

Figure 1.1 Reflecting TOF spectrometer showing the path of the parent (●), daughter ion (•) and daughter neutral (∘) when the mirror voltage is on.

$$t_f = L/v. \tag{1.3}$$

The ion mirror has a field E; it accelerates the ions according to

$$a = qE/m \tag{1.4}$$

so that the total time spent in the mirror is

$$t_m = 2v/a = 2(m/qE)v. \tag{1.5}$$

The total flight time then is

$$t = t_m + t_f = 2(m/qE)v + L/v. \tag{1.6}$$

When small variations due to an initial velocity spread exist, t(v) is minimized when

$$2(m/qE)v_o = L/v_o. \tag{1.7}$$

This means that the times in the mirror and in free flight are equal to first order.
In other words, if the mirror field E is set constant as above, then the optimum accelerating voltage, V_o, is chosen by satisfying

$$E = (2m/qL)\, v_o^2 = 4V_o/L, \tag{1.8}$$

When this V_o is used, the initial velocity spread has been corrected to first order and the resolution is optimized.

A more complete treatment has been given by Tang [Tang '91].

1.2.4.2 Correlation Technique

In the simplest mode of operation of a reflecting spectrometer, there is no field in the electrostatic mirror, so the TOF spectrum (the "direct spectrum") is observed in detector

1 (Fig. 1.1) and the device operates as a linear TOF spectrometer. If the molecular ions or the prompt fragment ions decay as they pass along the flight tube, their neutral and charged daughters continue with approximately the same velocity as their respective parent ions. Therefore, the daughters appear as a broadened peak at the same position as the parent ion peak.

When the spectrometer is operated in the reflecting mode, the voltage on the mirror is normally set to a value that optimizes the resolution for the parent ions [Tang '88]. Under these conditions, undecayed ions (*both* the molecular ions and the prompt charged fragments) are reflected by the mirror and observed with improved resolution in detector 2. If an ion decays in free flight between the target and the mirror, the neutral daughter, which is not affected by the mirror, continues to detector 1 where its measured flight time serves to identify its parent. The charged daughter is reflected into detector 2, where its mass is determined by the ratio of its flight time to the flight time of its parent, as will be shown below [Tang '88].

The ion mirror can be used to study the metastable or photon-induced decay of ions passing through the first field free region, figure 1.1 as developed by the Orsay group and by ourselves (§2.3.4.3, §3.4.2, Appendix 2.6) [Tang '91, '89, '88a, '88b, Brunelle '90, Standing '90a, '90b, '90c, '89, '86, Della-Negra '86, '85, '84]. In TOF SIMS, the primary ion current can be set so that for each primary ion pulse, only one or two ions are desorbed and ionized. If a primary ion pulse produces a secondary ion which decays into a neutral daughter and a charged daughter, the neutral will be detected at detector 1 and the ion at detector 2, as described above. Time windows are set for detector 1 corresponding to the neutral daughter's arrival. For any primary ion pulse after which a neutral arrives at the detector in this time window, a daughter ion arrives at detector 2 and is stored in a correlation spectrum. Of course, if a background neutral fragment arrives at detector 1 during the expected time window, the spectrum at detector 2 will be saved with the correlated spectra, resulting in a false correlation. As well, if more than one ion is desorbed in a particular pulse, there will be false correlations. Such false correlations must be removed from the correlation spectrum before it can be analyzed.

Analysis of the correlations between charged and neutral daughters then enables one to determine the decay of each parent ion, *i.e.* the decays of both the molecular ion and the

prompt fragment ions. Theoretically, *any* ions which decay can be examined, although those with low decay rates may require an unreasonably long data acquisition time. The only exceptions would be those decaying with loss of an electron or a hydrogen ion, because the charged particle may have too high a transverse velocity to reach the detector.

The flight time of the daughter ion is simply the sum of its free flight time (before and after metastable decay) and its time in the mirror. The daughter free flight time t_{fd}, is given by

$$t_{fd} \cong L/v_o \tag{1.9}$$

where L is the total length of the free flight region and v_o is the parent ion velocity, which is approximately the same as the daughter ion's velocity. The time spent in the mirror is

$$t_{md} = 2(m_d/qE)v_o \tag{1.10}$$

where m_d is the daughter ion mass. The daughter ion flight time t_d is then

$$t_d = t_{fd}+t_{md} = L/v_o + 2(m_d/qE)v_o \tag{1.11}$$

When the mirror is optimized for the parent ion mass as in 1.7 (i.e. $L/v_o = 2(m_p/qE)v_o$) , then

$$t_d = (L/v_o)(1+m_d/m_p) = (t_p/2)\,(m_p+m_d)/m_p \tag{1.12}$$

or

$$m_d = (2t_d/t_p - 1)m_p \tag{1.13}$$

Note that the mirror is not optimized for the daughter ions. To optimize it for a particular daughter ion m_d, its field must be reduced to allow the daughter ion to spend as much time in the mirror as in free flight. As mentioned above, after a metastable decay, the daughter ion and neutral have essentially the same velocity as the parent ion had.

Therefore the daughter's free flight time is the same as the parent's, and its optimum time in the mirror must also be the same. Thus we get, similar to equation 1.7,

$$2(m_d/qE_d)v_o = L/v_o \tag{1.14}$$

where E_d is the optimum mirror field for the daughter ion. By comparison with equation 1.7 which holds for the parent ion, we get

$$m_d/V_{md} = m_p/V_{mp} \tag{1.15}$$

where V_{md} and V_{mp} are the optimum mirror voltages for the daughter and parent, respectively.

When daughter ion resolution is important, it may be necessary to examine the correlation spectra at several mirror voltages. Even in such a case, however, many daughter ions of interest will not satisfy equation 1.15. In that case, their masses can simply be calculated as follows:

$$m_d = (2t_d/t_p - 1)\, m_p\, (V_{mred}/V_{mp}) \tag{1.16}$$

where V_{mred} is the reduced mirror voltage (which is, of course, the optimum V_{md} for a different value of m_d).

If data logging is used, all ions which decay can be examined in a single spectrometer run and no scanning of the parents is necessary. Only if the daughter ion resolution is very important do spectra need to be acquired at several mirror voltages, usually no more than three, for a linear single stage mirror. It has been shown that a curved mirror field may allow daughter ions of all masses to be observed with good resolution at one time [Cornish '93], although perhaps with reduced sensitivity. TOF correlation measurements are thus much more sensitive than sector field or quadrupole MS/MS in which both the parent and daughter spectrum need to be scanned to obtain the same information.

Unlike sector field or triple quadrupole tandem MS, which can examine both CAD and a narrow range of metastable ions, the TOF correlation method can examine only metastable ions, although these are spread over a long time (§3.4.2). Thus in the TOF

method, the decay cannot be controlled. Fortunately, with the SIMS desorption ionization technique used, many molecular ions are somewhat unstable and can easily be examined by this method.

1.2.4.3 Advantages and Disadvantages

The resolution of a TOF spectrometer, often quoted as $m/\Delta m_{FWHM}$ (although it is defined as the reciprocal), is $t/2\Delta t$, for all masses. Historically, due to velocity and time spreads in the initial beam pulse and due to metastable decay, the resolution was not very good. Narrow incident beam pulses and a velocity focussing ion mirror have been used to improve the attainable resolution to 13000 [Tang '91]. The ion mirrors can also be used to study metastable decay in a manner analogous to the MS/MS performed in other instruments using CAD.

TOF instruments have several advantages over other spectrometers for analyzing biological molecules:

1)They have no theoretical mass limit, and the only mass limitation is due to desorption and detection capabilities.

2) The resolution limited only by the metastable decay, the initial energy spread, and the isotope distribution; this is an advantage at high mass.

3)Because of the open geometry and straight flight tube, TOF spectrometer sensitivities are much higher than those of magnetic sector spectrometers.

4)The whole spectrum can be examined at one time because no scanning of the spectrum is involved; this improves the sensitivity.

5)The daughters of metastable decay are not lost in the spectrometer but continue their flight to the detector with approximately the same velocity as the parent and therefore arrive at the detector close to the time at which the undecayed particle would have arrived. Thus the spectrum seen is essentially that occurring immediately after acceleration (*i.e.* < 200ns).

6)Using an ion mirror allows metastable analysis comparable to that in MS/MS, but with much better sensitivity because neither the parent nor the daughter spectra needs to be scanned.

The disadvantages of TOF machines include the relatively low resolution, the need for a pulsed ion source, low count rates leading to long run times, and the inability to fragment ions controllably, as is possible in CAD. However, the resolution is usually adequate and pulsed ion sources are available. All things considered, TOF machines are generally very well suited to the study of small amounts of high mass biological molecules.

1.3 DETECTORS

Once the ions have been mass analyzed, they must be detected and recorded. Various different approaches can be used. In most spectrometers excluding FTMS (§1.2.3), the ions are detected when they collide with a detector such as a photographic plate, a Faraday cup, a scintillator, or some type of electron multiplier. When high mass ions (i.e. with less energy/u or less velocity) collide with a surface, more secondary ions than electrons are produced [Verentchikov ' 93, Kaufmann '92, Martens '92]. However, for the masses examined in this thesis (up to ~2500 u), the traditional detection techniques [Tang '91, Ens '84] are perfectly adequate.

Electron multipliers, which can be used to detect either single ions (SIMS) or ion currents (MALDI), must produce very high secondary electron yields. Incident ions generate electrons by impinging upon a special electron-producing surface. The electrons which are produced are then multiplied by being accelerated to collide with more of such electron-emitting surfaces. Electron multipliers are available in various geometries, including single tubes, called channel electron multipliers, which are coated inside with an electron emitting material. Such channels, when fused together into arrays, can be used as position-sensitive detectors, greatly increasing the sensitivity of sector field instruments. Very thin arrays of very small, angled channels, called microchannel plates, are often used in TOF spectrometers (*eg.* Fig. 1.1). For two such plates in a chevron arrangement, gains of 10^7 are common.

1.4 MANITOBA TOF II

The spectrometer used for this work, Manitoba TOF II, is a reflecting time of flight machine with both secondary ion and MALDI sources. Its ion sources, the spectrometer itself, and the detection and data acquisition systems will be outlined separately. Five to 35 femtomoles of peptides up to ~3000 u have given well-resolved molecular ions [Tang '91]. A resolution of 13000 has been obtained for $(CsI)_2Cs^+$ (652.5 u), and γ-endorphin (1859 u) has been observed with a resolution of 7000 [Tang '91] (note that resolution is defined as ΔM/M, but the resolving power, M/ΔM, is usually quoted as the resolution). Operating pressures of 0.5 to 5 $x10^{-7}$ Torr were maintained using titanium sublimation and ion pumps which have recently been replaced by a turbomolecular pump. TOF II has been used for analyzing peptides, proteins, and oligonucleotides as well as for fundamental SIMS, MALDI, and metastable decay studies.

1.4.1 ION SOURCES

Two different secondary ion sources were used in this work. A pulsed Cs^+ ion gun was used for the studies of an unknown peptide (§2.2). A dual I/Cs^+ ion gun was used for the monolayer work (§3.3) and the alamethicin work (§2.3). The MALDI source was also used to study the alamethicins.

1.4.1.1 Ion Guns

Each ion gun comprises a source of primary ions, a set of pulsing plates, and a target (figure 1.2). Resistive heating produces a beam of ions. An einzel lens is used to focus the beam in the plane of a narrow slit and deflection plates sweep the beam across it, producing a pulsed beam. The pulsed beam reaches a sample target, often a peptide deposited onto electrosprayed nitrocellulose, and desorbs and ionizes some sample ions (usually one or two per pulse).

The pulses were at least 2.0 ns (sometimes as high as several ns) long for the Cs^+

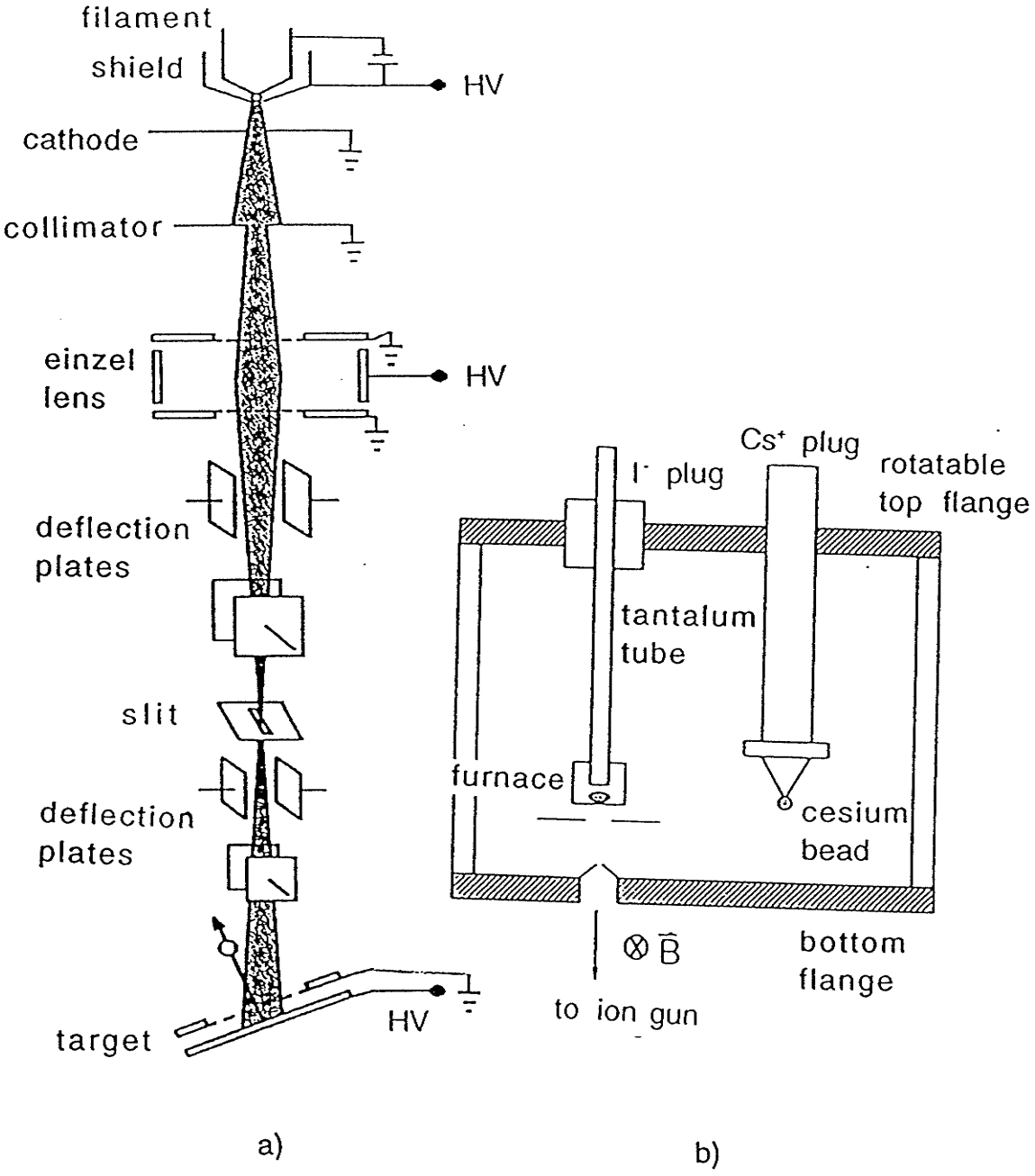

Figure 1.2 Secondary ion sources used. a) primary Cs^+ source and ion gun, and b) primary dual Cs^+ / I^- source (Figures adapted from Tang '91 and Zhou '93].

ion gun, and at least 4 ns (often 8-10 ns) long for the I^- gun, as measured from the electron -peak width for electrons desorbed from the target. The repetition rate was either 2kHz or 4kHz, and primary ion currents of several nA, measured at the slit, were routinely used. The primary ions were extracted using a potential of ~15 to 25 kV.

1.4.1.1.1 Cesium ion gun

A bead of cesium aluminosilicate silicate is coated onto a tungsten filament which, when resistively heated, emits Cs^+ ions [Tang '91, Ens '84]. They are extracted from the high voltage filament and shield region by a grounded extraction plate. Positioning of the bead with respect to the shield is crucial to maximize the ion current and the spectrum resolution, and can be done while the ion gun is at a high voltage using insulated micrometer adjustment screws. For high resolution, such fine adjustment must be repeated every time the ion gun is turned on because the filament often shifts slightly. If the shield has a small positive pulse applied to it with respect to the filament, the beam is first bunched inside the shield and is pulsed out only when the beam path will pass through the slit, enhancing the primary ion current. The voltage (and timing) of the deflection plates are crucial in obtaining good resolution in a spectrum and must be optimized every time the Cs^+ gun is turned on.

Steering deflection plates were constructed beyond the slit to steer the beam onto a specific spot on the target so that the sample may be deposited onto just a small part of the target, increasing the sensitivity. Using these plates to deflect the primary ion beam in steps across a 5 mm CsI strip, vapor-deposited on the target, the diameter of the Cs^+ primary ion beam was determined to be ≤ 3 mm.

1.4.1.1.2 Dual cesium-iodide ion gun

The cesium part of this ion gun [Zhou '94] is similar to the one described above but without the pulsed extraction. The filament cannot be aligned easily because no micrometer screws are available and the source is at a high voltage. As mentioned above, the optimization adjustments must be repeated on-line every time the voltages are turned on for optimum resolution and ion currents; with the dual source this is very difficult.

The iodide part of this ion gun produces I^- ions when iodine vapor is passed through a heated sintered plug of LaB_6, which is much larger and more robust than the

aluminosilicate bead of the Cs^+ gun. Because of the plug size, the beam spot size and the resolution are never as good as for the Cs^+ gun. However, because the iodide gun can be aligned satisfactorily with the voltage off and need not be realigned every time the voltage is turned on, and because it sparks less, it is much easier to use (although, of course, the analysis is complicated due to poorer resolution). Further, it is simpler to replenish the iodine than to coat a new cesium aluminosilicate bead.

The Cs^+ and I^- guns can be exchanged without breaking the vacuum by rotating the large flange. Each ion source itself is mounted on a rotatable plug which can move up and down for alignment.

1.4.1.1.3 Sample Target

The target is a circular metal (Al, Fe, Ag) surface on which nitrocellulose has been electrosprayed from a 5g/l acetone solution. The peptide sample is deposited on this surface from solution in aqueous 0.1% TFA. It is usually air dried but can be spin dried using a modified centrifuge [Nielsen '88][4]. If the target must be rinsed to remove impurities (*e.g.* alkali metal ions such as Na^+) , aqueous 0.1% TFA is used and drying is accomplished as above.

The target is introduced into the spectrometer through a vacuum interlock which allows targets to be replaced and pumped down in about five minutes.

1.4.1.2 The MALDI Source

A nitrogen laser beam (Laser Science ND337, which operates at 337 nm), passing just beneath the acceleration grid, is used to desorb ions from samples deposited on an etched silver target. The laser beam position and power density are adjusted using a lens, a beam attenuator, two wedge beam displacers and a bending prism (all of quartz) before reaching the target. Power densities used are ~10^6 W/cm^2, which is near the threshold for desorption. Part of the beam is reflected into a Scientech photodetector and is used as a start signal for the data acquisition system.

The target is usually etched silver (etched with HNO_3, and rinsed well) covered with

[4]The spin drying system was constructed by G. Westmacott.

a matrix solution containing ~5g/L protein and a large molar excess of matrix. The matrix solution used is ~10 g/L matrix (sinapinic acid, 2,5-dihydroxybenzoic acid (DHB) or α-cyano-4-hydroxycinnamic acid (CHC)) in a (1:3) acetonitrile:water mixture. Careful air drying of the solution on the target allows good matrix crystallization. Rinsing the target in nanopure ice water [Beavis '90] did not seem to affect spectrum quality and therefore was not always done.

1.4.2 SPECTROMETER

The spectrometer has been described in great detail [Tang '91]. The sample ions are accelerated across 12-25 kV in the electric field between the HV target and the grounded acceleration grid and enter the field free region. If the mirror field is off, all ions and neutrals are observed in detector 1 (figure 1.1), but, as explained in §1.2.4.3, if the field is on, the parent and daughter ions reach detector 2 and the neutrals reach detector 1.

The mirror field, established by 28 rings at constant potential differences and grids at the entrance and exit, is long enough to compensate for ion velocity spreads at the target. The acceptance of the spectrometer is effectively increased by an Einzel lens as mentioned in §1.2.4.2.

1.4.3 DETECTION AND DATA SYSTEM

Chevron microchannel plates, composed of micron diameter continuous dynode electron multipliers at a small angle, form the main detection system [Tang '91]. Two plates with opposing multiplier angles are mounted in succession, with a voltage of ~1kV across each plate (the voltage is lower for MALDI when the signal is strong). The electron gain of this system is ~10^7. To improve resolution and sensitivity, a CsI electron converter plate with 1 kV postacceleration is used before the microchannel plates of detector 2. The electrons produced are bent in a semicircle to the microchannel plate by a magnetic field, following Lorentz's force law.

The output current from the microchannel plates passes through a differentiating circuit so there is a voltage pulse corresponding to each ion detected. This pulse must be

preamplified. If there are only a few ions as in SIMS, they can be counted using a time to digital converter (TDC), but if there are many as in MALDI, the ion current with respect to time is recorded using a transient recorder.

1.4.3.1 SIMS

As described above, a tremendous amount of data is available from a typical experiment. To record this complex array of data it is essential to have an efficient data system [26]. For most of this work, the system was controlled by an Atari TT030 microcomputer, which uses a 68030 microprocessor running at 32 MHz. The Orsay model CTN/M2 time to digital converter (TDC) is connected to the VME bus of the computer with a custom interface, designed and constructed in our laboratory. This TDC has one common input (for the start signal) and three individually coded stop inputs, of which two are used here. For each primary ion pulse, the TDC receives a start signal from the ion gun clock in the common input. If events are measured in detector 1 or 2, the TDC generates an individually coded stop signal for each event. For each primary ion pulse the stop times are grouped together with their start time in a 512 byte buffer. The TT030 polls the TDC sixty times a second for data from the common start and the two stops. Flight times from detector 1, occurring within a particular time window, will trigger storage of the corresponding flight times from detector 2 as a histogram into a reserved area of computer memory; a correlated spectrum is then constructed from the stored information.

In some of the early correlation measurements (§2.2 and some of §3.4), the spectra were recorded in real time during the spectrometer run [Tang '91, '89, '88, Standing '90a, '90b, '90c, '88, '86]. However, this method requires a trial run to determine the time windows for the detection of neutrals, and the measurement may have to be repeated if any mistakes are made in setting the windows. Also, the method requires a good deal of memory, and several experiments may be necessary if many correlated spectra are to be recorded. For these reasons, we have developed an alternative procedure for most of the experiments reported here (§2.3 and most of §3.3); the flight times are recorded directly onto magnetic tape, event by event, instead of sorting them into histograms on line. Thus, the experiment may be "replayed" later with the taped data substituting for those normally

coming directly from the spectrometer's detector. As many as ten correlation spectra can be recorded simultaneously in such a "replayed" experiment. Furthermore, this can be done in less time than the actual spectrometer experiment because the restrictions on counting rate imposed by the instrument and the data system no longer apply. Because multiple replays of a run allow extraction of a daughter ion spectrum from *every* ion that decays, the sensitivity of the experiments is greatly increased. Also flexibility is considerably improved; the effect of changes in the time window can be investigated easily by replaying the tape with new window settings. Although a spectrometer run is typically ~4 - 5 hours, the data can be "replayed" from the tape in ~75% of the time.

For this procedure an Exabyte EXB-8200 8 mm tape drive is connected to the TT030 through its SCSI port. Each 8 mm tape can store up to 2 gigabytes of data, corresponding to about 15 hours of acquisition time. The acquisition software writes blocks of raw neutral and ion flight times onto tape at a maximum rate of about 17000 events/second (events include both stop and start signals).

1.4.3.2 MALDI

Because MALDI produces large sample ion currents, a transient recorder (Lecroy TR8828D) which is sensitive to both the timing and the amplitude of a signal, was routinely used after preamplification. The signal was recorded by an Atari MEGA ST, using a version of the acquisition software which allowed peak height selection to avoid saturation and improve resolution. The MALDI system could be used to record spectra from only one detector at a time.

1.5 OVERVIEW OF THESIS

The first part of this thesis is about peptide sequencing by SIMS. Dynorphin A (1-17) was sequenced as an unknown peptide using SIMS, enzymatic digestions and chemical derivatization. Several alamethicin peptides were also sequenced, and in these

cases the TOF SIMS correlation technique and MALDI TOF were used. The fragmentations observed will be discussed.

The second part is a study of the SIMS of Langmuir Blodgett multilayers. The apparatus and procedures to make the monolayer are presented in enough detail to be used as an instruction manual. Results of yield versus monolayer thickness studies for various ions are reported. The differences between the prompt and the metastable fragments of parent ions are also discussed.

Although the link between the different topics is not obvious, it turned out that they are all most easily studied by our method than by other mass spectrometric techniques.

Highlights of this work will be reviewed and future directions will be outlined in the conclusion.

CHAPTER 2

PEPTIDE SEQUENCING

2.1 INTRODUCTION

Many biologically significant substances, such as hormones, enzymes, neuropeptides, and immunological molecules, are peptides and proteins, usually consisting of different linear sequences of the twenty most common amino acids. The sequences, encoded by DNA in a peptide's gene, ultimately determine the molecule's tertiary structure. To understand a molecule's function, *i.e.* its chemical interactions, one must know its three dimensional structure. Obviously, then, it is important to know these amino acid sequences. A classical approach involving various cleavages, Edman degradation, and separations is traditionally used. Since DNA sequencing has gained popularity, peptide sequences may be deduced from the cDNA sequence. A third increasingly popular approach is to use mass spectrometry in conjunction with the other techniques [McCloskey '90].

This chapter outlines these three main sequencing techniques and describes two TOF-SIMS sequencing projects in detail. In the one project, sequencing the highly basic dynorphin A(1-17) as an unknown, enzymatic digestions (on and off the target) and chemical derivatizations were performed. In the other project, sequencing various alamethicin peptides, extensive metastable decay allowed the TOF correlation technique to be used.

At the time these studies were begun, FAB MS/MS was the sequencing method of choice; the power of MALDI and ES was not apparent. However, even now, TOF SIMS using single ion counting has a useful role in sequencing small amounts of peptides of masses < 2500 u. Very basic peptides are difficult to examine using the other standard MS

techniques (§1.1.2, 2.2) [Curtis '93, Poppe-Schriemer '91]. The experience our laboratory has gained with SIMS of these peptides may be applied to peptide and protein studies using ESMS and MALDI.

2.1.1 TRADITIONAL PROTEIN SEQUENCING TECHNIQUE

Once the protein has been purified, it is cleaved using fairly specific enzymes (e.g. *staphylococcus aureus* V8 protease [which cleaves at Glu-X], clostripain [Arg-X], endoproteinase Lys-C [Lys-X], trypsin [Arg-X, Lys-X]) or specific chemical cleavages (e.g. cyanogen bromide [which cleaves at Met-X], o-iodobenzoic acid [Trp-X], hydroxylamine [Asn-Gly], mild acid [Asp-Pro], 2-nitro-5-thiocyanobenzoic acid [X-Cys]) [Hermodson '90]. The resultant peptides are separated and purified using chromatography or electrophoresis, and then subjected to the Edman degradation either manually (for an average of ~10 residues) or automatically (for an average of 30-40 residues). Using one of the other cleavage methods, another peptide mixture is produced; these peptides are separated, purified and sequenced as before. The overlapping sequences are then used to order the different peptides and the protein may be cleaved again to determine the entire sequence.

Although this classical approach has provided the sequences of many proteins, it has limitations. Peptides with blocked N termini are not amenable to the Edman degradation. Problems can occur with His residues, Asp-Gly bonds, Glu and s-carboxymethylcysteine residues, Trp, Ser and Thr residues, and glycosylated Ser and Thr residues [Allen '89]. As well, post-translational modifications which add to or alter a protein can interfere with the Edman degradation or may not be detected. Modified or uncommon residues are often not detected [Yates '87]. Since each step of the reaction is less than 100% complete, preceding residues as well as the residue of interest are released, and this may cause difficulties.

2.1.2 USE OF DNA SEQUENCES IN PROTEIN SEQUENCING

Once a partial sequence of a protein is known (and it can be determined using

traditional and/or mass spectrometric methods), corresponding oligonucleotide probes can be synthesized [Allen '89]. These probes are used to select cDNA clones from a genomic library [Voet '90]. The protein sequence may be deduced from the cDNA sequence using the standard genetic code. This method is very powerful and for a time it seemed to render protein sequencing obsolete.

Contrary to earlier expectations, however, the cDNA sequence may not give the mature protein primary structure. There are various reasons:

1) The standard genetic code is not universal [Voet '90]. (For example, in many kinds of systems, the usual termination codon may code for an amino acid. In some mitochondrial systems, the traditional codon meaning has been altered [Fox '87]. In fact, more than eight codes are presently known.)

2) Errors may have occurred in the DNA sequence determination [Allen '89, Biemann '89].

3) There may be errors in the reading frame, due to difficulty in identifying the correct reading frame, or to ribosomal frame shifting during translation [Craigen '86].

4) Errors due to overproduction (*e.g.* due to a shortage of amino acids, tRNA or enzymes [Chait '93a]), may arise if the protein is genetically engineered.

5) Post-translational modifications such as acylation, glycosylation, phosphorylation [Allen '89], removal of some N and/or C terminal residues [Biemann '89], or removal of an internal section of the protein [Allen '89] may have taken place in the host cell [Scoble '90, Chernushevich].

In fact, many genetically engineered proteins have unexpected sequences or added groups [Chait '93a]. Thus, the protein sequence deduced from the cDNA must be checked with the protein itself. Traditional techniques are often used but mass spectrometry, combined with enzymatic digestions (especially tryptic digestions) and with CNBr cleavages, is becoming a method of choice [Shimonishi '90, Allen '89, Biemann '89].

2.1.3 USE OF MASS SPECTROMETRY IN PROTEIN SEQUENCING

Mass spectrometry, combined with enzymatic and chemical degradations, can be used to sequence some peptides completely, although it is most useful in conjunction with the other two approaches to sequencing. Because it is based on entirely different physical properties and techniques, it is complementary to the other approaches and can be used to

examine peptides with blocked N termini and modified or uncommon amino acids as well as enzymatic digestion product mixtures. Mass spectrometry gives the molecular weight of the parent ion(s), and sequence information may result from the molecular weights of fragment ions.

Since its discovery, FAB has been the workhorse of peptide sequencing by mass spectrometry. Although the other particle induced desorption ionization techniques, PDMS and SIMS, can be at least as successful in sequencing, they have not been widely available and have therefore been developed more by mass spectrometrists than by biochemists. MALDI and ESMS are also being applied and show great promise. These techniques are useful both for the molecular weight determination capabilities of mixtures (*e.g.* after digestions) and for the peptide fragmentation they produce.

Mass spectrometry has been used in conjunction with Edman degradation and exopeptidase digestions (most often carboxypeptidases, although aminopeptidases have been used as well) to generate peptide sequence information [*e.g.* Chait '93, Nielsen '90, Morris '89, Biemann '89, Hong '82, Bradley '82]. Often the mass spectrometry permits less purification, and is more amenable to unusual or modified amino acids, than is usual.

Subtractive Edman is often used and spectra are examined after each Edman cycle using field desorption mass spectrometry [Biemann '87], FAB [Morris '89, Bradley '82], or PDMS [Nielsen '90]. The mass difference between the molecular ions, in the spectra taken after successive cycles, gives the sequence. Edman degradation in conjunction with mass spectrometry has many of the same difficulties as conventional Edman degradation, but if subtractive Edman-MS is used, unusual or modified amino acid residues which will cleave can be observed, and the nature and location of the modification can often also be determined. If long coupling steps are used (*e.g.* 45 to 60 min at room temperature), phenylthiocarbamoyl adducts form; these may be helpful in counting the number of reduced Cys and Lys residues and in differentiating Lys and Gln [Nielsen '90]. If exopeptidases are used, different amino acids may be removed from the peptide at different rates, often resulting in mass differences between adjacent molecular ions corresponding to two amino acid peaks.

A slightly different combination of Edman degradation and MS uses the termination agent phenylisocyanate along with phenylisothiocyanate to generate a whole ladder of peptides; each successive Edman cycle results in some terminated peptides [Chait '93].

After a certain number of cycles, the entire peptide mixture is examined by MALDI, and the peptide sequence can be read directly from one spectrum. If phenylthiocarbamoyl and phenylcarbamoyl adducts were to form at Cys and Lys in this technique, the different masses of the two adducts and the single step MS readout could be a source of great confusion. However, under the conditions used (3 min coupling step at 50° C) there is no indication of such adducts forming.

2.1.3.1 Molecular Weight Information

The molecular weight of a protein or peptide can be used to confirm an expected sequence. In such cases, the masses of a chemical or enzymatic digestion product mixture are often also examined, sometimes after chromatographic separation. If all the experimental masses agree with what was expected, it is likely that the expected amino acid sequence is correct. If the molecular mass and/or some of the digestion product masses do not agree, the expected sequence is obviously not correct, and the relevant digestion products may be sequenced by tandem mass spectrometry or purified and sequenced traditionally.

Even though the common amino acids (see appendix 2.1) have unique masses (excepting Lys and Gln; Leu and Ile), molecular weight information alone gives little information about a true unknown. In fact, the molecular mass of even a small peptide cannot give its sequence and cannot even give its amino acid composition. For example there are a total of 2669 amino acid combinations which give ~695 u, and all of these fall between 695.15 u and 695.55 u (see Appendix 2.2). For TOF-SIMS with a mirror, the total mass uncertainty (accuracy and precision) is normally less than ~ 0.2 u, but this is clearly inadequate to determine a peptide's amino acid composition from its molecular weight alone. However, knowing the number of exchangeable hydrogens from H-D exchange can reduce the number of possible amino acid combinations by a factor of 5 to 100 [Sepetov '93].

2.1.3.2 Use of Fragmentation Information

To determine the sequence, fragmentation, whether prompt (*i.e.* at the target), metastable, or collision-induced, is necessary. Since most fragmentation occurs along the

peptide backbone, fragment mass differences between adjacent peptide bonds may be used to determine amino acid identities. Higher-energy dissociation or collisions may induce fragmentations of the amino acid side chains as well. Common positive ion fragmentation patterns and their usual nomenclatures [Johnson '88, Roepstorff '84] are shown in figure 2.1. Deprotonated peptides are being examined but do not seem to give as much useful information [Waugh '93].

The probabilities of various fragmentations occurring have been studied extensively [Johnson '89, Seki '85, Westmore '82]. Because peptide fragmentation patterns occurring in various kinds of biological mass spectrometry usually exhibit only slight differences [Fabris '93, Kaufmann '93, Dass '92, Tang '91] these predictions can often be applied to most methods. (However, it is necessary to note that fragmentation patterns may depend on the kind of decomposition and if CAD is used, the energy of decomposition is also important [Dass '92].) Based on these studies, several computer programs have been written to predict fragment ions for a given peptide. Two such programs were used in this work, MacBioSpec (from Sciex, written by T. Lee and S. Vemuri) and an in-house program (by J. B. Westmore) which could be modified to accommodate unusual amino acids. COMPOST [Papayannopoulos '91] from K. Biemann's laboratory had also been obtained, but since it required a prohibitively large amount of space (at the time) on a VAX computer, it was never used. Programs used to sequence FAB and FAB CAD spectra have also been written [Johnson '89]. The fragmentation principles they are based on are useful to develop sequencing protocols for these other desorption methods.

As shown in figure 2.1, several fragmentations can occur between any two residues, and either the C-terminal or the N-terminal portion of the peptide may retain the charge and be detected as X, Y+2, and Z ions or A, B, and C+2 ions, respectively. In such cases, one can use the characteristic mass differences between the various peaks from each terminus to determine from which end of the peptide the fragments were derived, as shown in figure 2.2.

Mass differences between adjacent clusters of peaks (as in the "unknown" peptide, section 2.2), identify the amino acid residue involved. Side chain ions, such as D, V, and W ions, include characteristic portions of amino acid residues and therefore their masses do not follow a pattern independent of the residue as those for backbone fragmentation do. This may confuse the initial understanding of the spectrum if the peaks are large, as D ions

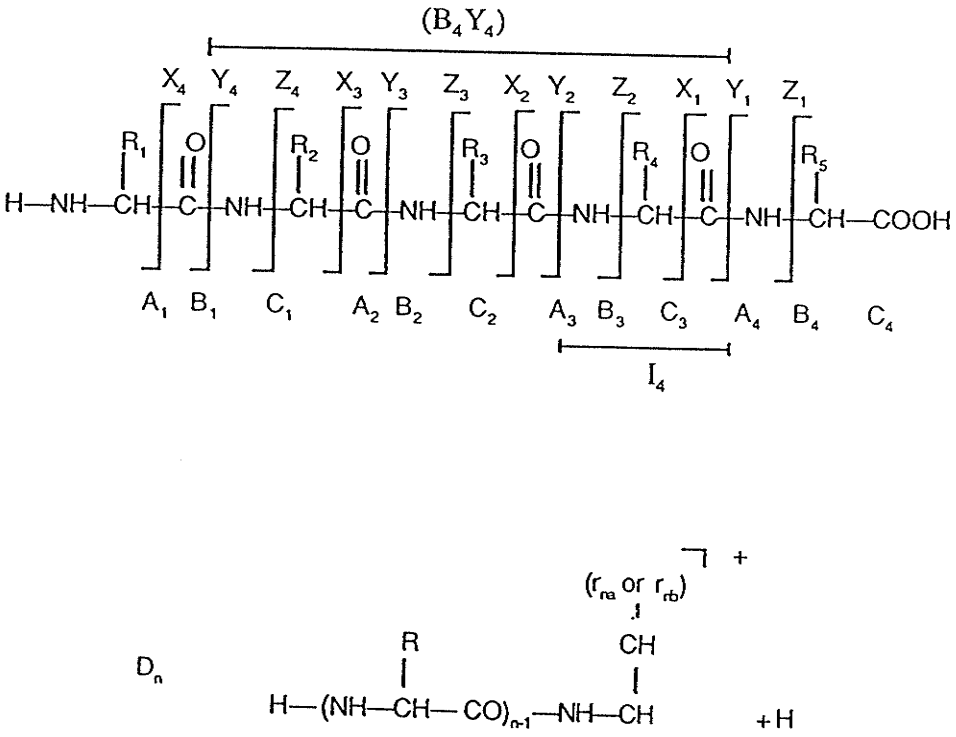

Figure 2.1 Peptide fragmentation nomenclature.

N-Terminus	C-Terminus
$(C_n+2) - B_n = 17$	$Z_n - (Y_n+2) = 17$
$(C_n+2) - A_n = 45$	$Z_n - X_n = 43$
$B_n - A_n = 28$	$(Y_n+2) - X_n = 26$

Figure 2.2 Characteristic mass differences between fragment peaks

occasionally can be. However, the side chain fragmentations are often invaluable to confirm amino acid identity; D and W ions provide the only means of differentiating Leu and Ile by MS. Gln and Lys, which also have the same masses, cannot be distinguished by side chain fragmentations. Acetylation (onto Lys, not Gln), tryptic digestion (after Lys, not Gln), or treatment with phenylisothiocyanate (which combines with Lys *via* the ε-amino group) can be used to distinguish between Lys and Gln [Biemann '89, Johnson '89].

If both N-terminal and C-terminal ion series are present, extra sequence information is available, but determining the sequence of an unknown peptide may become very difficult because of the large number of peaks present. In such cases, a combination of enzymatic or chemical digestions, computer interpretation, and experienced manual interpretation may be a necessity[1].

Internal fragment ions occur when both the N-terminal end and the C-terminal end have been cleaved off. The accepted nomenclature is shown in figure 2.1. Such fragments may be formed at the target, but can also be metastable decay products of N- or C- terminal ions formed at the target.

Individual amino acids may influence the fragmentation pattern. Basic residues, such as Arg or Lys attract the charge, and their presence at either terminus can drastically affect the appearance of the spectrum, giving rise to either N-terminal or C-terminal fragments in the spectrum. Such residues seem to have the greatest influence. For this reason trypsin, which gives peptides with basic C-terminal residues, is used to cleave a protein or peptide in the hope of getting a complete series of Y ions from each peptide produced [Biemann '89]. Pro, especially in a peptide without basic residues, has a great effect on fragmentation as well and may cause large Y+2 and B ions adjacent to it [Bunk '91]. Some unexpected masses may be observed because the Pro iminium structure is more stable [Williams '82]. Pro also inhibits C, D, V, and W ion formation and promotes the occurrence of fragment ions (§2.3) [Poppe-Schriemer '95, Biemann '89]. In negative spectra, the effect of acidic residues is important [*eg.* Williams '82].

Fragmentation may be altered by chemical modifications. For example, by fixing a positive charge at the N-terminus, sequence-specific fragments which are normally neutral become ions and can be observed. Increasing the basicity of Lys by guanidization also

---

[1]For an example in which a sophisticated computer program was not adequate, see Johnson '89.

enhances prompt fragmentation [Bunk '93]. Removing the basic sites of a peptide may both alter its prompt fragmentation patterns and render it more susceptible to metastable decay [Bunk '93] [§2.3]. Lithiating peptides has also been proposed as a means of controlling fragmentation [Leary '89].

2.2 SEQUENCING AN UNKNOWN PEPTIDE

2.2.1 INTRODUCTION

A workshop organized by the Biomedical Interest Group at the 1990 meeting of the American Society for Mass Spectrometry (ASMS) featured reports on the analysis of two "unknown" peptides in order to "illuminate some of the strategies and mechanics of characterizing peptides of unknown sequence by mass spectrometry" [Carr '90]. The peptides (a sample stated to contain ~1.5 μg of a peptide of mass ~1800 u, and a second sample stated to contain ~30 μg of a peptide of mass ~5000 u) had been distributed previously to some 35 laboratories requesting them . Participants were requested to restrict their methods of analysis to mass spectrometry (i.e. no Edman degradation or amino acid analysis). Whether or not the peptide was blocked at either terminus was not specified.

Three groups reported analyses of the 30 μg sample but ours was the only laboratory to submit results on the 1.5 μg sample (the smaller peptide). The organizers commented that "unfortunately there was too little time for any of the groups to discuss in sufficient detail how they interpreted their spectra, and the steps involved in building a sequence that they (or the audience) could be confident in" [Carr '90]. As pointed out by Biemann and Martin [Biemann '87], "it is by no means as straightforward to deduce the sequence of a peptide of unknown structure from its FAB mass spectrum as is often implied by the successful rationalization of a spectrum of a peptide of known structure". For these reasons, and because of the scarcity of data in the literature on the analysis of true

unknowns using only mass spectrometric methods, the work was published [Poppe-Schriemer '91]. Moreover, the measurements included a combination of features not normally found in peptide sequence determinations: production of secondary ions by keV Cs^+ bombardment of a solid sample film (on a nitrocellulose substrate); mass measurement in a reflecting time-of-flight mass spectrometer; deduction of the sequence from observation of fragment ions produced directly on the target without resorting to collisional dissociation; enzymatic digestions of the peptide on the nitrocellulose substrate.

2.2.2 EXPERIMENTAL

The ~1.5 μg sample was dissolved in 7.5 μL 0.1% aqueous trifluoroacetic acid in the plastic micro test tube in which it was supplied. For most targets 0.5 μL (~50 pmol) of this solution was dropped from a micropipette onto a 2 mm diameter spot of nitrocellulose that had been electrosprayed onto aluminum foil [Lafortune '87]; in two cases twice this amount was used. At the time of the ASMS report, nine targets had been prepared and about 3/4 (~5.5 μL) of the sample had been consumed. After each target was prepared the remaining sample was frozen, and later thawed for preparation of the next target. Significant sample deterioration was observed (a decrease in the ratio of the $[M+H]^+$ intensity to background by a factor ~2 from the 1st to the 9th target), presumably as a result of the many freeze-thaw cycles. [In retrospect, it might have been better to divide the original solution into several fractions and to thaw one at a time, even though this procedure would in principle give more losses from adsorption onto the walls of the tubes.]

Mass measurements were carried out in the reflecting time-of-flight mass spectrometer described in §1.4. Secondary ions were produced by bombardment of the target with 10 keV Cs^+ ions. They were then accelerated to an energy of 12.5 keV (with additional postacceleration across 1 kV at the detector).

2.2.3 RESULTS

2.2.3.1 Measurement of the Molecular Weight

An approximate mass scale for the reflected spectrum was determined by extrapolation

from measurements on H^+ and $[C_3H_3]^+$. The most prominent ion in the high mass spectrum, assumed to be $[M+H]^+$, was observed at a mass greater than 2140 u, a somewhat surprising result in view of the stated value ~1800 u. Because of the long extrapolation involved in the approximate calibration, a measurement was made on a molecule of known mass (ACTH 1-17) that happened to be available in the laboratory; this gave a correction of ~0.2 u to the approximate mass scale at ~2100 u. The high mass spectrum of a mixture of the unknown peptide and ACTH 1-17 is shown in figure 2.3. Note that the isotopic peaks are well resolved, thanks to the velocity focusing produced by the ion mirror. This measurement yielded a monoisotopic mass of 2147.2 u for the $[M+H]^+$ ion, a value we reported at the workshop. The $[M+H]^+$ assignment was confirmed by observation of the $[M-H]^-$ ion in the negative spectrum.

2.2.3.2 Fragment Ions From The Unmodified Peptide

In addition to the protonated molecule, the reflected time-of-flight spectrum contained many sharp peaks resulting from production of fragment ions at the target. These were superimposed on a continuous background resulting from unimolecular decay in the acceleration region and in free flight. Our previous peptide measurements [Standing '90a , '90b, '90c, '88, Tang '91, '89, '88] had provided a small data base for interpreting the spectra. In particular they had shown that the fragment ions observed in our technique were often more similar to those observed in collisional dissociation measurements than in FAB spectra [Martin '87], probably because of the increased energy transfer in bombardment of a solid sample, although the different spectrometers used may have had an effect [Ens '93a], as mentioned in §1.1.6. For example, our reflected spectrum from Substance P [Standing '90b] was almost identical to the one reported by Martin and Biemann from collisional dissociation in a four-sector tandem mass spectrometer, and quite different from their FAB spectrum [Martin '87].

For the present "unknown" sample the positive fragment ion spectrum showed many peaks between ~100 u and ~600 u, but none assignable, and a confusing medley of small peaks above ~1900 u, so it was not possible to start the sequence from either terminus. However, the spectrum between 600 u and 1800 u, shown in figure 2.4, contained some 24 major peaks together with a large number of smaller ones. Differences

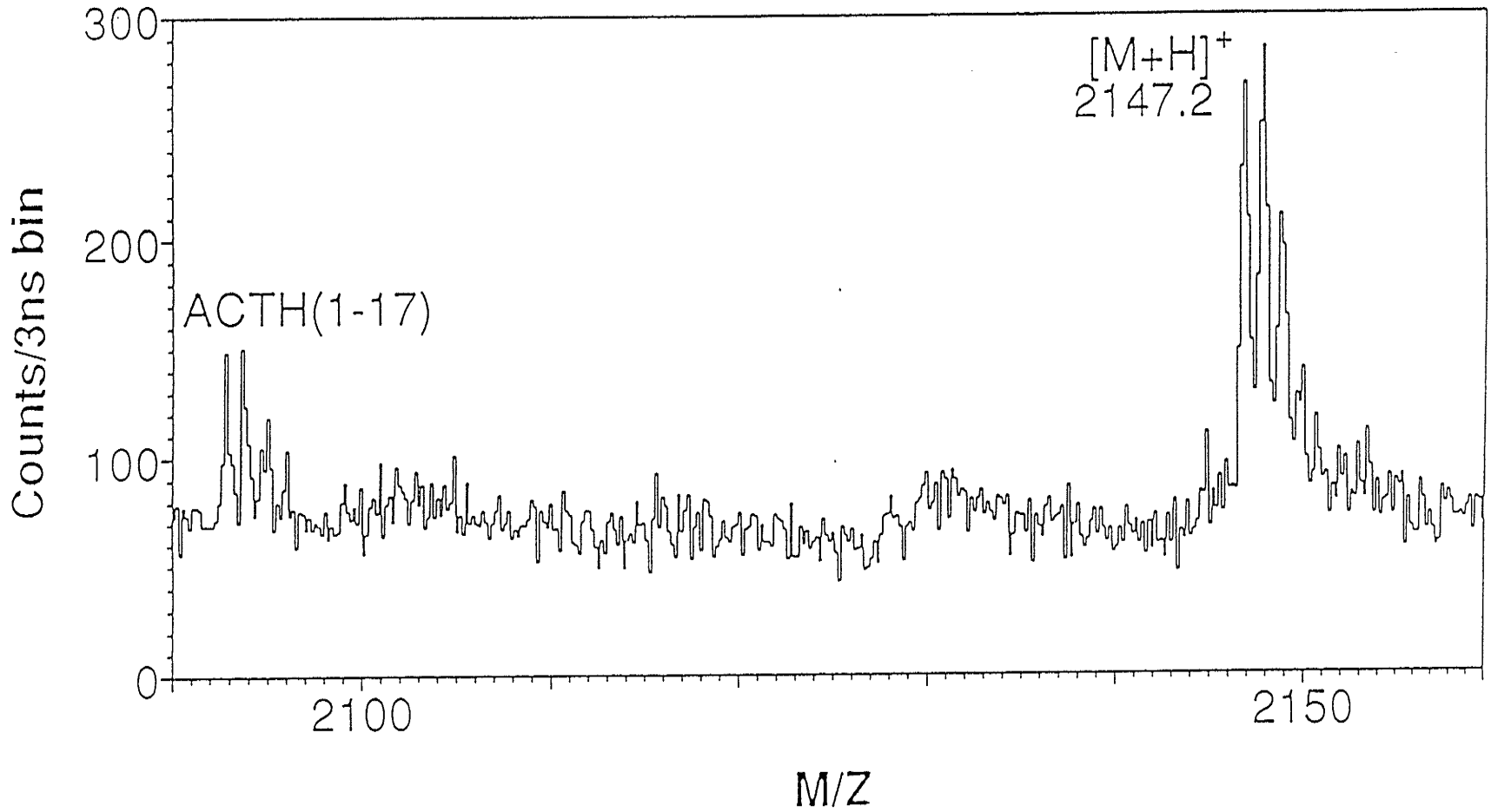

Fig. 2.3 Mass spectrum of a mixture of the "unknown" peptide and ACTH 1-17 in the molecular ion region: 0.5 µL (about 50 pmol) "unknown" solution, about 4 hr measurement.

between the measured masses of the major peaks were calculated as a first step in the analysis. This yielded a number of values corresponding to the masses of amino acid residues, but the most definitive feature was the presence of five pairs separated by 45 u, indicated in boldface under the spectrum. Such values characterize the mass difference between N-terminal A and C+2 ions as discussed in §2.1.3.2. Thus the assignments A_6, A_7, A_8, A_{10}, A_{12} and the corresponding C ion assignments could be made (the subscripts were of course unknown at that stage, but we have used their correct values to avoid cumbersome n, n+1, etc. labels). The mass differences A_6-A_7 and A_7-A_8 correspond to Arg/(Val+Gly) and Ile/Leu respectively (where "/" separates alternatives), lending support to the assignment as A and C+2 ions.

Only two combinations of amino acid residues correspond to the measured mass difference of 253 u between A_8 and A_{10} as assigned above: Arg+Pro, or Val+Gly+Pro. Proline cannot be at the N-terminal side of the interval because C_8+2 is clearly observed. Placing proline at the C-terminal side yields an assignment of three major peaks in the interval as A_9, B_9 and A_9- 17 (loss of 17 u, as observed previously in Substance P [Tang '89]); neither valine nor glycine in this position receives any support from the data. The resulting sequence Arg/(Val+Gly)-Pro is also consistent with the absence of C_9+2 ions.

The measured mass difference of 241 u between A_{10} and A_{12} yields eight possible combinations of amino acid residues. However, there are only two major unassigned peaks in this interval; if one is assigned as A_{11} (and its companion as D_{12}, see below), two of the combinations are ruled out and the sequence is (Gly+Ala)/Gln/Lys-Ile/Leu, supported by the presence of a small C_{11}+2 peak.

If the remaining major peaks beyond A_{12} at the high mass end are assumed to be A ions, the sequence is tentatively defined as (Gly+Ala)/Gln/Lys-Trp/(Ala+Asp)/(Ser+Val)/(Gly+Glu)-Ala, given some support (except for alanine) by the presence of small C+2 ion peaks.

The arguments above have considered only fragment ions from cleavage of the peptide backbone. However, about five major peaks remain to be assigned, and ions corresponding to losses from the amino acid side chains may also be important at keV energies, as shown by Johnson et al. [Johnson '88]. In particular, these ions distinguish between leucine and isoleucine. In our case a major peak (labelled D_{8a}) is observed corresponding to the loss of one branch of the isoleucine side chain, and a smaller peak

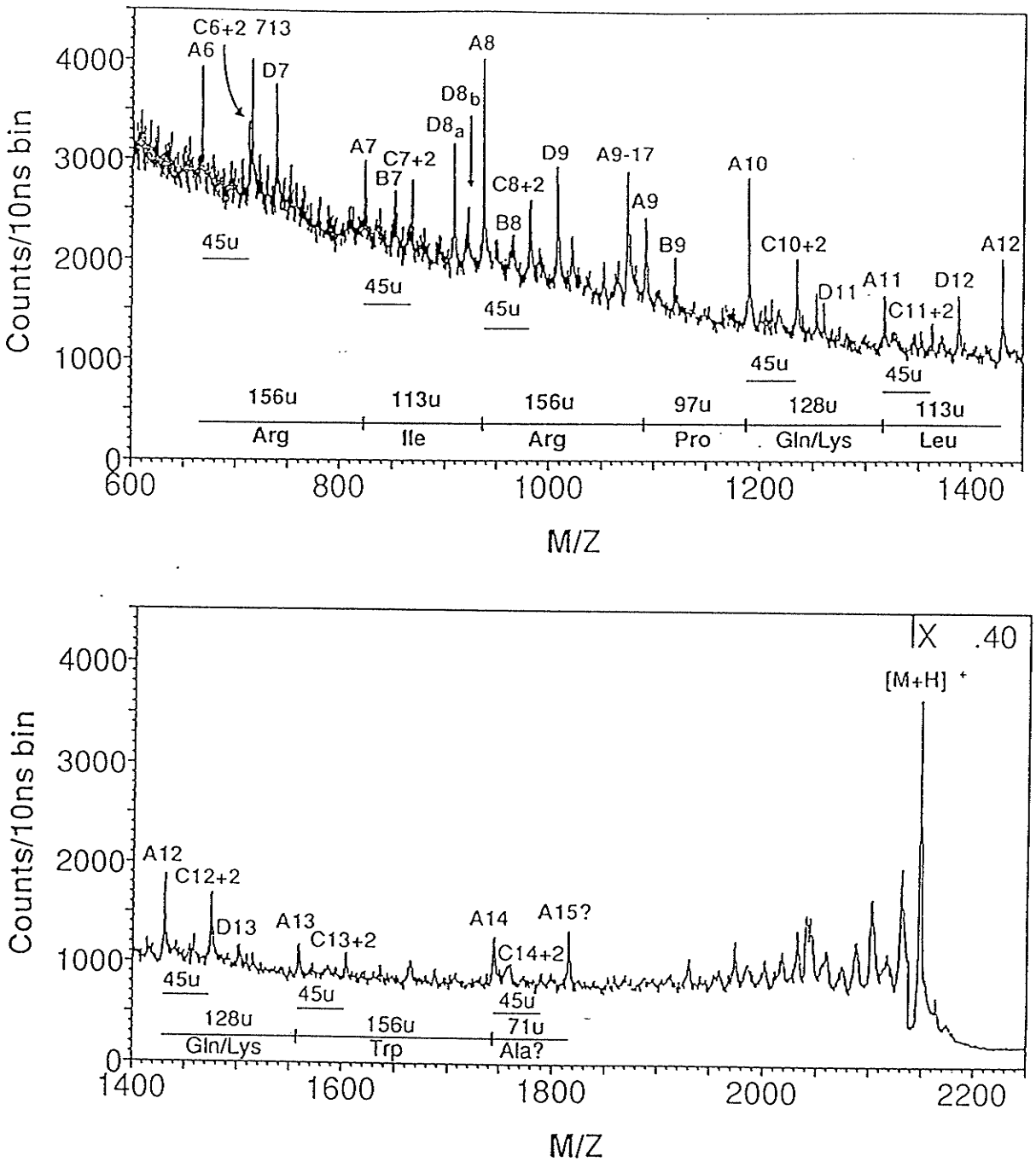

Fig. 2.4 Mass spectrum of the "unknown" peptide from m/z 650 to 2250: 1 μL (about 100 pmol) "unknown" solution, about 9 hr measurement.

(labelled D_{8b}) corresponding to loss of the other branch; the 8th residue is therefore isoleucine. The major peak labelled D_{12} defines residue 12 as leucine.

Identification of the remaining major ions as D_7 and D_9 yields further information. Their presence rules out glycine as the residue on the N-terminal side of the intervals, and their measured masses rule out valine, so both residues 7 and 9 must be arginine. The absence of D_{10} is consistent with the above assignment of proline in the 10th position. Finally, the identification of the small peaks labelled D_{11} and D_{13} as D ions eliminates both glycine and alanine as the corresponding residue on the N-terminal side of the intervals, and the small ratio of the D/A intensities favors lysine rather than glutamine in these positions [Johnson '88].

Thus the positive ion mass spectrum of the unmodified peptide led to assignment of the partial sequence:

-Arg$_7$-Ile$_8$-Arg$_9$-Pro$_{10}$-*Gln*/Lys$_{11}$-**Leu$_{12}$**-*Gln*/Lys$_{13}$-

-*Trp*/*(Ala+Asp)*/*(Ser+Val)*(*Gly+Glu*)$_{14}$-*Ala*$_{15}$-

where boldface type indicates the assignments that appeared to be reasonably reliable, ordinary type those less reliable, and italics those least reliable. The residue numbers were not known, but their correct values are added, here and later, for the convenience of the reader. All the major peaks observed were accounted for by this sequence except the one at 713.4 u, believed to be an impurity. No C-terminal ions were identified. The negative ion mass spectrum failed to yield useful sequence information.

2.2.3.3 Enzymatic Digests

Additional sequence information was obtained from the action of various enzymes on the sample [Lee '90, Allen '89, Caprioli '87, Keesey '87]. Because of the small amount of material available the reactions were carried out directly on the target [Hafok-Peters '90, Chowdhury '89, Klarskov '89, Nielsen '89, Roepstorff '88a, '88b, Craig '87, Chait '86a, 86b, 85], *i.e.* on the thin layer of sample deposited on the nitrocellulose substrate. We note that the $[M+H]^+$ ions of N-terminal cleavage products have a mass only 1 u

greater than the mass of the corresponding C+2 ion in the original spectrum, so it is necessary to distinguish carefully between them, particularly if the digestion is incomplete.

Trypsin cleaves at the C-terminal side of arginine or lysine unless the next residue is proline, so it might be expected to produce a number of cleavages if the above sequence is correct. Several tryptic digests were carried out under various conditions of time, temperature and pH (see Appendix 2.3). Figure 2.5 shows a mass spectrum from one of the digests. Here new peaks were observed (with masses equal to C+3 fragments) for cleavage after residues 6, 7, 11 and 13. Some C+2 fragments were observed as well, but are not resolved on the scale of the figure. Thus the new peaks confirm residue 7 as arginine and define both residues 11 and 13 as lysine rather than glutamine. In addition, a prominent peak at 712.4 u (between those previously observed at 711.4 u and 713.4 u) shows that the 6th residue is arginine or lysine. The absence of an observed cleavage on the C-terminal side of the 9th residue (arginine) is consistent with the assignment of proline in the 10th position.

Cleavage at the C-terminal side of tryptophan, phenylalanine, tyrosine, leucine or methionine is produced by α-chymotrypsin, except for adjacent proline. The action of this enzyme on a target (see Appendix 2.3) led to a spectrum with poorer signal to background ratio than in the case of the tryptic digest. However a clear peak was observed at the C_{14}+3 mass value, defining the 14th residue as tryptophan. In addition, a prominent peak was observed at 1252.8 u; this was consistent with the above assignments only if residue 6 was arginine rather than lysine. It would then correspond to a double cleavage at both the C-terminal side of tryptophan and the N-terminal side of the arginine, requiring residue 5 to be one of the five possibilities above that produce cleavage with α-chymotrypsin.

Attempts were made to determine the sequences at the C- and N-terminal ends of the peptide using the enzymes carboxypeptidase Y and leucine aminopeptidase, but these were unsuccessful. Some correlation measurements were carried out to look for daughter ions from metastable decay; they confirmed some of the previous assignments but did not yield new information. Thus at the workshop we reported the partial sequence:

-*(Trp/Tyr/Phe/Leu/Met)*$_5$-Arg$_6$-**Arg$_7$-Ile$_8$-Arg$_9$-Pro$_{10}$-Lys$_{11}$-**

Leu$_{12}$-Lys$_{13}$-Trp$_{14}$-*Ala*$_{15}$-

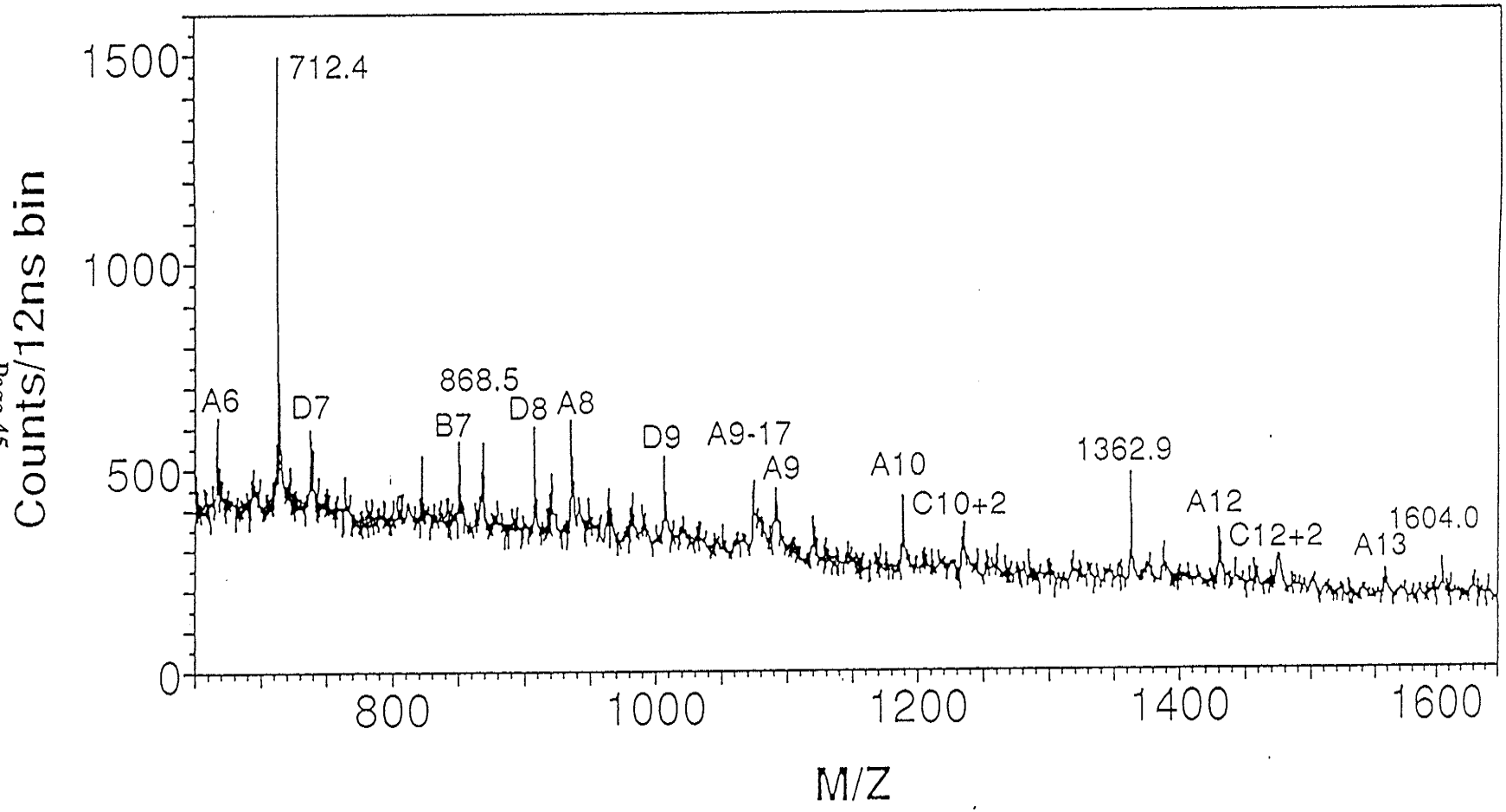

Fig. 2.5 Mass spectrum of the "unknown" peptide after digestion with trypsin: 1 µL (about 100 pmol)"unknown" solution, about 1 hr measurement.

where again the assignments believed reasonably reliable are shown in boldface type, plain type indicates those less certain, and italics indicate the most uncertain.

2.2.3.4 The Workshop

At the workshop the organizer (D.Hunt) announced that the "unknown" peptide was dynorphin 1-17 (Dynorphin A) with a monoisotopic mass for the $[M+H]^+$ ion of 2147.20 u. This compound has the sequence:

Tyr_1-Gly_2-Gly_3-Phe_4-Leu_5-Arg_6-Arg_7-Ile_8-Arg_9-

-Pro_{10}-Lys_{11}-Leu_{12}-Lys_{13}-Trp_{14}-Asp_{15}-Asn_{16}-Gln_{17}

Our mass measurement therefore was correct, as were the "reliable" assignments for residues 7-14 indicated above. The tentative assignment of residue 6 was also correct, and the correct assignment of residue 5 was one of the alternatives proposed above. The tentative assignment of alanine as residue 15 was wrong. It appears that the prominent ion identified as A_{15} in figure 2.4 was in fact D_{15} and we were misled by the accidental coincidence between their mass values. We were aware of this possibility but clearly did not give it sufficient weight.

2.2.3.5 Subsequent Measurements - C terminal end

As shown above, we were able to define about half the peptide sequence correctly by the time of the workshop, but the other half remained undetermined. More recently, in order to investigate whether the technique used was capable of doing better, given more time and more experience with enzymatic digestions, we carried out some additional measurements on the compound. A second 1.5 μg sample was obtained from the organizers and a much larger sample (1 mg) of Dynorphin A was purchased (Bachem Inc., Torrance,

CA).

Clearly the most straightforward method of defining the C-terminal end of the sequence is a carboxypeptidase digestion. As remarked above, our earlier attempts to do this were unsuccessful. However, we repeated the digestion with more careful control of the experimental procedures (and a new lot of carboxypeptidase Y); this gave the spectrum shown in figure 2.6. Here two prominent cleavages appear. The upper one defines the C-terminal residue as (Gly+Ala)/Lys/Gln and the lower one is a cleavage at the C-terminal side of the previously assigned tryptophan. Similar results were obtained with carboxypeptidase P.

There are six possible combinations of common residues that correspond to the measured mass difference of 229 u between the cleavages; two include the previously suggested alanine. Several attempts were made to produce another cleavage in this interval by varying the conditions of the digestion, but without success. The six residue combinations give a large number of possible permutations, but only nine of these are consistent with the observed major ion in the interval (as A_{15} or D_{15}). Calculations were made of the ion masses that might normally be expected to appear in the spectrum of figure 2.4 (A, B, C+2 and D ions) for each of the nine permutations, and compared with the small peaks in that spectrum. A perfect score was obtained only for the sequence Asp-Asn, and no more than 60% of the spectrum peaks matched the calculated peaks for any of the other eight permutations. For this sequence the major peak (A_{15} of figure 2.4) is of course D_{15}. Attempts were made to produce a cleavage at aspartic acid with the enzyme V-8 protease, but without success.

In order to define the C-terminal residue and perhaps obtain further sequence information, the peptide was acetylated (with methanol and water as solvents -- see Appendix 2.3). The reflected spectrum after the reaction (methanol present) is shown in figure 2.7. Many sharp peaks are observed, confirming the sequence presented at the workshop, in particular the lysine residues. The absence of an extra acetyl addition at residue 17 rules out lysine in that position. The peak at 14 u higher than $[M+H]^+$ of triacetylated Dynorphin A is ascribed to partial methylation of the C-terminal carboxyl group. The small peak 28 u higher than $[M+H]^+$ is consistent with a second methylation at the aspartic acid residue proposed above.

Prominent features of the spectrum are the peaks labelled $C_{15} + 17$ and $C_{16} + 17$;

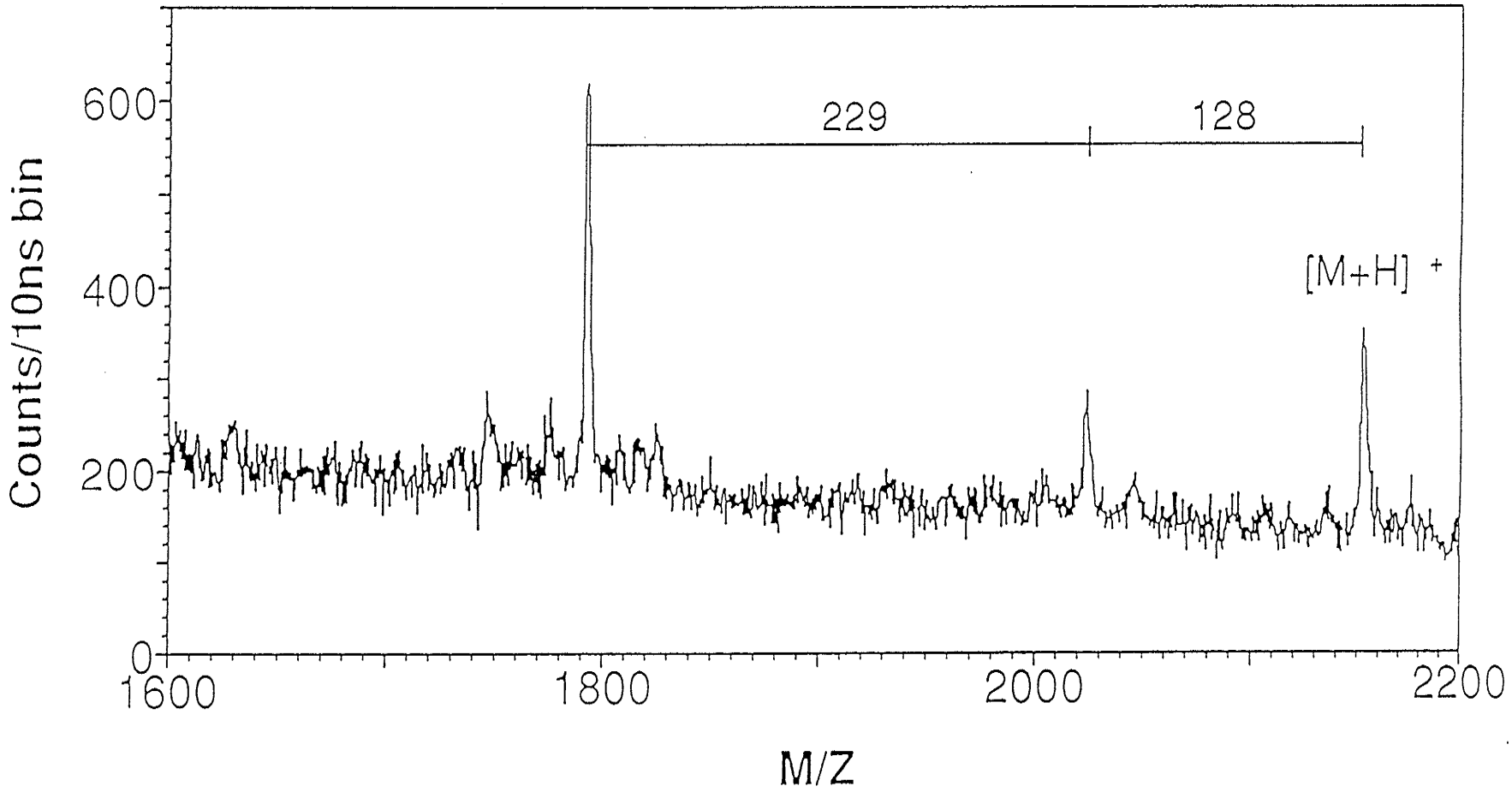

Fig. 2.6 Mass spectrum of Dynorphin A after digestion with carboxypeptidase
Y: about 0.5 µg (250 pmol) Dynorphin A, about 1.8 hr measurement.

no corresponding features are observed in the spectrum with methanol absent. Their masses differ by 114 u, the mass of the asparagine residue, so they offer support to the sequence Asp-Asn proposed above. At present we can only speculate as to their mode of formation. One possibility is that, during the acetylation in methanol, methanolysis has occurred at the C-terminal side of the aspartic acid and asparagine residues, as suggested by the early weak acid hydrolysis experiments of Partridge and Davis [Partidge '50]. A second possibility is a mass spectral rearrangement at the C-terminus of the $[M+H]^+$ ion of the methylated peptide, analogous to the one previously observed in cationized peptides [Grese '89, Tang '88a]. We plan to investigate the question.

2.2.3.6 Subsequent Measurements - N terminal end

Attempts were again made to define the sequence at the N-terminal end of the peptide by digestion on and off the target with leucine aminopeptidase and leucine aminopeptidase M, but again without success, suggesting that the N-terminus might be blocked; (we have more recently been informed that on-target digestions with these enzymes may require several days of incubation [Woods].)

This result suggested that chemical modification of the N-terminus be attempted; failure would provide further evidence for blocking. Moreover, the same strategy is appropriate if the N-terminus is not blocked, since obviously much of the difficulty in obtaining ions that characterize the N-terminal region is caused by the presence of the five basic residues in the interior of the sample molecule. As Vath and Biemann have pointed out [Vath '90], a possible solution to this kind of problem is addition of a quaternary ammonium ion to the N-terminus in order to place a fixed positive charge at that location; a slightly modified version of their procedure was adopted. The reaction was first carried out directly on a target, with unsatisfactory results; the reagents apparently attacked the nitrocellulose substrate. The procedure was then repeated on a glass slide and the product transferred (Appendix 2.3). The resulting target yielded spectra in which most of the N-terminal fragments expected from the correct sequence could be identified (with addition of 99 u): A_6, D_6, A_5, D_5, A_4, A_3, $(C_2 + 2)$? and A_1. This tells us that the N-terminus was not previously blocked. Ions defining the division between the two glycines are absent (with the possible exception of $C_2 + 2$), so asparagine is an alternative assignment.

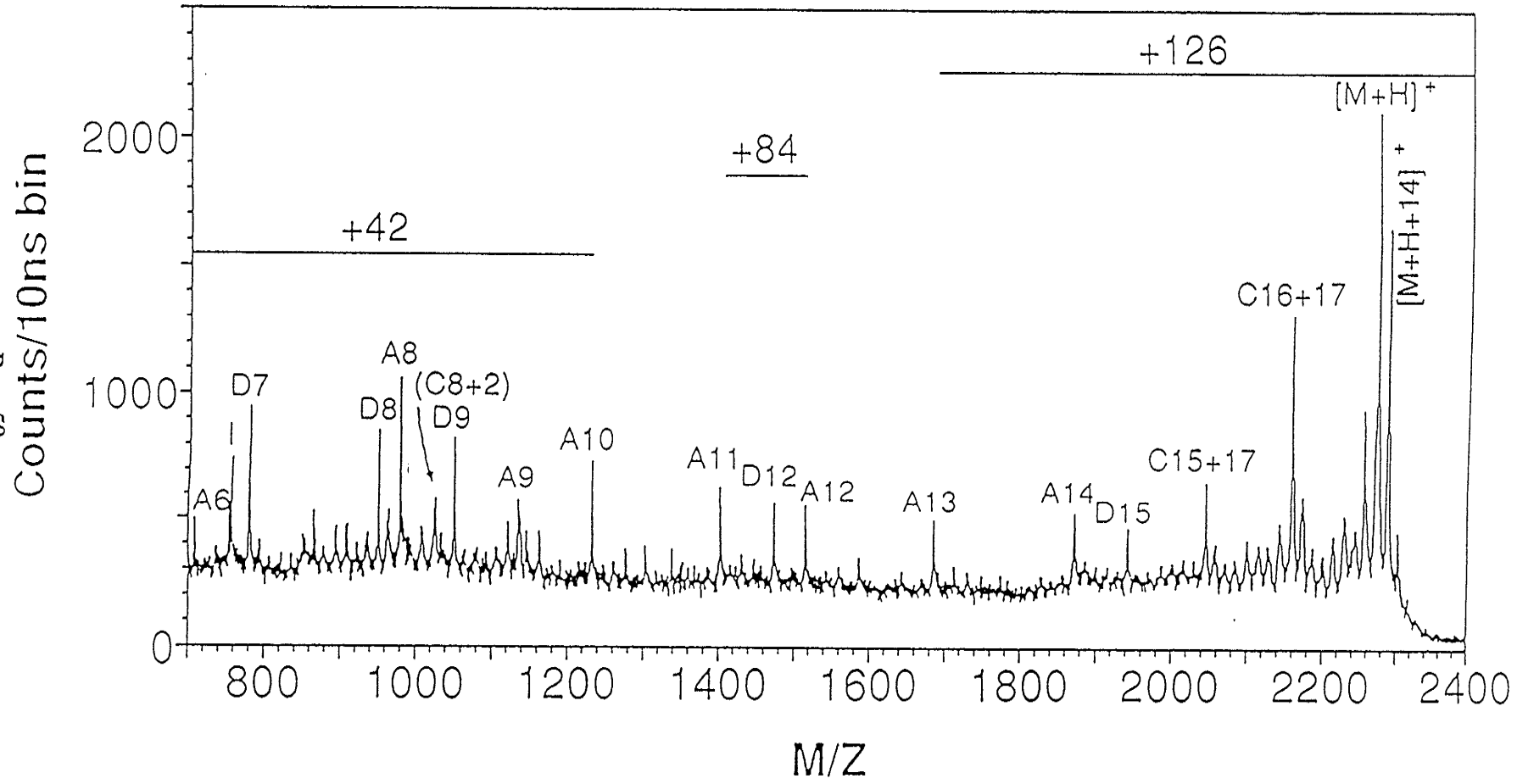

Fig.2.7 Mass spectrum of Dynorphin A after acetylation (methanol present): about 1.4 µg Dynorphin A, 0.5 hr measurement. The numbers at the top correspond to addition of one, two, or three acetyl groups to the indicated ions.

However, many peptides are reluctant to cleave at glycine in any case [Vath '90], and asparagine should produce a corresponding D ion, which is not observed, so the sequence Gly-Gly is favored. The presence of D_6 and D_5 and the absence of the other D ions are consistent with the correct sequence. Thus the measurements define the following sequence with some remaining uncertainty:

Tyr-(Gly-Gly)/Asn-Phe-Leu-Arg-

A number of prominent peaks were observed in the low mass region in addition to those mentioned above. Most were known impurity peaks (from nitrocellulose, etc.) but there were a few that could not be identified. However, it turned out that in this case none of the unknown peaks could be fitted into a sequence consisting of the common amino acid residues and with an unblocked N-terminus, whereas the above sequence is well accounted for, so the assignment can be made with reasonable confidence.

2.2.4 DISCUSSION

As the N-terminus of the sample peptide was in fact not blocked, it could be analyzed by Edman degradation, so that method would normally be preferred. On the other hand, the same peptide with the addition of a blocking group at the N-terminus (or other modifications) cannot be handled by the Edman method, whereas our mass spectrometric analysis would probably yield results similar to the present ones. There might, however, be some difficulty in the final step described above (derivatization at the N-terminus), depending on the nature of the blocking group.

A similar compound that would indeed cause difficulties for the Edman degradation is dynorphin A with p-benzoylphenylalanine replacing isoleucine in position 8. This peptide has in fact been examined by Chowdhury and Chait using a sample of 1 nmol and fission fragment bombardment [Chowdhury '89]. Their measurements were made with a linear time-of-flight spectrometer, so the resolution is lower, but apart from that and the significant absence of D_8 ions, their spectrum is very similar to ours in figure 2.4, consistent

with the previously reported similarity between the results of keV and MeV bombardment in this mass range [Ens '88].

For comparison with FAB, Dynorphin A was submitted to our Chemistry Department service laboratory. Rather large amounts of the peptide were used to prepare two targets (~0.25 mg and ~0.5 mg), which were examined in a VG 7070E-HF mass spectrometer (accelerating voltage 6 kV, 8 keV Xe atom bombardment, matrix ~80% glycerol + ~15% thioglycerol + ~5% trifluoroacetic acid). With wide slits a clear $[M+H]^+$ peak (isotopes unresolved) was observed together with a few of the expected fragment ions. However, even with this much sample it seems doubtful that much sequence information could be derived from a true unknown. Measurements on various dynorphins and other endorphins using LSIMS and CAD on a four-sector instrument with an array detector and unlimited sample amounts, produced no extended coherent fragment series. Results using low energy CAD of multiply-charged peptides produced by ES were similar (§1.1.3) [Curtis '93].

On the basis of the original measurements and those subsequent to the workshop, the sequence of the sample peptide can be defined as:

$$Tyr_1\text{-}(Gly_2\text{-}Gly_3)/Asn\text{-}Phe_4\text{-}\mathbf{Leu_5\text{-}Arg_6\text{-}Arg_7\text{-}Ile_8}\text{-}$$
$$\text{-}\mathbf{Arg_9\text{-}Pro_{10}\text{-}Lys_{11}\text{-}Leu_{12}\text{-}Lys_{13}\text{-}Trp_{14}}\text{-}Asp_{15}\text{-}Asn_{16}\text{-}Gln/(Gly+Ala)_{17}$$

There is no evidence for division within residue 17, so the (Gly+Ala) alternative is given less weight, but we have left it as a possible alternative because of the previously mentioned reluctance to cleave at glycine. The sequence is determined correctly within the uncertainties indicated.

As mentioned above, about 3/4 of the sample had been consumed at the time of the workshops, although much of this was used in unproductive experiments. The useful results obtained subsequently (carboxypeptidase digestion, acetylation and N-terminal derivatization) consumed considerably more sample than this remainder (see Appendix 2.3), but largely for the sake of experimental convenience. Thus it seems possible that the above result could have been obtained with the original sample provided an appropriate strategy had been followed. The ideal strategy depends on the particular peptide being examined, so a certain amount of trial and error is inevitable. However, we believe that we

could have carried out the operations in a more intelligent way with more experience. In particular, acetylation and N-terminal derivatization could have been applied at a much earlier stage of the analysis.

If the sample had been presented as one component of a mixture, the problem would have been more difficult. Separation by liquid chromatography or perhaps capillary electrophoresis is certainly a possibility, but might involve significant losses of material. The alternative is analysis by tandem mass spectrometry without separation. In our case similar information can be obtained by correlated measurements on the products of unimolecular decay in the flight tube.

As our method is almost non-destructive, some targets can be used for two purposes, e.g. an ordinary spectrum followed by one or more enzymatic digestions. On the other hand, it is considerably slower than some competing techniques; note the measurement times in the figure captions. At the time the factor limiting our analysis speed was the data processing capability of the computer (Atari ST, based on a 68000 chip running at 8 MHz) [Ens '89]. The speed has since been improved by a significant factor by substituting the faster Atari TT computer (based on a 68030 chip running at 8 MHz) (§1.4.3) [Poppe-Schriemer].

2.2.5 CONCLUSION

TOF SIMS and enzymatic digestions were used to sequence Dynorphin A as an unknown peptide with good results. Other mass spectrometric methods encountered difficulties.

2.3 SEQUENCING SEVERAL ALAMETHICIN PEPTIDES BY THE TIME-OF-FLIGHT CORRELATION TECHNIQUE

2.3.1 INTRODUCTION

The alamethicins, produced by the fungus *Trichoderma viride*, are members of the peptaibol class of peptides, which comprises linear, amphiphilic, antibiotic polypeptides (~2000 u) with acetylated N-termini and amino alcohols at the C-termini. The peptaibols contain many α-aminoisobutyric acid (Aib) residues and may contain some isovaline (Iva) residues [Bruckner '84]. Because they are all produced enzymatically (not from an RNA template), amino acid interchanges occur, resulting in whole families of closely-related peptides.

The alamethicins are widely used to model voltage-gated ion channels because, when incorporated into bilayer lipid membranes [Cafiso '94, Tien '74] (*i.e.* membranes consisting of two monolayers (see §3.2), with the hydrophilic sides facing each other), they induce a conductance that increases with increasing applied voltage [Eisenberg '73]. This behavior is apparently a result of the formation of pores with five discrete voltage-dependent conductance levels [Eisenberg '73] in the membrane. Determination of the sequence of the peptides involved is a first step in understanding the formation and structure of these pores.

Because the compounds are so similar, it is very difficult to separate them completely by HPLC [Iida '90]; in fact samples pure enough to crystallize may not be homogenous [Bruckner '84, Fujita '84]. Even if a sample consists of only one peptide, the nature of the peptaibols renders sequencing quite difficult [*eg.* Iida '90]. As mentioned above, the N-terminus is acetylated, so the Edman degradation cannot be used for determining the sequence of amino acids in the peptide, and the C-terminus is an alcohol ($-CH_2OH$), ruling out the use of degradations from that end of the peptide. Additional problems are the resistance of the compounds to proteolytic digestion, and the unusual amino acids, namely

Aib and perhaps Iva, that are present. For this reason, mass spectrometry (field desorption, electron impact, and plasma desorption mass spectrometry (PDMS)) has played an important role in determining the primary structure of these compounds [Chait '82, Pandey '77, Rinehart '77]. Other techniques have also contributed [Balasubramanian '81, Martin '76] and additional information has been provided by gas phase chromatography / mass spectrometry of a hydrolysate of alamethicins [Konig '80]. Tandem mass spectrometry has been applied to other peptaibols, the trichosporin compounds [Iida '90], for example, but not to the alamethicins themselves.

The amino acid sequences of the two main alamethicin components (I and II) grown under standard (Upjohn) conditions [Upjohn '66] (Fig. 2.8b) are known. The sequence of alamethicin I is [Pandey '77a, '77b]:

$Ac\text{-}Aib_1\text{-}Pro_2\text{-}Aib_3\text{-}Ala_4\text{-}Aib_5\text{-}Ala_6\text{-}Gln_7\text{-}Aib_8\text{-}Val_9\text{-}Aib_{10}\text{-}$

$Gly_{11}\text{-}Leu_{12}\text{-}Aib_{13}\text{-}Pro_{14}\text{-}Val_{15}\text{-}Aib_{16}\text{-}Aib_{17}\text{-}Glu_{18}\text{-}Gln_{19}\text{-}Phe_{20}\text{-}ol.$

Alamethicin II differs from this only by the replacement of Ala by Aib in position 6 [Pandey '77, Rinehart '77]. As well, the GC/MS study indicated that Aib-Ala interchanges may occur at residues 4, 5, and 6, and that Aib-Val interchanges may occur at residues 9, 16, and 17 [Konig '80]. Several different families of fungal antibiotics that are very similar to the alamethicins have also been analyzed by mass spectrometry [*eg.* Iida '90, Bruckner '84, Fujita '84, Przybylski '84], with similar results.

However, even mass spectrometric sequencing is not trivial. Most peptaibols contain at least one Aib-Pro bond (usually between positions 13 and 14), which is very easily fragmented in FAB MS [Iida '90, Przybylski '84]. Fragmentation in CAD also occurs preferentially at Pro [Loo '93]. As a result, the mass spectrum is very complicated, with most spectral peaks in the low mass region; generally two or three acylium ion series are present. It turns out to be relatively simple to sequence the first 13 or so residues, but the remainder of the peptide, from the $Aib_{13}\text{-}Pro_{14}$ bond to the C-terminus, is significantly more difficult.

It has been noted that "...chemical treatment, such as partial hydrolysis, or NMR measurements must be performed in order to confirm the peptide sequences" [Iida '90].

One method used involves acid hydrolysis of the Aib-Pro bond. When the resulting hydrolysis mixture is examined by FAB using a glycerol matrix, the prolylheptapeptaibol product gives the most abundant peak, and its sequence specific fragment ion peaks are also abundant, allowing the remainder of the peptide to be determined [Przybylski '84].

The amount of each alamethicin peptide produced by the fungus is sensitive to the environment in which the fungus is grown [Brewer '87]. A method for preparing the alamethicins [Brewer '87] differing from the standard (Upjohn) one has recently been applied in one of our laboratories for preparing the alamethicins [Yee '92]. HPLC of the resultant peptide mixture exhibits an abundant component (denoted by III in Fig. 2.8a) not prominent in the standard preparation, as well as some others. These other components include the two main peaks produced by the standard preparation, but there also appear to be additional compounds, as yet uncharacterized.

Our results indicate that some of the chromatographic peaks consist of more than one component, so the situation is quite complicated. Since the chromatogram contains so many peaks, it is difficult to determine which of these are due to coeluting peptides using only HPLC. (In the case of the peptaibols, the amino acid exchanges can affect peptide properties so subtly that separation of different components is not trivial, although HPLC is often successful [Bruckner '84, Fujita '84]. A similar situation involving other closely-related peaks has been reported [Chou '94].) Mass spectrometry can not only distinguish the different peptides in an HPLC fraction but can also give their molecular weights.

From studies of other peptaibols, it is expected that the structure of the major component, which we call alamethicin III, is similar to those of the two known components, I and II, whose chromatogram is shown in Fig. 2.8. It has been examined by Yee and O'Neil using NMR spectrometry [Yee '92]. Their results are consistent with the same sequence as for alamethicin I above, except for the substitution of Gln for Glu at position 18. However, the NMR measurement required 1 μmole (2 mg) of sample, and insufficient material was available to make NMR measurements on the less abundant components.

In this work, we determine several alamethicin sequences without chemical treatments or NMR (except for Leu/Ile and Val/Iva differentiation). We describe the detailed sequence verification of the new abundant component, alamethicin III, using the correlation method described previously (§1.2.4.3). Some results on the other alamethicins are also reported. Noteworthy features of the alamethicin mass spectra will be compared to the results

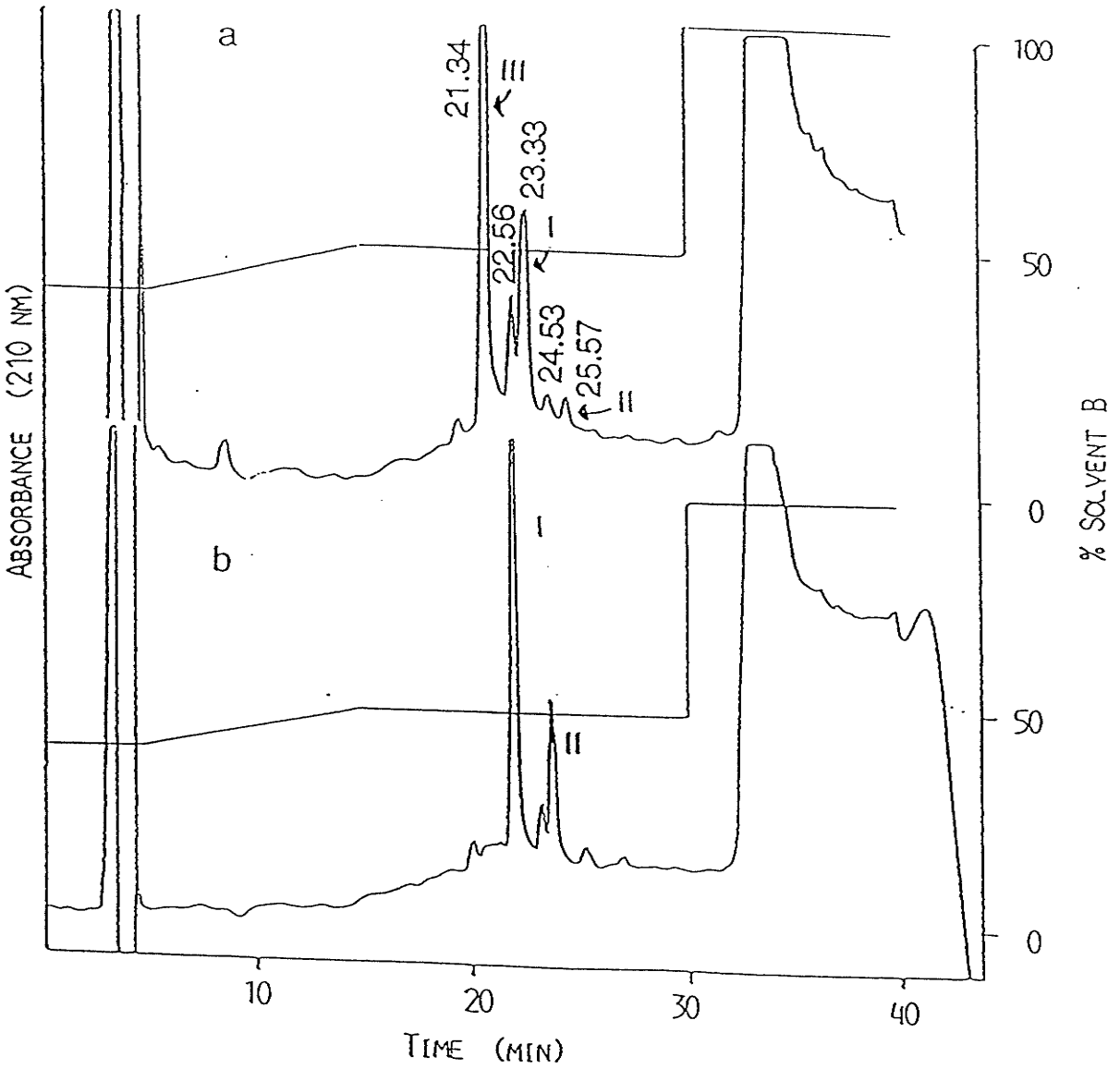

Fig. 2.8 HPLC of crude alamethicin preparations. a) Yee and O'Neil preparation [Yee '92] used here. (Peak elution times are given in minutes), b) The standard alamethicin preparation (Upjohn method [Upjohn '66]).

Samples of 100-500 µL were loaded onto a Beckman Spherisorb 5 µm C-18 reverse-phase column (10 mm i.d., 150 mm length). Solvent A is 0.05 N acetic acid adjusted to pH 3.5 with triethylamine. Solvent B is tetrahydrofuran/acetonitrile/solvent A (8:2:1). Isocratic elution (40% solvent B) at 1 mL/min for 5 min, was followed by a gradient elution at 1.5 mL/min for 10 min to 49% solvent B, then by isocratic elution at 1 mL/min for 15 min, and finally by elution at 1mL/min for 10 min at 100% solvent B [Yee '92]. (Note that the elution times differ slightly for the two chromatograms.)

obtained by other investigators for closely related peptide antibiotics.

Our previous investigations of peptide ions which undergo decay, using this correlation method [Tang '91, '89, '88, Standing '90a, '90b, '90c], dealt with fairly simple cases, where the decays of only a few parent ions were examined. However, we believe that the real strength of the technique lies in its ability to examine the decays of many parent ions at the same time, and thus to examine a given daughter ion produced by several different parents; this provides additional confidence in the deduced structure. In addition, it may be of some interest to obtain the metastable decay pattern of a whole series of similar ion types, such as the series of prompt alamethicin III fragment ions observed here, corresponding to successive deletions of a single amino acid residue. Because most of the prompt fragment ions of the alamethicins show metastable decay and because many of the HPLC fractions contain more than one peptide, the present work serves as a test of the utility of the technique in a fairly complicated case. Moreover, the conclusions can be tested by comparison with the result of the NMR measurement mentioned above and with mass spectral results for closely related peptaibols.

2.3.2 EXPERIMENTAL

Alamethicin III was separated from the crude alamethicin mixture by reverse phase HPLC, as described in the caption to Fig. 2.8. A fraction collected from the central part of the largest peak (21.34 min, denoted by III, in Fig. 2.8a) was recrystallized to remove impurities, then dissolved in 0.1% trifluoroacetic acid, and deposited onto electrosprayed nitrocellulose. An estimated 5 nmol were deposited on each target used; the collected fraction yielded sufficient material after recrystallization that no particular effort was necessary to conserve sample. This rather large amount was used for convenience; previous measurements have shown that complete sequence information can be obtained with our technique on 200 femtomoles of peptide [Tang '91, '91a, '90]. The other HPLC fractions examined were treated as alamethicin III, except that they were not recrystallized; details are given in Appendix 2.4.

The amounts of the alamethicins used were estimated visually (when they could be seen) and an attempt was made to use a concentration of ~1 mg alamethicin / ml of .1%

TFA (see Appendix 2.4). Since the peptides were so insoluble, ultrasonic agitation often had to be used to dissolve them. At times there would still be a precipitate, but the solution above it contained enough peptide for TOF SIMS correlation experiments. An ammonia impurity was present in the fractions which were not recrystallized. However, a comparison of the major component with and without recrystallization showed that this impurity did not seem to affect the spectra at all.

The measurements were carried out on our reflecting TOF mass spectrometer, TOF II (§1.4). Secondary ions were formed by bombardment of the solid sample target by I^- primary ions at 25 keV [Zhou '93, in prep]. (The I^- ions were produced with an energy of 15 keV and then accelerated to an energy of 25 keV at the target by the secondary ion accelerating voltage (+10 kV) for positive ion spectra. In the few cases where negative ions were examined, the incident I^- ions were slowed to an energy of 5 keV by the -10 kV accelerating voltage.) The secondary ions were then accelerated to 10 keV and they, or their decay products, were detected at the appropriate detectors, as explained in §1.2. A few MALDI measurements were also performed.

Ion bombardment produces a variety of charged molecules and fragment ions from the peptide at (or very near) the surface of the solid target. We shall refer to these fragments as "prompt" fragment ions. Both molecular ions and prompt fragment ions are accelerated to an energy of 10 keV and they (or their decay products, called "metastable" daughter ions or neutral daughters) are detected either at the end of the flight tube or after reflection in the mirror.

2.3.3 RESULTS

2.3.3.1 Molecular weight

Many secondary ions from alamethicin III, including the $[M+H]^+$ ions, were found to undergo an unusual amount of decomposition along the flight path. This facilitated the correlation measurements, described later, but made it difficult to extract much information from the reflected spectrum, which is usually used to obtain the molecular weight. In the molecular ion region (Fig. 2.9) the $[M+H]^+$ ion peak is barely visible at ~1963.1 u. Fortunately, the $[M+Na]^+$ ions are more stable and give a prominent peak; the principal

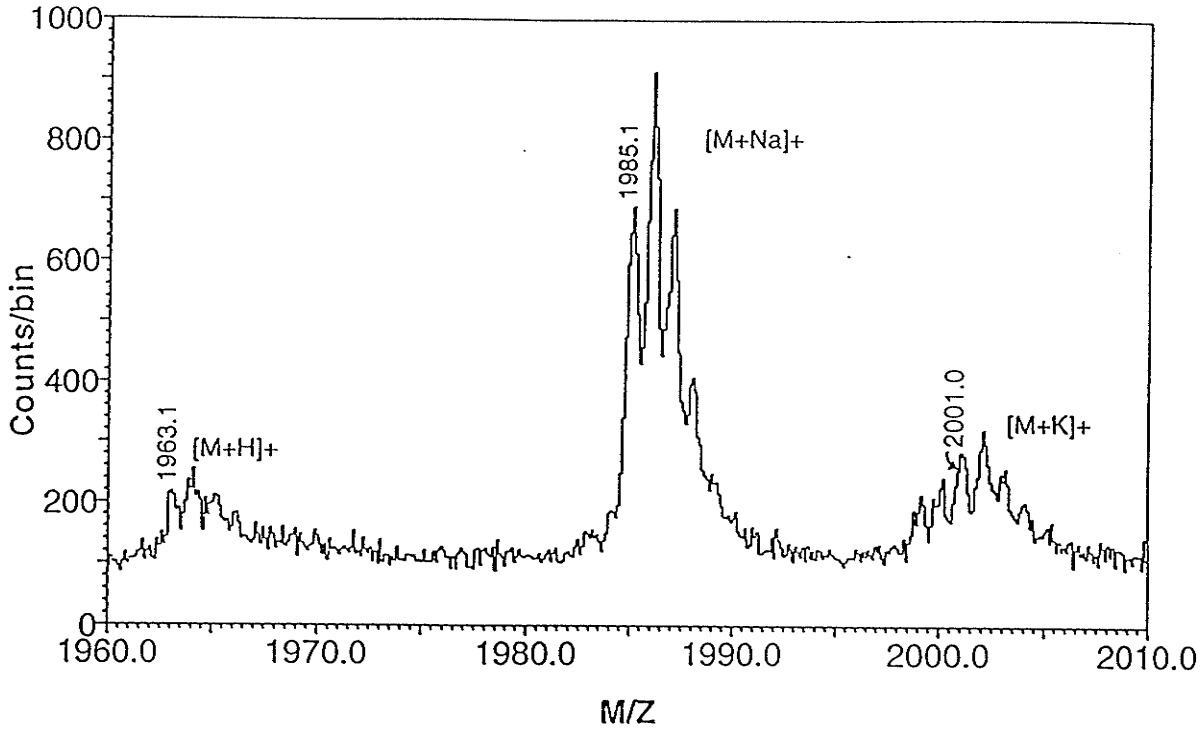

Fig. 2.9 The molecular ion region of a reflected spectrum of alamethicin III. The principal mass of $(M+Na)^+$ was measured to be 1985.1 u on the basis of a calibration with the H^+ and $C_3H_3^+$ ions, which has been found to give masses accurate to ~0.1 u for peptides as large as 2000 u in previous measurements [Tang '91]. A calibration using H^+ and $[Substance\ P+H]^+$ gave identical results. The small cluster of peaks at 2001 u corresponds to $[M+K]^+$.

The $[M+Na]^+$ peak at 1986.1 u is larger than expected, consistent with the presence of an impurity of that mass, probably alamethicin I. The peaks at 1999 u, interfering with the $[M+K]^+$ peaks, suggest the presence of another impurity. Rechromatographing the sample under the conditions previously used showed that it did, in fact, contain two impurities, consistent with this interpretation.

mass is measured as 1985.1 u on the basis of a calibration with the H^+ and $C_3H_3^+$ ions, which has been found to give masses accurate to ~0.1 u for peptides as large as 2000 u in our previous measurements [Tang '91]. A calibration using H^+ and [Substance P + H]$^+$ gave identical results.

The [M+Na]$^+$ assignment was confirmed by observation of the [M-H]$^-$ ion in the negative ion spectrum. A calibration on H^- and C_2H^- gave a principal mass of 1961.3 u for [M-H]$^-$ and 2089.3 u for [M+I]$^-$. In a calibration run with renin substrate there were no molecular ions, and in one with substance P, the substance P molecular ion was suppressed. Because the H^- and C_2H^- calibration had not been examined extensively to verify its accuracy, the mass value was not as reliable as in the positive mode.

Because the peak for the protonated molecule is so small, MALDI was also used as a desorption/ionization method to verify the mass. The positive ion spectra were calibrated using LHRH and insulin and the calibration itself was verified on substance P and melittin. In this case also, the alamethicin peak was mainly a [M+Na]$^+$ ion, and [M+K]$^+$ ions were present as well. The [M+H]$^+$ alamethicin peak was very small or nonexistent while the calibration peaks corresponded to [M+H]$^+$ ions; no other [M+Na]$^+$ peaks were evident [compare Chait '82]. The principal mass obtained was 1985.4 u in one case and, in another case with worse resolution, the chemical mass was 1986.5 u. In the negative mode, this mixture produced only the alamethicin peak, which was highly unusual in MALDI, and no calibration was possible.

The measured mass of the peptide is then 1962.1 u, *i.e.* 1.0 u less than that of alamethicin I, consistent with the proposed replacement of Gln_{18} for Glu_{18}.

2.3.3.2 Sequence

As mentioned above, a sequence similar to one of the known alamethicins is expected, and the measured molecular weight supports this expectation. Therefore, mass spectral peaks were compared with those expected for alamethicin I on the basis of the fragmentations generally observed for collisionally induced dissociation of peptide [M+H]$^+$ ions produced by FAB. As noted above, a similar positive ion spectrum is produced by SIMS. The fragment ions are denoted in the usual way [Biemann '87, Roepstorf '84], shown in Fig. 2.1 and described in §2.1.3.2. Although Iva occurs in some peptaibols, it does not occur in the known alamethicins and only very rarely in the closely related hypelcins, paracelsins

and trichosporins [Iida '90, Bruckner '84, Fujita '84]. Therefore, it has been assumed to be absent, although for other peptaibols it has been distinguished by variants of NMR spectroscopy.

For the alamethicins it is necessary to examine the direct and correlation spectra to obtain sequence information, because the reflected spectra, which one would usually examine, are too difficult to interpret. This is because of the many "metastable" daughter ions that appear so that in some cases, in fact, prompt fragment ions created at the target and daughter ions created by metastable decay form overlapping peaks (Fig. 2.10) as explained in Appendix 2.5. Unfortunately, a direct spectrum's resolution is never as good as that of a reflected spectrum, due largely to metastable decay of the ions and to the low resolution inherent in the linear TOF configuration. Although the extensive metastable decay rendered the reflected spectrum less useful, it generated an unusually large number of correlation spectra which provide a wealth of sequence information.

2.3.3.2.1 Sequence information from the direct spectrum

The direct spectrum reveals many fragment ions (Fig. 2.11a). The B_n ion series is prominent up to B_{13} (which gives a very large peak) and extends, at low abundance, to B_{19} (excluding B_{18}). The Y_7+2 ion is the only significant C-terminal ion; peaks for both it and Y_{19}+2, which also occurs, are much wider than the nearby peaks. The amino acid residues Aib, Pro, Gln and Leu produce abundant immonium (or iminium) ions. A fairly strong series of internal fragment ions beginning with Pro_2 (assigned as $Y_{19}B_n$+1) and a weaker one beginning with Pro_{14} (assigned as Y_7B_n+1) appear, but often their peaks coincide with expected peaks from other series. Internal fragment ions of the form Y_mB_n+1 are more likely than fragments of the type X_nA_m+1 or Z_nC_m+1 ions. This is evident from their decay, as well as from the decay of B_n ions and of Y_7+2 (see Table 2.1) Many A_n, C_n+2, D_n, Y_m+2 (besides the Y_m+2 ions mentioned above), Z_m, V_m and W_m ions are observed, but they are quite weak and peaks can often not be distinguished from each other. Such fragment ion overlap occurs both because of the many repeated amino acids and because of the low resolution available in the direct spectrum. Unexplained peaks include 426.4 u, which is about as intense as the weak series mentioned above, and the much weaker 454.9 u, 794 u and 1071 u, all of which correspond to many possible internal fragment ions. (It is interesting to note that the first three of these could correspond, with an error somewhat

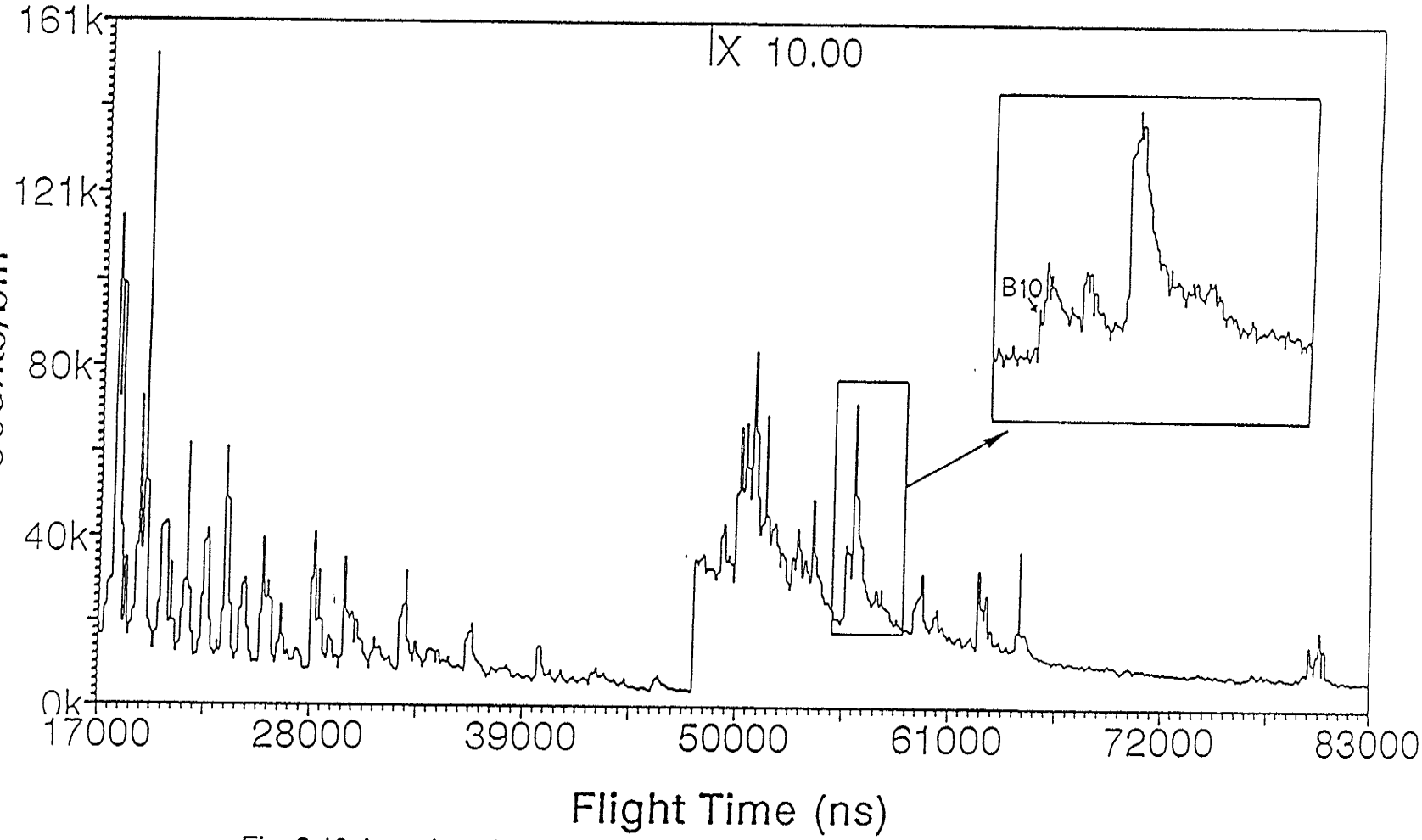

Fig. 2.10 A portion of a reflected spectrum showing near overlap between prompt B_{10} ions and the daughter B_{10} ions arising from metastable decay of heavier ions, such as B_{11},B_{12},B_{13} and $[M+H]^+$. The prompt B_{10} ion is the tiny peak labelled in the insert, and the daughter B_{10} ions appear to its right [Appendix 2.5].

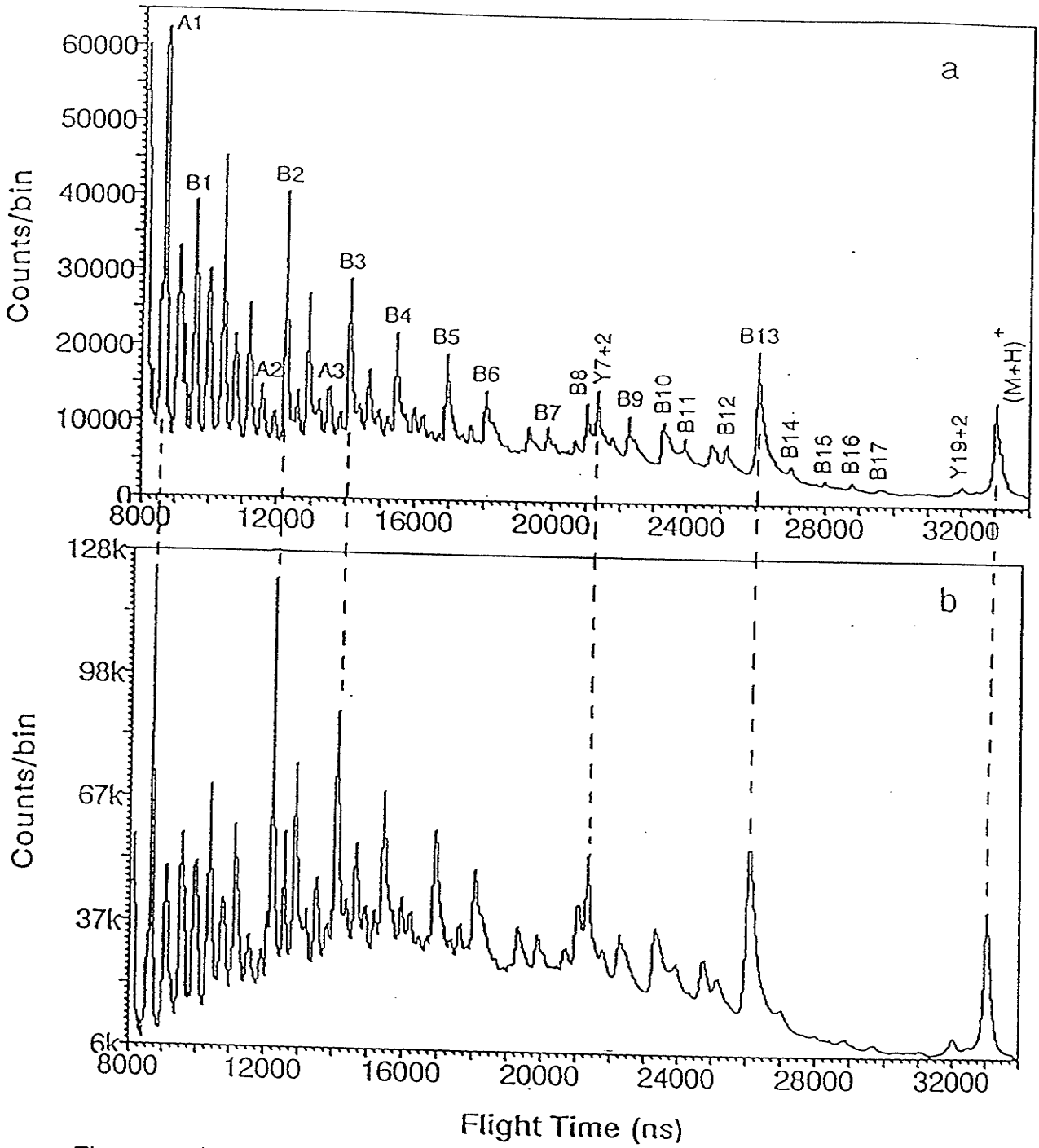

Fig. 2.11 a)"Direct" spectrum of alamethicin III observed in detector 1 with zero voltage on the mirror. The sequence given in equation 1, with Gln_{18} substituted for Glu_{18}, was assumed. b)"Neutral" spectrum of alamethicin III observed in detector 1 when a reflecting voltage was applied to the mirror. (Note that the acquisition times differ for the two spectra.)

larger than expected, to Y_3+Na , X_3+Na, and Y_7+Na. Although the data are far from conclusive, this may indicate that the Na^+ is attracted to the C-terminus. On the other hand, 426.4 u could also relate to $Y_{19}B_6$+1 for an impurity with 14 u extra.)

The masses of the prominent B_n ion series suggests that alamethicin III has the same sequence as alamethicin I up to amino acid 13 within a mass uncertainty that varies from >~0.5 u at low mass to >~2 u at higher mass. However, there could be replacements of Gln by Lys or Glu at position 7, of Val by Pro at position 9, of Ser by Aib at positions 10 and 13, and of Ile by Leu at position 12. The much weaker B_n ion series from B_{14} to the C-terminus is consistent both with the sequence of alamethicin I and with the NMR suggestion mentioned above in which Glu (alamethicin I) or Gln (NMR suggestion) occupy position 18. In this range, the mass uncertainty leads to a possible partial amino acid sequence of -(Val/Pro)$_{14}$ -(Pro/Val/Thr)$_{15}$ -(Ser/Aib)$_{16}$ -(Ser/Aib)$_{17}$ -(Glu/Gln/Lys)$_{18}$ -(Glu/Gln/Lys)$_{19}$- . Of course, the various amino acid interchanges would have to compensate for each other so that the expected mass of subsequent fragments would still be within experimental error.

Other arguments can be applied to reduce the possibilities. Within the experimental uncertainty, the masses of B_{12}, B_{13} and B_{14} permit the alternative sequence (Aib/Ser)$_{13}$-(Pro/Val)$_{14}$. However, it has been shown [*eg.* Iida '90] that the Aib-Pro bond cleaves preferentially under bombardment, so that the prominence of the B_{13} and Y_7+2 ions, and the existence of a set of internal sequence fragments corresponding to cleavage between amino acids 13 and 14, strongly support the assignment Aib$_{13}$-Pro$_{14}$. This is expected from the alamethicin I sequence. (Similarly, another set of internal sequence fragments corresponds to cleavage at the Aib$_1$-Pro$_2$ bond.) Because there is no such cleavage observed between Aib$_8$-(Val/Pro)$_9$, residue 9 is probably Val, as in the alamethicin I sequence. The internal fragment peaks, and the other weaker ion series, are consistent with this sequence but overlap too much with each other to be conclusive. If present, D_n ions can be used to discriminate easily between Aib/Ser and Leu/Ile and often also among Pro/Val/Thr. In most cases the D_n ions overlapped with other expected masses and could not be used to decide between these amino acids. However, Leu$_{12}$ is more likely because it is present in the alamethicin I and II sequences. The characteristic termini of the alamethicins and other peptaibols are consistent with the fragment masses found. However, the N-terminus could be H-(Gln/Lys), formyl-Val, or methyl-(Leu/Ile) as well as Ac-Aib. The most likely

choice is Ac-Aib, both because the acetyl group is characteristic of the peptaibols, and because all the other alamethicins have an Aib residue at the N-terminus.

Thus the sequence resulting from the direct spectrum is:

Ac-Aib$_1$-**Pro$_2$-Aib$_3$-Ala$_4$-Aib$_5$-Ala$_6$**-(Gln/*Lys/Glu*)$_7$-Aib$_8$-Val$_9$

-(Aib/*Ser*)$_{10}$-Gly$_{11}$-(Leu/*Ile*)$_{12}$-Aib$_{13}$-Pro$_{14}$-(Val/*Pro/Thr*)$_{15}$

-(Aib/*Ser*)$_{16}$-(Aib/*Ser*)$_{17}$-(Gln/*Lys/Glu*)$_{18}$-(Gln/*Lys/Glu*)$_{19}$-Phe$_{20}$-ol,

where the bold face type denotes firm assignments, plain type denotes probable assignments, and italic type denotes less certain assignments. (The amino acids in parentheses are either isobaric (*i.e.* Lys/Gln and Leu/Ile) or within the experimental uncertainty.)

2.3.3.2.2 Correlation spectra (metastable decay)

Primary ion bombardment produces a variety of secondary ions at the target, both molecular ions and prompt fragment ions. If the ion survives acceleration but subsequently decays before it enters the mirror, the flight time of the neutral daughter (observed in detector 1) defines the parent ion (§1.2.4.3). The parent ion can itself be the product of the decay of a precursor close to the target. What the neutral spectrum actually measures is the parent ion distribution that exists ~ 100 ns after desorption, as discussed in Appendix 2.6.

On the other hand, the time of arrival of the correlated daughter ion at detector 2 measures the daughter ion spectrum at the entrance to the mirror, *i.e.* ~ 10μs after the desorption event (but only those which do not decay further inside the mirror). Thus the technique measures decays of the parent ion that occur during the time they travel from the acceleration grid to the mirror, ~ 0.5 μs to ~ 10 μs after desorption.

The correlation spectra for the decay of the $[M+H]^+$ ion and many of the prompt fragment ions are summarized in Table 2.1, and representative spectra are shown in Fig. 2.12 to 2.14. The results have been used to verify and to clarify the sequence given above.

The $[M+H]^+$ ion, which decays much more than the $[M+Na]^+$ and $[M+K]^+$ ions, produces mainly B_8, B_9, B_{10}, B_{13} and Y_7+2 ions as well as some weaker B_n ions (n=4-7, 11, 12), internal fragment ions, and C_n+2 ions and a few D_n ions as well as A_8 (Fig. 2.12).

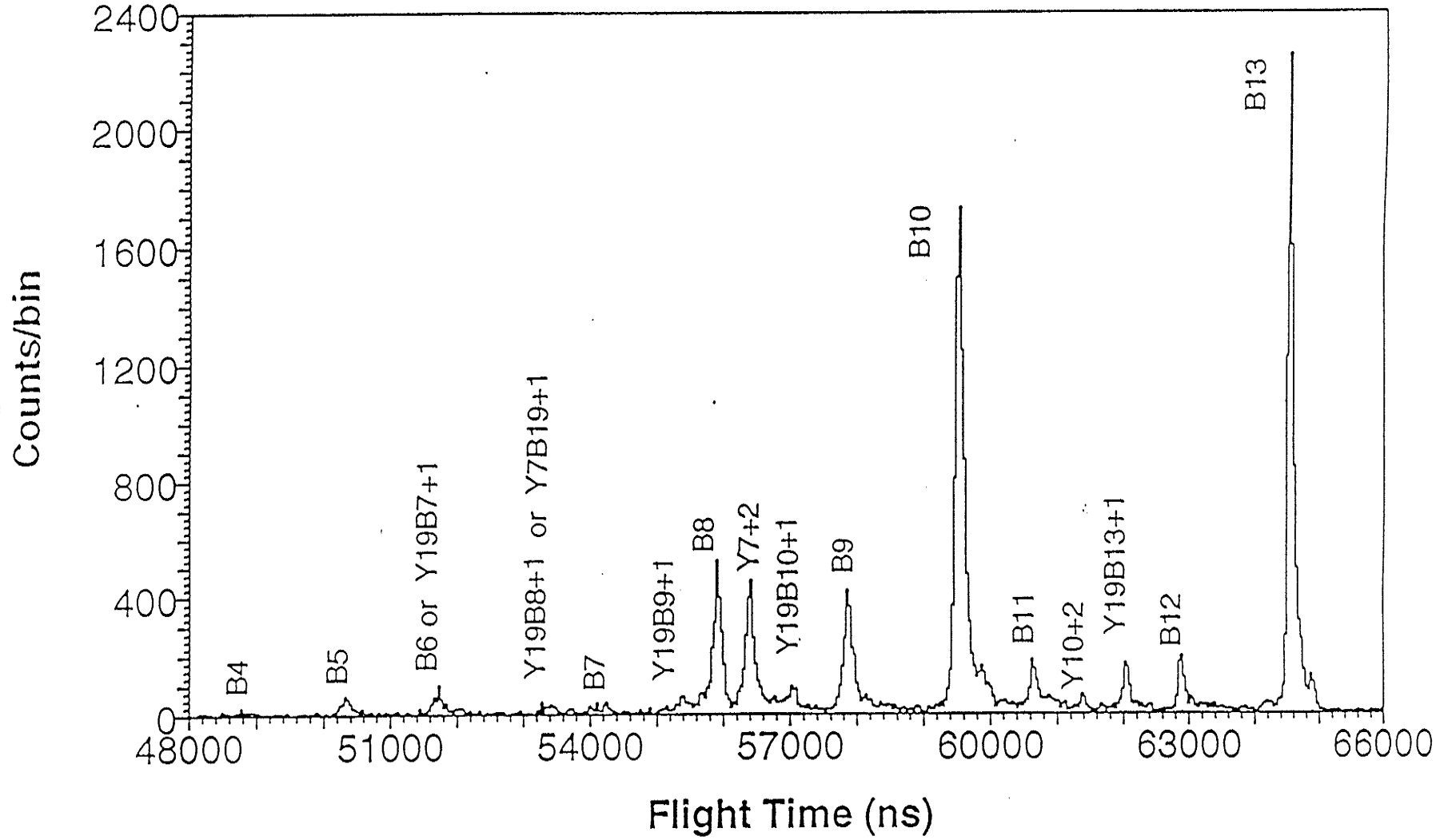

Fig. 2.12 Daughter ion spectrum of $[M+H]^+$ parent ions.

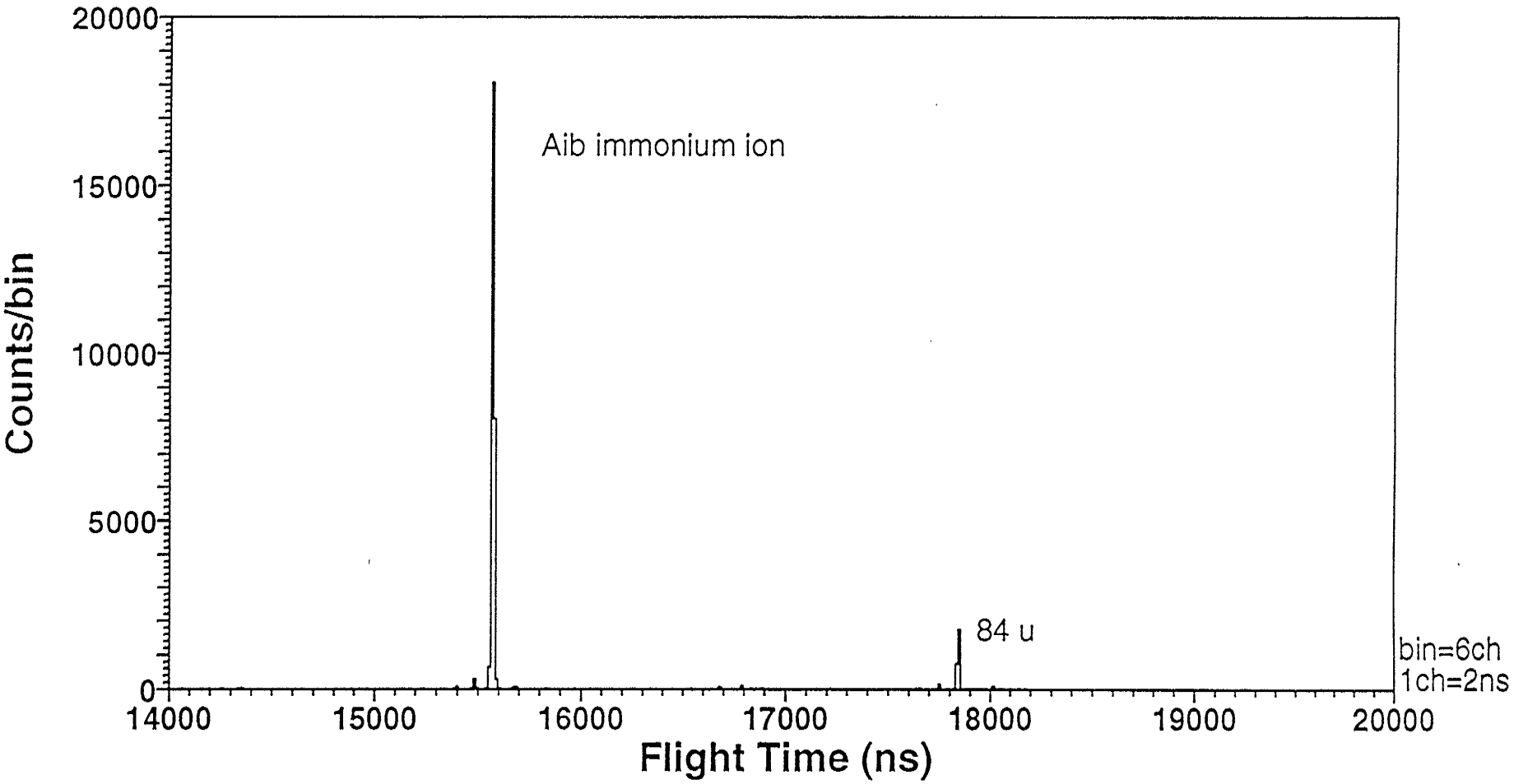

Fig. 2.13a Daughters of A1.

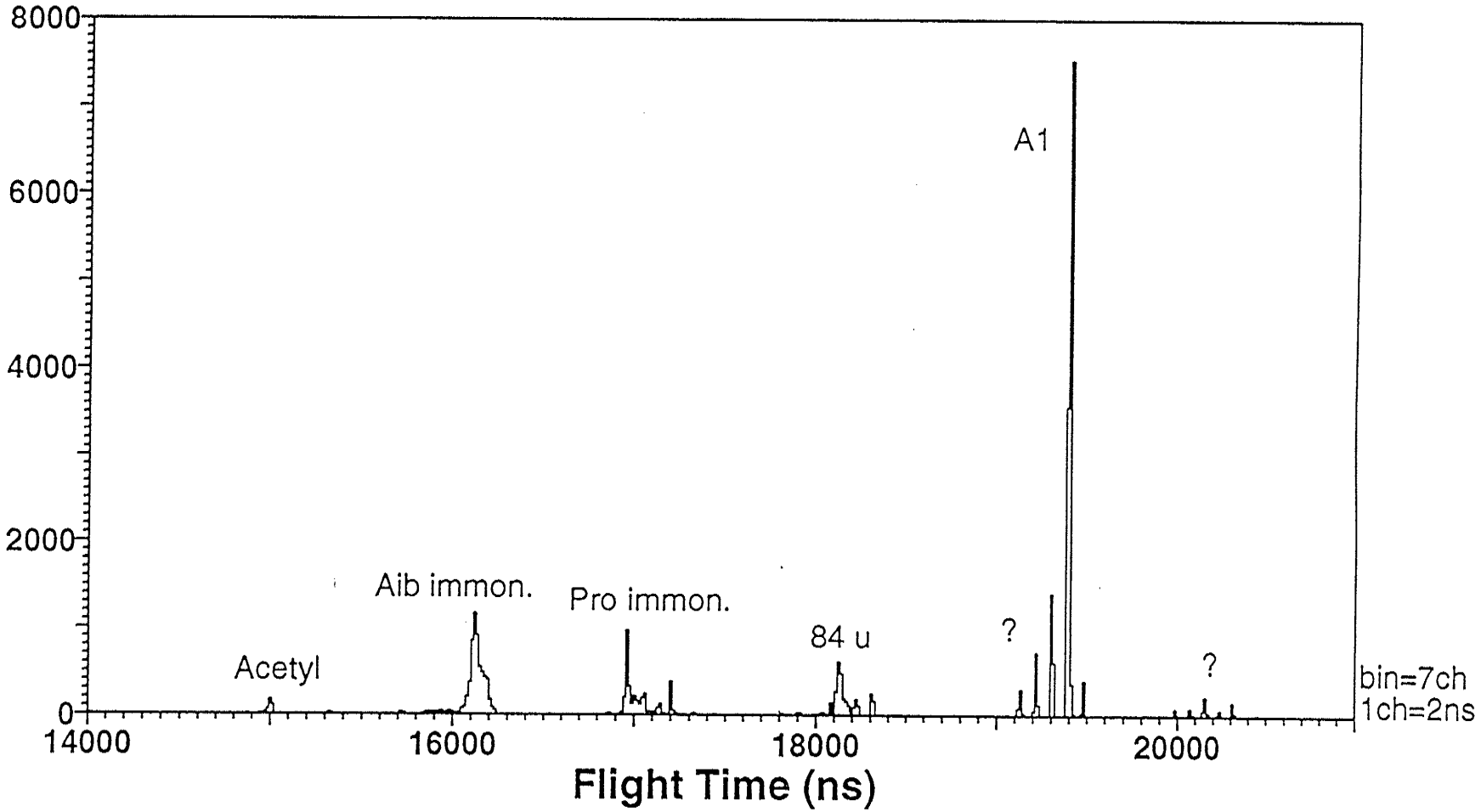

Fig. 2.13b Daughters of B1.

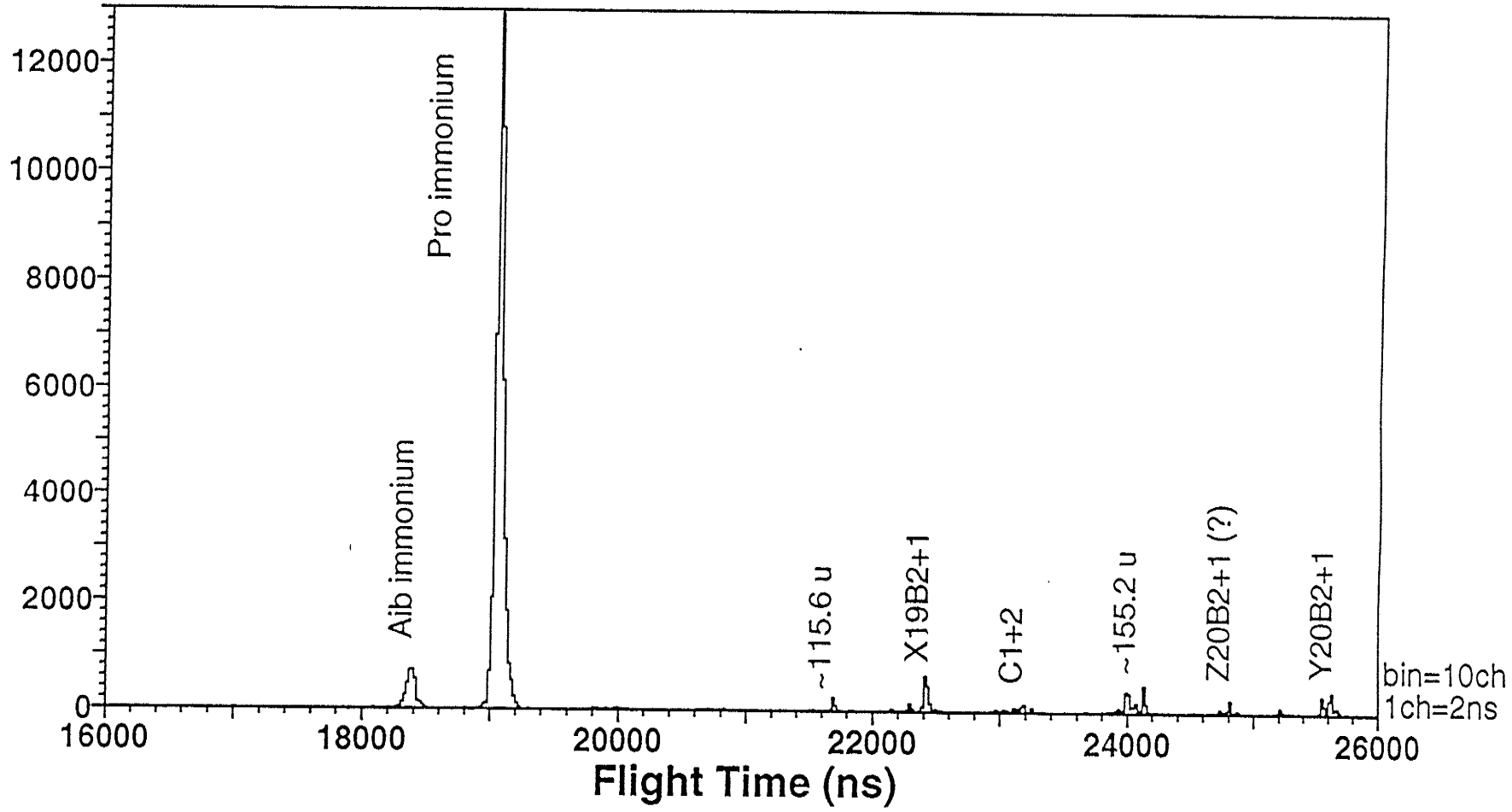

Fig. 2.13c Daughters of B2.

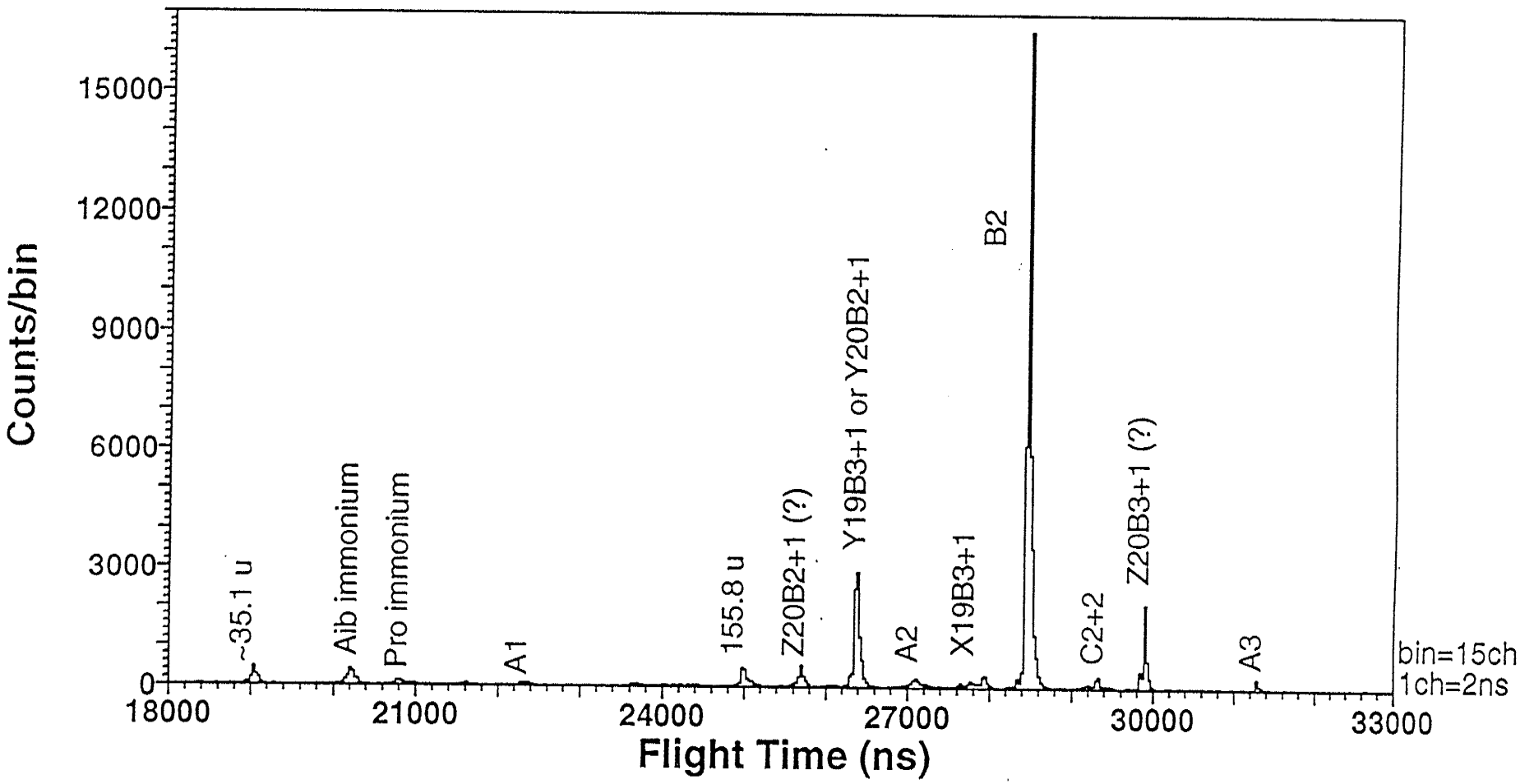

Fig. 2.13d Daughters of B3.

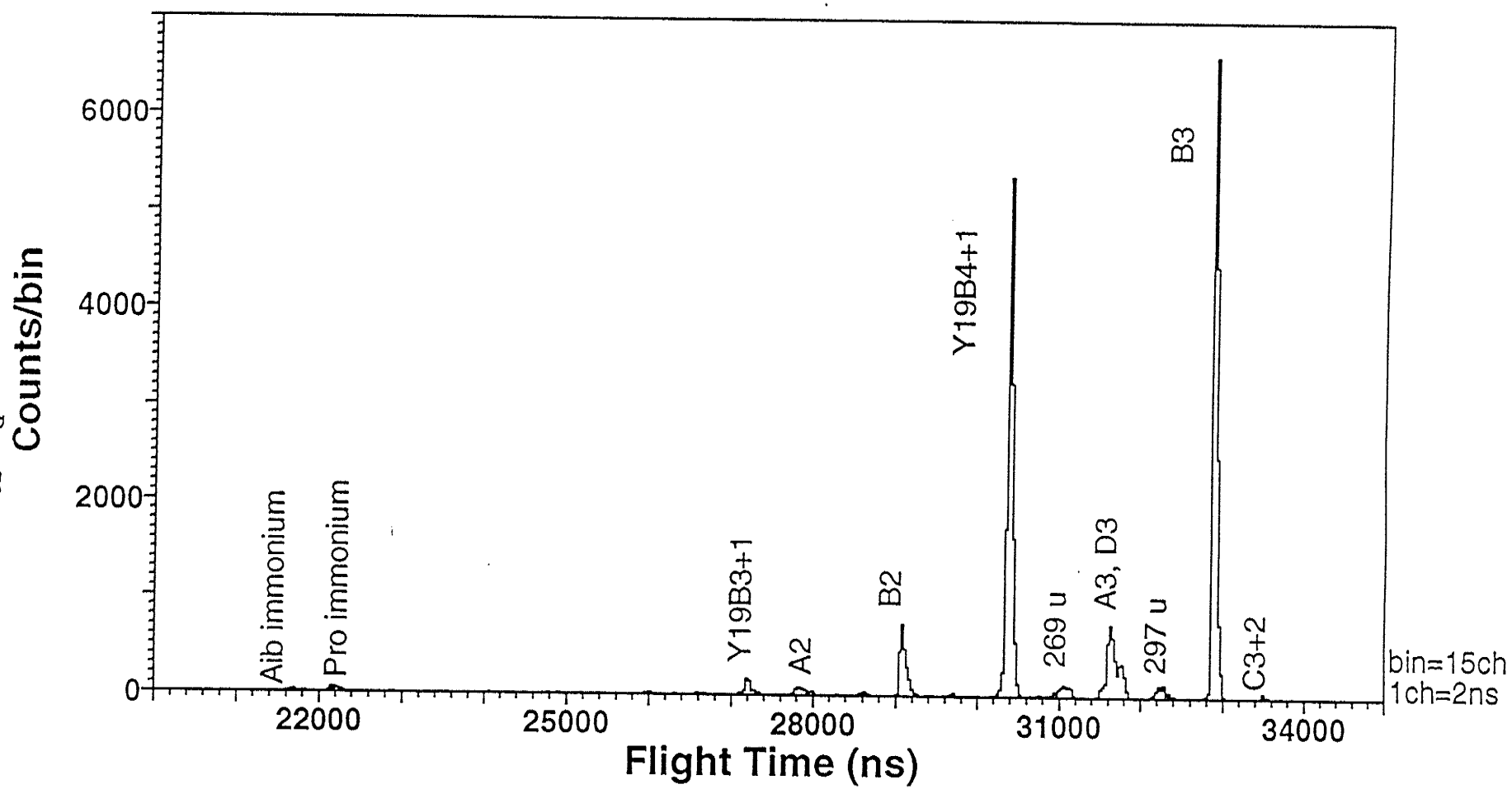

Fig. 2.13e Daughters of B4.

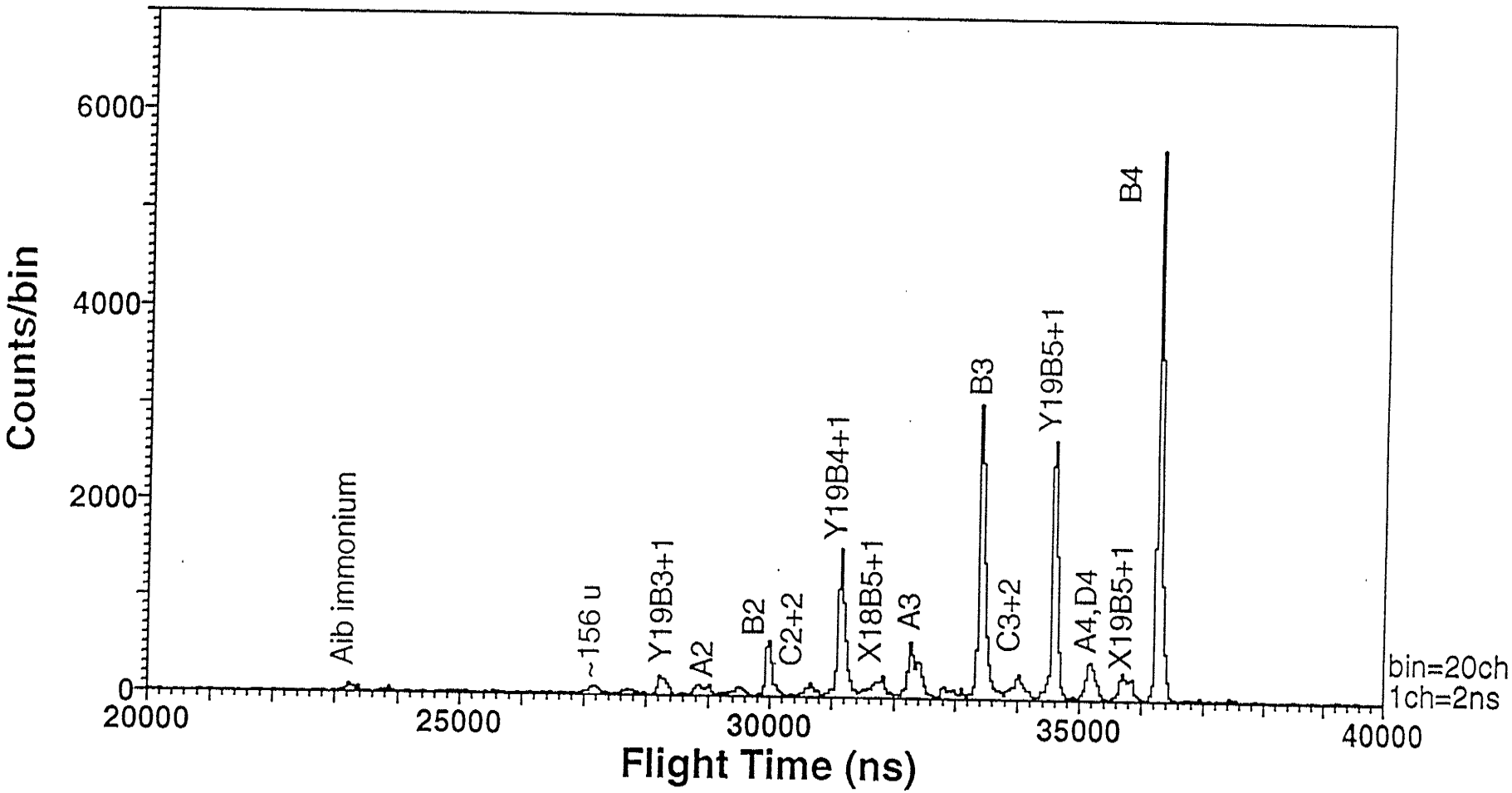

Fig. 2.13f Daughters of B5.

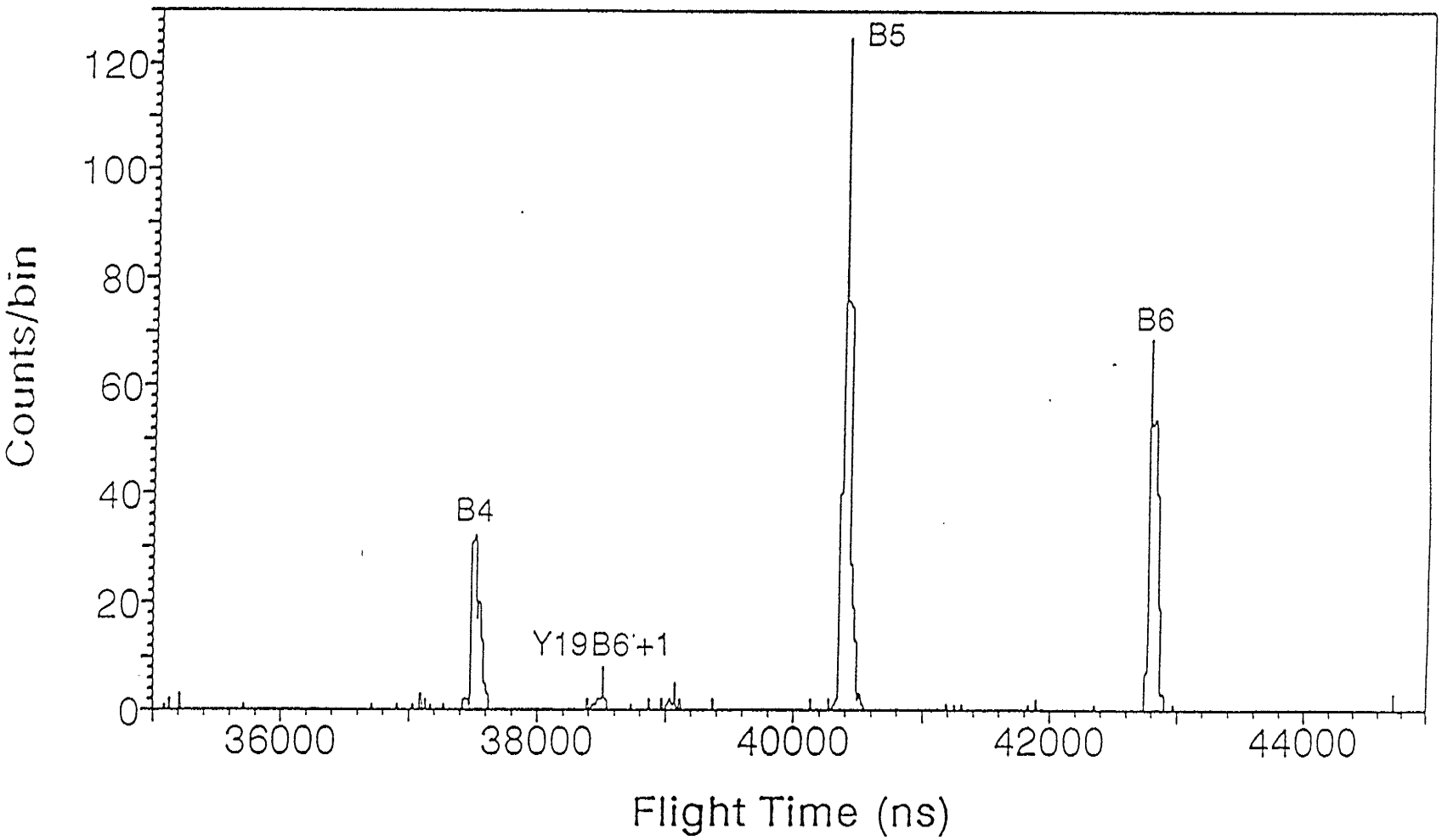

Fig. 2.13g Daughters of B7.

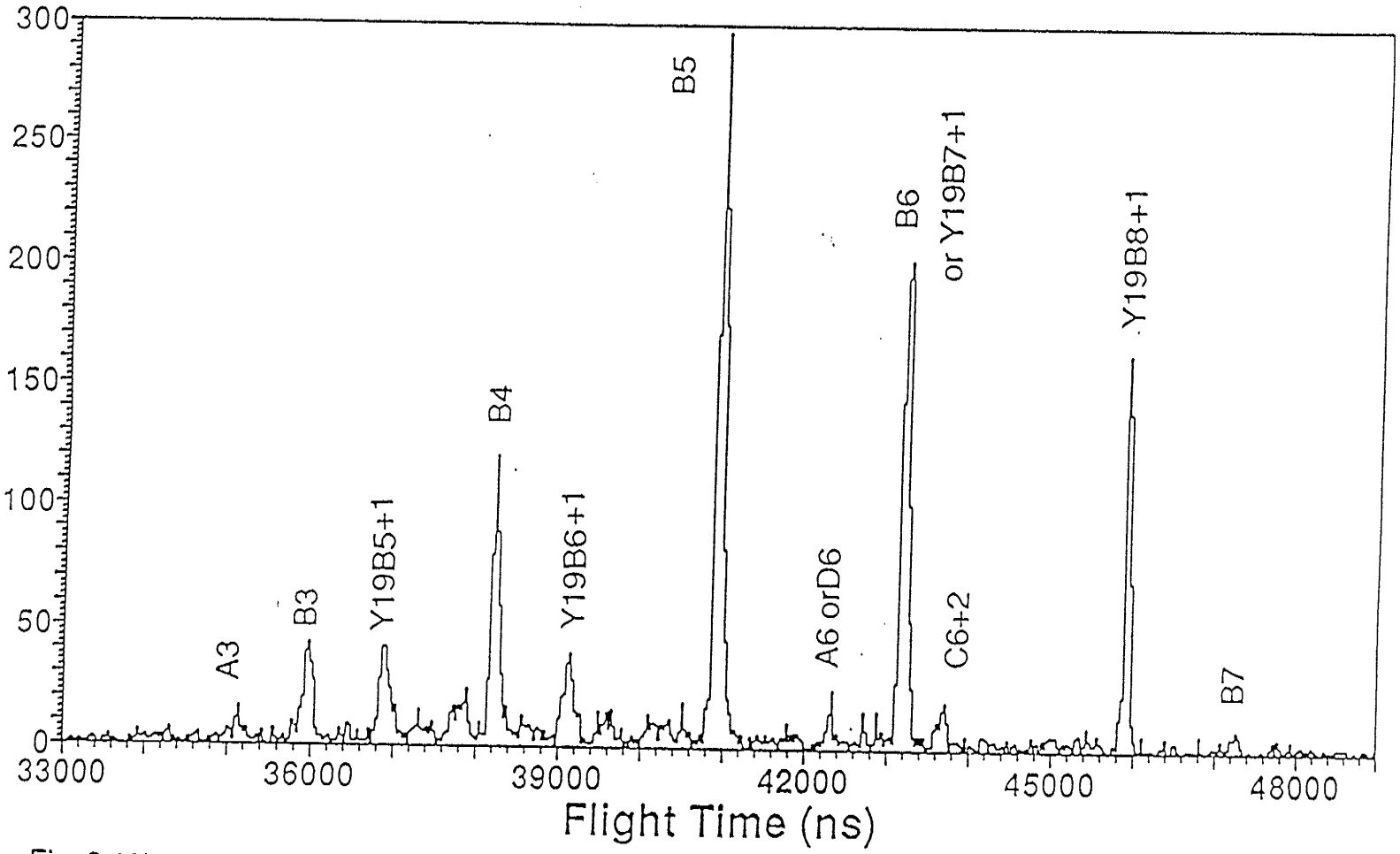

Fig. 2.13h Daughters of B8.

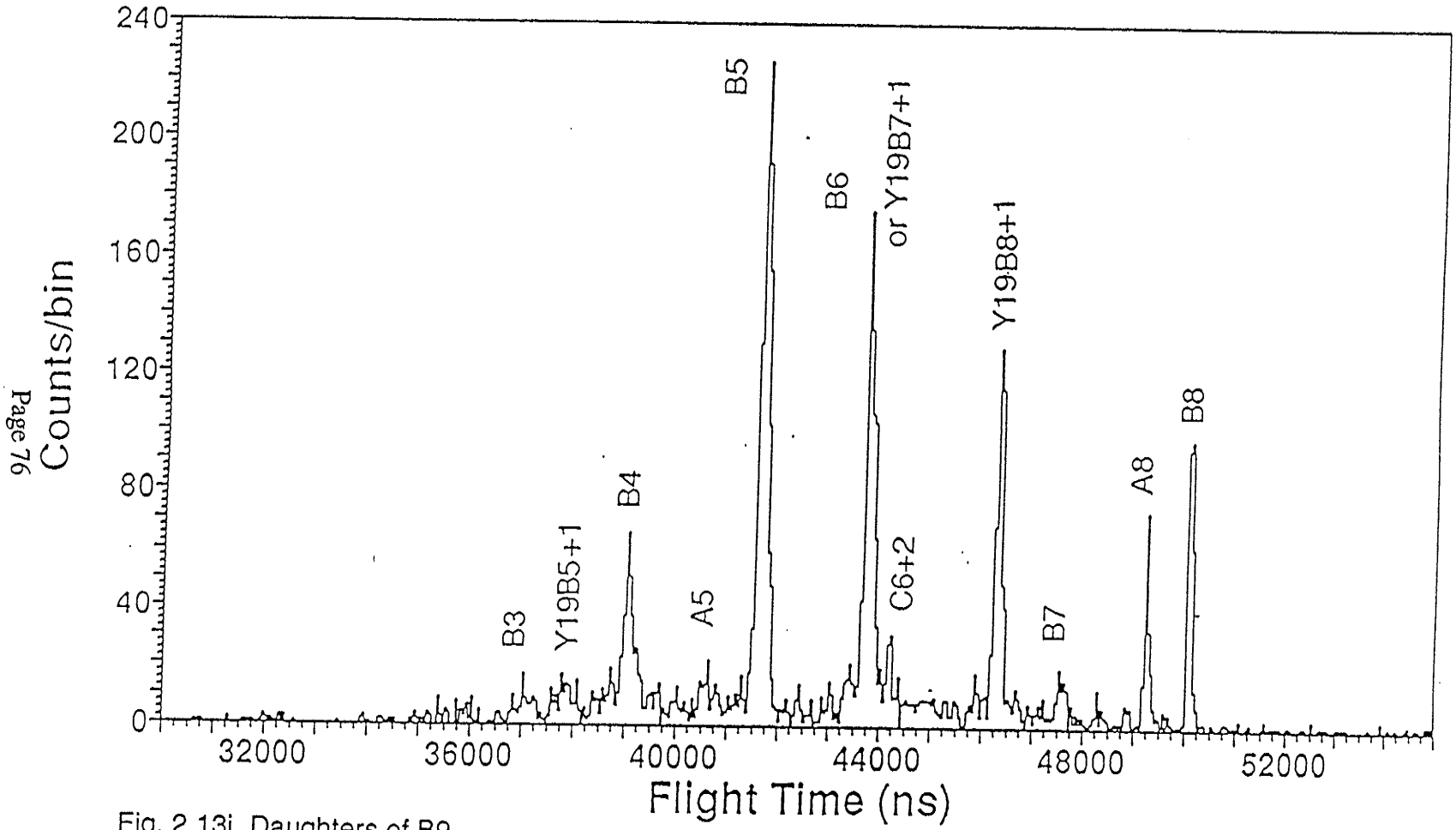

Fig. 2.13i Daughters of B9.

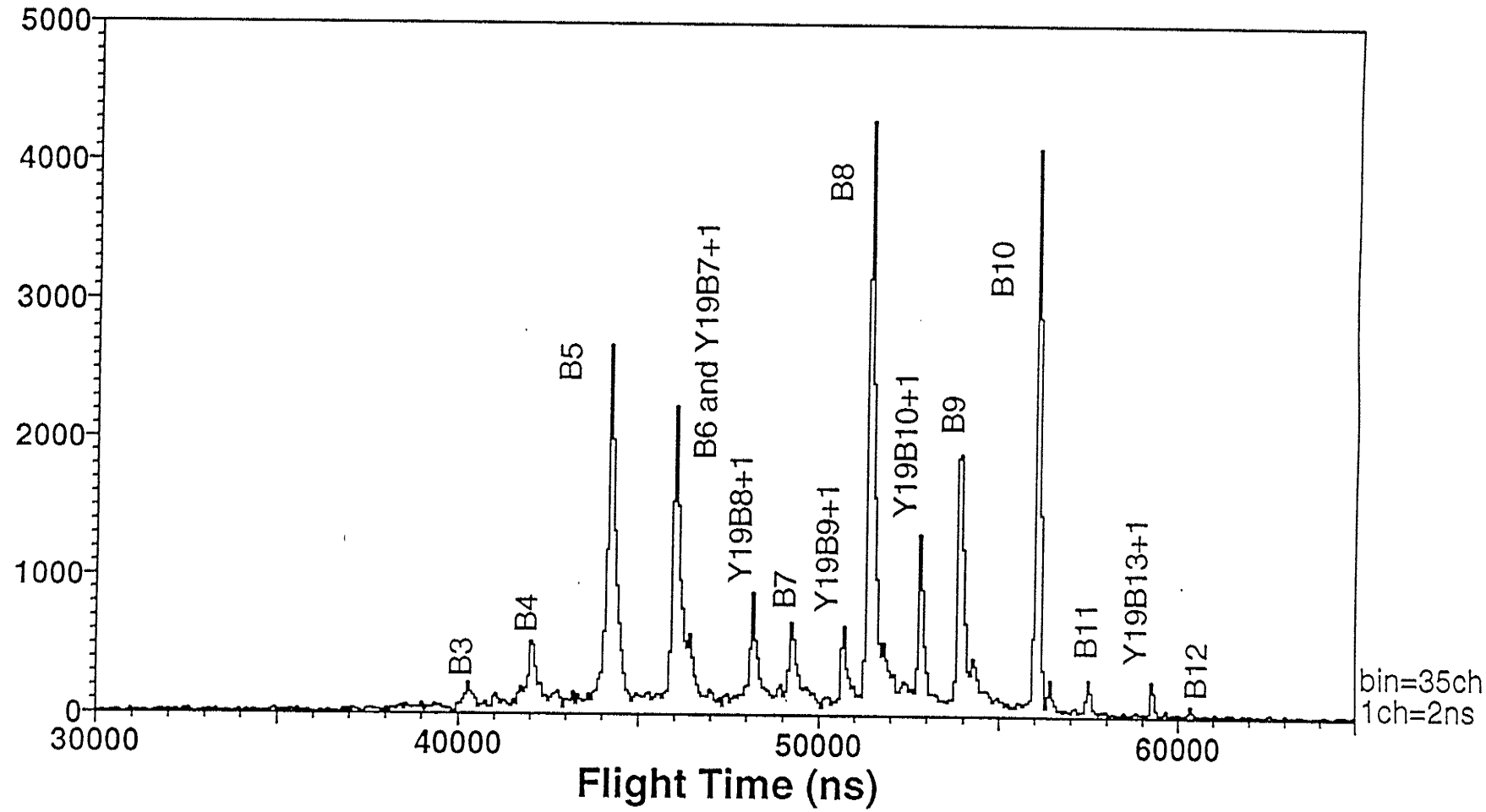

Fig. 2.13j Daughters of B13.

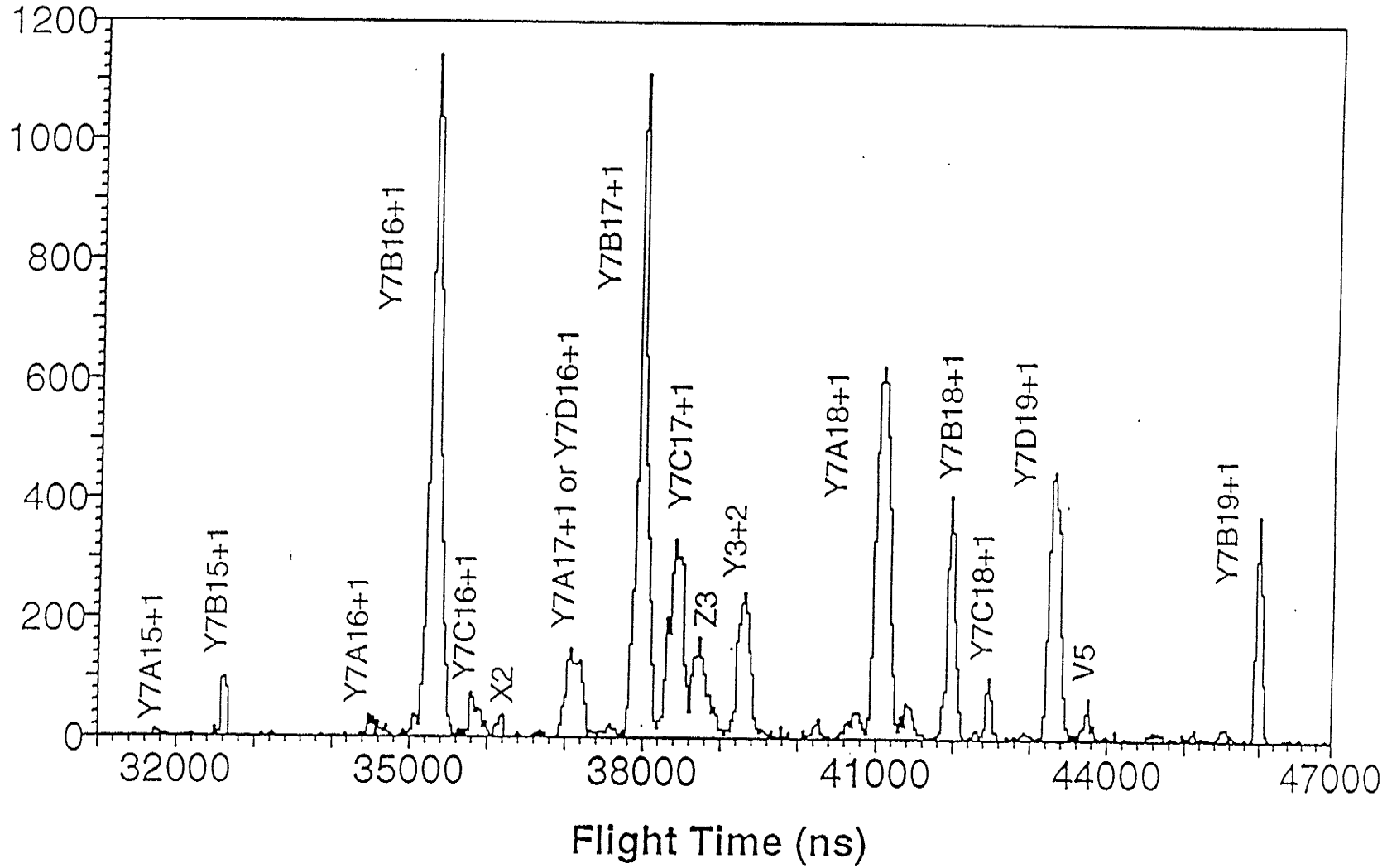

Fig. 2.14 Daughter ion spectrum of Y_7+2 parent ions.

It also has a fairly strong Y_7+2 daughter ion peak as well as weaker Y_{10}+2 and Y_{12}+2 ion peaks.

Many of the B_n ions (n=3-14 and 19) decay into lower mass B_m ions by loss of one or more residues from the C terminus, *e.g.* the daughters of B_{13} include ions from B_3 to B_{11} (Table 2.1) (*If* the B_{13} ion originated from decay of an $[M+H]^+$ ion near the target, these ions would then be granddaughters of the original $[M+H]^+$ ion.) For values of m for daughters of a given B_n ion see Table 2.1. These cleavages are sometimes accompanied by a cleavage at Aib_1-Pro_2 (as for $[M+H]^+$) to produce internal fragment ions beginning with Pro_2 (*i.e.* $Y_{19}B_n$+1). Some B_n ions (n=4-9, except 7) also decay to smaller A_n and D_n ions. As representative examples, a series of correlation spectra are shown in Fig. 2.13.

Most other ion series were weaker. Since we did not need any more sequence information on the first thirteen residues of the peptide, we did not examine these entire series in detail. However, the decays of several $Y_{19}B_n$ +1 ions were examined closely. Like the B_n ions, these ions decay into series of fragment ions containing the C- or N-termini of their parents, as well as internal fragments (Table 2.1b). Unfortunately, most of the parent $Y_{19}B_n$+1 ion peaks overlap with those of other expected prompt fragments, as shown in Table 2.1, so that the spectra can be exceedingly difficult to interpret.

The decay patterns discussed so far confirm the sequence from the N-terminus to B_{13}, with discrepancies in mass of ~<0.6 u, as determined mainly from B_n ion and internal fragment ion series in the correlation spectra. (These discrepancies were calculated by taking the mass difference between adjacent peaks in a series and subtracting the mass of the residue expected from previous information. Most of the discrepancies in the differences are due to poor statistics and to the poor resolution of daughter peaks, both because of the shorter times they spend in the ion mirror and because of the width of the parent ion peak.) The A_1 ion decays into an Aib immonium ion (m/z 58), and the B_1 ion into an acetyl ion (m/z 43), the Aib immonium ion, and others. These results define the N-terminus as Ac-Aib. Although an unusually wide or small peak in one correlation spectrum could increase the mass uncertainty for a certain residue, in all cases except for those of Aib_8 and Aib_{13}, the residue could be confirmed by another correlation spectrum. In these two cases, the correlation data support the assignments of Aib_8 and Aib_{13} but cannot confirm them. Residue 8 can be assigned as Aib_8 using data from both the direct and the correlation spectra. As mentioned above, the high abundances of Y_7+2 and B_{13} ions in both the

Table 2.1 Metastable Decay

		Parent Ion, Bn ——>												
	Daughter Ion	B14	B13	B12	B11	B10	B9	B8*	B7	B6*	B5	B4	B3	B2
a) losses from the C terminus of Bn	B13													
	B12													
	B11		.1*											
	B10	1*	0.8	.3*										
	B9	.3*	0.5	0.3	0.1									
	B8	.8*	1	1*	1	0.5	0.3							
	B7		0.1			0.1	0.1							
	B6*	.2*	.6*	.5*	.6*	.7*	.7*	.6*	.7*					
	B5	.3*	.7*	.6*	0.5	1*	1*	1*	1*	0.6				
	B4		0.3	.3*	0.1	.1*	.4*	0.5	.5*	1	1			
	B3		0.1	.1*			.1*	0.3	.1*	0.8	0.7	1		
	B2									0.1	.1*	0.2	1	
b) losses from the C terminus plus cleavage at Alb1-Pro2**	Y19B13*													
	Y19B12													
	Y19B11*		.1*											
	Y19B10*		.2*	.2*	.1*	0.1								
	Y19B9*		.1*	.1*	.1*	.1*	.1*							
	Y19B8	.1*	0.2	.4*	0.2	.3*	.5*	0.3						
	Y19B7*	.2*	.6*	.5*	.6*	.7*	.7*	.6*	.7*					
	Y19B6					0.1	.1*	0.2	0.1	0.5				
	Y19B5					0.1	.2*	0.3		.8*	0.6			
	Y19B4									.8*	0.4	0.9		
	Y19B3									.1*		.1*	0.2	

*The intensity reported may be partially or wholly due to overlap of this peak with another one.
In general**, B6~Y19B7; B8~Y7B20; Y19B9~A8~D8; Y19B10~D9; Y19B11~C9+2; Y19B13~A12.
B6 and B8 are more likely than the alternatives. (Note that this overlap also occurs for parent B6 and B8 ions.)
The other overlaps shown are specific to a particular parent**: B4 daughters, Y19B3~X18B4; B5 daughters, B2~V18B5~W18B5;
B6 daughters, Y19B3~X16B6, Y19B4~X17B6, Y19B5~X18B6; B7 daughters, B3~X16B7, B4~X17B7,
B5~X18B7; B8 daughters, B5~X17B8; B9 daughters, B3~Y14B9, B4~Y15B9, B5~Y16B9, B6~Y17B9~Y19B7, Y19B5~X14B9,
Y19B6~X15B9, Y19B8~Y18B9; B10 daughters, B4~Z14B10, B6~Z16B10~V16B10~W16B10~Y19B7
B5~Y15B10, Y19B8~Y17B10; B12 daughters, B3~V12B12, B4~X12B12, B5~X13B12,
B8~X16B12, B10~V19B12~W19B12, Y19B8~Z15B12~V15B12~W15B12; B13 daughters, B5~X12B13, B11~X18B13.
Note that because Bn and YmBn ions predominate, the other ions mentioned are less likely.
**Internal fragment ions appear with an additional proton, eg. Y19Bn+1

daughter ion spectrum of $[M+H]^+$, and in the direct spectrum, support the assignment as Aib_{13}-Pro_{14}.

Although they contain much information about the first thirteen residues, only two of the decay spectra discussed above provide any information about the sequence from amino acid 14 to the C-terminus. The decay of the $[M+H]^+$ ion to a Y_7+2 ion confirmed that the mass is approximately the same as that of the Y_7+2 ion of alamethicin I.

The decay of the Y_7+2 ion (Fig. 2.14) gives sequence information on the difficult C-terminal portion of the peptide. The correlation spectrum shows various internal fragments, Y_7B_n+1, Y_7 A_n+1, Y_7C_n+1, Z_m, and perhaps Y_7D_n+1 ions, with uncertainties arising from overlap of peaks corresponding to different ion types. The daughters included Y_7B_n+1 with n=15 to 19. From the adjacent peaks in a series, residue 16 is Aib or Ser within a 1 u error. The next three residues are Aib_{17}-$(Gln/Lys)_{18}$-$(Gln/Lys)_{19}$ with discrepancies up to 0.7 u. From the absolute masses of the fragments, using Pro_{14}, residue 15 is Val/Thr. The C terminus is Phe-ol. Thus, the sequence is $(Val/Thr)_{15}$ - $(Aib/Ser)_{16}$ - Aib_{17} - $(Gln/Lys)_{18}$ - $(Gln/Lys)_{19}$ - (Phe-ol). A second possibility for the C-terminus, Met-OH, was discounted because the mass difference is just beyond the expected maximum error range of 2 u, and because it does not have the C-terminal alcohol characteristic of the peptaibols. Due to the anomalously large width of the Y_7+2 parent ion peak, which can shift the entire calibration by a few u, there is a large error for absolute masses; however, this should not affect mass differences between the peaks. Thus the Y_7+2 decay spectrum supports the replacement of Glu_{18} by Gln/Lys in alamethicin III.

This measurement found residue 18 to be Gln/Lys, but we thought it desirable to verify the assignments more precisely, since it is the only change expected from the sequence of alamethicin I. In addition, there were indications of some Glu impurity (see below). Therefore we carried out measurements in which the mirror voltage was successively optimized for the Y_7B_{17}+1 ion and the Y_7B_{18}+1 ion, thus bracketing residue 18. This is carried out by reducing the mirror voltage until the flight time of the desired daughter ion coincides with the flight time observed previously for its parent (§1.2.4.2). The mirror then provides full correction for the velocity spread of the daughter, instead of the partial correction when the mirror is optimized for the parent. Under this condition, $m_p/V_p = m_1/V_1 = m_2/V_2$ where m_p, m_1 and m_2 are the masses of the parent and the two daughter ions, and V_p, V_1 and V_2 are the corresponding mirror voltages [Tang '88]. Although

statistics were poor, this procedure yielded well resolved isotopic peaks for the selected daughter and enabled residue 18 to be determined as Gln within an error ~<0.1 u by measurement of the principal masses as shown in Fig. 2.15. Resolution of the other peaks was also improved, thus defining residue 16 as Aib and residue 15 as Val.

The Gln/Lys ambiguities are not easy to resolve by mass measurements, since the mass difference is only ~0.04 u. N-acetylation of Lys, or some other chemical method, is often used to distinguish between the two. However, in this case the general appearance of the spectrum is adequate to distinguish them; because the alamethicins are nonbasic peptides, the presence of a basic Lys residue would greatly affect the spectrum by providing a protonation site that would promote the formation of other ion types at the expense of B_n ions. Added confirmation is provided by the spectra of other nonbasic peptaibols, such as the closely related hypelcins, trichosporins and paracelsins (all containing Gln_7 and Glu_{18}-Gln_{19})[Buko '90, Iida '90, Bruckner '84, Fujita '84], which have features similar to the present spectra. Thus the upper part of the sequence is defined as Val_{15}-Aib_{16}-Aib-$_{17}$-Gln_{18}-Gln_{19}-Phe_{20}-ol in accordance with the structure suggested by the NMR measurements.

2.3.3.3 Other alamethicins present in this sample

Close inspection of the isotopic peak heights of the $[M+Na]^+$ ion in SIMS and in MALDI show a discrepancy from that expected for the proposed alamethicin III sequence: the peak at principal mass + 1 u was much larger than expected. This could correspond to the presence of another peptide with a mass 1 u higher than that of alamethicin III. There is also a small peak, at m/z 1999, that interferes with the $[M+K]^+$ peaks (Fig. 2.9). This is a sodiated species, as confirmed by two tiny peaks at m/z 1977 and 2015, which would correspond to $[M^*+H]^+$ and $[M^*+K]^+$, respectively. Thus, this peptide would have a mass of about 1976 u, but the assignment cannot be verified from these data. (The negative ion spectrum also shows a peak at ~1976 u, as well as very small unexplained peaks at ~1992 u and 1948 u.)

Rechromatographing the sample under the conditions previously used showed that it did, in fact, contain two small impurities. As the original chromatogram (Fig. 2.8) shows, the various peptides eluted closely together, and it is likely that both impurities may arise from other HPLC fractions (§2.3.3.5).

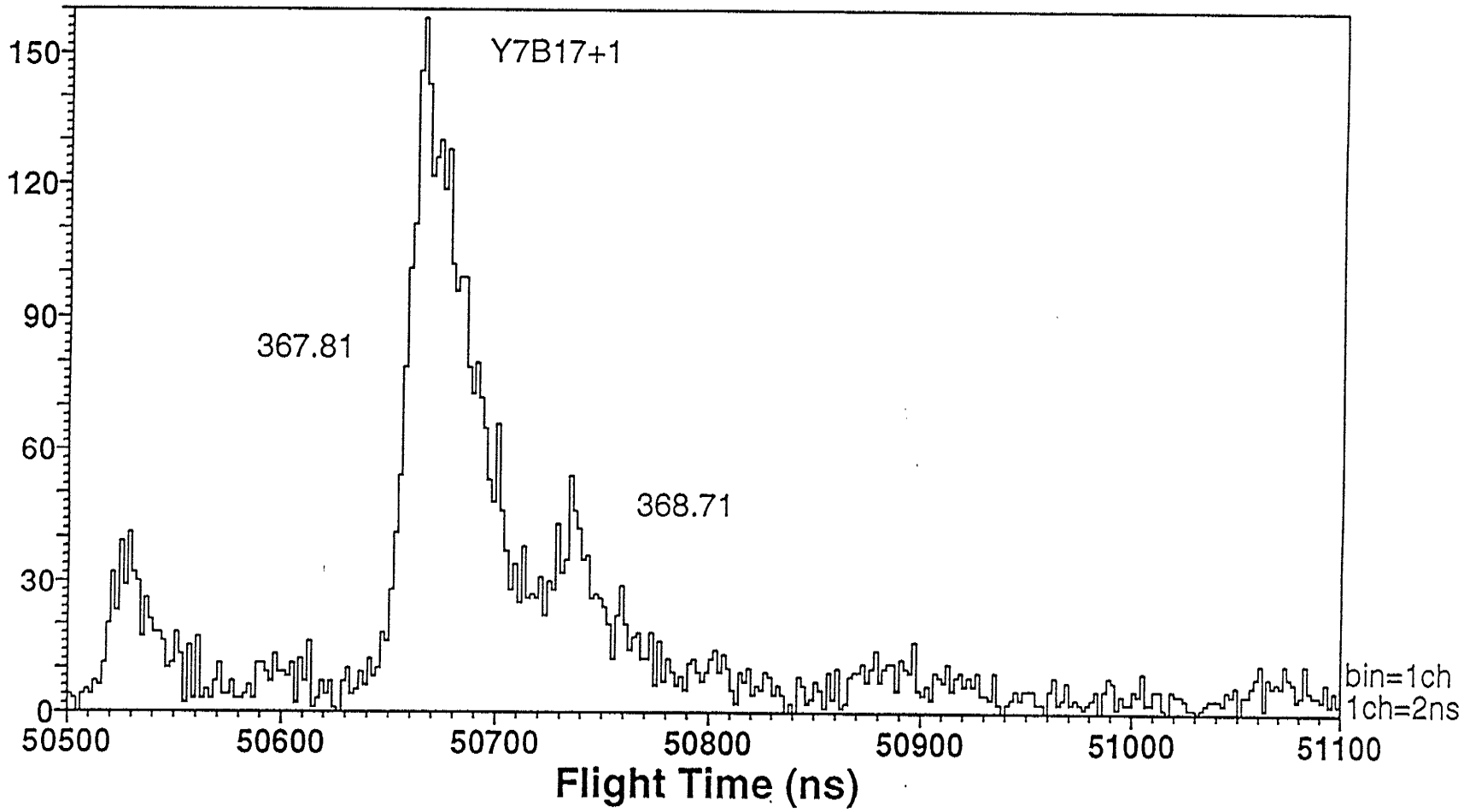
Y7B17+1
367.81
368.71
Counts/bin
150
120
90
60
30
0
50500
50600
50700
50800
50900
51000
51100
Flight Time (ns)
bin=1ch
1ch=2ns

Fig. 2.15a

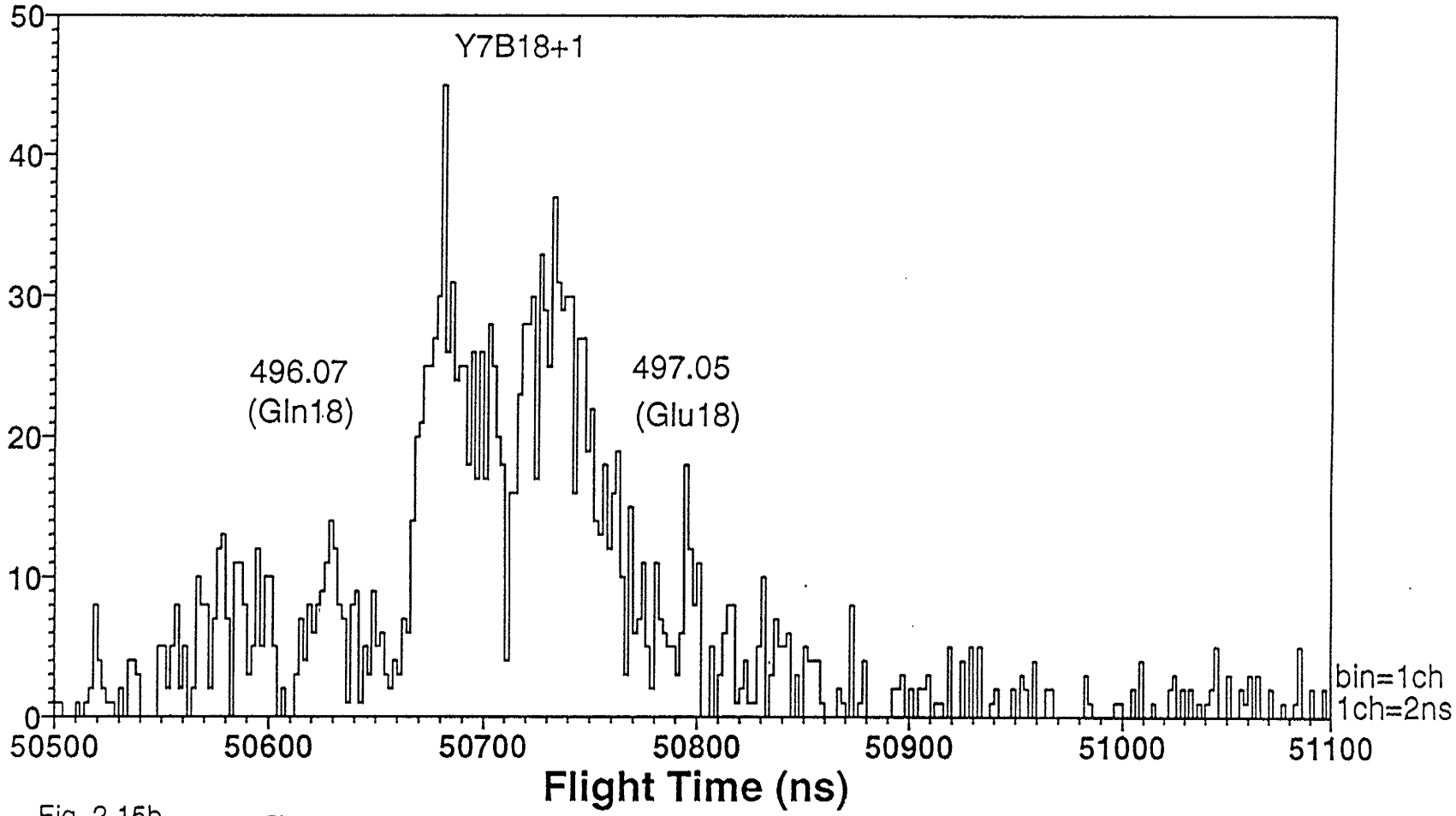

Fig. 2.15b

Fig. 2.15 Daughters of Y_7+2, taken with the mirror voltage optimized for a) Y_7B_{17}+1 and b) Y_7B_{18}+1.The mass difference between the first peak in each spectrum corresponds to Gln, defining residue 18. The second peak in a) is the ^{13}C isotope peak, but the second peak in b) corresponds to a superposition of the ^{13}C isotope peak and an ion containing Glu_{18}.

The data presented above indicate that the predominant amino acids at positions 18 and 19 are both Gln. The peak height ratios of the B_8 ion peak correspond to theory, however, and this suggests that the other peptide which, considering the enzymatic synthesis of the peptides is likely to be closely related to the other alamethicins, has one more mass unit between residue 8 and the C-terminus than does alamethicin III. It could have the same sequence as alamethicin III, but with replacement of Gln by Glu at position 18 or 19. The Y_7+2 ion resolution in the direct spectrum does not permit definitive confirmation.

The correlation spectra of $[M+H]^+$ and Y_7+2 decay provide support for this: The Y_7+2 daughter ion peaks in some $[M+H]^+$ decay spectra may be doublets, although low statistics and their large width make it difficult to be certain. Because there are no Y_6+2 and Y_8+2 peaks, mass differences cannot be measured to identify amino acid residues, but the Y_7+2 ion mass is close to that expected from the proposed sequence. However, the parent $[M+H]^+$ ion peak is very wide and the Y_7+2 daughter ion peak is also intrinsically wide itself because daughter ions do not spend the optimum amount of time in the mirror. As a result, the error in the absolute mass of the Y_7+2 ion may be as high as several u. Therefore, although this result for Y_7+2 ion is consistent with the direct spectrum, it does not yield more information. More definitively, however, some daughters of parent Y_7+2 ions seem to include double peaks, corresponding to the masses expected when both Gln_{18} and Glu_{18} are present. If the resolution is too poor to see a doublet, the daughter ion peaks are broad when they include residue 18. Those ions containing up to residue 17 only give single, narrow peaks.

The reduced mirror voltage experiment mentioned above provided resolution adequate to decide the question. The Y_7+2 daughter of the $[M+H]^+$ ion has somewhat resolved peaks, whose relative heights (100:~95:) differ from the expected ratios of (100:46), confirming the presence of a peptide, similar to alamethicin III, with a 1 u mass increase in the Y_7+2 fragment (Fig. 2.16).

Further information is available from the reduced mirror field experiments for daughters of Y_7+2 that bracket residue 18 (Fig. 2.15). The Y_7B_{17}+1 peak heights agree with the expected (100:22:3) ratios, but those of Y_7B_{18}+1 do not agree at all with the expected (100:29:5) ratios. Thus, the peptide is like alamethicin III up to residue 17, and residue 18 is anomalous, containing a mixture of Gln_{18} and Glu_{18}. Because the peak height ratios of fragments containing both residues 18 and 19 mimic those of fragments containing

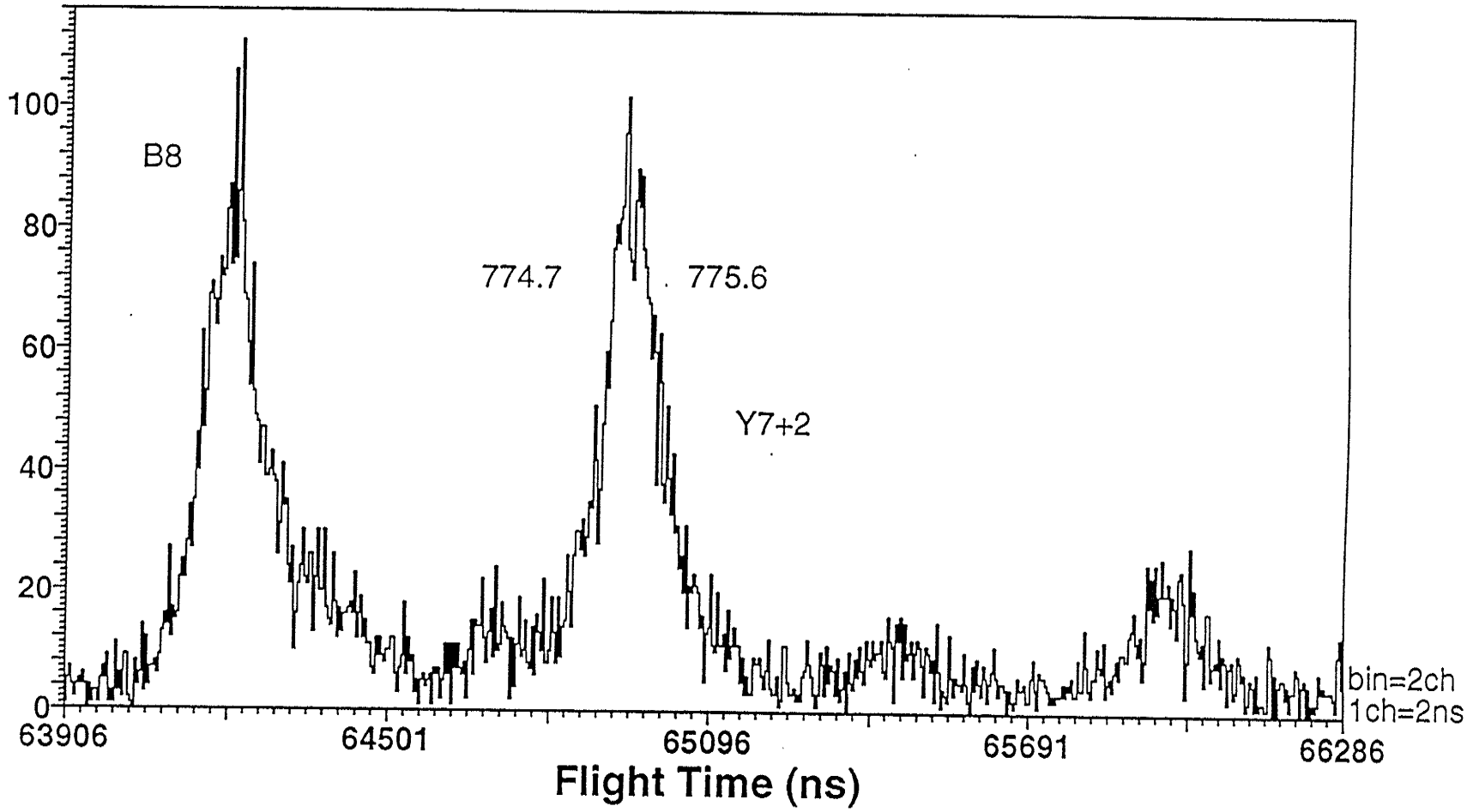

Fig. 2.16 The Y_7+2 daughter of $[M+H]^+$, taken with a reduced mirror voltage.

residue 18 only, residue 19 cannot consist of a mixture of Glu and Gln, but must be only Gln_{19}. Thus these two peptides are alamethicin III and alamethicin I.

2.3.3.4 Interesting Details

The $[M+Na]^+$ ion observed in the reflected spectrum with a normal mirror voltage in the second series of experiments (*i.e.* those including the reduced mirror voltage experiments) is surprising because it shows an even greater amount of alamethicin I than before. The solution had been stored for several months in an old freezer (which was unfortunately frost-free so that the peptides underwent freeze-thaw cycles), but one or more of the three proposed Gln residues may have changed to Glu. This may provide additional support for choosing Gln instead of Lys.

Another surprising fact is that the peak height ratios of the $[M+Na]^+$ ion and the Y_7+2 daughter of the $[M+H]^+$ ion do not, within experimental error, indicate the same relative amounts of impurity; the isotope peak height ratios of Y_7+2 indicate less of a peptide 1 u heavier than those of $[M+H]^+$. The relative abundances of detected ions depend upon both production and decay factors. Thus, the Gln residue that occurs at position 7 (*i.e.* which is present in $[M+Na]^+$ but not in Y_7+2) could have undergone some conversion to Glu. The peak height ratios of some B_n ions, and some internal fragment ions from both reflected and daughter spectra agree with this possibility, although the data are inconclusive. Another explanation may be that residue 7 is still Gln, but that the greater peak height anomaly observed in the $[M+Na]^+$ ion is due to preferential cationization of the Glu_{18}-containing peptide versus the Gln_{18}-containing peptide. (There was very little evidence of sodiated Y_7+2.) This assumes that amino acid cationization and protonation follow similar trends, which is not always true. Also, as discussed below, the Gln_{18} peptide may form Y_7+2 more readily than the Glu_{18} peptide because Glu competes more effectively than Gln for H^+. (The H^+ must be on the Pro_{14} amide, not on Glu or Gln, for Y_7+2 formation to occur.) One could distinguish between these possibilities by examining the Y_7+2 daughter ion peak of $[M+H]^+$ before the peptide solution was stored (i.e. before the peptide could have degraded). Unfortunately, however, this peak contained too few counts to give a valid peak height ratio.

The $[M+Na]^+$ ion peak height ratios seem to indicate a larger amount of alamethicin

I than indicated by the chromatogram. This could be due to preferential sodiation of the impurity [Gorman '92] or to differences in ion lifetimes of the Glu and Gln containing peptides. The $[M+H]^+$ ion peak was not sufficiently large to determine the peak height ratios from the signals observed.

It is interesting to speculate that the observed suppression of the other peptides in the negative MALDI spectrum could be due to preferential ionization of this Glu_{18} peptide in the negative mode.

2.3.3.5 Other Alamethicins

As shown in Figure 2.8, other alamethicins besides the one analyzed above are present. Each of the peaks has been collected and examined using mass spectrometry, some in more detail than others. Sequences have been determined with various degrees of confidence by using the methods detailed above and by comparing with the known alamethicins. Some highlights of the analysis will be given, and the sequences are presented in Table 2.2.

In all cases, the spectra showed similar characteristics: the first 14 amino acids were relatively easy to determine and the remainder were more difficult; much metastable decay occurred; the molecular ion was of low abundance; and the peak for the sodiated peptide was usually adequate for molecular weight determination (sometimes the negative spectrum was used). In some cases, the molecular mass uncertainty was considerable as a result of extensive metastable decay. The collected HPLC fractions all contained more than one peptide, often due to contamination from neighboring fractions, and were examined as mixtures. In the one case checked by HPLC (the 23.33 minute fraction), two peptides truly did coelute; these were rechromatographed and collected under different conditions, and analyzed by the TOF correlation technique to confirm the sequences determined from the mixture.

The molecular masses were obtained from the positive reflected spectra. In all cases the $[M+Na]^+$ ion predominated, and several alamethicin peaks were always present. Negative spectra were taken to confirm the masses using the $[M-H]^-$ and the $[M+I]^-$ ions, but MALDI was not used as previously because it did not seem necessary. The reflected spectra showed too much overlap to be useful in sequence determination.

As was the case for the 21.34 minute fraction, extensive series of B ions were observed in the direct spectra, with corresponding peaks in the neutral spectra. Series of internal fragment ions with Pro_2 at the N-terminus also appeared. The A and D ions, which often overlapped, were less abundant and only a few C+2 ions were present. The only C-terminal ions observed clearly were Y_7+2 and Y_{19}+2, corresponding to cleavage before Pro residues.

In all cases the $[M+H]^+$ ion decayed into a partial series of B ions, the Y_7+2 ion and a few internal fragments beginning at Pro_2. The daughters of the B ions were predominantly B ions and a series of ions with Pro_2 at the N-terminus. The internal fragment ions beginning at Pro_2 exhibited decay similar to the B ions. The daughters of the Y_7+2 ions are predominantly Y_7B_n+1 fragments although the corresponding Y_7A_n+1 and Y_7C_n+1 fragments appeared as well. A few Y_7D_n+1 ions, and some C-terminal ions were also present. Thus in most instances the analysis was similar to that for the 21.34 minute fraction described in detail above.

One interesting approach that was not used for alamethicin III but was used in the analysis of most of the other alamethicin fractions involves the identification of very closely related peptides approximately fourteen mass units apart using the correlation spectra, as occurred in the 23.33 minute HPLC fraction. The molecular ion region of this HPLC fraction shows peaks corresponding to two molecular ions with a mass difference of 13 u. The negative reflected spectrum, with two $[M-H]^-$ and two $[M+I]^-$ peaks, confirms this.

When a correlation window was set on the envelope of the entire B_{13} peak, which contained two peptides, it was evident that an amino acid substitution had occurred at position 6 as shown in figure 2.17. The one peptide contained Ala_6 and the other Aib_6 (with a mass difference of 14 u). This is 1 u more than that observed for the molecular ion. From the Y_7+2 correlation spectra, it seemed likely that a partial interchange between Gln and Glu had occurred, and from work with alamethicin III, residue 18 seemed a likely candidate. The molecular mass difference of 13 u suggested that this occurred in conjunction with the first interchange at residue 6. Similar analyses were performed for some of the other HPLC fractions, although not always with such clear results.

To test these results, the 23.33 minute fraction was rechromatographed with a pH of 5.14 instead of 3.5 as had been used previously. The new chromatogram showed that two peptides were present, one with an ionizable group. Subsequent mass spectrometry of

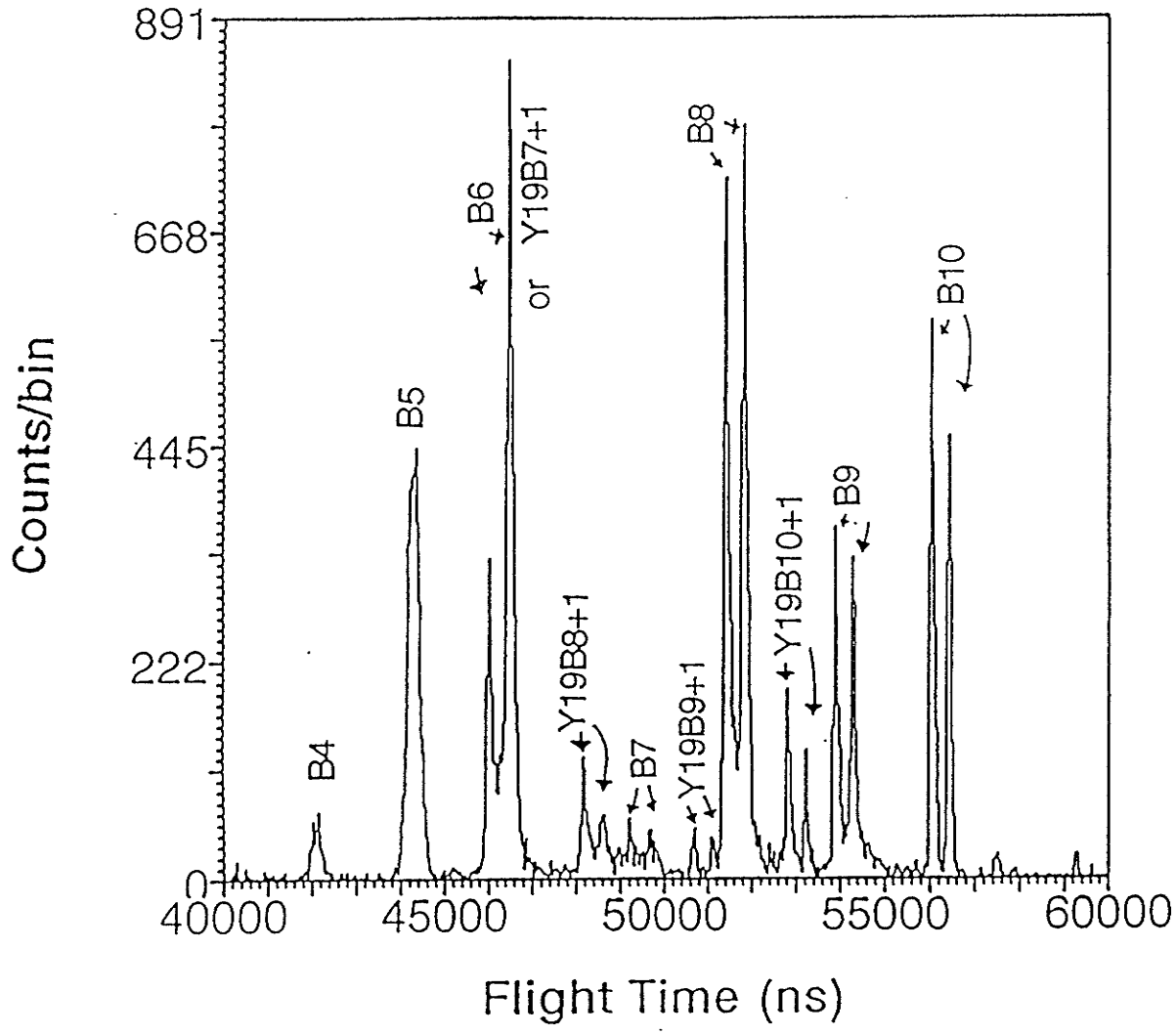

Fig. 2.17 Daughter ion spectrum of B_{13} parent ions of the 23.33 minute fraction of alamethicin. Up to position five the peaks are single and from position six on they are double, showing that two different amino acids are present at position six in the peptide.

the separated components confirmed the sequences suggested above, and the validity of our method. Note that this fraction and the 21.34 minute fraction discussed above are the only ones that were rechromatographed.

The compounds observed result from interchange of various amino acid residues, as expected from the measurements [Konig '80] on alamethicins prepared by traditional methods. The major components arise from combinations of the variations $Ala_4 \leftrightarrow Aib_4$ (14 u) and/or $Aib_5 \leftrightarrow Val_5$ (14 u), $Ala_6 \leftrightarrow Aib_6$ (14 u), $Aib_{17} \leftrightarrow Val_{17}$ (14 u), and $Gln_{18} \leftrightarrow Glu_{18}$ (1 u). For the 14 u interchanges, correlation spectra show both the mass change and the location of the modification, as illustrated in Fig. 2.17. For the Gln $\leftrightarrow$ Glu interchanges, no spectra at reduced mirror voltages were examined, so the 1 u difference was discernible mainly in the anomalous isotopic peak height ratios. Also, the molecular ions in the negative ion spectra sometimes seemed to be 1 u higher than expected from the positive ion spectra, perhaps due to the presence of small amounts of peptides containing Glu_{18} (which would be expected to produce $[M-H]^-$ ions much more readily than a peptide containing Gln_{18}). These data were sufficient to determine that both were usually present.

Using mass spectrometry alone to confirm these sequences would have been laborious. Because the amino acid interchanges always involved either 1 u or 14 u; because so many amino acids in the peptides are repeated; and because of the poor resolution (due to metastable decay), definitive confirmation by mass spectrometry may not even be possible in all cases.

Therefore we attempted to use the HPLC elution time data. Various tables of calculated HPLC retention coefficients [Guo '86, Browne '82] were used as an aid in choosing among the different peptides suggested by mass spectral sequencing. These tables did not include the Aib residue, and two different methods were used to estimate its value. The first, following Champney's method [Champney '90] (although he made an arithmetical error), assumed that the effect of replacing H with a methyl group in the replacement of Ala by Aib was the same as the replacement of Gly by Ala. In the second method, the retention coefficient of Aib was estimated from the coeluting peptides of the 23.33 minute fraction. No conclusive results were obtained from the retention coefficients. In fact, for the sequences proposed from MS, the predicted HPLC elution times are inconsistent. This is at least partially due to the different solvents involved, even though some claims are made for the universality of the retention coefficients.

Thus the sequences of the alamethicins proposed in Table 2.2 are somewhat tentative. The assignments of the first 14 residues are quite definite for the boldface alamethicins, but the remainder of the peptides are less certain. The proposed sequences show some agreement with previous GC/MS data [Konig '80] for alamethicins prepared by other methods, as expected. The various alamethicins have previously been separated by HPLC [Brewer '87, Balasubramanian '81, Bruckner '84], and in one case twelve components were detected [Balasubramanian '81]. Therefore it is not unreasonable to conclude that we have observed 11 to 14 alamethicins (see Table 2.2).

2.3.4 DISCUSSION

2.3.4.1. Sequence Determination from the Correlation Spectra

Observation of the daughter ions from decay of the $[M+H]^+$ ion is sufficient in principle to define the sequence, provided that the peak assignments are correct. In practice, however, some of the daughter ions may be absent, or of too low intensity, or may have poor resolution. In Fig. 2.12 the only B ions strong enough to give good measurements are B_8 to B_{13}. It is therefore necessary to observe also the decay of a number of prompt fragments. The Y_7+2 ion is particularly important in this case, since it is the only intense parent (besides $[M+H]^+$) covering the C-terminal region of the peptide.

A unique assignment for a daughter is not always possible in a given spectrum so it is helpful to have various daughter ion spectra available. This is especially true in alamethicin because of the large number of identical residues; ambiguous peaks are marked with asterisks in Table 2.2. These overlaps are often between the B ions and various unusual internal fragments (see footnote to the table), which usually depend on the parent ion. Therefore different parents tend to have different overlaps occurring in their daughter ion spectra, so that there is usually at least one correlation spectrum in which a particular ion peak is unambiguous. This increases our confidence in the interpretation even when, as is often the case, the alternative assignments seem quite unlikely. For example, the B_3 daughter ion appears in 8 different correlation spectra. It overlaps with other ions in the

Table 2.2 Alamethicins Observed

HPLC fraction (min)	principal mass (u) [1]	variations from alamethicin III (in boldface type)	principal mass (from sequence)[2]	assignment [3]
21.34	1962±.5 (la)	...Ala4 Aib5 Ala6 Gln7 ...Aib16 Aib17 Gln18 Gln19 ...	1962.1	alam III
	1963±.5(m)	...Ala4 Aib5 Ala6 Gln7 ...Aib16 Aib17 **Glu18** Gln19 ...	1963.1	alam I
	1976±2 (sm)	...??? ...		
22.56	1962.5±1.5 (m)	...Ala4 Aib5 Ala6 Gln7 ...Aib16 Aib17 Gln18 Gln19 ...	1962.1	alam III
		...Ala4 Aib5 Ala6 Gln7 ...Aib16 Aib17 **Glu18** Gln19 ...	1963.1	alam I
	1976.8±1.5(la)	...Ala4 Aib5 Ala6 Gln7 ...Aib16 **Val17** Gln18 Gln19 ...	1976.2	alam IV
		...Ala4 Aib5 Ala6 Gln7 ...Aib16 **Val17** **Glu18** Gln19 ...	1977.1	alam V
	1992±3 (sm)	...Ala4 Aib5 **Alb6** Gln7 ...Aib16 **Val17** Gln18 Gln19 ...	1990.2	alam VI
		...Ala4 Aib5 **Alb6** Gln7 ...Aib16 **Val17** **Glu18** Gln19 ...	1991.2	alam VII
23.33	1962.8±.5(la)	...Ala4 Aib5 Ala6 Gln7 ...Aib16 Aib17 **Glu18** Gln19 ...	1963.1	alam I
	1975.9±.5 (la)	...Ala4 Aib5 **Alb6** Gln7 ...Aib16 Aib17 Gln18 Gln19 ...	1976.2	alam VIII
		...Ala4 Aib5 **Alb6** Gln7 ...Aib16 Aib17 **Glu18** Gln19 ...	1977.1	alam II
24.53	1963.5±1.5(sm)	...Ala4 Aib5 Ala6 Gln7 ...Aib16 Aib17 **Glu18** Gln19 ...	1963.1	alam I
	1977.2±1(la)	...Ala4 Aib5 **Alb6** Gln7 ...Aib16 Aib17 Gln18 Gln19 ...	1976.2	alam VIII
		...Ala4 Aib5 **Alb6** Gln7 ...Aib16 Aib17 **Glu18** Gln19 ...	1977.1	alam II
	1990.4±1.5(la)	...Ala4 Aib5 **Alb6** Gln7 ...Aib16 **Val17** Gln18 Gln19 ...	1990.2	alam IX
		...Ala4 Aib5 **Alb6** Gln7 ...Aib16 **Val17** **Glu18** Gln19 ...	1991.2	alam X
25.57	1961.3±1.5 (sm)	...Ala4 Aib5 Ala6 Gln7 ...Aib16 Aib17 Gln18 Gln19 ...	1962.1	alam III
		...Ala4 Aib5 Ala6 Gln7 ...Aib16 Aib17 **Glu18** Gln19 ...	1963.1	alam I
	1977.1±1.5(la)	...Ala4 Aib5 **Alb6** Gln7 ...Aib16 Aib17 Gln18 Gln19 ...	1976.2	alam VIII
		...Ala4 Aib5 **Alb6** Gln7 ...Aib16 Aib17 **Glu18** Gln19 ...[4]	1977.1	alam II
		...Ala4 **Val5** Ala6 Gln7 ...Aib16 Aib17 Gln18 Gln19 ...[5]	1976.2	alam XI
		...Ala4 **Val5** Ala6 Gln7 ...Aib16 Aib17 **Glu18** Gln19 ...[5]	1977.1	alam XII
		...**Alb4** Aib5 Ala6 Gln7 ...Aib16 Aib17 Gln18 Gln19 ...[5]	1976.2	alam XIII
		...**Alb4** Aib5 Ala6 Gln7 ...Aib16 Aib17 **Glu18** Gln19 ...[5]	1977.1	alam XIV

[1] (la) represents a large peak, (m) a medium sized peak, and (sm) a small peak.
[2] The major peptide is in bold face; minor ones are in standard type. If no choice can be made, between peptides for a given mass peak, or if both are equally present, both are in the same type.
[3] Alamethicin I and II were previously numbered; the other alamethicins are numbered in order of HPLC elution; it is not known how these numbers relate to those of Brewer et al [14].
[4]Note, for the 25.57 min fraction, 1977.1 u, Aib6Glu18 is preferable to Aib6Gln18 because of the peak height ratios and the mass.
[5]These are represented by such small peaks that they cannot be differentiated. The Aib4 version seems more likely than the Val5 version.

daughter spectra of B_7 ($X_{16}B_7$+1), B_9 ($Y_{14}B_9$+1), and B_{12} ($V_{12}B_{12}$+1). Although some of these alternative assignments may be unlikely, it is reassuring to have five other spectra where B_3 is clearly assigned. Another example is the B_5 daughter which appears in nine different correlation spectra, in four of them as the major peak. In six cases there is some ambiguity, but in three the daughter B_5 is clearly assigned. As well A_n and D_n ions, and Z_m, V_m and W_m ions, often have identical, or very similar, masses.

Ambiguities may also arise in parent ion assignment. For example, B_6 and the internal fragment $Y_{19}B_7$+1 differ in mass by only 1 u, so both are included in the same peak in the neutral spectrum. Most of the ~20 daughter ion peaks could originate from either parent, but three can only come from B_6 and a different three only from $Y_{19}B_7$+1. Therefore both parent ions must be present. In such cases it is difficult to derive any sequence information from the data unless the one parent is much more likely than the other. Because the neutral peak, which is used for the correlations (see Appendix 2.6), is broadened in time due to kinetic energy released during metastable decay, the peaks of overlapping parent ions of low mass may be several u apart. For higher mass parent ions, which have poor signal to noise ratios, the neutral spectrum peaks are very wide and overlapping parent ions may be as much as 15 -20 u apart. Such overlap is usually a disadvantage, as mentioned. However, if the overlap is between two similar peptides with an amino acid interchange, it can provide an extremely simple and effective way of determining the nature and location of the interchange, as explained in §2.3.3.5 and Fig. 2.17.

The redundancy provided by measurements of daughter ion from a large set of parents, as in Table 2.1, thus leads to more accurate mass measurements and increased confidence in the assignments. The usual measurements may leave some uncertainty where possible residues differ by only one or two u, but such problems can be solved by bracketing the uncertain residue, as seen for the Glu_{18}/Gln_{18} case above, and impurity levels may sometimes be estimated, even for mass differences of one u. On the other hand, the ambiguity in the internal fragment parent ion identities renders most of their decay data useless for sequencing.

Although some peptide antibiotic series containing both charged and uncharged peptides have linear sequences for the neutral components and a cyclic structure for the charged ones [Tang '92], this is obviously not the case for the alamethicins observed.

2.3.4.2. Decay Pattern

As pointed out previously (§1.1.6, §2.2.3.2), bombardment of a *solid* target by primary ions at keV energies yields a variety of secondary ions at the target surface very similar to those produced by collisional activation of ions in a gas cell at similar energies. In particular, side chain fragmentations [Martin '87] are often observed, enabling leucine and isoleucine to be distinguished. In both methods continuous (or semicontinuous) sequences of one or more fragment ion species are normally produced, but in some cases our technique appears to be even more informative. For example, we were able to obtain considerable sequence information on the peptide dynorphin A, which has a large number of basic residues (five) in the central region of the molecule (§1.1.2). By comparison, an extensive investigation of the compound by tandem mass spectrometry, using both high energy CID of ions produced by LSIMS and low energy CID of electrosprayed ions, failed to yield any coherent series of fragments [Curtis '92].

Not only was sequence information gathered, but much fragmentation information was also obtained. The correlation technique uniquely allows one to acquire information on the decay of all metastable fragments, on all the neutral fragments, and on the prompt fragments simultaneously. This can be used to study both prompt and metastable fragmentation patterns.

A major part of the direct and correlated spectra consists of B_n ions, along with some of the complementary Y_m+2 ions, particularly the complementary pair B_{13}/Y_7+2. B_n ions are commonly found in N-acetylated peptides without basic residues, such as alamethicin III, in which the charge is delocalized [Johnson '88]. Formation of B_n and Y_m+2 ions for such peptides may be initiated by protonation at the amide nitrogens [Hunt '86], which have a competitively high proton affinity in a nonbasic peptide or by a delocalized proton [Kenny '92, Mueller '84].

It is clear that cleavage at Aib-Pro is favored in the alamethicins, especially from the intensity of the B_{13}/Y_7+2 pair of ions. The abundant internal fragment series $Y_{19}B_n$+1 and Y_7B_n+1 also correspond to cleavage at Pro_2 and Pro_{14}, respectively. Similar behavior is observed in studies of other peptides containing Aib-Pro bonds [Iida '90, Bruckner '84], and analogous effects are observed in some charged peptides [Martin '87, Hunt '86] and in nonbasic bradykinin derivatives [Bunk '91].

Measurements have shown that the proton affinity of Pro is exceeded only by Arg, Lys, and Glu [Gorman '92], and perhaps Gln [Wu '92]. (There is some disagreement between Amster's proton affinity results using the thermodynamic equilibria of isolated amino acids [Gorman '92] and other results using the less precise [Gorman '92, Wu '92] kinetic method for protonated peptides [Wu '92]. The latter measurements suggest Gln has a higher proton affinity than Pro, but the alamethicins show no evidence of this.) None of the first three residues mentioned is represented in alamethicin III. Neglecting the uncertain Gln, and because acetylation has reduced the proton affinity of the N-terminus, it might be argued that the charge is quite likely to reside on the amide nitrogen of Pro, leading to a preferred formation of the corresponding B_{13} and Y_7+2 ions, as observed in both prompt fragmentation and unimolecular decay. As mentioned above, however, basic peptides (*i.e.* those containing Arg and Lys) may also exhibit large amounts of cleavage at Pro, so proton affinities cannot be the only explanation for the lability of the bond. (For example, dynorphin A (§2.2) has no big peak at Pro_{10}, perhaps because the spectrum contains mostly A and C+2 ions and very few B ions, due to the large number of basic residues. As mentioned, however, this is an unusually basic peptide which does not behave as most peptides do (*eg.* see §1.1.2).) As discussed by Loo *et al.* [Loo '93], the behavior seems to be related to the great stability of peptide fragments containing Pro at the N-terminus. It may also be related to conformational changes induced by Pro [Loo '93]; such changes have been observed in the alamethicins [Fox '82] and are common.

For alamethicin III, this cleavage was observed for both metastable and prompt fragmentation. In both cases, the charge could be on either side of the broken bond, to give either B_{13} or Y_7+2 ions and either B_1 or Y_{19}+2 ions. B_{13} ions are favored over Y_7+2 ions in both prompt and metastable decay. Because Y_{19}+2 and B_1 are in different mass ranges, it is misleading to compare their peak intensities. However, the B_2 daughter ion spectrum shows that the Pro iminium ion is very strongly favored over the Aib iminium ion; these two ion peaks are the only significant ones present in this spectrum (see Table 2.1). It is not clear why the charge prefers to be on the Pro side of the bond in the one case (B_2 decay) and on the Aib side in the other case (cleavage of Aib_{13}-Pro_{14} bond), but this is undoubtedly due to the rest of the peptide in the latter case, and may be more directly related to the location of the proton and the nature of the cleavage in the former case. The X-ray crystal structure of alamethicin I shows that Pro introduces a bend in the helix [Fox

'82], and it is known that this is common. Perhaps such bends, which disrupt the stable helix form, also provide partial reason why the Pro bond is so labile. Such a dependence of fragmentation on secondary structure has been observed in FAB of peptaibols in organic solutions [Przybylski '85].

A related observation is the abundance of internal fragments series $Y_{19}B_n+1$, and Y_7B_n+1 ions, corresponding to cleavage at Pro_2 and Pro_{14} respectively.

The wealth of data accumulated allows some observations regarding the metastable decay of alamethicin and its prompt fragments. It is interesting to note that the direct spectrum peaks in Fig. 2.11a represent the total amount of each fragment ion *produced* (*i.e.* both the metastable decay products and the ions that reach the detector intact), although the peak intensities may also reflect some mass dependence of the detector efficiency of the microchannel plate detectors. The neutral peaks shown in Fig. 2.11b represent the amount of each prompt parent ion *decaying,* since they represent neutral daughters reaching detector 1 when the ion mirror field is on (§1.2.4.3). As is evident from Fig. 2.11, A_1 and B_1 exhibit less decay than average (probably because they contain no peptide bonds), and B_2 and Y_7+2 show more metastable decay than the rest of the fragments. The unusual susceptibility of B_2 to metastable decay confirms that the Aib-Pro bond is labile in the gas phase ion as well as during desorption/ionization and in solution chemistry. This is also shown by the internal fragment daughter ion series appearing in many of the correlation spectra. The slightly above average decay of the Y_7+2 ion is not understood.

The peptide maps shown in Table 2.1 also provide information regarding the decay of closely related ions. The uncertainties in the daughter ion assignments, as discussed in §2.3.4.1, are not a serious problem because the unusual daughter ions are less likely. Therefore, the intensity data for the B_n ions is expected to be valid in such cases. (On the other hand, ambiguities in the parent ion identity make it difficult to extract any meaningful fragmentation information from the decay data, so again the decay of the $Y_{19}B_n+1$ internal fragment ions (Table 2.1b) does not provide any conclusive data.)

Electron ionization (EI) stability data obtained many years ago [Biemann '62, see also Przybylski '84] indicate that fragments with C-terminal Aib residues are more stable than those with C-terminal Ala residues, and that peptides ending with Gln are much less stable. It is interesting to note that the amounts of *prompt* fragment ions produced do not seem to correspond to the stability considerations for EI gas phase dissociations, although

there is a low abundance of B_7 ions. However, the *metastable* fragments (as defined above, those arising from metastable decay) showed a correspondence with the EI gas phase stability data, suggesting that these data also apply to metastable decay. As can be seen in Table 2.1a, the daughter ions with Aib end groups are generally most abundant, and the daughter ions ending in Gln_7 are the least abundant. This is especially obvious when comparing the correlation spectra of the various different alamethicins (data not shown). Although these stability considerations do not seem to be valid for prompt ion formation in SIMS , they do seem to be valid in the FAB spectra of the paracelsins, which are similar to the alamethicins [Przybylski '84]. However, it is important to note that in the experiment with the paracelsins, a double focussing spectrometer was used; of course only the stable ions survived the flight through the spectrometer. On the other hand, in the direct TOF spectra examined for the alamethicins, *all* of the ions formed at the target are observed at the detector, not only the stable ones. Thus in the direct spectra, the amounts of fragment ions formed at the target are represented, not the gas phase stability. In the correlation spectra the gas phase stability is measured, however, and the data agrees with what is expected.

In the series of B_n ions, resulting from both prompt formation (direct and reflected spectra) and metastable decay (correlated spectra), B_7 has a very low abundance. This is not due to the metastable decay (*i.e.* the gas phase stability) of the B_7 ion, because its peak is small in both the neutral and the direct spectra; the probability for its *formation* is therefore low. The reason for this is not clear, but perhaps the amide group of Gln_7 reduces the proton affinity of the peptide bond nitrogen of residue 8 by non-bonding interactions, thus lowering the population of this form of decomposing ions.

As mentioned, the alamethicins have an anomalously large extent of metastable decay. We also observed such decay for a synthetic alamethicin in which Ala replaces all of the Aib residues and a carboxylic acid at the C-terminus replaces the alcohol. Data, similar to that described above for alamethicin III, were obtained for this synthetic alamethicin. They demonstrate that neither the Aib residues nor the terminal alcohol seems to be responsible for the tremendous amount of metastable decay. From previous work on alamethicin I and II [Chait '82, Pandey '77], it seems that the peptides containing Glu instead of Gln also undergo much decay. Thus the neutrality of the peptide does not seem to have an effect. However, the lack of basic residues in the peptide and of a basic NH_2 at the N-terminus

seem to be significant.

The fact that the peptide is not basic may also be related to the unusual intensities of sodiated molecular ion peaks in SIMS of all of the alamethicins, although it is just as likely to be related to the fact that the alamethicins form ion channels and therefore must have some special affinity for ions. The $[M+Na]^+$ and the $[M+K]^+$ ions are much more stable than the $[M+H]^+$ ions, but even so, the intensity of the cationized peaks is unusually high in comparison to the protonated peak, as the linear TOF data show. As pointed out in §2.3.3.1, the MALDI experiments on a mixture containing alamethicin III show explicitly that alamethicin III has a much higher affinity for Na^+ and K^+ than four other common peptides; only the alamethicin peak is cationized with almost no molecular ion present (even after rinsing in ice water as recommended by Beavis and Chait [Beavis '90]), and the other peaks are protonated and not cationized at all. Because alamethicins form ion channels, it is not unlikely that they would have a special affinity for ions such as Na^+ and K^+ and that these ions might stabilize the molecule in the gas phase. The results mentioned in §2.3.3.2.1 indicate that the cation may reside on one of the three C terminal residues, although the data is far from conclusive. A fragmentation process observed in FAB MS/MS of cationized peptides, in which the C-terminal residue is lost [Kulik '89], was not observed, presumably because this reaction is not favored for amino alcohols.

Varying degrees of cationization were also observed for alamethicin I [Chait '82], trichosporin-B[Iida '90], trichotoxin A-50 (although in this series of experiments the paracelsins showed no cationization at all) [Bruckner '84, Przybylski '84], the hypelcins [Fujita '84], and trichorzianine [Bodo '85]. No sodiation occurred in the synthetic alamethicin in which all of the Aib residues were converted to Ala residues, but because there was no sodium present in the sample at all, this is not significant. Similar effects were observed for nonbasic bradykinin derivatives [Bunk '91]. (The bradykinin showed $M^{\bullet+}$ ions rather than $[M+H]^+$ ions, but the alamethicins and other peptaibols show no evidence of this.)

As mentioned in §1.2, the flight time of a neutral daughter serves to identify its parent, *i.e.* a molecular ion or a "prompt fragment". The peaks in the neutral spectra are quite broad, e.g. ~190 ns for the $(M+H)^+$ ion corresponding to a mass resolution $M/\Delta M_{FWHM}$ ~75, consistent with previous results [Standing '88]. The peak width is determined mainly by the spread in velocity of the daughters produced by metastable decay; this results from the finite energy release in the disintegration. A "prompt fragment" can of course be

produced directly at the target by the primary ion impact. In addition, however, the fragment may itself be a product of the decay of a larger ion close to the target, as discussed in Appendix 2.6. For example, the B_{13} "prompt fragment" peak in the neutral spectrum defines B_{13} ions that are produced within ~100 ns after impact, and that subsequently decay in free flight. The low intensity of the B_n series ions beyond B_{13} indicates that any such ions produced at the target have lifetimes < 100 ns.

2.3.4.3. Correlation Technique

The principal advantage of the present method is seen in the large amount of data — all of the correlation spectra as well as the neutral and direct spectra — produced in a single experimental run. Since all daughter ions are produced at the same time, problems of normalization are minimized and the overall decay pattern shows up clearly. The redundancy provided is a considerable help in sequence determination.

A related advantage is the increased sensitivity inherent in the TOF correlation technique. Unlike in other spectrometers, ions are not lost when they decay, but can be used to obtain sequence information. The only scanning ever needed involves reducing the mirror voltage, and this is not often needed. Although ~5 nmol of sample were used on a target purely for convenience, we have previously reported [Tang '91, '90] that this technique is capable of giving almost complete daughter ion spectra from samples of ~200 femtomoles. However, if the smaller sample reduced the number of ions produced, we would have had to increase the primary ion current or else take data for a longer time.

A disadvantage is the limited resolution ($M/\Delta M < 100$ here) obtained for the neutral daughters which represent the parent ions; this is probably due partly to metastable decay both in and after the acceleration region (§1.2.4.3, §3.4.2 and appendix 2.6), as well as to the pulse widths of the I^- ion source (§1.4.1.1). This resolution is considerably lower than the resolution of MS-1 in most tandem spectrometers. Similar values to ours have been reported for TOF instruments where the parent ions are selected by opening a gate between the acceleration region and the mirror [Hoyes '94, Kaufmann '93], so the limit is not imposed by the correlation method; rather it is a result of selecting the parent in a linear TOF spectrometer. It may be possible to do better in a tandem TOF instrument where parent ions are selected after reflection [Cornish '93, Seeterlin '93], but at the cost of lower

sensitivity.

A second disadvantage is the large amount of time required for a run—several hours in general. Here there is an intrinsic limitation specific to the correlation technique; the overall counting rate must be limited to less than one correlated pair per pulse in order to define the correlated particle uniquely. However, the practical limitation at present is the speed of the data system, which restricts the counting rate to ≤ 4000 events/s. Consequently, the pulse repetition rate is limited to 4 kHz. In principle, this repetition rate is limited only by the longest flight time of interest. Recent improvements allow accelerating voltages up to 30 kV, and therefore shorter flight time, permitting a pulse repetition rate of 20 kHz. Thus an improvement in counting rate by a factor ~ 5 is expected with a faster data system, now under development; further improvements may be possible.

2.3.4.4. Comparison with other peptaibols

Various different families of fungal antibiotics, very similar to the alamethicins, have been analyzed by mass spectrometry and some results will be compared to the alamethicin results. The spectra observed by FAB MS and MS/MS techniques are similar to those obtained by TOF SIMS. For example, the hypelcins and the alamethicins which both contain Pro_2 give very similar spectra. The trichosporin-B's and the paracelsins contain Ala_2 in place of Pro_2, but are very similar to the alamethicins in other respects. Strong metastable decay, which can be exploited only by the TOF SIMS correlation method or theoretically by FTMS (but see the FTMS results below), is observed. A few primary sequences are shown in Table 2.3, and some of the mass spectrometry results will be discussed and compared to alamethicin results.

Alamethicin I, studied by TOF PDMS [Chait '82], also shows great affinity for Na, and even contains a substantial $[M+2Na-H]^+$ peak. A and D ion variants containing Na, B ions (except B_7) and C+2 ions occurred. Metastable decay occurred, as evidenced by the peak widths, but some daughter neutrals were probably lost due to the extremely long flight tube (3 m long, with an electrostatic particle guide). However, this could explain the absence of the metastable $[M+H]^+$ ion, which was present in our TOF SIMS results; perhaps excess Na was present in these experiments. The metastable B_{13} ion, which is very abundant in the TOF SIMS spectra, is also absent in these spectra. The $[M+H]^+$ ion does

Table 2.3 Sequences of some related peptaibols

Alamethicins and related peptaibols
The sequences are given in the usual single letter amino acid code: Ac=acetyl; ol=alcohol; A=Ala; B=Aib; E=Glu; F=Phe; G=Gly; I=Ile; J=Iva=isovaline; L=Leu; P=Pro; Q=Gln; S=Ser; V=Val

alamethicins
Ac-B_1-P_2-B_3-A_4-B_5-A_6-Q_7-B_8-V_9-B_{10}-G_{11}-L_{12}-B_{13}-P_{14}-V_{15}-B_{16}-B_{17}-E_{18}-Q_{19}-F_{20}-ol (I, 23.33a min fraction)
Ac-B_1-P_2-B_3-A_4-B_5-B_6-Q_7-B_8-V_9-B_{10}-G_{11}-L_{12}-B_{13}-P_{14}-V_{15}-B_{16}-B_{17}-E_{18}-Q_{19}-F_{20}-ol (II,)
Ac-B_1-P_2-B_3-A_4-B_5-A_6-Q_7-B_8-V_9-B_{10}-G_{11}-L_{12}-B_{13}-P_{14}-V_{15}-B_{16}-B_{17}-Q_{18}-Q_{19}-F_{20}-ol (III, 21.34 min fraction)
Ac-B_1-P_2-B_3-A_4-B_5-B_6-Q_7-B_8-V_9-B_{10}-G_{11}-L_{12}-B_{13}-P_{14}-V_{15}-B_{16}-B_{17}-Q_{18}-Q_{19}-F_{20}-ol (23.33b min fraction)

Ac-B_1-P_2-B_3-A_4-B_5-A_6-Q_7-B_8-V_9-B_{10}-G_{11}-L_{12}-B_{13}-P_{14}-V_{15}-B_{16}-B_{17}-E_{18}-Q_{19}-F_{20}-ol {alam I}
Ac-B_1-P_2-B_3-$\underline{B_4}$-$\underline{A_5}$-$\underline{B_6}$-Q_7-B_8-$\underline{B_9}$-B_{10}-G_{11}-L_{12}-B_{13}-P_{14}-V_{15}-$\underline{V_{16}}$-$\underline{V_{17}}$-$\underline{Q_{18}}$-Q_{19}-F_{20}-ol {all the different substitutions that have been observed so far, Pandey and Rhinehart, Bruckner et al, and Konig and Ayden. Note that this is not a sequence, but merely shows which amino acids have been interchanged, and at which locations. Compare table 2.2}

hypelcins [Fujita '84]
Ac-B_1-P_2-B_3-A_4-B_5-B_6-Q_7-B_8-L_9-B_{10}-G_{11}-B_{12}-B_{13}-P_{14}-V_{15}-B_{16}-B_{17}-Q_{18}-Q_{19}-L_{20}-ol (A-I(1))
Ac-B_1-P_2-B_3-A_4-B_5-A_6-Q_7-B_8-L_9-B_{10}-G_{11}-B_{12}-B_{13}-P_{14}-V_{15}-B_{16}-B_{17}-Q_{18}-Q_{19}-L_{20}-ol (A-II(2))
Ac-B_1-P_2-B_3-A_4-B_5-B_6-Q_7-B_8-L_9-B_{10}-G_{11}-B_{12}-B_{13}-P_{14}-V_{15}-B_{16}-B_{17}-Q_{18}-Q_{19}-($C_7H_{16}NO$)-ol (A-III(3))
Ac-B_1-P_2-B_3-A_4-B_5-B_6-Q_7-B_8-I_9-B_{10}-G_{11}-B_{12}-B_{13}-P_{14}-V_{15}-B_{16}-B_{17}-Q_{18}-Q_{19}-L_{20}-ol (A-IV(4))
Ac-B_1-P_2-B_3-A_4-B_5-B_6-Q_7-L_8-B_9-G_{10}-B_{11}-B_{12}-B_{13}-P_{14}-V_{15}-B_{16}-B_{17}-Q_{18}-Q_{19}-L_{20}-ol (A (5))

paracelsins [Bruckner '84]
Ac-B_1-A_2-B_3-A_4-B_5-A_6-Q_7-B_8-V_9-B_{10}-G_{11}-B_{12}-B_{13}-P_{14}-V_{15}-B_{16}-B_{17}-Q_{18}-Q_{19}-F_{20}-ol (A)
Ac-B_1-A_2-B_3-A_4-B_5-A_6-Q_7-B_8-L_9-B_{10}-G_{11}-B_{12}-B_{13}-P_{14}-V_{15}-B_{16}-B_{17}-Q_{18}-Q_{19}-F_{20}-ol (B)
Ac-B_1-A_2-B_3-A_4-B_5-B_6-Q_7-B_8-V_9-B_{10}-G_{11}-B_{12}-B_{13}-P_{14}-V_{15}-B_{16}-B_{17}-Q_{18}-Q_{19}-F_{20}-ol (C)
Ac-B_1-A_2-B_3-A_4-B_5-B_6-Q_7-B_8-L_9-B_{10}-G_{11}-B_{12}-B_{13}-P_{14}-V_{15}-B_{16}-B_{17}-Q_{18}-Q_{19}-F_{20}-ol (D)

trichosporin-Bs [Iida '90]
Ac-B_1-A_2-S_3-A_4-B_5-B_6-Q_7-B_8-L_9-B_{10}-G_{11}-L_{12}-B_{13}-P_{14}-V_{15}-B_{16}-B_{17}-Q_{18}-Q_{19}-F_{20}-ol (TS-B-Ia)
Ac-B_1-A_2-A_3-A_4-B_5-B_6-Q_7-B_8-L_9-B_{10}-G_{11}-L_{12}-B_{13}-P_{14}-V_{15}-B_{16}-B_{17}-Q_{18}-Q_{19}-F_{20}-ol (TS-B-IIIa)
Ac-B_1-A_2-A_3-A_4-B_5-B_6-Q_7-B_8-I_9-B_{10}-G_{11}-L_{12}-B_{13}-P_{14}-V_{15}-B_{16}-A_{17}-Q_{18}-Q_{19}-F_{20}-ol (TS-B-IIIb)
Ac-B_1-A_2-A_3-A_4-A_5-B_6-Q_7-B_8-I_9-B_{10}-G_{11}-L_{12}-B_{13}-P_{14}-V_{15}-B_{16}-B_{17}-Q_{18}-Q_{19}-F_{20}-ol (TS-B-IIIc)
Ac-B_1-A_2-A_3-A_4-B_5-B_6-Q_7-B_8-V_9-B_{10}-G_{11}-L_{12}-B_{13}-P_{14}-V_{15}-B_{16}-B_{17}-Q_{18}-Q_{19}-F_{20}-ol (TS-B-IIId)
Ac-B_1-A_2-A_3-A_4-B_5-B_6-Q_7-B_8-L_9-B_{10}-G_{11}-L_{12}-B_{13}-P_{14}-V_{15}-B_{16}-J_{17}-Q_{18}-Q_{19}-F_{20}-ol (TS-B-IVb)
Ac-B_1-A_2-B_3-A_4-B_5-B_6-Q_7-B_8-V_9-B_{10}-G_{11}-L_{12}-B_{13}-P_{14}-V_{15}-B_{16}-B_{17}-Q_{18}-Q_{19}-F_{20}-ol (TS-B-IVc)
Ac-B_1-A_2-A_3-A_4-B_5-B_6-Q_7-B_8-V_9-B_{10}-G_{11}-L_{12}-B_{13}-P_{14}-V_{15}-B_{16}-J_{17}-Q_{18}-Q_{19}-F_{20}-ol (TS-B-IVd)
Ac-B_1-A_2-A_3-A_4-B_5-B_6-Q_7-B_8-I_9-B_{10}-G_{11}-L_{12}-B_{13}-P_{14}-V_{15}-B_{16}-B_{17}-Q_{18}-Q_{19}-F_{20}-ol (TS-B-V)
Ac-B_1-A_2-B_3-A_4-B_5-B_6-Q_7-B_8-I_9-B_{10}-G_{11}-L_{12}-B_{13}-P_{14}-V_{15}-B_{16}-B_{17}-Q_{18}-Q_{19}-F_{20}-ol (TS-B-VIa)
Ac-B_1-A_2-A_3-A_4-B_5-B_6-Q_7-B_8-I_9-B_{10}-G_{11}-L_{12}-B_{13}-P_{14}-V_{15}-B_{16}-J_{17}-Q_{18}-Q_{19}-F_{20}-ol (TS-B-VIb)

not appear in spectra of alamethicins I and II using PD FTMS [Loo '87] either, presumably because of the time between ion formation and detection (1-2 min collection time, during which any metastable decay results in fragment ions in the spectrum; 6 ms rf excitation pulse; 65 ms detection time). There are very few fragment ions in this spectrum compared to the TOF PDMS spectra, however, and the authors suggest that is due to the time differences involved. On the other hand, it is remotely possible that the excess Na present in the TOF study and the K added in the FTMS experiments may have inhibited the formation of the $[M+H]^+$ ion. In comparison, TOF SIMS results in the direct spectra show the $[M+H]^+$ and other ion peaks clearly, and in the correlation spectra they provide sequence information; thus *much* less information is lost in our technique.

Hypelcin A, which is crystalline and uniform in thin layer chromatography (*i.e.* it seems pure), has been shown to be a mixture of peptides using FAB MS, NMR, HPLC and amino acid analysis [Fujita '84]. The hypelcins differ from the alamethicins at essentially three positions, residues 9, 12 and 20 (except for hypelcin A5 in which several pairs of adjacent amino acids are reversed), as shown in Table 2.3. None of these residues is expected to influence the mass spectrum very much. FAB-MS of each of the peptides showed the $[M+Na]^+$ and $[M+K]^+$ ions and three series of fragment peaks: the B ions up to B_{13}; a series of Y_7B_m+1 ions (m=15-19) ending with Y_7+2, and a series of $Y_{19}B_m+1$ ions (m=3-8, sometimes 9,10,11,12; if m=7, the peak is $Y_{19}B_7+0$). Leucine and isoleucine were distinguished by amino acid analysis. The metastable $[M+H]^+$ was not observed and many of the fragments were of low intensity, presumably due to decay in the spectrometer.

Leu-paracelsin, which differs from the alamethicins at residues 2, 9 and 12, has been examined using TOF PDMS and shows many similar spectral features [Buko '90]. Of course, since Pro_2 is not present, the internal fragment series $Y_{19}B_m+1$ is not expected, although the Y_7B_m+1 series is expected because Pro_{14} is present. The direct spectrum contains predominantly B ions up to B_{13}, excepting B_7. Although the published spectrum contains many other peaks, these are not identified. In the molecular ion region only the $[M+Na]^+$ peak was identified in the spectrum, although its shoulder suggests a $[M+H]^+$ peak. [Note: the BIOION 20 TOF MS used has a short flight tube length (only 14 cm) and an acceleration voltage of 19 kV, which could explain such poor resolution to some extent.] It is interesting to note that the non-peptaibol peptides in this study exhibited only the $[M+H]^+$ ion and no cationized species. All of the B ions up to position 13 are noted, and

Y_7+2 can be seen as well; very few other peaks seem to occur, suggesting that the Y_7B_m+1 series may decay more easily than the B ion series. Strong metastable decay was evidenced by the comparatively wide peaks. In another study of paracelsin using HPLC and FAB on a double focussing spectrometer, however, the $[M+H]^+$ ion is observed but no sodium adduct is seen, perhaps due to redistilling the HPLC eluents (although the similar peptaibol trichotoxin, which was also studied in these experiments using redistilled eluents, did contain a $[M+Na]^+$ peak) [Bruckner '84].

The trichosporin-Bs differ from the alamethicins at positions 2, 3, 9, and 17 and are otherwise quite similar [Iida '90]. The Ala_2 which replaces Pro_2, does not encourage internal sequence formation. Thus, in comparison with alamethicin III, the spectrum is simplified and contains less sequence information, but only due to the nature of the peptide, not due to the capabilities of the technique. It is instructive to compare the FAB MS and FAB MS/MS results reported for trichosporin-B-VIb with the TOF SIMS and TOF SIMS correlation results obtained for alamethicin III. Note that in the comparison (Table 2.4) peaks due to internal cleavage at Pro_2 in alamethicin are ignored because no such peaks are expected for the trichosporins.

It is evident from Table 2.4 that more information is available from TOF SIMS than from FAB MS, as has been reported previously. This is probably due to the larger energy transfer in a solid target compared to a liquid one, which leads to more sequence-specific fragmentation, although a difference in spectrometers also plays a role [Ens '93]. The extensive B_n ion data present in the TOF SIMS results provided a significant advantage in sequencing and reduced the need for extensive amounts of correlation data, although these data were obviously still necessary to refine and confirm the sequence. In FAB, sequence information on residues 7 to 20 could only be obtained from MS/MS experiments.

In the daughter ion spectra a larger amount of data is reported for alamethicin III compared to that reported for the trichosporin-B-VIb This is probably due to loss of metastable decay ions in the FAB MS/MS study. On the other hand, we can expect that the TOF SIMS correlation results, especially those with just one mirror voltage, have much worse resolution, leading to some difficulties in sequence determination as repeatedly noted above. Note that in FAB MS/MS, even when using a triple quadrupole spectrometer, it is possible to choose only the parent ion, whereas in the TOF-SIMS correlation method one must set a window on a broad neutral peak, which may include more than one parent

Table 2.4 FAB MS and MS/MS of a Trichosporin [Iida '90] compared to SIMS (direct and correlated spectra) of an Alamethicin

Entire spectrum
FAB MS: Bn, n=1-6,8,10,13; Y7+2; $[M+Na]^+$; some unidentified low mass and molecular ion region peaks
TOF SIMS direct spectrum**[1]; Bn, n=1-14; Y7+2; $[M+Na]^+$; $[M+H]^+$; $[M+K]^+$;Aib, Pro, Gln and Leu imminium ions; many small B_n, Y_7B_n+1, A_n, C_n+2, D_n, Y_m+2 (besides the Y_m+2 ions mentioned above), Z_m, V_m and W_m ions are observed, but they are all small and exhibit much overlap and are therefore considered to be unreliable.

$[M+H]^+$ daughters
FAB MS/MS: "no acceptable results"
corr-TOF SIMS**: Bn, n=8-13; A11,D9[2]*, Y7+2

B13 daughters
FAB MS/MS: Bn, n=8-13 and A12 or D12; the spectrum was shown from 600u to 1177u
corr-TOF SIMS**: Bn, n=4-12; A8, C8+2* or D9??

B8 daughters
FAB MS/MS: Bn, n=1-8; also some unlabelled peaks
corr-TOF SIMS**: Bn, n=3-7; An, n=3-6; C6+2; also some unidentified peaks

Y7+2 daughters
FAB MS/MS: Y7Bn+1, n=15-19; Y7A15+1, Y7+2
corr-TOF SIMS: Y7Bn+1, n=15-19; Y7A17+1 or Y7D16+1;Y7A18+1; Y7C17+1; Z3; Y3+2; Y7D19+1; other small Y7A15+1, n=15-18; note that the resolution of these peaks was quite poor

Y7B15+1 daughters
FAB MS/MS: Pro immonium; Y7B14+1; Y7A15+1
corr-TOF SIMS: the parent peak overlaps with A1, and the daughters present are diagnostic of A1

[1] **Note: These lists ignore the internal fragment peaks due to alamethicin cleavage at Pro2 which are irrelevant in the comparison, because no such cleavage is expected at trichosporin's Ala2.

[2] *this ion coincided with another peak expected due to cleavage at Pro2, so its assignment is not certain.

(§2.4.2). Although this may not always be a disadvantage (§2.3.3.5), it usually is. A comparison of the Y_7+2 peaks for the two peptaibols highlights the advantages of having a collision cell, good resolution throughout the mass range, and a large beam current. The daughter ion spectrum is very clear and informative for the trichosporins, whereas the TOF SIMS spectrum is obviously less informative (Fig. 2.14). Note that this is the among the worst spectra analyzed in these experiments. However, as mentioned, the TOF SIMS technique is more sensitive, because the metastable decay ions are not lost, because mass scanning is not necessary, and because of the data logging technique which allows decay information to be obtained on *every* decaying ion in the spectrum without repeating an experiment. FAB was no more successful at differentiating Leu and Ile than TOF SIMS was; these were differentiated by variants of NMR spectroscopy. Iva and Val were also explicitly differentiated by these techniques [Iida '90], unlike in the alamethicin work where this was not done.

2.3.5 CONCLUSION

Alamethicin III, like the two alamethicins known previously, has eight α-aminoisobutyric acid residues, an acetyl group at the N-terminus, and a phenylalaninol at the C-terminus. It has neither acidic nor basic residues, unlike alamethicins I and II which have an acidic residue. Its sequence, from mass spectrometry alone, is

Ac-Aib$_1$-Pro$_2$-Aib$_3$-Ala$_4$-Aib$_5$-Ala$_6$-Gln$_7$-Aib$_8$-Val$_9$-Aib$_{10}$-

Gly$_{11}$-(Leu/*Ile*)$_{12}$-Aib$_{13}$-Pro$_{14}$-Val$_{15}$-Aib$_{16}$-Aib$_{17}$-Gln$_{18}$-Gln$_{19}$-Phe$_{20}$-ol

This sequence agrees with the NMR data, which reveal that residue 12 is Leu and confirm that Val is present instead of Iva. Sequences are proposed for a number of the minor components of the mixture produced by the fungus. In addition, the data yielded by the TOF correlation technique have given an improved understanding of the fragmentation processes taking place in these compounds.

CHAPTER 3

SIMS OF LANGMUIR BLODGETT FILMS

3.1 FUNDAMENTALS

In ion bombardment as used in SIMS, a primary particle (ion or neutral) strikes a surface with several keV energy, disrupts the surface, and produces neutral and ionized secondary species. How this process can result in the desorption and ionization of large, labile biomolecules has not yet been elucidated, although many experimental investigations have been performed [Ens '93]. Much progress has, however, been made in the closely related sputtering theory of inorganic species from a solid target.

3.1.1 PRODUCTION OF SECONDARY IONS

The collision cascade model [Sigmund '72, '77, '81], which is the best-supported description of the sputtering process, explains the interactions of an incident particle and a monoelemental target mathematically. In this model, the incident particle undergoes elastic, binary collisions with target atoms until it comes to rest. Because the velocity of the incident ion is considerably less than that of the target electrons (the Bohr velocity), the incident particle interacts with the target atom as a whole (i.e. with its center of mass). In fact, because neither momentum nor energy is transferred from the incident ion to the target *electrons* (*i.e.* atoms are neither excited nor ionized), the collisions are considered to be elastic. The target atoms are considered to be free and at rest, because their binding and initial kinetic energies are small compared to the kinetic energy of the incident particle.

Target atoms which are set in motion by the incident particle collide with other molecules and generate a "collision cascade". In the case of a "spike", all (not just a small fraction) of the atoms within a certain volume are in motion; much energy is dissipated in a smaller volume than occurs in a spike, and the ions all share a high level of energy. By some definitions, the disturbance is a spike if the average energy in this volume is greater than the minimum energy necessary for a sputtering event. When the excitation (*i.e.* the cascade or the spike) intersects the surface with enough energy, sputtering (which refers to removal of mass from the target) of target atoms occurs.

The most successful description of the origin of the charge of large organic molecules is the qualitative precursor model [Benninghoven '83] which states that a precursor is formed at the target surface and is desorbed in a very short period of time ($<10^{-9}$ s) by a very fast ($<10^{-12}$ s) transfer of small amounts of kinetic energy. (Larger amounts of kinetic energy transferred to the molecule cause fragmentation.) The precursor tends to conserve its charge sign. Precursor formation is strongly influenced by the chemical composition of the surface, which in turn is determined by the substrate, by its pretreatment, and by sample deposition conditions. Noble metals, especially Ag, provide better $[M+H]^+$ yield than the reactive metals which often bind to organic molecules. (As mentioned, nitrocellulose is an even more favorable substrate, probably because it affects desorption.)

The bombarding particle properties, such as mass, energy, and charge have less pronounced effects on the nature of the spectrum than the target surface does [Ens '93]. In fact, a comparison of spectra resulting from particle induced desorption methods at keV and MeV energies led to the conclusion that desorption / ionization is an *indirect* result of the excitation induced by the primary ions, such as spikes and collision cascades. Other data suggest that thermal spikes are more likely than linear collision cascades to cause desorption. Secondary ion yields and mass range do increase for primary ions with increased energy, higher mass [Zhou '93, Benninghoven '87] and a more glancing incident angle [Ens '93]. It is interesting that the chemical reactivity of the primary ions can influence the spectrum (§3.4).

Primary ion-induced emission of secondary ions is the basis for SIMS. Because each incident particle damages an area of the target as well as causing desorption, the primary ion current must be very low when examining targets of large fragile molecules in order to prevent unnecessary damage. Under these conditions (static SIMS) the primary ion

current density is $\leq 10^{-9}$ A/cm^2, with a total primary ion dose of $\leq 10^{12}$ to 10^{13} /cm^2 [Benninghoven '76].

3.2 CONTRIBUTIONS FROM LANGMUIR-BLODGETT FILM STUDIES

A promising way to study the desorption/ionization of organic molecules by keV ion bombardment is to use SIMS on a molecularly organized system. Such systems exist and can be prepared as SIMS targets using the Langmuir Blodgett (LB) technique described below. The resulting targets have a definite number of monomolecular layers of vertically-aligned fatty acids, fatty acid salts, or other amphiphilic molecules.

In this work we made LB films of different thicknesses of stearic acid / Cd stearate (as well as the deuterated films) to study prompt and metastable fragmentation and the yield versus thickness of molecular ions and prompt fragments. The goal of the experiments, studying energy deposition at different depths, was not achieved but much preliminary information was obtained.

The integrity of LB films depends strongly on the conditions of their preparation [Peterson '90, Veale '85, Hasmonay '80, Kuhn '72, Spink '67, Gaines '66, Gaines '60], and unfortunately not all SIMS-LB experiments meet the stringent recommendations of those most successful in the field [Kuhn '72].

3.2.1 LANGMUIR-BLODGETT MULTILAYERS: AN INTRODUCTION

Oil films can be spread very easily on water as has been known for many centuries. To produce a highly ordered layer of aligned molecules, however, requires careful attention to detail and cleanliness [Peterson '90, Agarwal '88, Tredgold '87, Hasmonay '80, Kuhn '72, Gaines '66, Blodgett '34, '35, '37a, '37b]. Many kinds of molecules can be used to produce monolayer films: fatty acids, fatty acid salts, polymers, proteins, dyes, porphyrins, phthalocyanines and aromatic molecules [Peterson '90, Hann '90]. Monolayers, which are

like 2-dimensional analogues of 3-dimensional materials, exhibit 'solid', 'liquid' and 'gas'-like phases as evident in Fig. 3.1, where the steepest slope represents a 'solid' phase and the less steep slopes a 'liquid' and 'gas' phase. Other phases have been identified (often involving tilting of the hydrocarbon chains, stripe structures and buckling) [Bourdieu '94a, Bourdieu '94b, D. Schwartz '94a, D. Schwartz '94b, Bourdieu '93, Ruiz-Garcia '93, Henon '91, Qiu '91, Lin '90, Neuman '84] but we will only discuss the three main phases, realizing that they are idealizations and may, depending on experimental conditions, contain domains of other, more subtle, phases [Peterson '90]. Discontinuities and differences in orientation of the hydrocarbon tails are common, and it turns out that monolayers are quite similar to smectic liquid crystals [Peterson '90].

In the 'solid' phase, the molecules are aligned perpendicular to the water surface with the carboxylic 'heads' in the water and the hydrocarbon 'tails' above it often in a hexagonal close packing configuration [*eg.* Lin '90, Kuhn '72]. The average molecular area in the plane of the water is ~0.205 nm^2 and is similar to the molecular cross section which is ~0.185 nm^2 [Shaw '70]. Recently it has been shown [D. Schwartz '93] that the area per molecule is primarily controlled by the counter ion, added to the subphase, which becomes associated with the film itself. The lattice dimensions and the symmetry are influenced by alkane chain close packing.

In the 'liquid' or expanded phase, the surface area occupied by each molecule is several times larger than the molecular cross section but the film is still coherent and homogenous. Physically, the molecule's head is in the water, and its tail is randomly intertwined with those of its neighbors. Lower temperatures may 'freeze' a 'liquid' monolayer into a 'solid' one. Some suggest that the film is not homogenous but that hydrogen bonding between the head groups, or van der Waals' or dipole-dipole forces (also known as dispersion forces [Barker '91]) between the hydrocarbon chains keeps small islands of film together [*eg.* Schlossman '91, Ries '55]. Some such results may occur near phase transitions, and some have been attributed to experimental artifacts [Ferestehkhou '86, Sheppard '64, Ries '55].

In the 'gas' phase, the molecules are independent; their heads are in the water and their tails may lie nearly flat. Thus they each take up a larger surface area of ~1-2 nm^2 [Gaines '66]. Their behavior approaches that of a two dimensional analogue of the three dimensional ideal gas law at molecular areas of ~50 nm^2 (if the interaction with the aqueous

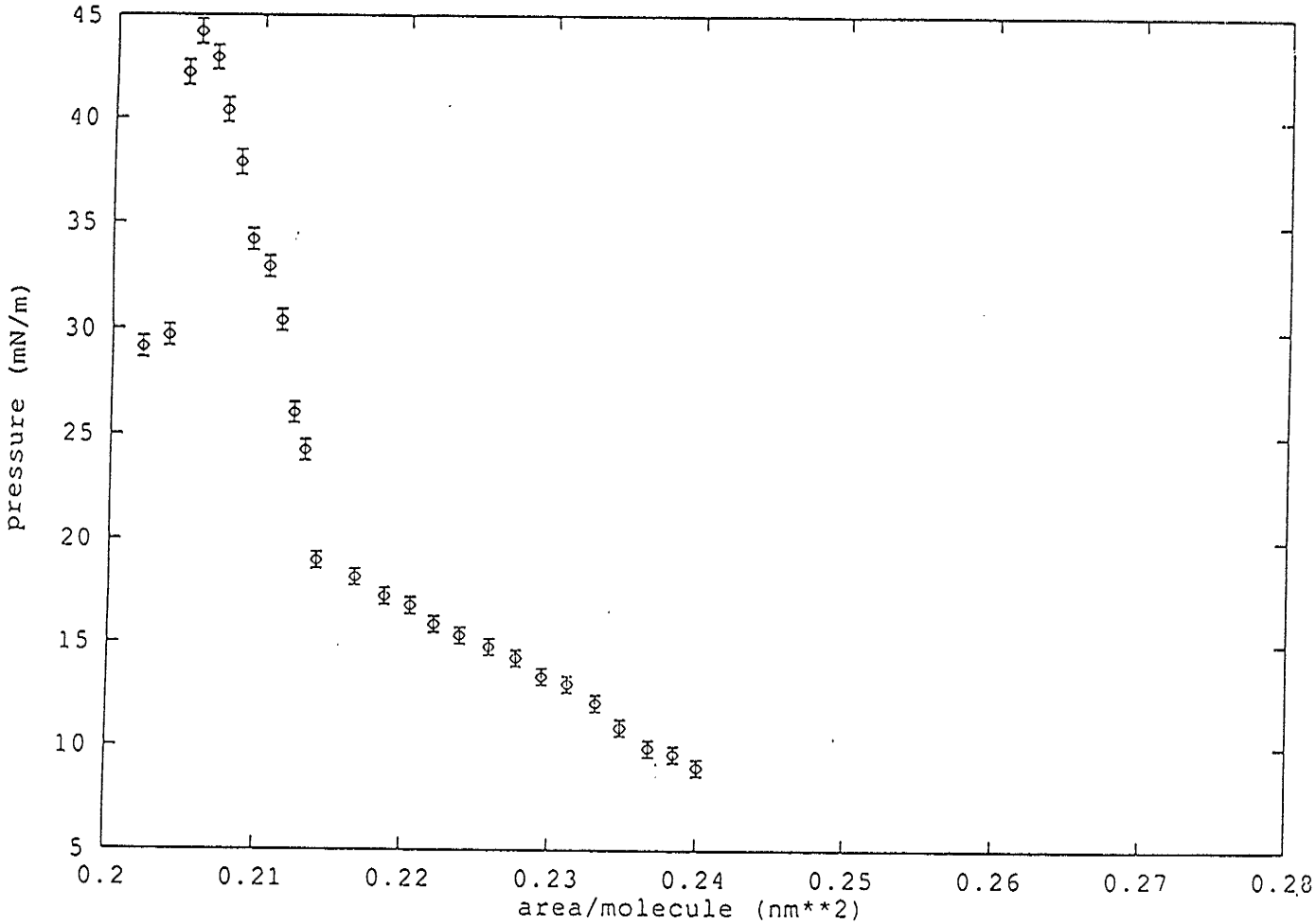

Fig. 3.1 Pressure area diagram of stearic acid on a subphase containing 5 x 10^{-4} M $CdCl_2$. (Errors in the area / molecule may be considerable, but do not affect the shape of the curve. See Appendix 3.1.)

subphase is ignored). Such a huge area is necessary for this approximation because the ideal gas law requires that the molecules must be of negligible size.

A monolayer in the 'solid' phase can be built up onto a slide using the Langmuir-Blodgett dipping technique shown in Fig. 3.2. While the surface pressure (§3.3.3.2.2) is kept constant (§3.3.3.2) a clean slide is dipped into the water. Depending on its surface properties it will attract its first layer when it is dipped into the subphase (hydrophobic slide) or when it is pulled from the subphase (hydrophilic slide) Once the first monolayer has been deposited, the slide gains another monolayer each time it passes through the surface, and a multilayer film of well-organized, ordered monomolecular layers is produced. Such films are called Y multilayers; those which are coated only on immersion are X layer films, and those coated only on emersion are Z-layer films [Peterson '90, Popowitz-Biro '88, Gaines '66].

The X, Y, or Z nature of film deposition depends strongly on the aqueous subphase, especially its pH and the concentration of any counter ions present [Hasmonay '80]. To determine this experimentally, the transfer ratio τ

$$\tau = \frac{\text{area of ML removed from the subphase}}{\text{coated substrate area}} \qquad (3.1)$$

is determined by measuring the change of monolayer area at constant surface pressure. In pure Y films $\tau_{up}=\tau_{down}=1$. XY films are defined by $\tau_{up}<\tau_{down}=1$; it seems that many fatty acid salts gradually develop some X type characteristics after many layers of the LB film have been deposited [Honig '74]. The value of τ is also affected by the LB substrate.

Obviously, coating films one molecule thick is a delicate procedure. The aqueous subphase, the monolayer itself, and the substrate to be coated must be as clean as possible. This requires a dust free working area. As well it requires careful cleaning of equipment subphase and substrate. Vibrations must be avoided to prevent breakage of the monolayer during coating; otherwise the coated film will have striations of thicker and thinner films than expected. The choice of counter ion, subphase pH, surface pressure during coating, dipping speed and film substrate all influence the resulting multilayer structure [*eg.* Peterson '90, Bolbach '88a, Hasmonay '80, Spink '67, Gaines '66]. Even though films have been shown to be quite stable outside vacuum [Peterson '90], they should be stored carefully in

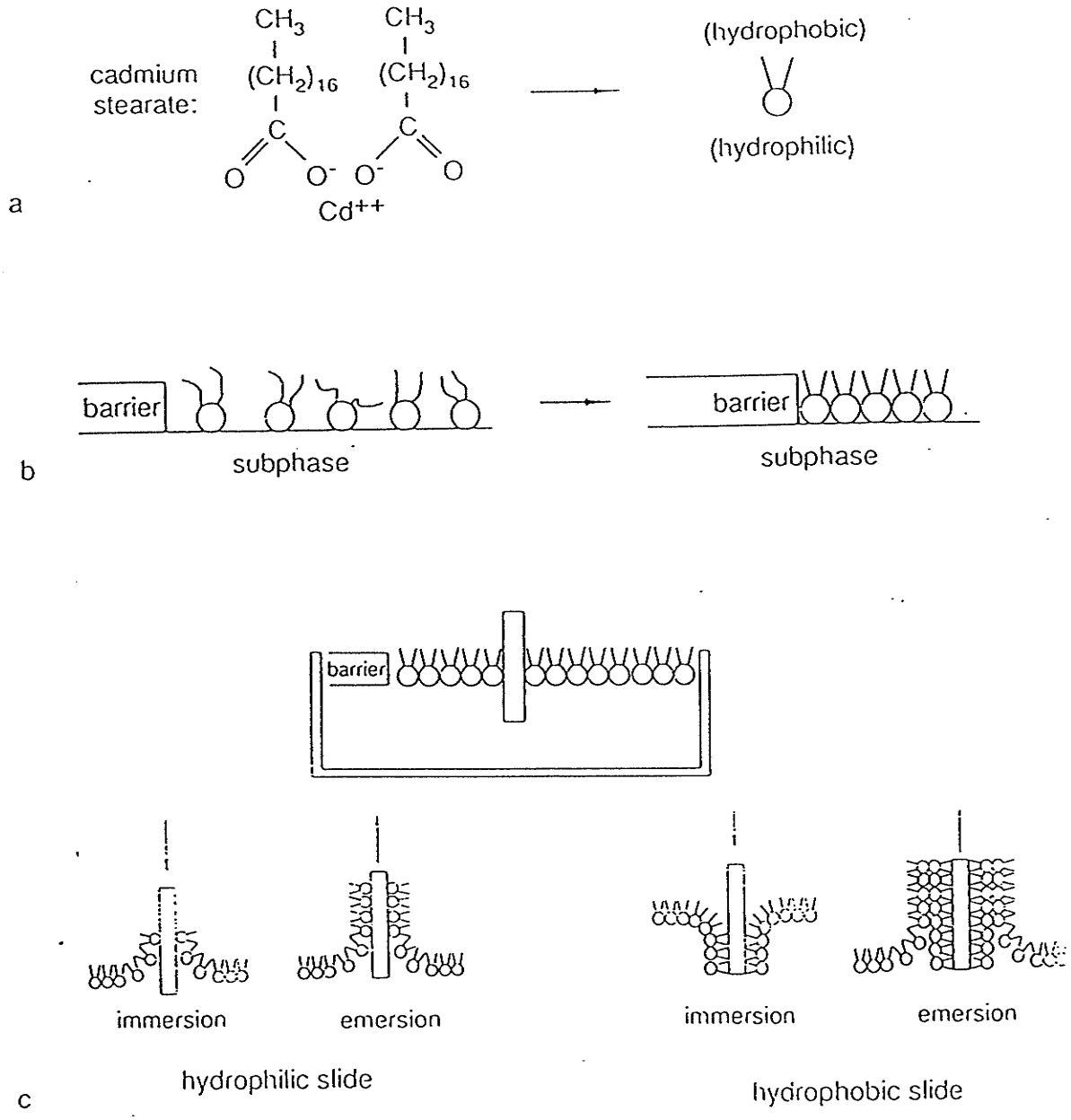

Fig. 3.2 Dipping Langmuir-Blodgett films. a) example of the molecules used, b) compression of the monolayer, c) coating of the LB film.

a clean environment, and used as soon as possible.

3.2.2 EXPERIMENTAL RESULTS FOR SIMS OF LBML'S

The tacit assumption in SIMS of LB films has always been that the film structure has few imperfections and can be used as a model surface. This has been tested, with varying degrees of rigor, by many investigators using a variety of methods: the value of the transfer ratio τ (§3.2.1)[*eg.* Spink '67, Gaines '66], the value of the contact angle θ (§3.3.3.2.2) throughout monolayer coating [Hasmonay '80], radiography [Spink '67, Gaines '60], ellipsometry [Henon '91], energy transfers across LB layers using dyes and fluorescence [Kuhn '72], fluorescence microscopy [*eg.* Meller '88], x-ray diffraction [Dutta '87], electron microscopy [Ferestehkou '86, Neuman '84, Spink '67, Sheppard '64], electron diffraction [Peterson '83, Kuhn '72], LB film capacitance and conductivity (which are very sensitive to defects and inhomogeneities) [Peterson '90, Kuhn '72], atomic force microscopy [Florsheimer '93, D. Schwartz '93a, D.Schwartz '93b, Ulman '91, Burnham 90], and other more specialized techniques [Hickel '89].

Some recent work using atomic force microscopy (note that the scanning tip affects the film [Florsheimer '93]) and fluorescence microscopy (note that the fluorescent material added may affect the monolayer behavior) shows defect structures (holes in a bilayer, dislocations) [Bourdieu '91]. Stripe textures, film buckling and other larger scale film textures have been reported and it is uncertain whether they represent new phases or are unexplained defects [Bourdieu '94a, Bourdieu '94b, D.Schwartz '94a, D.Schwartz '94b, Zasadzinski '94, Bourdieu '93, Ruiz-Garcia '93]. Significant substrate effects have also been reported [D. Schwartz '93], although reports of film disorder do not always take this into account [*eg.* Kinzler '94]. Evidence of subtle phase changes on the water [Qiu '91, Schlossman '91, Seul '90] and even in the meniscus during LBML coating [Riegler '88] have also been found. One study [Bourdieu '91] of arachidic acid / barium arachidate (the experimental conditions suggest a mixture [Hasmonay '80]) showed that μm defects occurred in this bilayer and also clearly showed dislocation pairs, characteristic of 2D solids and related to melting. Unfortunately, since many of the ML characterization papers do not report the recommended [Kuhn '72] extreme care in LB film preparation, some of the

reported results may have been influenced by the film preparation conditions, and it is difficult to judge their validity. (The characterization methods are discussed in most LB film reviews as well as elsewhere [*eg.* McConnell '91, Mohwald '90, and many of those mentioned elsewhere in this chapter])

3.2.2.1 Mohwald, Laxhuber and Coworkers

Mohwald, Laxhuber et al have used LB films in several dynamic SIMS studies [Laxhuber '83] and determined the SIMS depth resolution to be ~1 nm [Laxhuber '84]. Evidence of the primary ion backscattering off the LB film substrate was observed [Wittmaack '87]. They also concluded that the ion escape depth in an organic matrix is below 2.5 nm, and that the amount of substrate sputtered within a given time depends on the thickness of the LBML on it. For normal incident Ar^+ (2.5 keV), the damage cross section for organic molecules is ~1.25 nm^2; in the dynamic SIMS mode, the decay of the organic ion signal is due to damage, not to sputtering.

3.2.2.2 Bolbach and Coworkers

Bolbach and various coworkers have contributed extensively to this field with carefully controlled and performed static SIMS experiments. In an early paper [Bolbach '85], they noted that the $[M-H]^-$ ion is very unstable, even for a 9 layer film on Ag. The Ag substrate ions ejected from a ML-covered surface have a different angular distribution from, and slightly less energy than, those ejected from an uncovered surface. This suggested that substrate ions may channel through the LB film in the space between the carbon chains. Later studies [Bolbach '88] of Cd stearate LB films on various surfaces in SIMS lead to the following conclusions: the $[M-H]^-$ yield decreases with increasing ML coverage for noble metals and approaches a plateau at $\geq$ 8 ML coverage. (The noble metals are most suitable for studying the thickness effect in SIMS because, for reactive substrates, chemical effects may dominate.) Here keV experiments were compared to similar experiments using MeV incident ions in which the yield of $[M-H]^-$ increases with film thickness. The difference in behaviors was attributed to the presence of collision cascades in the metal

substrate under keV bombardment and their absence under MeV bombardment, although this interpretation has been disputed [Galera '91]. The dependence of yield on sample thickness is valid for other organic samples examined by SIMS and PDMS, and is why SIMS samples are thin and PDMS samples are thick.

In another set of experiments [Galera '91, Bolbach '89] multilayer LB films were made under very carefully controlled conditions, and analyzed at several angles and 2 energies, with known primary ion beam spot sizes. The data for primary ions impacting the target at a 20° angle of incidence suggest that the ejection and damage volume associated with primary ion impact is a cylinder (~1.9 nm radius, 10-15 nm depth for Cs^+ ions at 5 keV), with sputtering dominating at the surface and damage dominating at larger depths. At a higher angle of incidence (76°), much of the sputtering is essentially due to recoils from the side of the cylinder. Differences in the monolayer response to the excitation travelling along two different directions (along the hydrocarbon chains and perpendicular to the chains) may also be important [Bolbach '89].

For keV ions, the maximum depth of ejection is ~15 nm (from studies of LB films composed of layers of different fatty acids, and assuming, with some experimental evidence, that significant numbers of pinholes are not present) [Galera '90]. This result is simlar to that for MeV ions which showed conclusively that ions are ejected from well below the surface [Save '87]. Both primary ion energy and adsorption energy between molecule and substrate may affect the internal energy transferred to quasimolecular ions, although if the primary ion's linear energy loss exceeds a certain threshold, the secondary ions' internal energies seem to be independent of energy deposited in the film. The authors conclude that a fraction of the deposited energy seems to be redistributed in a microvolume inside which the molecules are vibrationally excited, a phase which precedes molecular ion emission in both keV and MeV particle induced desorption. In other words, ion ejection does not seem to be directly induced by collision cascades in the ML film. This is because most of a cascade is at half the primary ion range into the target (i.e. at ~8.5 nm for 5 keV Cs^+ ions at 20°), and collisions directed backwards, to the surface, are essentially produced beyond even this depth. Collision cascades seem to transport the energy in the film and ejection seems to be controlled by other processes. Furthermore, for a monomolecular film on Au the cross section of sputtering and damage for an incident ion varies linearly with the energy lost in the *monolayer* ; the energy lost in the substrate does not contribute directly

[Galera '91]. For a surface LB film on a substrate composed of a different LB film, however, the cross-section does not seem to depend only on energy lost in the surface LB film [Galera '91]. In earlier work [Bolbach '88] in which the yield of $[M-H]^-$ was highest for the thinnest films it was suggested that this might be due to the high nuclear stopping power of the substrate.

This group has also studied SIMS of barium arachidate films and noticed that as Ba concentrations in the film increased, fewer $[M-H]^-$ and $[M+H]^+$ ions were ejected [Bolbach '89], and only a small increase in Ba cationized molecules was observed. On the other hand, in similar experiments in which Cd is used instead of Ba, Cd salts show an increase in the spectra; this may be related to the polymeric structure which Ba stearate films have [Bolbach '88a]. Also, it had previously been shown that Cd stearate films have a monoclinic structure and that Ba films have a triclinic structure [Hasmonay '80].

Another study [Bolbach '88a] showed that the $[M-H]^-$ yield of LB films of stearic acid and Cd stearate deposited on Au and Ag at 3 different pH values, seems to be independent of the molecular environment, suggesting that the ion is preformed on the surface. Metal-containing secondary ions depend strongly on the environment, and do not seem to be ejected as preformed ions, but instead seem due to metal species, ejected from the substrate, interacting with the monolayers they pass through (note that these results are for both Cu and Au substrates). $[M+H]^+$ emission is only observed for LB films containing more than one monolayer; this seems to be related to interactions between the carboxylic acid groups in multilayer structures. In fact, it seems plausible that for LB films, $[M-H]^-$ ejection is attributed to chemisorbed molecules in the monolayer range, and $[M+H]^+$ ion ejection is attributed to physisorbed molecules in the multilayer range; similar behavior seems to occur for amino acids.

3.2.2.3 Gardella and Coworkers

Gardella et al have also studied the static SIMS of LB films. Their early experimental methods did not show the care often recommended for monolayers (§3.3) [1]. Later

[1]For example, the trough was housed in a plywood box; it was often cleaned only by rubbing it with paper towels (detergent washing occurred only after protein monolayers had been used or if the trough had stood unused for a long time); the LBML-covered slides were stored in kimwipes and plastic bags

experiments show a more rigorous approach, but even the early ones gave useful results, indicating that perfect film preparation conditions are not always necessary if the data are interpreted carefully and if no conclusions are drawn about the fundamental nature of the films.

In a study of 5 fatty acids on Ag [Wandass '86, 85], Ag^+ was observed from a depth of 37.5 nm, at an intensity three orders of magnitude less than from a depth of 2.5 nm. For various reasons the authors concluded that $[M+Ag]^+$ was not ejected as a preformed ion; later experiments by Bolbach and Blais [Bolbach '88a] confirmed this conclusion. These conclusions were dramatically confirmed in experiments with alternating ML films: $[M+Ag]^+$ ions were observed only if M was the *outermost* monolayer, and not if it was the first monolayer deposited on Ag [Cornelio-Clark '91].

Barium stearate was found to attenuate the substrate signal more than stearic acid for films from one to fifteen monolayers thick, consistent with Bolbach's results [Bolbach '89]. The stearic acid molecules seemed to be somewhat unstable on the surface, and after desorption the monolayers decomposed easily [Wandass '86].

SIMS and ESCA (Electron Spectroscopy for Chemical Analysis) results [Cornelio-Clark '91] of 1 ML arachidic acid on Ag suggest that for this case the $[M-H]^-$ ion in the spectrum is not preformed on the surface (although ML's formed on a basic subphase are expected to be deprotonated). As mentioned, Bolbach and Blais [Bolbach '88a] found no intensity difference between the ions deposited at different pH values for single monolayers of stearic acid/ Cd stearate and therefore concluded that the ion was "preformed on the surface whatever the substrate and the impurities adsorbed during [LB film] transfer". The ESCA experiments seem to involve less interpretation, and may therefore be more reliable.

It seems that the orientation of fatty acid LB films is important in $[M+H]^+$ emission, because only LB multilayers (not fatty acids deposited from solution) form $[M+H]^+$; on Ag surfaces monolayers do not form protonated molecular ions either, although they have been observed for Au and Ge substrates [Cornelio '90]. Since primary ion damage affects the order of the films, it has been suggested that the amount of damage affects $[M+H]^+$ emission because the film order is affected as well as because the molecules themselves are destroyed.

Results with alternating ML's [Cornelio-Clark '91] indicate that the $[M+H]^+$ ion

during transportation to another state [Wandass '86].

comes from only the first three layers of the LB film and show that the $[M+H]^+$ behenic acid ion is at 56% of its original intensity after 20 minutes. On the other hand, the $[M-H]^-$ ion can originate from deeper than 5 ML and after 20 minutes of the same 4 keV Xe^+ ion beam bombardment, the $[M-H]^-_{BA}$ signal was 79% of the original signal. (Note that a negative acceleration voltage would increase the incident Xe^+ impact energy, so the signal might be expected to decrease even sooner than that for the positive molecular ion.) These results suggest that quasimolecular ions of opposite polarity have differing desorption / ionization mechanisms (compare Bolbach's work, §3.2.2.2).

The main conclusions of this group's studies are that the sampling depth (depth from which ions can be observed) of molecular ions depends on the nature of the matrix, varies from ion to ion, is related to secondary ion stability, and depends on the substrate [Johnson '92].

3.2.2.4 Benninghoven and Coworkers

Benninghoven and coworkers studied LB films using ion-imaging TOF SIMS and came to the unexpected conclusion that monomeric molecules are not suitably stable, defect-free structures for studying SIMS desorption from different depths [Hagenhoff '92]. Polymeric molecule LBML films were shown to be more stable than stearic acid LB films.

In these experiments, static SIMS conditions were maintained. The stearic acid was coated at 20-25 mN/m, at a transfer rate of 10 mm/min. The transfer ratio was $1.0 \pm .1$, and ellipsometry, traditionally relied on to verify ML quality, showed good quality films. Unfortunately, no information was given about the salt content of the water or about the pH, both of which need to be optimized for high quality monolayers [Hasmonay '80, Gaines '66], as the authors themselves noted. Shipping conditions between the LB lab and the SIMS lab were not mentioned, and the time elapsed before the LB films were examined by SIMS was not given.

Ag^+ was observed up to 9 ML of stearic acid and even at 7 ML coverage, it was the base peak; the intensities of the Ag^+ and $[M-H+2Ag]^+$ peaks were found to vary strongly with the position probed by the primary ion beam. This is indicative of some defects, due either to poor LB film deposition and to contamination [Pitt '77], to the structure and stability of stearic acid specifically, or to the nature of monomeric ML's, which often show

variations in the orientation of the hydrocarbon tails [Peterson '90]. (Note that holes have been observed after several weeks in air for Cd arachidate/ arachidic acid films [Kuhn '72], and that, whereas Cd salt films are quite stable with time, other films seem to show less stability [Peterson '90].) The authors do not deal with the first two possibilities, and for the third possibility they discuss only pinholes and not such observed ML phenomena as twin boundaries, dislocations or disclinations. Furthermore, they do not discuss the possibility of ion channelling [Bolbach '85]. They also do not address the probability that the Ag surface, which was not stated to have been plasma or rf oxidized (as is often done to provide a controlled hydrophilic surface [Bolbach '88, Wandass '85]), was very reactive and had contacted different surface contaminants at different positions, influencing local Ag^+ desorption. It has been said that, "...gross inhomogeneities can occur in LB films if the substrate surface properties are not uniform..." [Peterson '90]. These considerations are especially important in light of the fact that a *clean*, freshly evaporated Ag surface coats an *even* number of LB monolayers (*i.e.* it is oleophilic; there is some disagreement whether it is hydrophilic or hydrophobic [Peterson '90, Kuhn '72]), whereas the monolayer coating showed that in this work the Ag coated an *odd* number of LB monolayers.

In contrast, the polymethyl acrylate LB spectra show no Ag^+ peak beyond 5 or more layers, and signal intensities are independent of the primary ion beam impact point. This indicates either a defect-free film through which no channelling can occur, or a great affinity for Ag^+ in the layers, so that it is absorbed by the layers. The first option is more plausible, even though it has been shown for monomers that Ag adducts form at the outermost parts of the LB film (§3.2.2.3). It is true that polymethyl acrylate films are remarkably stable (9 months in air, 15 minutes at high (boiling) temperatures in water), as checked by SIMS, and that they may be good candidates for detailed studies of SIMS mechanisms.

In the same work, experiments suggesting that monomers in a monomer/polymer LB layer may diffuse through overlayers, were performed. No information was given about precautions or tests to prove that this was not due to a difficulty with coating (e.g. it is quite possible that some of the already-coated monolayers slipped off the slide during the coating of the overlayers and so were incorporated into these overlayers). Furthermore, in comparison to these results, Kuhn report "no diffusion of cyanine dyes in the layer spectra", with a technique far more sensitive to molecular order than SIMS [Kuhn '72]. (Kuhn and

coworkers have long been associated with extremely precise work with LB films [Kuhn '71]; in fact, one reviewer has stated that "...the films of Kuhn et al had much better orientational alignments than those produced in other laboratories...." [Peterson '90], and sometimes LB films are referred to as Langmuir-Blodgett-Kuhn films.)

In a 125μm x 125μm ion image of 6 layers of stearic acid on Au, various ion intensities increased or decreased in streaks along the target, suggesting folds in the LBML's. Although it was not stated whether this image was taken at the center of the slide to eliminate edge effects [Hasmonay '80], the striations are too close to assign them to edge effects without any further evidence. Monolayer vibrations during coating, which were not addressed, could have caused such striations. Intermittent coating, with the smooth meniscus rising in tiny jerks, as has been observed for stearate films might also give rise to such effects. There has been some evidence that slow dipping (<24 mm/min) gives striations due to instabilities in the meniscus [Peterson '83] for films contaminated with small amounts of cations leached from the trough [Veale '85]. Similar stripe patterns have been observed by others in both polymeric and monomeric films, usually on surfaces such as mica [D. Schwartz '94, Zasadzinski '94, Ruiz-Garcia '93], and have been attributed to the conflict of ideal area / molecule betwen the head group and the hydrocarbon tail; in these studies the effects of substrate, dipping speed and contaminants were not usually addressed. Unlike other methods, SIMS imaging gives chemical information about the stripes and can therefore provide new information, but this group has not published any work exploring the possiblity.

It seems that the general conclusion of pinholes in monomer monolayers may be valid for the monolayers produced in this work; it is not clear that monolayers prepared with the rigor suggested by Kuhn would show the same defect density. On the other hand, since many investigators are not this rigorous, some of these results may apply to other work. For example, overlayer thickness versus yield data may overestimate the yield for a certain depth of emission, but the general trends of the data are expected to be valid. In relation to other workers who had difficulty with electron tunneling LB film experiments, with which Kuhn's group was quite successful, Kuhn et al stated that, "the difficulties they faced indicate that the preparation of ... [LB films] ... is a critical test of the quality of equipment and monolayer technique" [Kuhn '72]. Their statement may apply to these experiments as well. Furthermore, discoveries of unusual levels of disorder have been made in the past and were later shown to be due to artifacts [Ferestehkhou '86]. Therefore

the data obtained previously on monomeric ML's is not invalidated by these experiments; on the contrary, questions about the validity and relevance of this work remain. Although some experimental issues need to be addressed, the evidence for stripe structures seems valid and SIMS imaging could be a powerful probe of such stripes.

3.3 PRODUCING LANGMUIR BLODGETT FILMS

This section of the thesis is meant to be a practical guide for anyone wishing to make monolayers. General outlines have been written [Peterson '90, Agarwal '88, Blinov '88, Tredgold '87, Roberts '85, Hasmonay '80, Kuhn '72, Gaines '66, Blodgett '37a, '37b, '35, '34] and a helpful video exits of Langmuir and Blodgett themselves, making LB films [General Electric Company, Schenectady, NY]. Since many details which can cost weeks or months of work are assumed in the literature, this description will be very detailed and some specific instructions will be included in the appendices. In all experiments, it is crucial to remember that "scrupulous cleanliness is one of the most important requirements in handling monolayers and producing monolayer assemblies" [Kuhn '72]. For most monolayer work it is important to follow the recommendations of Kuhn et al [Kuhn '72], unless there are clear reasons not to, or unless the highest film quality is not necessary. For example, many groups use fatty acids without recrystallizing them; for fundamental studies characterizing ML's this may not be wise, but for studies such as ours the extra effort may not be worthwhile.

3.3.1 APPARATUS

To coat LB films one needs a trough in which to spread the film on a subphase, a compression/feedback system to keep the film at the required surface pressure and a slide dipping system. The whole apparatus must be set up in a dust and vibration free area. Many such systems have been described in the literature [*eg.* Grunfeld '93, Bohanon '92,

Armen '87, Miyano '87, Gaines '66, '63] and some are commercially available although very expensive. The system described below is simple, inexpensive, and relatively easy to make and is adequate for some LB film work. Some experimental parameters are given in Appendix 3.1.

3.3.1.1 Trough

The trough (~530 mm x 120 mm x 14 mm) was made of a solid block of teflon bolted onto a stainless steel base. A groove which had been cut into one corner was filled with a matching piece of teflon screwed into place. This corner of the trough was always cleaned carefully and no contamination has been noticed from the crack. Even so, it was always kept far from the slide dipping region. The top edges of the trough are smooth and flat so that the teflon barriers used to clean the subphase surface and to compress the monolayers can glide easily across it. A millimeter scale on the side of the trough allows accurate measurements of barrier positions to be made.

3.3.1.2 Compression and Feedback System

Originally a piston oil system [Gaines '66] was used to compress the monolayer to a constant value, but it has been replaced by an electronic system. This electronic system can compress a monolayer and allow examination of its pressure area characteristics, or it can compress the monolayer to a specified surface pressure and keep it at this pressure. It is composed of a surface tensiometer, a barrier and barrier drive, and a feedback circuit, Fig. 3.3.

3.3.1.2.1 Piston oil system

The original feedback mechanism to keep a constant surface pressure used the special qualities of the piston oil oleic acid [Gaines '66]. When spread in excess onto a clean water surface, the oleic acid maintains a constant surface pressure by forming lenses of the excess oil on the water surface. After being cleaned, a fresh water surface was divided into two sections with a waxed silk thread (black silk sewing thread rubbed along a clean block of household paraffin). Stearic acid was deposited on one side of the string,

and a drop of oleic acid on the other side; the waxed silk thread floated on the water between the two monolayers. Such a "molecular feedback system" is, of course, very sensitive. The monolayers were usually prepared in large glass petri dishes set on graph paper (1mm/division) and placed under a plexiglass cover. The string position on the graph paper was traced after each passage of the dipping slide through the monolayer. At times the dish was set on a transparent 1mm/division grid on a mirror to reduce parallax errors in locating the string. The area the string moved was obtained using a planimeter. Because of the difficulties of tracing the string position, this system was abandoned in favor of the automated system.

3.3.1.2.2 Surface tensiometer

Two general ways of measuring the surface pressure, π, of a monolayer film exist. One, used in Langmuir-Adam balances, involves directly measuring the pressure of the monolayer exerted against a barrier. The water surface on the other side of the barrier must be perfectly clean, so that no surface pressure is exerted on the barrier from that side. The other kind of measurement of surface pressure uses a Wilhelmy balance and involves measuring the reduction of surface tension of the liquid beneath the film. (Recall that surfactants reduce the surface tension [Shaw '70].)

In a Wilhelmy balance, a plate is suspended in a liquid and the forces exerted on the plate are measured. These consist of the gravitational force and the surface tension downward as well as the buoyant force and the pull of the tensiometer upward. In the stationary plate mode of operation, the torsion balance is adjusted to counteract any changes in surface tension; the gravitational and buoyant forces do not change. The surface pressure, π, which is simply the difference in surface tension, γ, between a clean surface (γ_o) and the one being measured, becomes simply

$$\pi = \gamma_o - \gamma = -\Delta F/[2 \cos\theta\ (t+w)] \qquad (3.2)$$

where F is the force on the plate as measured by the tensiometer, t and w are the plate thickness and width and θ is the contact angle of the liquid and the plate, which will be discussed below. Note that the force exerted by the tensiometer to keep the plate stationary

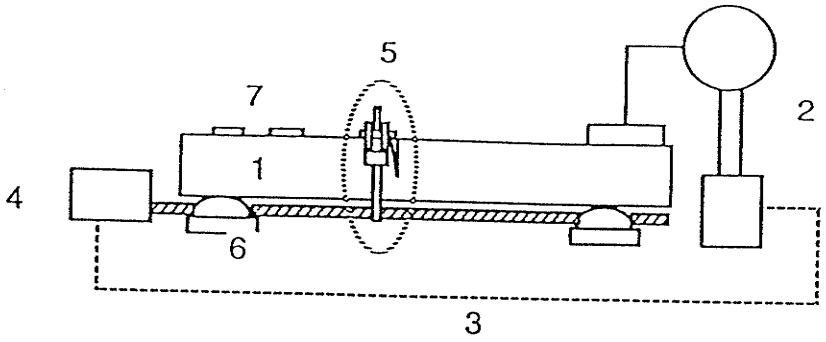

1 trough
2 tensiometer schematic
3 feedback system
4 motor
5 barrier and barrier drive (see detail below)
6 vibration isolation
7 sweeping barriers

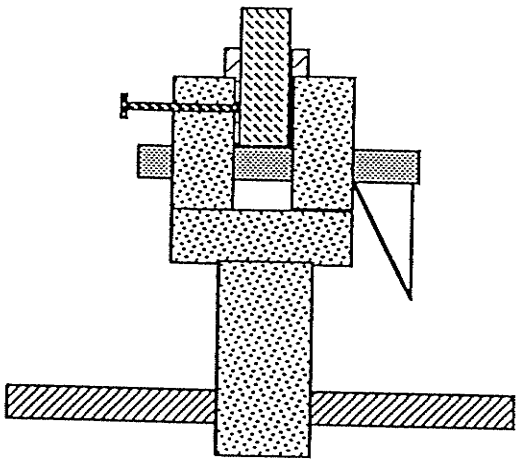

Barrier:

connection to barrier holder

held in place using screws at the ends of the barrier

barrier

pointer

Barrier drive:

barrier holder

driveshaft

thumbscrew

Fig. 3.3 Schematic of monolayer compression and feedback system with a detail of the barrier and barrier drive.

is greater when the surface tension is high; this explains the negative sign.

The contact angle, θ, is the angle between the water meniscus surface and the plate, Fig. 3.4. It applies all around the slide, hence the factor of 2(t+w). Since liquid surface tension is due to a tendency to draw the surface molecules into the bulk phase (i.e. the force is perpendicular to the surface), the force on the plate depends on the meniscus shape at the plate and is largest when the plate is completely wet and the contact angle is zero.

Obviously it is important to keep θ constant and to be able to measure it, which is difficult unless $\theta = 0°$, so the usual procedure is to ensure that the Wilhelmy plate is uniformly wetted to fulfill this condition. Usually Wilhelmy plates are glass, quartz, mica or platinum, cleaned and treated to be hydrophilic. However, if the liquid surface through which the slide moves is covered with a monolayer, the slide very easily becomes partially coated [Gaines '60] so that its surface becomes partially hydrophobic because of the CH_3 groups of the monolayer; then θ is no longer constant. This can cause large errors in the measured surface pressure. To overcome this problem, a filter paper was used in place of a traditional Wilhelmy plate [Peterson '83, Kuhn '72]. The paper is wet and its contact angle has never been observed to vary from 0° over hundreds of hours of measurement. Although filter paper may bend, so that it enters the water as a curve instead of a straight line, this has no effect on the measured surface tension.

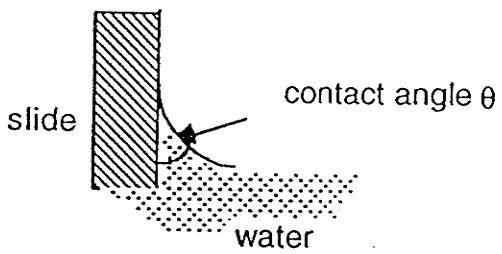

Figure 3.4 Definition of the contact angle θ.

In this work surface pressure was measured using a modified Wilhelmy balance consisting of a Cenco Du Nuouy interfacial tensiometer and a filter paper Wilhelmy plate. The tensiometer was calibrated with small weights and found to be linear.

If a careful measurement of surface pressure changes is necessary, as for a π-A plot, the tensiometer slide position can be kept constant manually by checking a pointer's position in a small mirror. If feedback will be needed during the experiment, however, the feedback system (see § 3.3.3.2.4) must be installed. In this case, the tensiometer can be kept stationary manually with respect to two reference points on the light shield.

3.3.1.2.3 Barrier and motorized barrier drive

The monolayer is compressed by using a motor-driven barrier, as shown schematically in Fig. 3.3. The barrier, barrier holder, and motorized drive were designed to work with fatty acid monolayers and the trough described above.

Several barriers have been used. The optimum design (Fig 3.3, detail) allows a final sweeping of the water surface before connecting the barrier to the drive via the barrier holder. The barrier is a simple teflon bar with two adjustable stainless steel screws at either end. A pointer at one end allows one to measure the barrier's location using the scale on the side of the trough. The barrier is laid onto the surface as close to the Wilhelmy balance filter paper as possible and is swept to the barrier holder. When it is properly aligned, a piece of plexiglass is inserted into the U's of the barrier holder and between the screws of the barrier itself. It is fastened to the barrier holder with thumb screws adjustable from the 'dirty' side of the barrier. Even though the barrier drive, and hence also the holder, show some slow vertical wobble, this has no effect on the barrier itself. No effects of the wobble could be observed on the water or monolayer surface.

The position of the barrier on the trough could be measured manually. However, a computer interface which connected the rotating barrier drive to the mouse control of an Atari Mega was also constructed. Although it was not completely linear, it allowed the barrier position to be measured adequately and simplified experimental work.

The barrier holder was fastened to the barrier driveshaft with foam to damp vibrations. The two teflon U's were fastened to the rest of the barrier holder using the same foam. Vibration isolation was so good that turning the barrier drive motor on produced no noticeable vibrations on the water or monolayer surface.

The threaded driveshaft was turned by a reversible stepping motor (a camera rewind motor) via a reduction gear set. The barrier velocities used ranged from stationary to ~1cm/min forward and backwards, and were controlled by a feedback system.

3.3.1.2.4 Feedback circuitry

To keep the monolayer surface pressure constant, a feedback circuit connected the tensiometer and the barrier drive. A small light and a photoresistor were mounted on the tensiometer frame, underneath a matt black shield. The tensiometer balance arm, which swings between the two, has attached to it a piece of dull black cardboard with a V-shaped hole to regulate the amount of light reaching the photoresistor. If the film pressure is too high, the tensiometer arm rises and allows less light to reach the photoresistor and so adjusts the motor's speed. Feedback sensitivity depends on the light's brightness, which can be adjusted. The system was able to keep the surface pressure constant, even during monolayer transfer. (Note that, due to film viscosity and to the time it takes the barrier to move, the surface pressure is not completely constant near the LB dipping slide [Pitt '77].)

3.3.1.3 Slide Dipping System

To coat monolayers onto a surface, a clean slide must be dipped smoothly into and out of the subphase with as few vibrations as possible. A very simple system which proved vibration free and versatile was used in the single substance multilayer experiments, Fig. 3.5a. It did, however, require considerable care and dexterity to operate successfully so an alternative system has been designed, Fig. 3.5b.

A low vibration reversible motor drives a microscope raising and lowering system by means of a thread gear. A nylon monofilament fishing line is connected to the bottom of the microscope focus and passes under one pulley and over another, as described below. The slide can be positioned at the end of this monofilament thread. The pulleys are on square rods which do not transmit vibrations or transfer them to the pulleys as easily as round ones do. To set the starting height of the slide, pulley A (see Fig. 3.5a) can be adjusted. The slides are clipped using alligator clips with stainless steel plates at the end; these are hung onto the nylon string so that the slides enter the water approximately vertically (with an error less than 5°). The string on which the slide is hung is put over

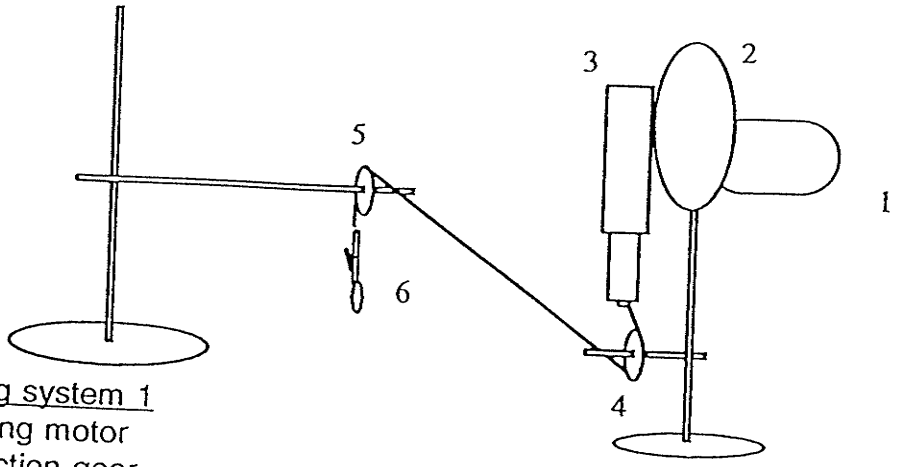

Dipping system 1
1 dipping motor
2 reduction gear
3 microscope focusing system
4 pulley A
5 pulley B (this one is moved over the monolayer)
6 clip with slide to be dipped

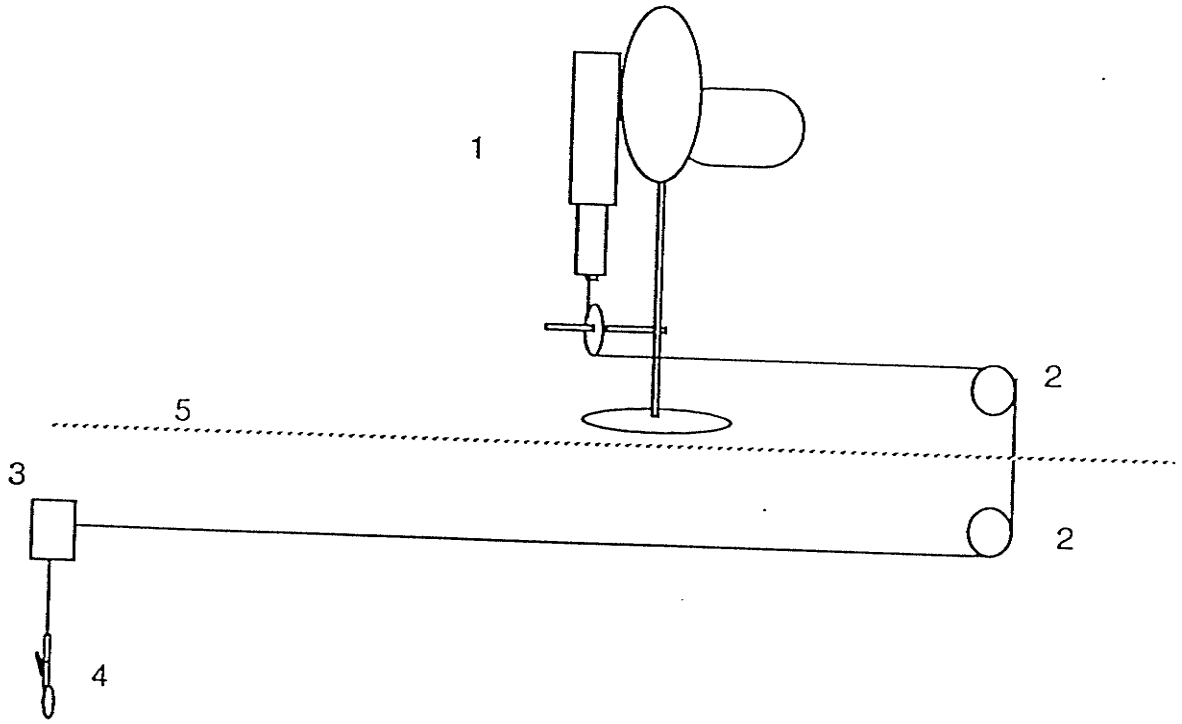

Dipping system 2
1 original dipping system
2 pulleys
3 curtain rod which is moveable along the length of the plexiglass box
4 slide, which can be moved across the width of the box, along the curtain rod
5 plexiglass box which houses the monolayer experiments

Fig. 3.5 Schematic of the two dipping systems used

pulley B in front of the trough. Pulley rod B is then moved over the monolayer-covered trough while pulley rod A is moved to adjust the height of the slide. Dipping speed is very slightly adjustable (2 to 4.5 mm/min), and is usually ~ 4 mm/min. Ideal dipping speeds have been discussed [Peterson '90, '83, Veale '85, Hasmonay '80], but may depend on contaminants present; in general, the first layer needs to be dipped more slowly than subsequent layers.

3.3.1.4 General Precautions Taken to Produce Good Monolayers

Some of the precautions needed to produce good monolayers have already been outlined while describing the monolayer apparatus. Others will be described in the section on making monolayers. Here the general methods used to reduce dust (which physically disrupts a monolayer and may often carry contaminants as well), vibrations, and contaminants will be outlined. The temperature was not controlled, but was fairly steady at room temperature; the water used was at room temperature.

3.3.1.4.1 Dust and airborne contaminants

To reduce the amount of dust falling onto the apparatus and the monolayer a plexiglass box was constructed. The front panel swings up for large scale adjustments of the apparatus and for cleaning. It had mounts for gloves but these are awkward to use and not necessary. Now it has a small horizontal sliding door at one side and a large vertical one in the center. These sliding doors are used during monolayer preparation since swinging the front panel open and closed introduces a large movement of air which can reduce cleanliness. Holes of adjustable sizes were drilled in the sides of the box for wires to pass through.

It seemed important to have a clean airflow from the back of the box to the front to ensure that only clean air surrounded the apparatus. New, clean poly-flo tubing, with holes punched along its length and a stainless steel stopper at its end, was clipped in a zigzag pattern along the back wall. Dry air was passed through this at a constant rate as checked with a flowmeter. Later it was found that by leaving the box closed, except when removing the trough, and by keeping it scrupulously dusted, this extra air flow was not necessary. In fact, it could stir up any small bits of dust that still remained in the clean box.

3.3.1.4.2 Vibration control

The whole plexiglass box was set on a counter top attached to a cinderblock wall. The box was set on a double layer of bubble camping mattress. Inside, the trough was positioned on semicircles of sorbothane polymer (Edmund Scientific) shock absorbent plastic resting on four homemade vibration isolation mounts. The tensiometer was also on the homemade antivibration mounts. Bumping the counter caused only slight vibrations on the water surface. Door slamming, which occurred infrequently, caused strong vibrations which could not be filtered out.

Any remaining vibrations could be monitored by looking at the reflections of the room lights on the water surface using a mirror set up behind the trough. When the monolayer was spread and compressed, however, the vibrations largely disappeared due to the monolayer's vibration damping ability. This damping persisted during Langmuir Blodgett film deposition and no vibrations were noticed.

3.3.1.4.3 Contamination

Contamination of the monolayer was reduced by scrupulous attention to cleanliness and by careful handling of solutions. Clean gloves (freshly washed pvc or latex gloves; disposable were preferred because they cannot pick up contaminants from repeated use) were worn, care was taken not to breathe or cough over the LB trough, and the box was opened as little as possible. Anything teflon that contacted the subphase was freshly washed with detergent, rinsed thoroughly with hot tap water (after allowing water which may have been standing in the taps to drain away) and rerinsed with the cleanest water available. Glass was cleaned in chromic acid and rinsed as above or treated as described in Appendix 3.2. The filter paper cleaning is described in Appendix 3.3. The substrates were cleaned with a glow discharge [Bolbach '88].

Water was filtered through a nanopure purification system and stored only if absolutely necessary and for very short periods of time, because ultra pure water can leach impurities from any container [Millipore Company].

All solutions were stored well-sealed to prevent evaporation, in quartz or glass containers cleaned as described above, and were prepared with great attention to cleanliness. The spreading solutions (without the fatty acids) were checked for contamination using

blank spreading experiments to test that they produced no change in the surface tension. Small amounts of the solutions were periodically poured into vials to be used in the experiments. All pipette tips, which were either disposable or dedicated to a particular solution, were rinsed well before inserting into the vials. Such precautions may seem excessive, but they consumed very little time. They are important since a contaminated solution may inhibit monolayer formation or it may affect monolayer structure subtly so that the effects are not noticed until the experiments are being analyzed.

3.3.2 MATERIALS

The stearic acid (>99%) was from Aldrich Chemical Co., Inc.; the 1% impurities seemed to cause no problems in previous experiments [Bolbach '88]. If surfactant impurities exist which spread more easily than the film molecules or if the impurities act like counter ions, poor film spreading on the water and poor LB film deposition may occur. In other cases the films may behave quite normally, except that the detailed transitions between phases are not observable in the π-A diagrams; this would not affect multilayer quality for our experiments. The heavy stearic acid (d35, 98% deuterated) was from Cambridge Isotope Laboratories. Cadmium chloride and n-hexane from Fisher Scientific Company were 80% (as $CdCl_2.2^1/_2H_2O$) and 99 mol% pure, respectively; again, the impurities seemed to cause no problems in previous experiments [Bolbach '88].

Water was purified in a nanopure system (Chemistry, Dr. A. Chow's lab), transported in the plastic boxes in which Fisher Scientific sells distilled water, and after purification it was used within one day (for LB film deposition) or a few days (for pressure area experiments). The filter paper used (589 black and 589 blue) was a gift from Schleicher and Schuell. Glass slides were 12 mm diameter microscope slides from Calbiochem. The silver (99.9985%) was from Johnson Matthey. The detergent used for cleaning was 10% Extran 300 in water.

Note that Kuhn et al [Kuhn '72] recommend recrystallization and fractional distillation of the fatty acids and spreading solvents respectively, but very few groups are so careful. For our experiments, it did not seem necessary since previous experiments using the same chemicals had produced good results, and because we did not need totally defect-free

structures for our work.

3.3.3 METHODS: SPREADING FILMS ON WATER

The step by step procedures used to spread monolayer films on water are noted in Appendix 3.4 and experimental parameters are tabulated in Appendix 3.1 Here the procedure will be outlined generally.

3.3.3.1 Subphase Preparation

First of all, the teflon trough was washed with hot tap water and 10% Extran 300 detergent and scrubbed with a bottle brush. It was then rinsed with copious amounts of this water so that the trough edges were also rinsed well. Finally, it was rinsed with several liters of nanopure water.

Enough water was added to the trough that the water surface formed a meniscus several mm high. (If it is much higher it will creep onto the trough edges after the monolayer has reduced the surface tension. If it is much lower there will be an air gap between the trough barrier and water surface, and the surface films can pass beneath the barrier. This can be checked by spreading talc on the surface where leakage is suspected and watching its movement.) If a counter ion was needed in the subphase, it was added when about one third of the water had been added to ensure proper mixing. Usually a concentration of 10^{-4} M $CdCl_2$ was used. The pH was ~5.5 due to the effect of CO_2 in the atmosphere; since this was the desired pH range [Hasmonay '80] no additional buffers were used.

The subphase was always covered with surfactants which needed to be removed before a monolayer could be spread. Teflon rods, cleaned as the trough was, were placed on the edge of the trough and swept along its length with a simple stainless steel rack. (Sliding the rod along by hand can cause contamination and also easily leads to bumping it so that the compressed surfactants slip underneath it into the cleaned area.) The rods were left lying across the trough after sweeping; once a few barriers were lying across the trough

the first ones were removed, washed carefully, and reused. Four sweeps generally produced a fairly clean surface, and after this the tensiometer with its filter paper slide was set up. The subphase was swept another time to remove any contamination arising from the filter paper, and then its tensiometer reading was noted. After this, the teflon barrier was swept back to the filter paper to check that the surface was free of surfactants: if so, the tensiometer reading for a stationary plate *remained the same* whether the barrier was close or far, showing that no surfactants were present to exert a force on the filter paper. If, however, it was not clean, this barrier was swept back to the far end of the trough and remained there. Other barriers were used to sweep the surface until it was clean (*i.e.* the tensiometer readings for the barrier at the far and the near end of the trough were identical.

Surface cleanliness can be checked qualitatively by sprinkling on talcum powder and blowing gently by mouth. If the talcum powder can be blown to one end of the trough and will stay there, the water was clean before the talcum powder was spread. If it can be blown to one end, but drifts back when the blowing is stopped, some surfactants were present in a 'gas' phase before the talcum powder was added. If it cannot be blown to one end of the trough at all, the surfactants are in an incompressible phase, either 'liquid' or 'solid'. A 'liquid' phase will flow when blown upon, but a 'solid' phase is rigid until the blowing becomes so vigorous that the surface fractures. This can also be used to check the phases of a monolayer once it is spread. Note that the talcum powder must be swept away to obtain a clean surface again and that any monolayer covered with talcum powder is not suitable for further experiments.

3.3.3.2 Spreading the Monolayer

Once the subphase is clean the monolayer can be spread. Since a monolayer will reduce the surface tension, the filter paper slide may leave the water as the monolayer is spread, causing strong surface vibrations which could lead to local monolayer collapse. Also, when the filter paper is reinserted it will most likely have a different orientation (i.e. 'w' will change, see Eqn. 3.2) which will invalidate all the surface pressure measurements since they depend on the surface tension without a film. Therefore the tensiometer must be adjusted to a low value before spreading the monolayer so that it cannot leave the water once the monolayer is spread.

A 100 µl metal syringe, devoted to spreading monolayers, was first rinsed using pure hexane and then used to deposit the stearic acid / hexane solution (~5 x 10^{-4} M) onto the surface, drop by drop. In all cases the first few drops spread across the surface immediately. Generally, later drops break into little droplets which spread apart and disappear more slowly. If any more drops are added, they may not spread at all, but may become whitish spots on the subphase. These spots are due to increased surface pressure of the stearic acid and the unevaporated hexane which inhibits the spreading of any additional surface active material. The spots' appearance corresponded to a linear plot of amount of solution deposited versus monolayer area. Although the required amount of stearic acid solution was estimated from this plot, droplet behavior on the water surface was used to determine the amount of solution actually deposited. The stearic acid / hexane droplets were deposited all over the monolayer area to promote good spreading, but the last drops were deposited near the barrier in case any whitish spots appeared. Some time was allowed for the spreading (approx 2 or 3 minutes) so that the hexane could begin to evaporate. Once the solution had been put on the water, the hexane was allowed to evaporate and stabilize for about twenty minutes before film compression began. (Some recent work suggests that several hours may be necessary to reach equilibrium [Schlossman '91], some work suggests that aging may cause poor films [Peterson '83] if cations are present [Veale '85], and some work shows that bacterial growth can be a problem in an aged film [Tredgold '87]).

3.3.3.3 Checking Monolayer Quality

If there were no noticeable imperfections (e.g. a white drop of dried up stearic acid / hexane, or a dust particle), and there was no bumping, jarring or other accident during the spreading, then the monolayer's quality was verified more precisely. With the feedback off and the compression barrier moving at a constant velocity of ~ 2.2 mm/min, the barrier position was noted either manually or using the computer interface, and the tensiometer was manually zeroed approximately once every minute. When the film reached the 'solid' phase (§3.2.1), the surface pressure changed very rapidly and measurements were taken twice as often. The data were plotted (e.g. Fig. 3.6) and the area/molecule and compression

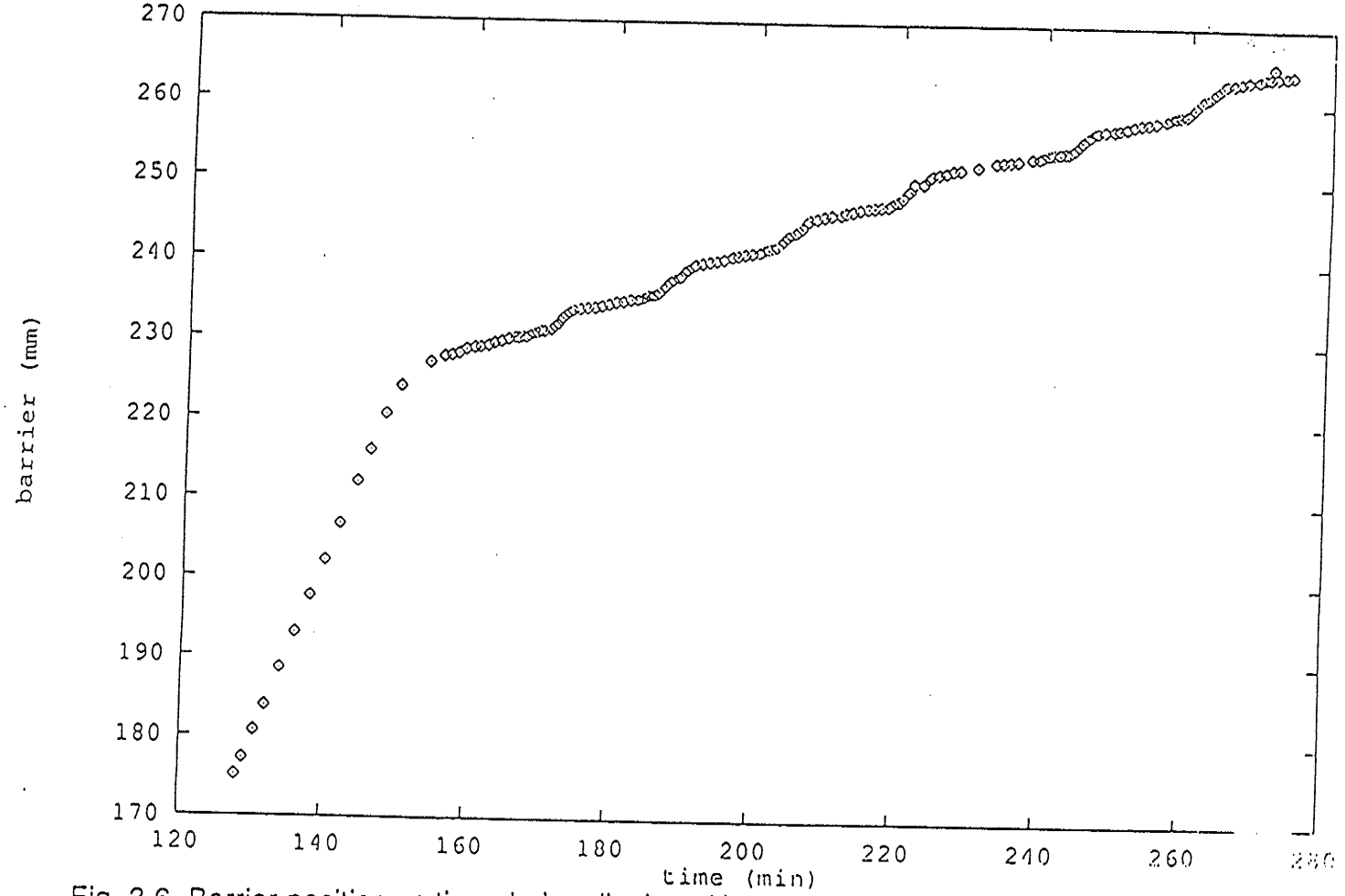

Fig. 3.6 Barrier position vs time during dipping. Note how the first and fifth steps are single because a fresh slide was dipped and coating occurred only on emersion. The other steps are double and represent both an immersion and an emersion. In these steps the jag is due to the meniscus contact angle changing from 180 ° during immersion to 0 ° for emersion. (See Appendix 3.5 for calculation of τ values.)

behaviors were noted. If the shapes of the π-A curves were as expected, the monolayers were considered to be satisfactory. Problems with pressure area curves have been associated with a contaminated sheet of filter paper, with improper trough meniscus, with the slide 'jumping' out of water, with dust, contaminated water or solutions, and with mistakes like dropping water from gloves onto the subphase or bumping the barrier during sweeping. Therefore, before commencing LB coating, at least one good π-A curve was obtained after any change in solvents, equipment or procedure.

Since the pressure vs area curve is sensitive to subphase pH and to temperature as well as to contaminants, the water used was always at room temperature. The pH was measured to be ~5.5 with an Accumet (915) pH meter, using a combination glass Ag/AgCl electrode, after any significant changes in procedure or solutions. Because the subphase was so pure, the electrode itself would contaminate it; therefore pH was usually measured after an experiment. For the same reason the measured pH value changes in such a pure unbuffered system [Fisher Scientific], and is therefore impossible to determine with great accuracy.

3.3.4 METHODS: LANGMUIR BLODGETT FILM COATING

To transfer the monolayer film from the water subphase to a solid substrate (i.e. the spectrometer target), it is necessary to prepare the substrate, to do the actual dipping and to verify that a monolayer was indeed transferred. The detailed procedure is given in Appendix 3.4 and the experimental parameters in Appendix 3.1.

3.3.4.1 Substrate Preparation

The substrates used in this work were 12 mm diameter glass microscope slides, vapor-coated with silver which was oxidized using a glow discharge in air. The glass was cleaned as described in detail in Appendix 3.2, and were clipped onto a holder which fits into the vacuum evaporator (Edwards High Vacuum coating unit, 12EA/620). Two strips

(20 mg each) of silver were used to coat the glass slides on both sides; both sides needed silver coating to ensure good LB deposition. First the glass slides were cleaned by 2-3 minutes of ionic bombardment using a glow discharge of ≤ 1A. At a pressure of ~3 x 10^{-5} Torr, the silver was evaporated onto one side of the slides. The slides were rotated 180° in atmosphere to coat the other side. Afterwards another short glow discharge in air was performed to oxidize the silver surface so that it would be hydrophilic. (If the glow discharge lasts too long, the surface becomes pitted and rough [Bolbach], which hampers monolayer deposition.)

3.3.4.2 Monolayer Deposition

The subphase and monolayer were prepared exactly like those which had, immediately previously, given good π-A diagrams. The feedback system was used to control barrier motion and in this case anomalies in the ML were detected by unusual barrier motion, which was always recorded, instead of by an unusual π-A diagram. If there were absolutely no indications to the contrary (e.g. poor ML spreading, dust on the surface, unusual vibrations, etc.) the monolayer was assumed to be of good quality. If there was any doubt about a spread monolayer, however, it was not used to coat slides; it could be tested to obtain a pressure area curve, or to study monolayer compression/decompression in order to gain more data and experience regarding sources of bad monolayers. If the cause of the inferior monolayer quality was not apparent, no coating would be attempted until a monolayer with a good π-A curve had been obtained, proving that the problem had been overcome. Otherwise, depending on the nature of the problem, a good pressure area curve was not always needed before LB film deposition.

The deposition set up was described in §3.3.3.3. If any problems arose in attaching the slides to the setup (e.g. dust, drop of water, vibrations) the slide was carefully stored away and a new monolayer was spread on the water. Usually the first slide was set up before compressing the monolayer.

After the spread ML had equilibrated (~20 min), the tensiometer value was set to the dipping value of ~30 mN/m. The feedback/compression system was turned on and barrier position vs time were recorded. The feedback was inactive until the actual surface pressure approached the dipping pressure, and the tensiometer arm rose (§3.3.1.2.4), reducing the

light reaching the photoresistor. At this time, the barrier would slow down, and become stationary, a signal that the desired surface pressure had been attained.

Then the dipping system was activated, and the slide entered the water. When it had entered as far as possible without wetting the clip, the direction of motion was reversed, and it rose out of the water with a ML coating which gave a hydrophobic surface.

The meniscus on both sides of the slide was recorded throughout each dipping; a mirror was set up behind the trough for this purpose. The meniscus of the ML on the slide showed clearly whether or not ML deposition was occurring. If for immersion the contact angle θ (§3.3.1.2.2) was 0°, as occurred for the first immersion, no coating occurred. If the contact angle on emersion was 0°, the hydrophilic part of the ML contacted the slide and could adhere to it, and coating occurred. On a subsequent immersion, the hydrophobic part of the previous monolayer caused a contact angle of 180° as the monolayer was transferred to the slide. If the contact angles were as expected and the meniscus was smooth, good coating was assumed. For good films the plate emerged from the trough dry after all but the first dipping; if it had more than a drop of water at the bottom of the slide, the film was obviously of inferior quality. In all cases, drops of water were allowed to evaporate before the next ML was coated. At times the meniscus was uneven; such slides were of poor quality, and the side of the slide with the best quality meniscus throughout dipping was examined by SIMS.

The time the slide entered the water was recorded, along with the barrier position at ~20 s intervals. This barrier position information was later converted to monolayer area vs time plots. If coating occurred, the monolayer area was observed to decrease as shown in Fig. 3.6. For each dipping the value h, which is the distance from the meniscus at its highest point to the top of the slide, was estimated so the approximate coated area could be calculated. Then τ (see Eqn. 3.1) was calculated; the films exhibited Y-type deposition (§3.2.1). If the τ values are not approximately 1, the ML film is unlikely to be of good quality. If $\tau \sim 1$, then the meniscus behavior is used to determine ML quality.

Many studies of ML's have shown that if coating occurs in the solid region of the π-A diagram, if the substrate is smooth, if the usual ML quality is such that the π-A diagrams are normal and reproducible, and if the ML's are carefully made, the ML structure is relatively good although, as mentioned, some studies suggest pinholes exist. (For our work, which is concerned with thickness effects and fragmentation patterns, the occasional

defect is not crucial; however for most ML work it is and more careful methods are required.)

After each slide was dipped the desired number of times, the coated slide would be moved away from the trough, and be returned to its spot on the holder. The next slide would be set up, and the whole dipping procedure would be repeated. At the end of each dipping run, the pH was measured.

3.4 SIMS EXPERIMENTS ON LB FILMS

3.4.1 METHOD

Films 1, 3, 5, 7, 9, 11, and 13 layers thick of stearic acid / cadmium stearate and deuterated stearic acid / cadmium stearate were coated onto silver-covered glass slides as described in the previous section [Poppe-Schriemer '92].

As soon as possible after being coated, the slides were examined by SIMS on their best side, as determined from the meniscus data and from the appearance of each side. Slides were examined in the order of decreasing quality, determined by the same criteria. (Because the calculation of τ was too time consuming to do before the SIMS experiments, τ values were not used to determine slide quality.) If the slides needed temporary storage, they were either put in petri dishes or hung in a clean area as before coating.

The spectrometer was optimized using a peptide sample to prevent unnecessary radiation damage to the LB films. Pumping down the spectrometer took less than half an hour, and any film in vacuum was examined immediately, since there are some indications of yield variations from LB films left under vacuum for more than a few hours [Bolbach '88].

During the experiments the primary ion charge was measured at the slit of the ion gun pulser (§1.4.1). In other words, we measured the current that did *not* reach the target. From a consideration of the pulsing mechanism [Ens '84], it is evident that this slit current is greater than the current actually reaching the target (the primary ion beam which hit the

target had a width of ~4 to 10 ns and a pulse frequency of either 2 or 4 kHz; the rest of the beam hit the slit plates and was measured as the slit current (§1.4.1.1)). Therefore, even though the recorded slit current and total charge barely satisfied static SIMS conditions (3.1.1), these conditions were easily maintained at the target. This means that most ions were recorded from previously undamaged portions of the target. The measured slit current was used to normalize peak intensities.

Both positive and negative spectra were examined, each with the mirror off (direct spectra) and with the mirror on (reflected, neutral and correlation spectra). Often the negative spectra were examined before the positive spectra because the negative incident I^- ions were slowed down by the negative acceleration voltage, reducing the sample damage. For both polarities all the ions formed in the spectrometer could be identified, except for the ones which decayed in the first ~ 45 ns (Appendix 2.6 and §3.4.2), and their desorption, stability, prompt fragmentation and metastable decay could be examined. Such a wealth of information could be obtained while satisfying static SIMS criteria because of the very high sensitivity of the TOF correlation technique with datalogging.

Correlation windows were set on $[M-17]^+$, $[M+H]^+$, $[M+Ag]^+$, $[M-H+2Ag]^+$, $[2M+H]^+$, $[2(M-H)+Ag+Cd]^+$ and $[3(M-H)+2Cd]^+$ in the positive mode and on $[M-H]^-$, $[2(M-H)+Ag?]^-$ [2], $[3(M-H)+Cd]^-$, and two unassigned peaks, which will be referred to as unassigned 1 and unassigned 2, in the negative mode.

The data taken before the data logging system was developed suffer because the correlation time windows were set using the direct spectra. Because the direct and neutral spectral peaks often have different peak shapes, setting windows on the direct peaks is not totally accurate. The usual procedure is to acquire a neutral spectrum, then set the correlation windows based on it, and then acquire the correlation data. However, for fragile LB film targets, such a procedure would have caused unproductive radiation damage before the important measurements. Due to experimental difficulties, the data for these correlation windows was not actually acquired for all of the LB films in the early work without datalogging.

[2]Note that this assignment is not certain; although the mass of the peak (~748.5 u) corresponds more closely to a Cd adduct, this does not easily give a negative ion. Also, the peak is quite wide and may be a mixture of different compounds including Ag and Cd, both of which have more than one abundant isotope.

To verify and extend the data obtained with Cd stearate, we repeated the experiments with better LB films using deuterated Cd stearate / deuterated stearic acid, datalogging, and better spectrometer resolution. Data taken with the datalogging system allow correlation time windows to be set during the read back, which can, of course, be repeated without damaging the target. Datalogging also can allow the time evolution of various ion peaks to be observed in the direct and reflected spectra. However, most of the correlation spectra do not have sufficiently high count rates to examine the time evolution of the daughter peak intensities and of the decay rate.

Prompt and metastable decay patterns were compared for both positive and negative spectra, with the assignments based on the undeuterated films being confirmed by the deuterated films. Peak heights were normalized to the slit current and plotted as a function of the number of monolayers involved. The spectra taken after different amounts of primary ion bombardment were also compared.

3.4.2 RESULTS AND DISCUSSION

As has been mentioned (§1.2.4.3, §2.3.4.2 and Appendix 2.6), the essential difference between the correlation, reflected and direct spectra is one of molecular stabilities on different time scales. The *direct* spectrum (mirror off, detector 1, see §1.2.4, Fig. 1.1) records the ions present at approximately 45 ns. (For a resolution giving ~ $\Delta t/t = .01$, the time is 55 ns if the precursor decays into an ion of 2/3 its mass, and 39 ns if it decays into an ion 1/3 of its mass (Appendix 2.6); note that all ions produced before this time are defined as prompt fragment ions.) Any ion that decays after 225 ns (*i.e.* after the acceleration grid) is detected at or very near its expected position; the main effect of the decay is a widened peak due to release of internal kinetic energy. The *reflected* spectrum (mirror on, detector 2) records the ions present at approximately 6μs (*i.e.* at the start of the mirror; the time value is for the molecular mass of ~ 300 u); the products of any decay in the mirror are lost, and any decay in the second leg of the flight tube, *i.e.* after the mirror, merely widens the peaks. However, any decay in the first leg of the flight tube (225 ns to 6 μs) causes the resultant daughter ions to be detected earlier than the parent in the reflected spectrum (Appendix 2.5). Such peaks can be analyzed in the *correlation* spectra (mirror on, detector 2). The *neutral* spectrum (mirror on, detector 1) records the neutral daughters

of any decay occurring in the first leg of the flight tube. They appear at or very near the expected position for their parent ion, and can therefore be used to correlate daughter ions with specific parents. Note that not all decays can be observed [Bolbach '88], although our sensitivity allows previously undetected daughters to be recorded (§3.4.2.1). Comparisons between the neutral and direct spectrum can be used to determine the amount of ions produced promptly and their stability between the acceleration grid and the mirror entrance (225 ns to 6 μs). Ions decaying in the mirror are not recorded at all, but this is not expected to be a problem unless the entrance and exit grids of the mirror affect the decay; otherwise the usual exponential decay law is expected to hold and all of the fragmentation information should still be available.

3.4.2.1 Negative ions

Although the relative intensities of the peaks vary with the number of layers in the LB film (§3.4.2.3), several features of the direct, reflected and neutral spectra remain constant. In general, the major peaks include $[M-H]^-$, $[2M-H]^-$, $[2(M-H)+Ag?]^-$, $[3(M-H)+Cd]^-$, and unassigned peaks 1 and 2, shown in Fig. 3.7 for deuterated stearic acid / cadmium stearate. "M" refers to deuterated stearic acid.

Note that the direct spectra (Fig 3.7a) are dominated by the $[M-H]^-$ ion. A series of moderate intensity fragment ions separated by a CH_2 or a CD_2 unit lead up to it. FAB MS, without collisional activation, of fatty acids in a triethanolamine matrix does not show such a series of ions [Tomer '83], although they are seen in tandem MS [Wysocki '88, Tomer '83]. This is most likely due to the softer ionization produced by FAB MS than by desorption from a solid ML although, as Fig. 3.7c shows, there is some decay of these ions which would lead to a reduced intensity in a magnetic sector machine. High mass clusters are more significant in direct spectra than in the reflected spectra, indicating that they decay more than the smaller ions. This information is confirmed by the neutral spectra which show that the decay of $[M-H]^-$ is very large, the higher mass clusters decay substantially, and the fragment ion series also decay.

In the reflected spectra the three adjacent fragment ion series (spaced 4 u apart) are similar to those in the direct spectra, with each group of three peaks spaced by the mass of a CH_2 or CD_2 unit, as shown in Fig. 3.7a. Some higher mass clusters appear, as well as

a large $[M-H]^-$ ion.

In the daughter ion spectra of $[M-H]^-$, there are two fragment ion series spaced 6 u apart as shown in Fig 3.8a. This is noteworthy because earlier metastable investigations of LB film fatty acids revealed no charged daughters of $[M-H]^-$ although the ion itself was very unstable [Bolbach '88]. Low energy CAD and SID of fatty acids not in a LB film configuration also resulted in a loss of $[M-H]^-$ but no fragment ion series [Wysocki '88] although high energy CAD did give a fragment ion series [Wysocki '88, Tomer '83]. The negative LB film and low energy results lead to the conclusion that, in these experiments at least, both dissociation and electron detachment were occurring [Bolbach '88, Wysocki '88]. Our $[M-H]^-$ correlation spectrum shown (Fig. 3.8a) has low statistics, and it is possible that the processes postulated above could account for the low daughter ion intensity. The prompt and metastable decay patterns are compared in Fig. 3.9. Daughter spectra of $[2M-H]^-$, $[2(M-H)+Ag?]^-$, and $[3(M-H)+Cd]^-$ contain only the $[M-H]^-$ peak, as shown in Fig. 3.8b. The two unassigned ion peaks also decayed to a single peak, $[M-H]^-$, indicating that they contain at least one stearate anion; even so, we have not found a reasonable assignment for these peaks.

3.4.2.2 Positive ions

Although again the relative intensities of the peaks vary with the number of layers in the LB film (§3.4.2.3), several general features of the spectra are constant. As shown in Fig. 3.10a and b, the major peaks in the direct and reflected spectra include Ag^+ (which is often the base peak, especially in films with few ML's and in films with poor quality, but which is not shown), $[M-17]^+$, $[M+H]^+$, $[M+Ag]^+$, $[2M+H]^+$. Smaller peaks include $[M-H+2Ag]^+$, $[2M+Ag]^+$, $[2(M-H)+Ag+Cd]^+$ and $[3(M-H)+2Cd]^+$. Although the positive reflected spectra show no series of fragment ions, the correlation spectra do.

The daughter ion spectra of the $[M-17]^+$ and $[M+H]^+$ ions, which contain four different series of fragments, are shown in Fig. 3.11a and b. The decay patterns are given in Fig. 3.12. The base peak in the $[M+Ag]^+$ daughter ion spectrum is Ag^+, and some $[M-17]^+$ and $[M+H]^+$ are present, although the statistics are poor (Fig. 3.13a). The closely related $[M-H+2Ag]^+$ decays into a relatively large $2Ag^+$ ion peak and into Ag^+, $[M+Ag]^+$ and $[M+H]^+$. The statistics were inadequate to determine whether or not $[M-17]^+$ was also

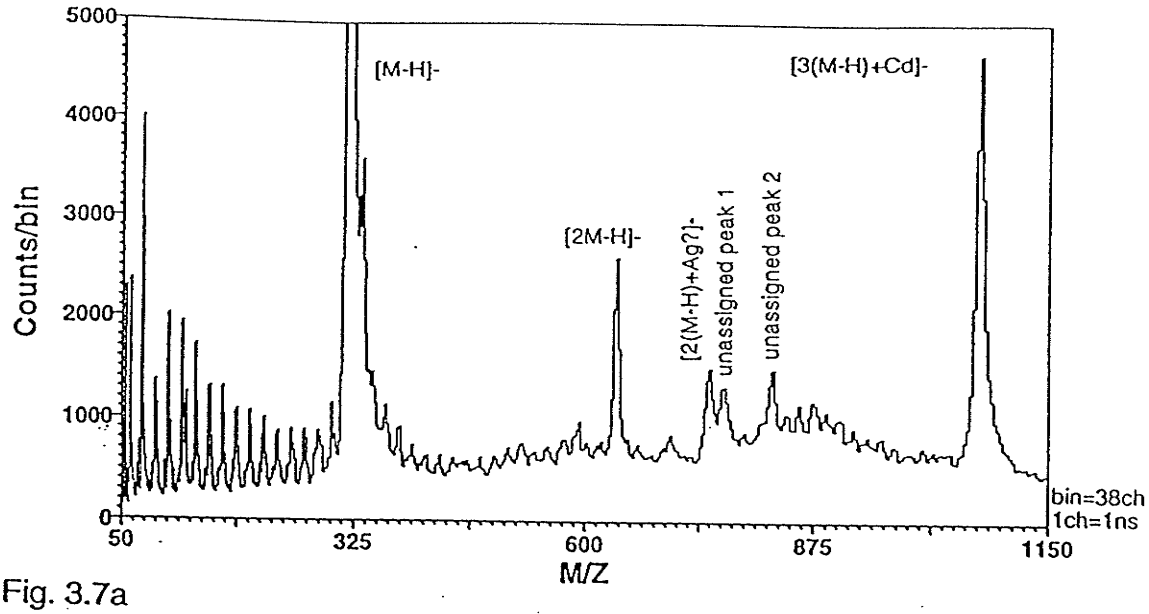

Fig. 3.7a

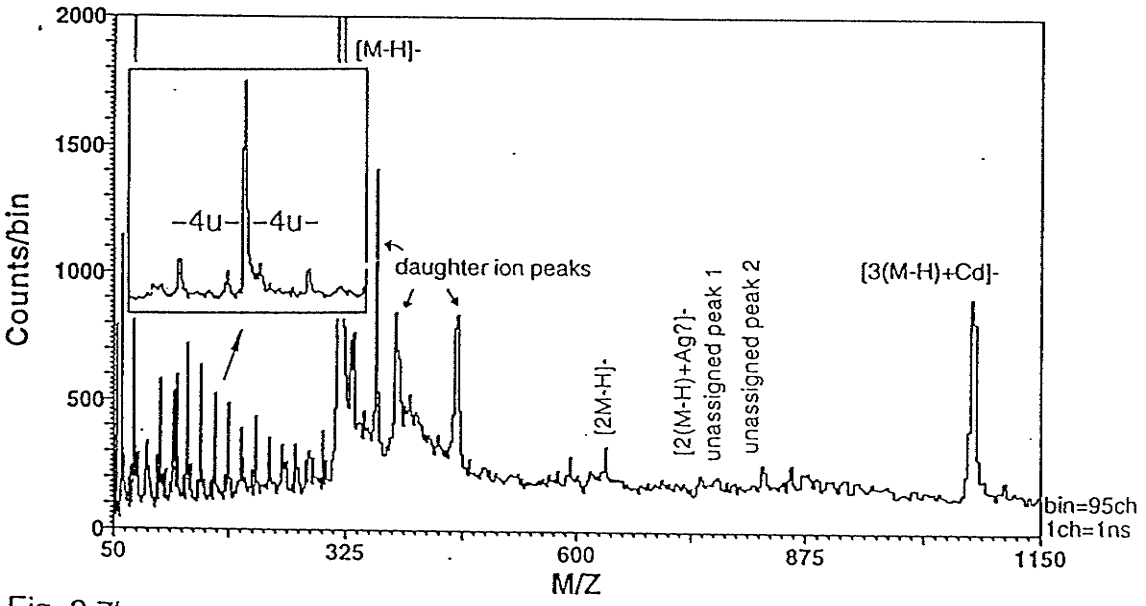

Fig. 3.7b

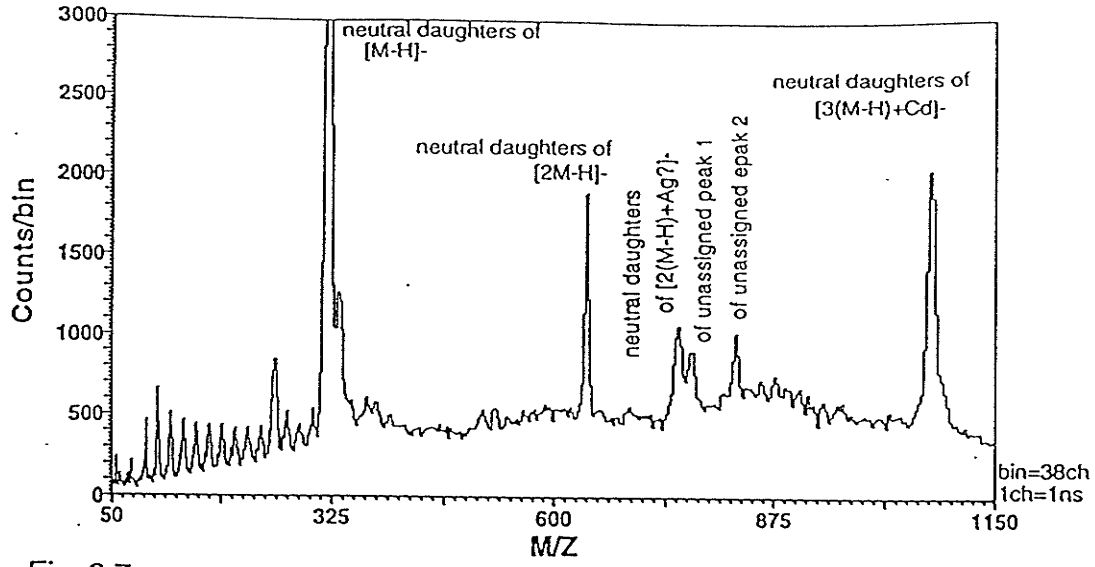

Fig. 3.7c

Fig 3.7 Negative ion spectra of a 9 ML LB film of deuterated stearic acid / Cd stearate; a) direct spectrum, b) reflected spectrum, and c) neutral spectrum.

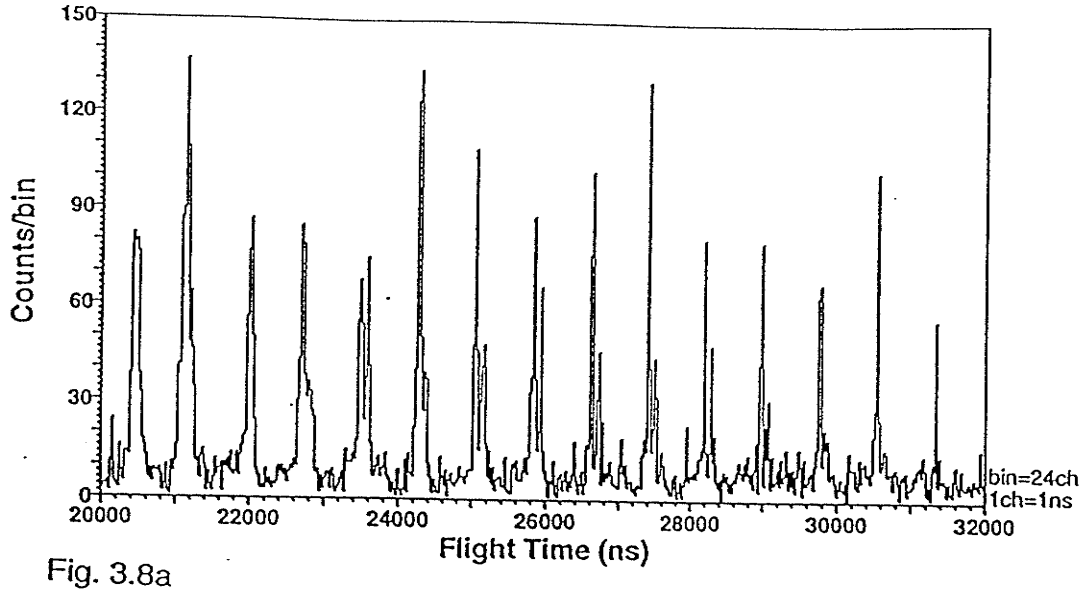

Fig. 3.8a

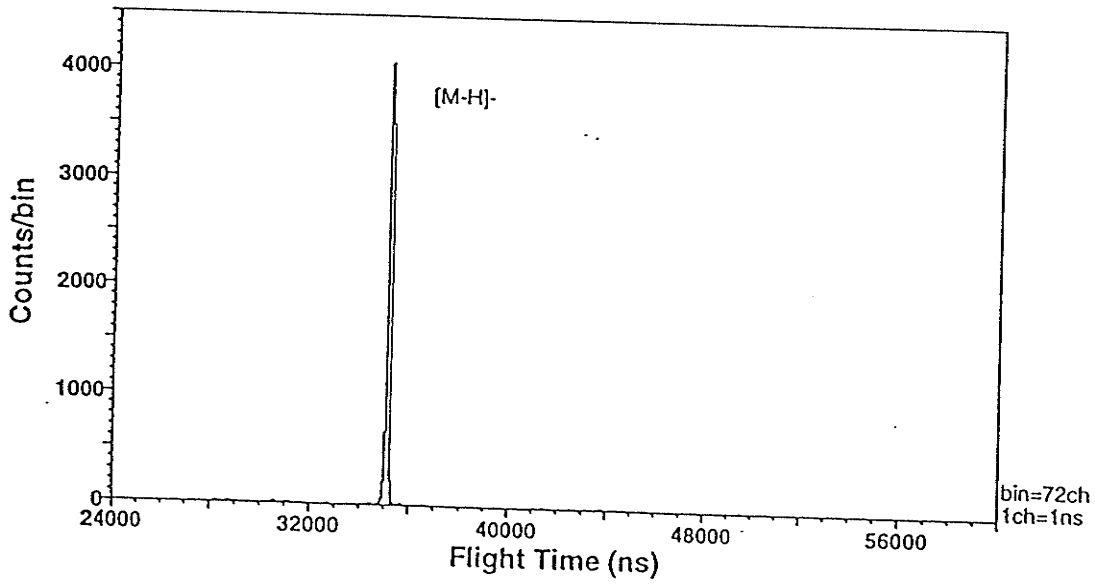

Fig 3.8b

Fig. 3.8 Decay a) of $[M-H]^-$ into a series of fragments (the peaks are defined in Fig. 3.9) and b) of $[2M-H]^-$ into $[M-H]^-$ for a 9 ML LB film of deuterated stearic acid/ Cd stearate (the decay of the other negative prompt ions produces spectra similar to b).

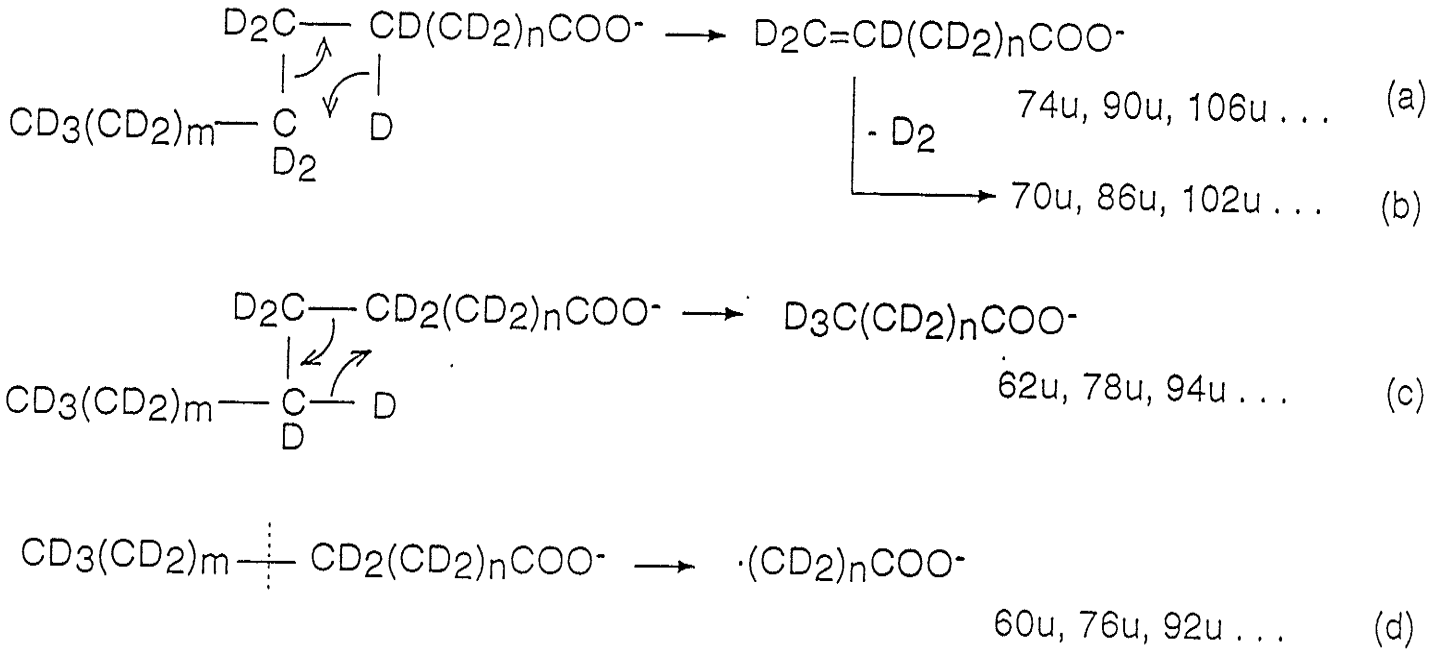

fast fragmentation gives series a, b and c

unimolecular decay of $[M - H]^-$ gives series b and d, but the intensity is variable

Fig. 3.9 Identities and possible reactions of the fragment ion series.

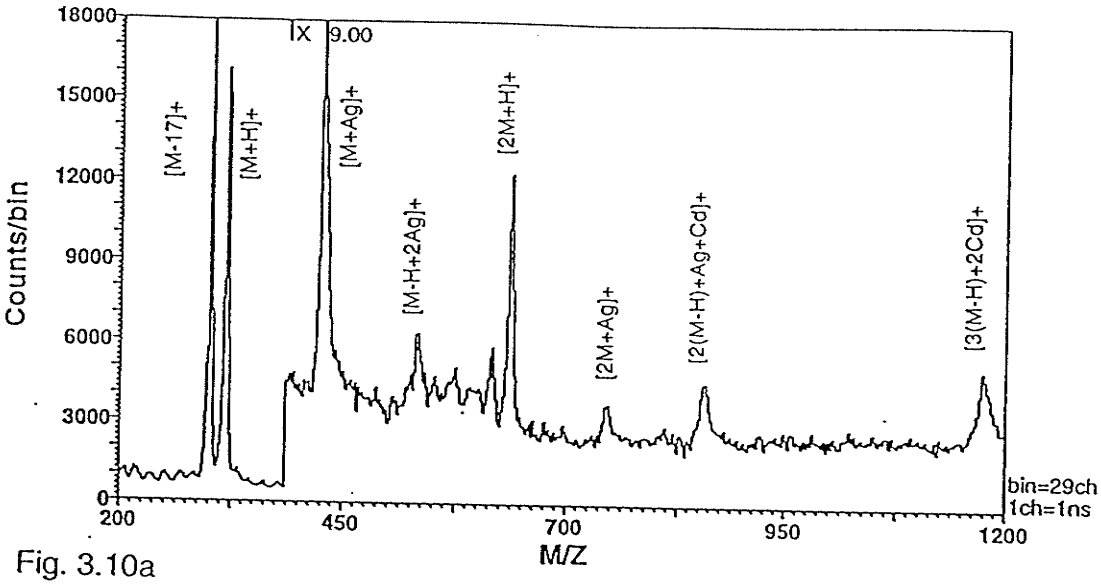

Fig. 3.10a

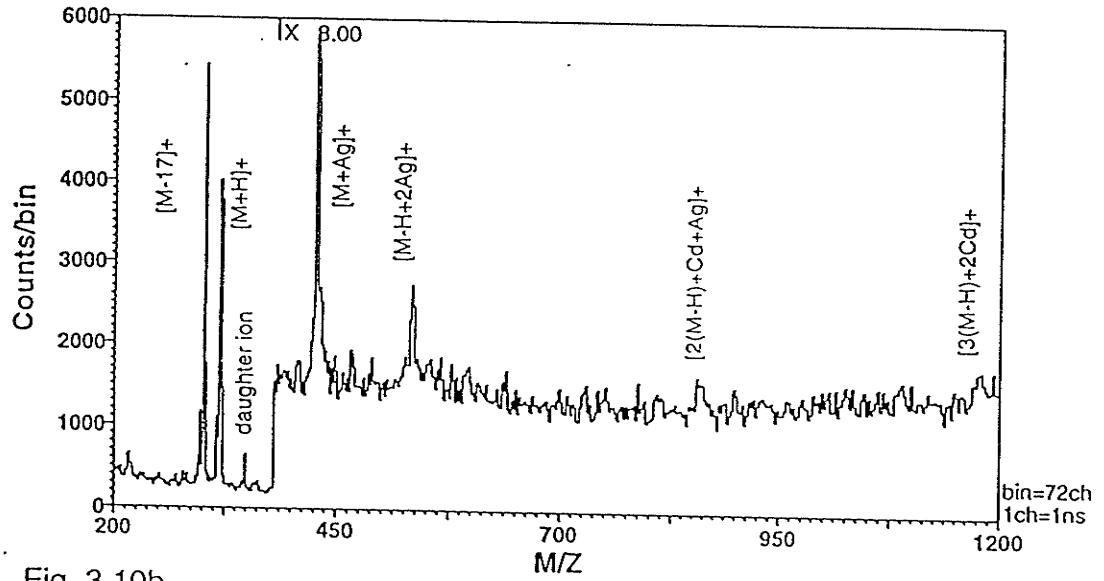

Fig. 3.10b

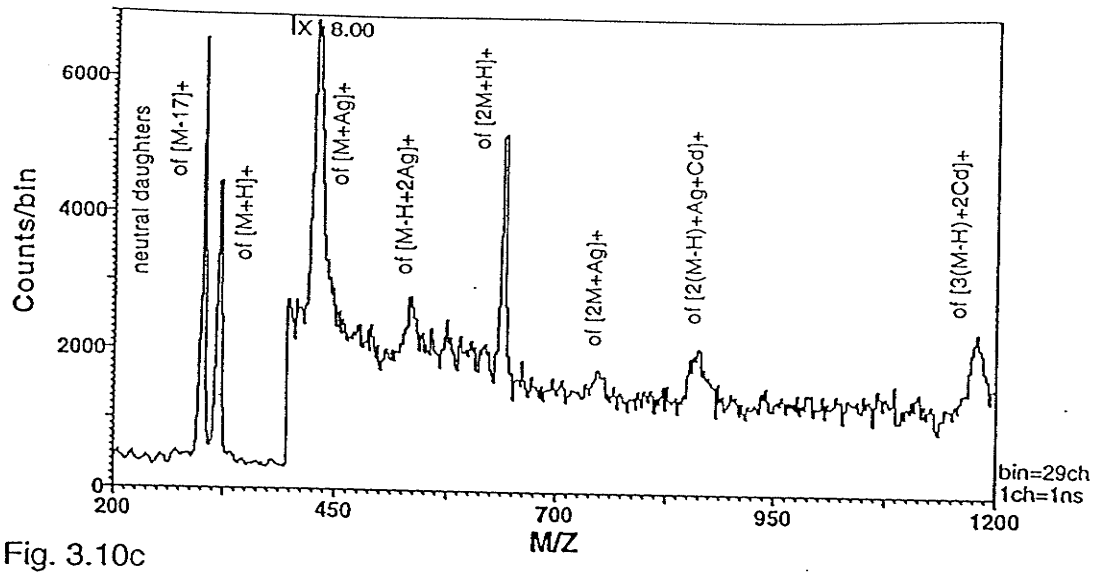

Fig. 3.10c

Fig 3.10 Positive ion spectra of a 9 ML LB film of deuterated stearic acid / Cd stearate; a) direct spectrum, b) reflected spectrum, and c) neutral spectrum.

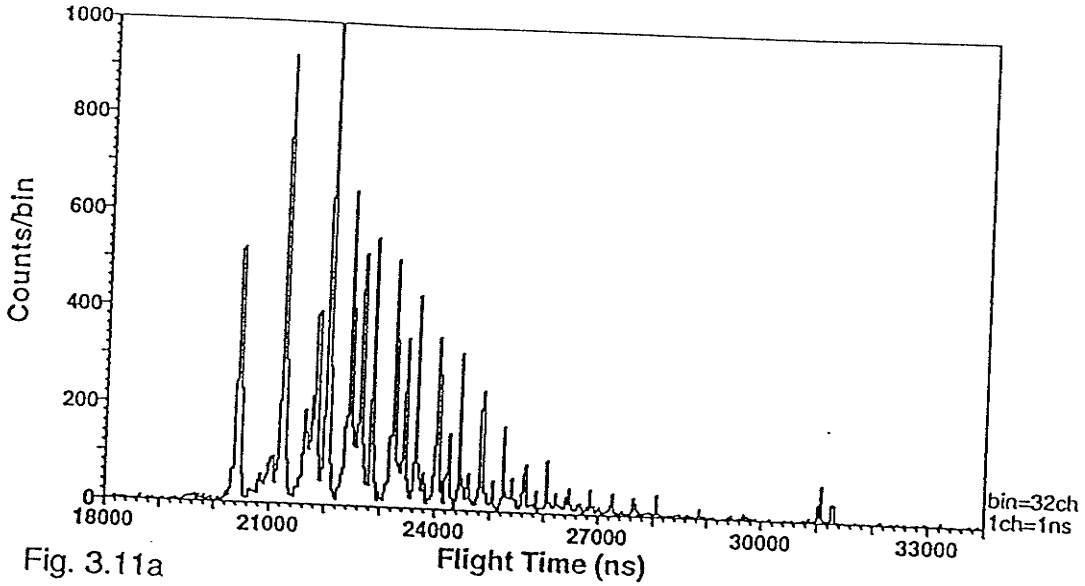

Fig. 3.11a

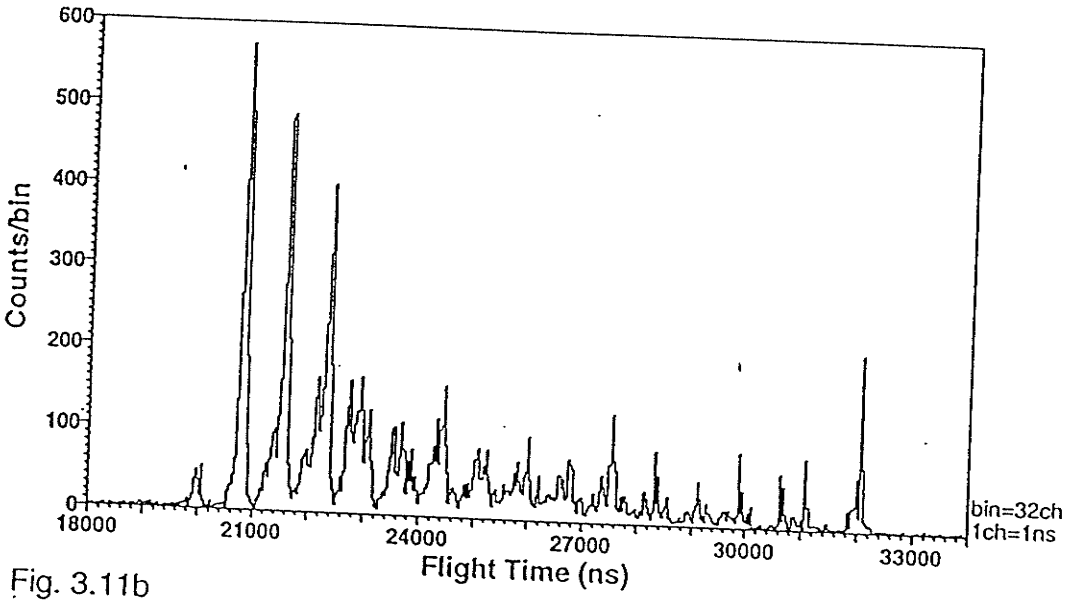

Fig. 3.11b

Fig. 3.11 Decay of the a) $[M-17]^+$ parent and b) the $[M+H]^+$ parent (the peaks are defined in Fig. 3.12).

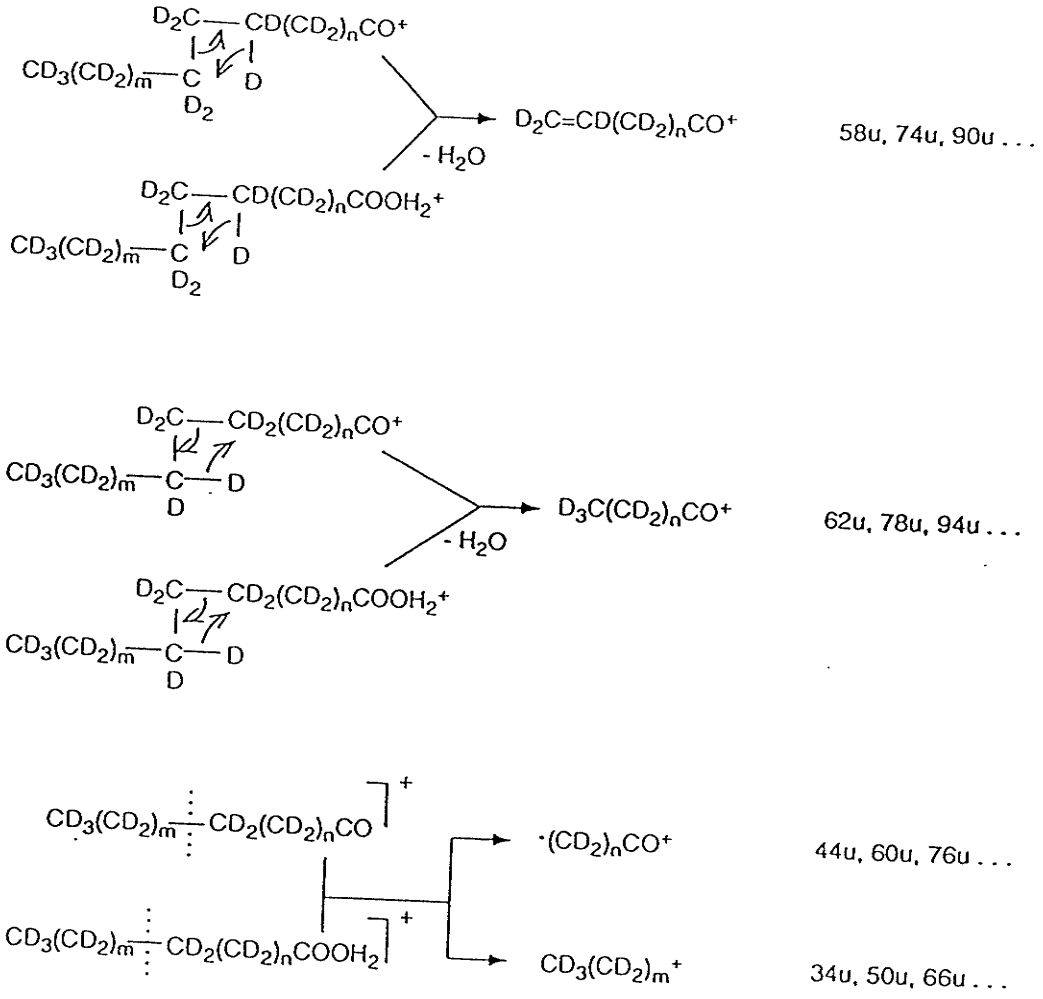

all series are observed in unimolecular decay of $[M + H]^+$ and $[M - 17]^+$ ions

fast fragmentation does not yield a series of ions spaced by 16u

Fig. 3.12 Identities and possible reactions of the fragment ion series.

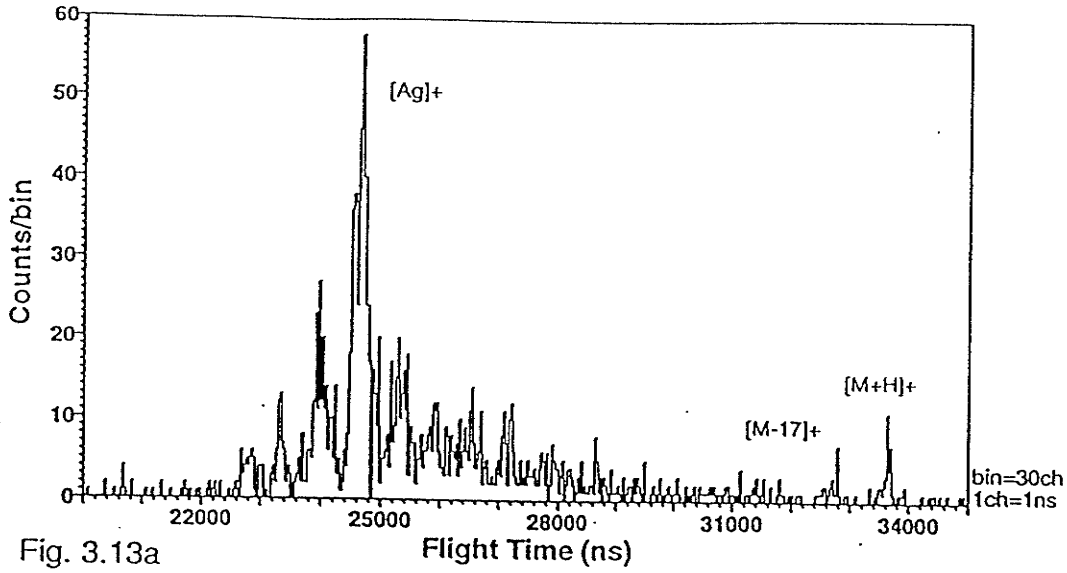

Fig. 3.13a

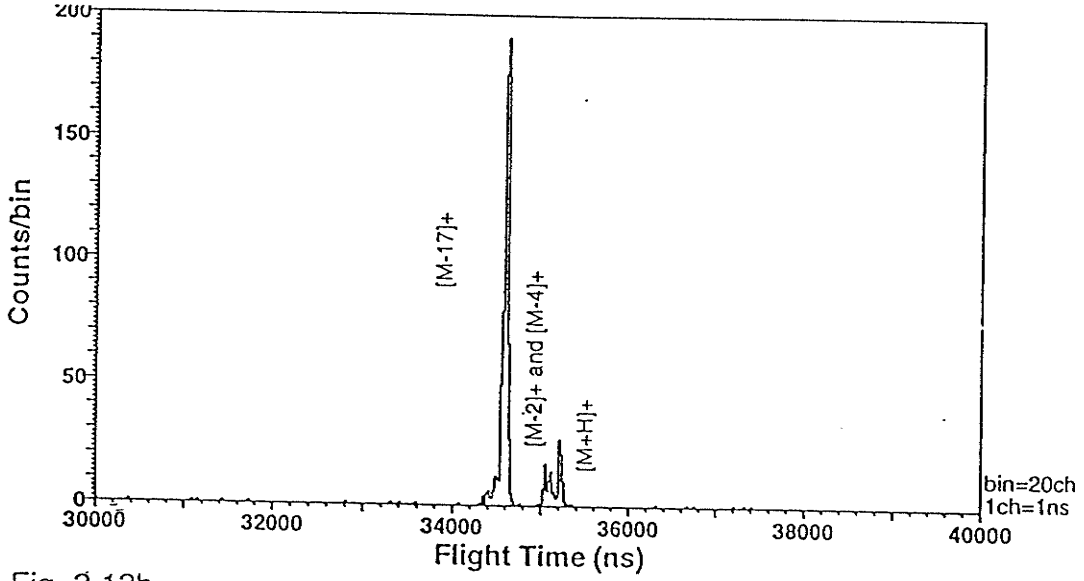

Fig. 3.13b

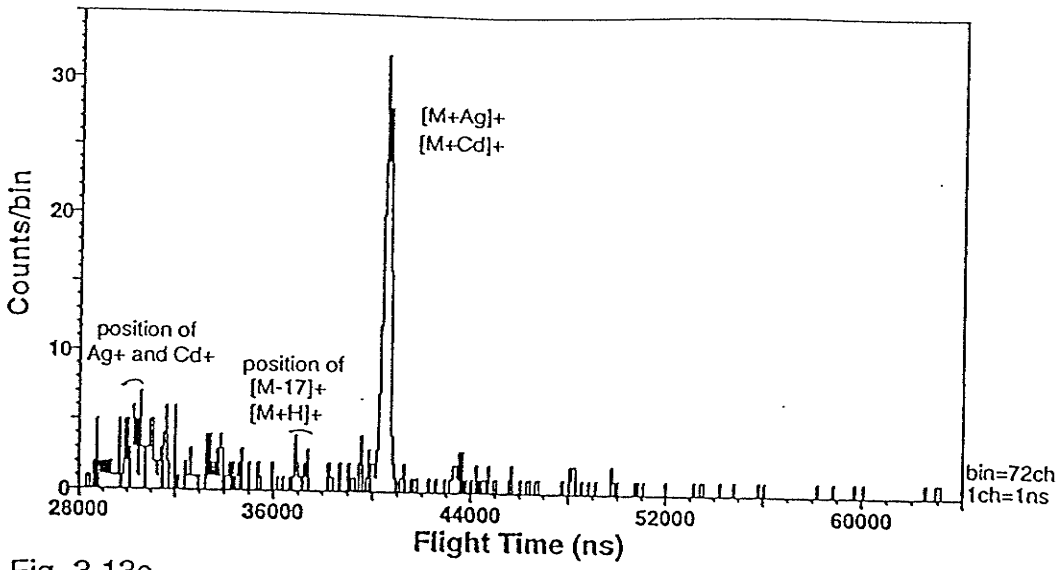

Fig. 3.13c

Fig. 3.13 Decay of a) the $[M+Ag]^+$ parent (the decay of $[M-H+2Ag]^+$ is analogous but has poorer statistics); b) the $[2M+H]^+$ parent; and c) the $[2(M-H)+Ag+Cd]^+$ parent (the decay of $[3(M-H)+2Cd]^+$ is analogous but has poorer statistics).

present. $[2M+H]^+$ decays mainly into $[M-17]^+$, with some $[M+H]^+$ and a tiny peak at a mass of ~M-2 or M-4 (for a deuterated LB film) (Fig 3.13b). As expected, the two closely related clusters, $[2(M-H)+Ag+Cd]^+$ and $[3(M-H)+2Cd]^+$ both decay mainly into $[M+metal]^+$ peaks; the former shows some hints of Ag^+ or Cd^+, but the statistics of the latter are too low to tell whether or not these ions are present (Fig. 3.13c).

3.4.2.3 Yield vs Thickness for various ion species

The yield of various ions, normalized to the integrated ion current, has been measured as a function of multilayer thickness in both the direct and reflected spectra. Two very different behaviors were apparent in both the positive and negative ion data (Fig. 3.14 and 3.15), with some ions producing a maximum yield at 1 monolayer, and some at 5 or 7 monolayers. The direct and reflected spectra give similar plots as had been expected. Because of the monolayer imperfections, the data do not give detailed information about the actual emission depths in SIMS, but they do represent the relative trends of yields versus thickness for the different molecules. Some effects of the sample are observed in the values for the 9 layer film, but they have not been explained. (Note that all of the data presented in the other sections of the results, which are mostly for a 9 layer film, were taken using a *different* film.)

The ions whose yields peaked at one monolayer and then decreased with film thickness were Ag^+, $[M+Ag]^+$, $[M-H+2Ag]^+$, $[2(M-H)+Ag+Cd]^+$, $[3(M-H)+2Cd]^+$, $[Ag]^-$, $[M-H]^-$, $[2(M-H)+Ag?]^-$, $[3(M-H)+Cd]^-$. In all cases (except $[M-H]^-$) these ions include either the substrate (Ag), or the counter ion (Cd^{2+}) which is expected to be on the substrate for the first monolayer and between the head groups of adjacent layers for subsequent pairs of monolayers. Although other experiments have shown that Ag complexes only with the outermost layer of the ML film (§3.2.2.3), these data suggest that it may do so most efficiently if the outer layer is also the only layer. The data also imply that Cd^{2+} complexes either form more easily or are more stable when only one monolayer is present. This is a surprising result for the $[3(M-H)+2Cd]^+$ molecule which is not be expected to form easily from the first monolayer where the Cd^{2+} ion has been observed to bind lightly to the polar group [Laxhuber '83]. Either the three deprotonated molecules' carboxylic acid groups are arranged to maximize their attraction for each other and for the two Cd^{2+} ions, or the

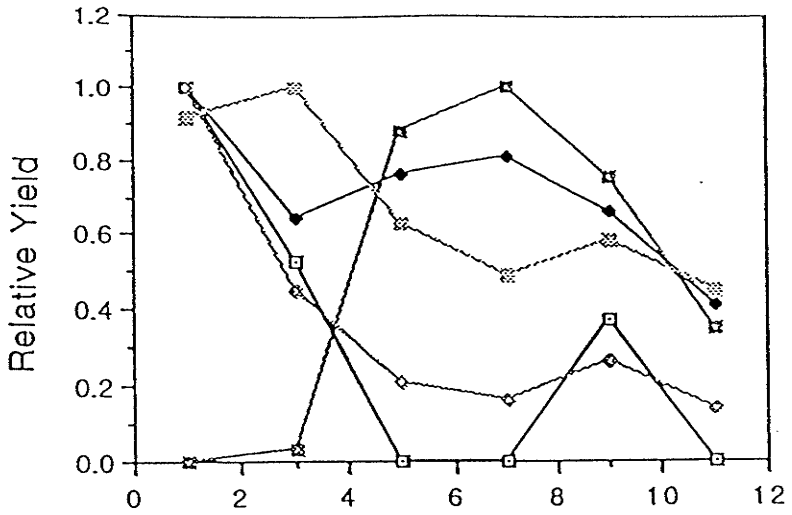

Fig. 3.14a

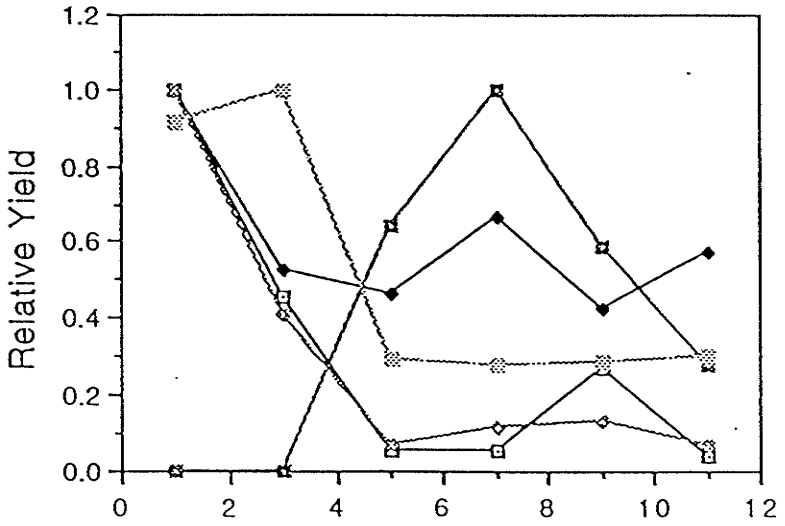

Fig. 3.14b

LB Film Thickness (monolayers)

Ag^-
$[M-H]^-$
$[2M-H]^-$
$[2(M-H)+Ag?]^-$
$[3(M-H)+Cd]^-$

Fig. 3.14 Yield vs thickness for negative spectra: a) direct spectra and b) reflected spectra. The anomaly observed at 9 layers seems due to the film itself, but it is not understood.

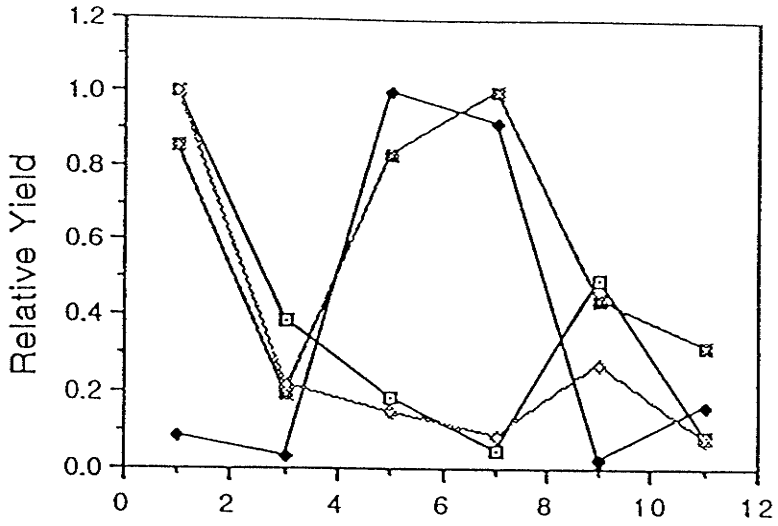

Fig. 3.15a

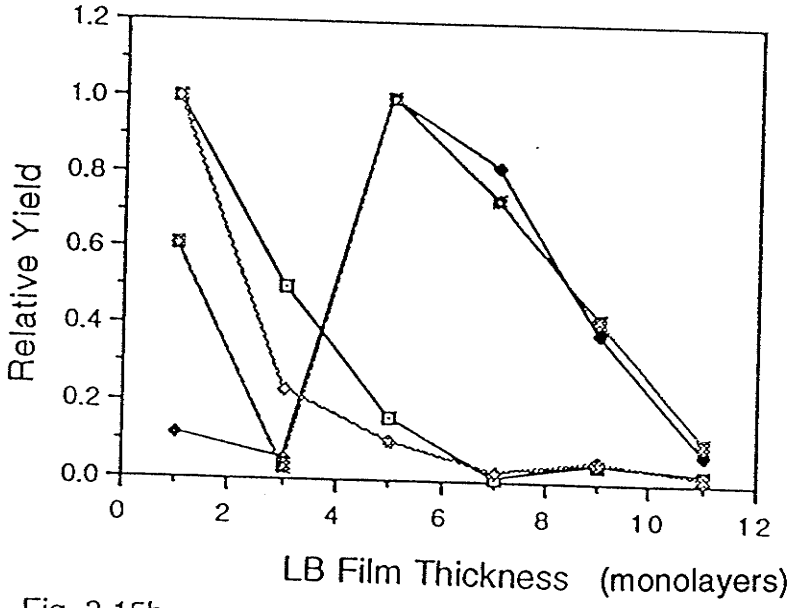

Fig. 3.15b

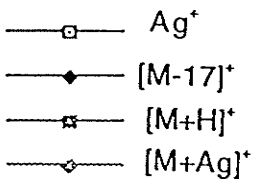

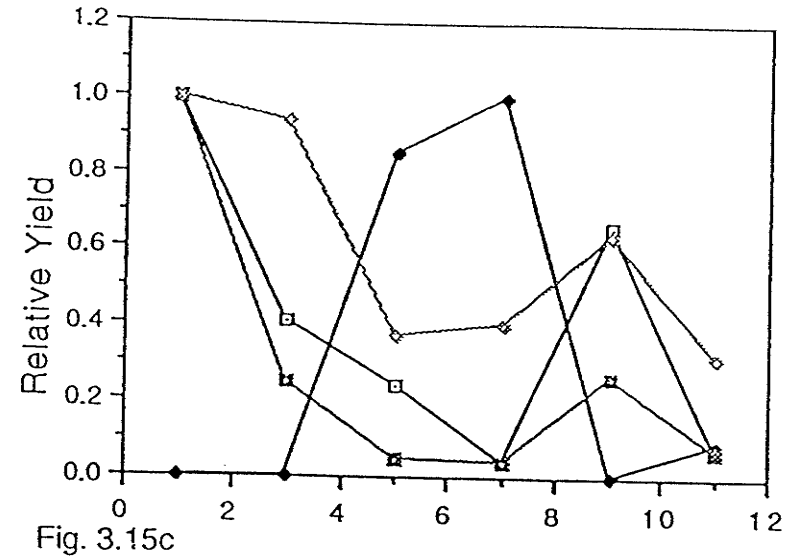

Fig. 3.15c

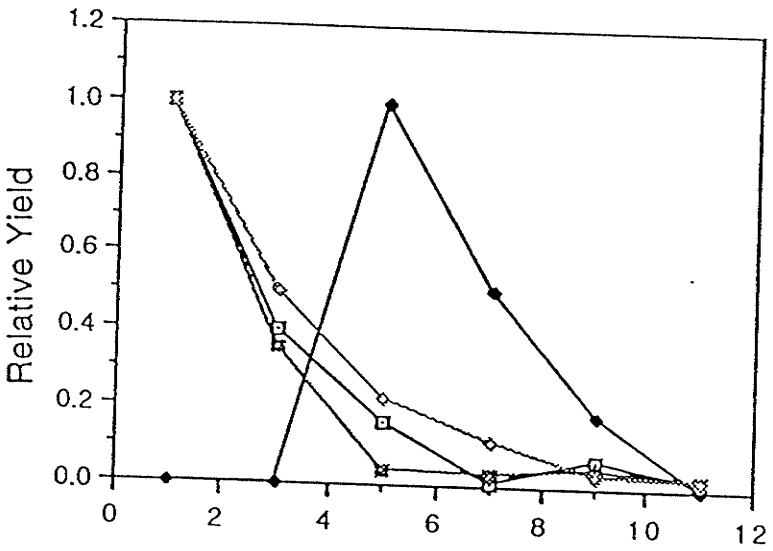

Fig. 3.15d

LB Film Thickness (monolayers)

[M-H+2Ag]$^+$

[2M+H]$^+$

[2(M-H)+Ag+Cd]$^+$

[3(M-H)+2Cd]$^+$

Fig. 3.15 Yield vs thickness for positive spectra: a) low mass peaks, direct spectra, b) low mass peaks, reflected spectra, c) high mass peaks, direct spectra, and d) high mass peaks, reflected spectra. The anomaly observed at 9 layers seems due to the film itself, but it is not understood.

complex cannot be formed as easily when Cd^{2+} is bound strongly between two layers as occurs when more layers are present [Laxhuber '83].

Previously the $[M-H]^-$ ion was shown to have a maximum yield at 1 monolayer for Cd stearate on Ag [Bolbach '88], which was confirmed in these experiments. This has been attributed to chemical adsorption of the preformed ion to the metal substrate [Bolbach '88a], which is supported by the observation that the intensity depends strongly on the nature of the metal substrate [Bolbach '88]. This behavior is like that of the metal-containing complexes and unlike that of the other ions involving only the fatty acid, indicating that these ions may arise from unstable metal-containing clusters. However, others have noted that the spectra of $[M-H]^-$ and metal-containing ions depend differently on the pH at which the monolayer was coated [Bolbach '88a], so their mechanism of formation is expected to be different. In PDMS as well, the yield versus thickness curves for $[M-H]^-$ and $[3(M-H)+Cd]^-$ are like each other, although they are different than the results for SIMS [Bolbach '88].

Ion yields peak at a film thickness of 5-7 monolayers for ions involving only the fatty acid (i.e. $[M-17]^+$, $[M+H]^+$, $[2M+H]^+$, and $[2M-H]^-$). This undoubtedly reflects the increase in the available amount of these species with increasing film thickness, and may also reflect the previously observed phenomenon that some of these ions have a very low yield at small coverages. The decrease in intensity after this maximum yield may reflect a decrease in the effect of the substrate, although this effect has been debated (§3.2.2.2).

Others have observed no $[M+H]^+$ emission for 1 ML LB films [Cornelio '90, Bolbach '88a] which we observed in both the direct and reflected modes. It is extremely unlikely that our film quality was so poor that the 1 ML films contained some 3 ML film or molecular solid, for which the protonated ion has been observed. The reasons for this discrepancy are not known. It is interesting that the $[M-17]^+$ yield is low for 1 and 3 ML's for the deuterated films, but is similar to that of $[M+H]^+$ for the undeuterated films; this might imply the presence of some impurity or film defect.

3.4.2.4 Time Evolution of Various Ions, Including I^- Adducts

Datalogging allows the time evolution of the ion peaks to be examined to determine whether there is any change with time under static SIMS conditions; by definition this is

not expected. However, there is one very unusual set of changes, observed also in the work with the alamethicins: the negative spectrum shows I^- adducts after a considerable primary ion flux (note that these conditions may still fulfill the static SIMS current and charge conditions (§3.1.1) although we are not certain). After a very small primary ion flux, there are no I^- adducts, as demonstrated in Fig. 3.7. After 3 hours of primary ion bombardment at 15 and 25 keV impact energy, a strong I^- peak appeared in the direct spectrum, as well as clusters such as $[3I+Cd]^-$, $[(M-H)+2I+Cd]^-$, and $[2(M-H)+I+Cd]^-$. In the datalogging readback, spectra were taken after 0-10 min and 50-60 min. The later reflected spectra show a much larger I^- peak, a less intense $[M-H]^-$, and less intense fragment ions, as well as the same three new peaks as in the direct spectrum. In contrast the neutral spectra before and after bombardment were very similar with only one new peak, corresponding to decay of $[2(M-H)+I+Cd]^-$. It is interesting that no Ag-containing ions were formed although Cd was present in the new ions. This could be because the Cd is present in the film itself, whereas the Ag is only underneath the film. Even more curious is the complete lack of $[M+I]^-$ in these spectra (compare the negative alamethicin spectra which all showed peaks corresponding to the molecular ions with an I^-). Another study of stearic acid with Cl^-, Br^-, and I^- present showed no evidence of anionization [Wandass '85], perhaps because the concentrations of these molecules were low, but if HCl had been added to the subphase, Cl^- adducts were present in the spectra [Bolbach '88a].

The positive spectra do not seem to be greatly affected by long I^- ion bombardment. For example, the ions $[M-17]^+$, $[M+H]^+$, $[M+Ag]^+$, $[M-H+2Ag]^+$, $[2M+H]^+$, and $[3(M-H)+2Cd]^+$, are still present in the direct spectrum after 3 hours of primary ion bombardment. Some effects of primary ion-induced damage are expected to be evident, but may be masked by the fact that the 1.5 hour negative ion experiment was performed first and had already damaged the target before this 1.5 hour experiment was performed. Comparing this bombarded target with another fresh one shows no great difference in the direct spectra with and without the extended bombardment except that the bombarded sample has a relatively lower yield of Ag^+ and higher yield of $[M+Ag]^+$ (although this is likely an artifact because different LB films were used in the comparison). The reflected spectra taken in the first 10 min and from 50 to 60 min are very similar; the latter had higher relative intensities of Ag^+, $[M+Ag]^+$, $[M+2Ag]^+$, and $[2(M-H)+Ag+Cd]^+$. The corresponding neutral spectra showed that the data taken from 50 to 60 min had slightly lower intensities of

$[M+Ag]^+$, $[M+2Ag]^+$, and $[2(M-H)+Ag+Cd]^+$. Unfortunately we did not record the corresponding direct spectrum, but it seems possible that the same amount of ions were desorbed but with different stabilities. This would correspond to the results obtained for another LB film before and after a long primary ion bombardment time; in that case the direct spectra showed no significant change.

Cs^+ adducts are not seen in the positive ion spectra, and it is obvious that the chemical properties of the I^- ions must influence the negative spectra for I^- adducts to occur. Chemically reactive ion beams can introduce large modifications into the sample surface even at a low flux, and can strongly affect secondary ion emission [Benninghoven '87]. Because secondary ion emission depends very strongly on the chemical composition of the surface layer of the target [Benninghoven '83], any implanted I^- ions, even under conditions which are usually referred to as static SIMS , may have a considerable effect on the mass spectrum. These results suggest that for a reactive incident beam like I^- the charge and current requirements of static SIMS may not be quite stringent enough to ensure that most of the secondary ions arise from a sample spot unaffected by the ion beam. It does, however, seem reasonable to assume that for the short data acquisition times normally used, when static SIMS conditions were more than fulfilled and when no I^- adducts were observed, the LB films were not significantly affected by the primary ion beam. Also, it seems obvious that the cross sections for I^- and Cs^+ are different.

The presence of adducts after a considerable data acquisition time can be useful and can cause difficulties. If it causes overlapping peaks or if too many clusters are present it can significantly complicate a spectrum, as it did for the negative spectrum discussed above. On the other hand, in some cases it may contribute an extra peak to assist in molecular weight determination, as in the alamethicin work. Here only the deprotonated molecule showed adducts, and one check on the number of molecular ions present in the spectra was the number of I^- adducts. It is conceivable that the I^- source may also be used to study on-target iodine reactions under controlled conditions.

3.4.2.5 Discussion

As explained (§3.2.2 and §3.3), unless the chemical purity and coating conditions meet very high standards, the resultant LB films are not perfect but may contain pinholes

and other imperfections such as striations due to meniscus instabilities (Appendix 3.1) or vibrations. Although some of the films reported in the literature do seem to be of high quality (§3.2), many have not been prepared rigorously enough for fundamental studies. This can be a problem when film preparation conditions are not given in adequate detail to assess the film quality so that the validity of the results cannot be judged, or when possible problems are not acknowledged and fundamental conclusions are drawn from possibly defective data (§3.2.2.4). On the other hand, as the work of Gardella's group (3.2.2.3) shows, interesting and useful results can be obtained from films prepared with less than optimum rigor; in fact, in some cases, the effort and expense necessary to produce near-perfect films is not justified. Therefore, although our LB films are by no means perfect, the results obtained in this work are valid as presented above.

For our pH and Cd^{2+} concentration, the multilayers were composed of microdomains of both stearic acid and Cd stearate [Hasmonay '80] (similarly for the deuterated films). Although this could cause difficulties for any study at the molecular level, it did not affect our results because our primary ion beam spot was significantly more than 3 mm in diameter (§1.4.1), allowing detection of an average surface composition.

Although it is not true for all LB films that the structure of the deposited monolayer is identical to that on water, it has been shown for Cd fatty acid salts that the molecules are perpendicular to the surface both before and after deposition [Peterson '90]. All carboxyl groups except those in the first layer face another layer of carboxyl groups. It is also not true that most LB films, even of fatty acids and fatty acid salts, are stable, but Cd soap films are stable even at somewhat elevated temperatures [Peterson '90].

Our films can be expected to give reliable information about the general trends in yield versus LB film thickness, although not about the actual thickness at which the yield has decreased by a certain percentage. The fragmentation patterns are expected to be independent of the film quality as long as it is reasonable. The time evolution of the yield of various ions is also expected to be largely independent of film quality.

Fragmentation patterns at different times are of interest in that they may give some information about the energy required for different decay channels [Van Veelen '91, Wysocki '91, '88]. Often one can say that the reactions occurring early are due to large amounts of internal energy deposited into the molecules, and that those occurring later seem to require less energy. The simple view is complicated by the possibility of a kinetic shift occurring,

in which the average energy required for decomposition increases as the observation time decreases. As explained above, our method allows examination of two time windows simultaneously (*i.e.* both prompt and metastable fragmentation).

The fragmentation information we obtained could be useful to any workers who had the capabilities of preparing high quality LB films of alternating layers and were interested in studying the energy deposited by primary ions at various depths in LB films. A comparison of the fragmentation of ions from different depths in the films could give some information about the internal energy at different depths. This could be interpreted in terms of energy distribution in the LB film immediately preceding and during desorption/ionization. The greatest amount of data could, of course, be obtained if the spectrometry were done using TOF-MS with the correlation technique and datalogging, although other techniques could give the same information using several LB film targets for each data set.

3.4.3 CONCLUSIONS

Stearic acid / cadmium stearate LB films were examined by TOF-SIMS to acquire data about prompt and metastable fragmentation patterns, about the yield of various ions versus film thickness, and about the time evolution of ion intensities under I^- ion bombardment. We were able to obtain such a wealth of fragmentation information while meeting static SIMS requirements because of the very sensitive TOF SIMS correlation technique with datalogging.

CONCLUSION

TOF SIMS was used to sequence Dynorphin A (1-17) as an unknown peptide. The sequencing procedure and the enzymatic and chemical treatments were described in detail. This and similar peptides have proven difficult to sequence by other mass spectrometric methods. Directly related future work includes determining the mode of formation of the unusual C_{15}+17 and C_{16}+17 ions observed in the dynorphin spectrum after acetylation in methanol (§2.2.3.5).

The TOF SIMS correlation technique with datalogging was used to verify an alamethicin sequence and to obtain sequence information for several more. These peptides are extremely unstable and are therefore well suited to analysis by the correlation technique. In other mass spectrometric methods, much of the information we obtained would have been lost. Much of the fragmentation information obtained has not yet been analyzed in detail to study ion stabilities and fragmentation energies of closely related peptides in the two different time scales observed (§2.3.4.2). Simple model peptides could also be useful in such work.

Langmuir-Blodgett film preparation was described in enough detail to guide anyone wishing to prepare reasonable quality films at a minimum cost. TOF SIMS was used to acquire secondary ion yield versus film thickness data for various ions. Prompt and metastable fragmentation (representing decay in different time windows, hence with different internal energies) were compared. The bombarding I^- ions affected the negative spectra over time, but did not seem to influence the positive spectra. In these experiments, the sensitivity of our technique was crucial to obtain the data without unduly disrupting the fragile LB films. LB film studies could be extended to alternating ML's. The reasons for different series of CH_2 / CD_2 loss in the prompt and metastable regimes should be elucidated (§3.4.2.1, §3.4.2.2).

TOF SIMS, with or without the extra sensitivity provided by the correlation technique and datalogging, proved to be uniquely suited to each of these experiments, providing

significant advantages over other mass spectrometric methods. This work represents three classes of experiments which are uniquely suited to our method: sequencing of very basic peptides, sequencing of very unstable peptides, and studying very fragile films.

APPENDICES

2.1 Table of Amino Acid Masses and Associated Mass Spectral Fragments

Name	Symbol	Mass in u Principal (Average)	Related Low Mass Ions and *Neutral Losses from $[M+H]^+$* *
Alanine	Ala A	71.04 (71.08)	44.1,** *15*
Arginine	Arg R	156.10 (156.19)	129.1, 59,70,87,100,112, *100*
Asparagine	Asn N	114.04 (114.10)	87.1, 70, *58*
Aspartic Acid	Asp D	115.03 (115.09)	88.0, *59*
Cysteine	Cys C	103.01 (103.14)	76.0, *47*
Glutamic Acid	Glu E	129.04 (129.12)	102.1,84,91, *36,45,60,62,73*
Glutamine	Gln Q	128.06 (128.13)	101.1, 30,56,84,128,129,130, *45,59,72*
Glycine	Gly G	57.02 (57.05)	30.0,** *1*
Histidine	His H	137.06 (137.14)	110.1, 82, *81*
Isoleucine	Ile I	113.08 (113.16)	86.1, 44, *44,57*
Leucine	Leu L	113.08 (113.16)	86.1, 44, *44,57*
Lysine	Lys K	128.09 (128.17)	101.1, 30,56,84,128,129,130, *45,59,72*
Methionine	Met M	131.04 (131.19)	104.1, 56,61, *48,75*
Phenylalanine	Phe F	147.07 (147.18)	120.1, 91,103, *91,92*
Proline	Pro P	97.05 (97.12)	70.1, *41*
Serine	Ser S	87.03 (87.08)	60.0, *31*
Threonine	Thr T	101.05 (101.11)	74.1, *45*
Tryptophan	Trp W	186.08 (186.21)	159.1, 77,117,130,132, *130*
Tyrosine	Tyr Y	163.06 (163.18)	136.1, 91,107, *107, 108*
Valine	Val V	99.07 (99.13)	72.1, 41,55,69, *31,43*
α-Aminoisobutyric acid	Aib B	85.05 (85.11)	58.1, *???*

*monisotopic masses are used for the immonium ions (underlined); nominal masses are used for the other ions and for the neutral losses (italics) [Papayannopoulos '91, Johnson '89, Lee].

**note, these masses can also be formed by rearrangements from other aliphatic amino acids [Johnson '89], so they cannot be used as indications of these amino acids.

2.2 Number of Amino Acid Combinations Near 695 u.

Mass Range	Number of Amino Acid Combinations
694.55-694.65	0
694.65-694.75	0
694.75-694.85	0
694.85-694.95	0
694.95-695.05	0
695.05-695.15	0
695.15-695.25	221
695.25-695.35	1244
695.35-695.45	1079
695.45-695.55	125

Since these combinations are composed of the same elements, H, C, N, O, and S, their mass excesses are expected to fall within a narrow mass range, as shown above. Calculations were done using a VAX computer. A similar pattern occurs at other masses. (Note that for each of the amino acid combinations mentioned above, many permutations of the amino acids are possible, so the number of sequences is much larger than the number of combinations.)

2.3 Enzymatic Digestions Used in Dynorphin Sequencing

Trypsin (T), α-chymotrypsin (CT), carboxypeptidase Y (CPD-Y), carboxypeptidase P (CPD-P), staphylococcus aureus V8 protease (V8) and leucine aminopeptidase (LAP) were purchased from Sigma (St. Louis, MO), and leucine aminopeptidase M (LAP-M) from Boehringer Mannheim (Montreal, Canada).

The following aqueous buffer solutions were used: A = 0.05 M ammonium bicarbonate (pH 7.8); B = 0.10 M ammonium acetate adjusted to pH 6.0; C = 0.08 M ammonium acetate adjusted to pH 6.0; D = 0.10 M ammonium acetate adjusted to pH 4.5; E = 0.001 M phosphate buffer (pH 7.9; K_2HPO_4:KH_2PO_4 = 3.9:1)

Enzymatic digestions were performed according to two general procedures:

(a) On target. Approximately 1-5 μL of the buffered enzyme solution was deposited on ~0.1 μg of the substrate on nitrocellulose that had been electrosprayed onto aluminum foil or etched silver. This was covered with a glass microscope slide during the course of the digestion; alternatively it was left uncovered, and buffer was added if evaporation was more rapid than expected.

(b) In solution. Approximately 2 μg of the substrate was dissolved in 30 μL of the buffered enzyme solution in a small cavity drilled in a teflon block.

Specific conditions for the digestions are given in Table 1. While T, CT, CPD-Y and CPD-P gave the expected cleavages, the other digestions were not successful. Digestions attempted with LAP and LAP-M under a variety of conditions, including the presence of $MgCl_2$ for LAP, both on target and in solution, did not yield any useful mass spectra.

Chemical Derivatizations

Conversion of the N-terminal $-NH_2$ group to $-NHCOCH_2N(CH_3)_3^+$ was based on the method of Vath and Biemann [Vath '90]. Dynorphin A, deposited on a glass slide by evaporation of its 0.1% aqueous trifluoroacetic acid (TFA) solution, was reacted with gaseous chloroacetyl chloride at 45°C for 1 hour. The reaction product was then reacted with the vapor in equilibrium with 25% aqueous trimethylamine at 45°C for 2 hours. The product on the glass slide was dissolved in 0.1% aqueous TFA and frozen until used. About 0.5 μg of the derivatized peptide was then deposited on a nitrocellulose target.

Acetylation of amino groups (N-terminal + lysine) of Dynorphin A was performed by two procedures, based on methods described in the literature [Gaskell '88a, '88b, LeVine '87, Morris '74, Hunt '73]: (a) 0.15 μg in 11 μL of methanol was reacted with 11 μL of acetic anhydride for 70 min at room temperature; (b) 7 μg in 20 μL of 0.1% aqueous TFA was reacted with 20 μL acetic anhydride for 15 hours at room temperature. (Note that to avoid incomplete acetylation and methyl ester formation, acetylation could be done using acetic anhydride/water (1:1, v/v) for 1/2 hour at room temperature [Williams '82].) From both products, the solvents were evaporated in vacuo and stored frozen. For use, each was dissolved in 0.1% aqueous TFA, and about 1 μg was deposited on

nitrocellulose.

TABLE A2.1. Summary of the Enzymatic Digestions

Substrate	Enzyme	Buffer	Procedure	Temp °C	Time(min)
≈0.2 µg* "unknown"	1 µL of 3.3 µM T	A	a	39	24
≈0.1 µg* "unknown"	1-1.5 µL of 3.4 µM CT	A	a	25-38	10-12
≈0.54 µg Dyn-A	52 ng of CPD-Y in 5.2 µL	B	a	35.5	≈8
31 µM Dyn-A	0.55 µM CPD-Y	C	b	≤45	10,20,30, 40,50,60**
≈0.54 µg Dyn-A	26 ng of CPD-P in 5.2 µL	D	a	≈37	12
0.1-0.5 µg Dyn-A	160-300 ng of V8 in5 µL	A,E	a	25-40	12-35

*Based on the assumption that 1.5 µg of "unknown" was supplied.
**Six 1 µL aliquots were removed at 10 min intervals and put on the target.

2.4 Solution Conditions for the Alamethicins

recrystallized 21.34 minute fraction: ~1mg[1] /1 ml .1% TFA; ultrasonic shaking used to dissolve the peptide; not totally dissolved

21.34 minute fraction (no crystallization): <.1 mg, dissolved in 200 µl .1% TFA; 1 hr ultrasonic shaking; not totally dissolved

23.33 minute fraction : ~.1mg/ 100 µl; dissolved more easily than the 21.34 minute fraction

23.33a minute fraction): could not see sample; added 50 µl .1% TFA

23.33b minute fraction : could not see sample; added 50 µl .1% TFA

24.53 minute fraction : <.1mg / 100 µl .1% TFA; ultrasonic shaking

25.57 minute fraction : sample was a spheroid , 2mm diameter; added 100 µl .1% TFA; ultrasonic shaking; not totally dissolved

22.56 minute fraction : vial contained yellow spots and a bit of white fluff; added 100 µl .1% TFA; ultrasonic shaking

ala/aib alamethicin : ~.5mg / 1.5 ml .1% TFA ; ultrasonic shaking for 1 hr; seemed totally dissolved (added so much TFA because this peptide was said to be especially insoluble)

2.5 Positions of daughter ions and parent ions in reflected spectra

As Figure 2.10 shows, the reflected spectrum of alamethicin contains many overlapping peaks, some of which are daughter ions and some of which are parent ions. Often several peaks which represent the same mass occur at different flight times.

Case 1: A parent of mass m_p and its own daughter, mass m_d [Tang '91].

The parent flight time t_p is $t_p = 2L/v_o$, where L is the length of the field free region of the flight tube, and v_o is the parent velocity for the optimum acceleration voltage for a given mirror field.

The daughter flight time, t_d, is $t_d = L/v_o + 2m_d v_o/qE = (1+m_p/m_d)L/v_o$, where E is the

[1]Weights of alamethicin peptides were estimated from the amount of powder visible in the vial.

mirror field [Tang '91].

Then $t_d/t_p = (m_p+m_d)/2m_p$.

If $m_d \sim m_p$, then $t_d \sim t_p$, and if $m_d << m_p$, then $t_d \sim t_p/2$. In other words, daughter ions of a parent ion arrive at the detector between $t_p/2$ and t_p.

Case 2: A daughter of mass m_d and a parent ion of the *same* mass m_d [Tang '91]. Note that this daughter ion is the daughter of a *larger* parent of mass m_p, and is unrelated to the parent ion it is being compared with.

The flight time of the parent, m_p, is t_p, as given above.

The flight time of the *daughter*, m_d, is t_d, as given above.

The flight time of the unrelated parent of mass m_d is $t_p^* = 2L/v_o^* = (2L/v_o)\sqrt{(m_d/m_p)}$ because the velocity of this parent ion is $v_o^* = v_o\sqrt{(m_p/m_d)}$.

Then $t_d/t_p^* = (m_p+m_d)/[2m_p\sqrt{(m_d/m_p)}]$.

If $m_d \sim m_p$, then $t_d \sim t_p^*$, and if $m_d << m_p$, then $t_d >> t_p^*$. In other words, daughter ions of mass m_d appear at higher flight times than parent ions of the same mass.

Case 3: Daughter ions of the same mass but from two *different* parent ions.

Flight time of daughter of parent #1 is $t_{d1} = L/v_{o1} + 2m_{d1}v_{o1}/qE = (1+m_p/m_{d1})L/v_{o1}$.

Flight time of daughter of parent #2 is $t_{d2} = L/v_{o2} + 2m_{d2}v_{o2}/qE = (1+m_{p2}/m_{d2})L/v_{o2}$.

Here $m_{d1}=m_{d2} = m_d$, and v_{o1} is related to v_{o2} by $v_{o1} = v_{o2}\sqrt{(m_{p2}/m_p)}$, so that

$$\frac{t_{d1}}{t_{d2}} = \frac{(m_d+m_p)\sqrt{(m_{p2})}}{(m_d+m_{p2})\sqrt{(m_p)}}$$

If $m_{p1} >> m_{p2}$, then $m_{p1} >> m_d$ as well, and $t_{d1}/t_{d2} \sim (m_{p1}/2m_{p2})\sqrt{(m_{p2}/m_{p1})}$ or $t_{d1}/t_{d2} \sim \sqrt{(m_{p1}/m_{p2})}$, as expected, and the daughter with the heavier parent will arrive later.

These three cases explain the complexity of the reflected spectrum as shown in Fig. 2.10. Some of the peaks at a shorter flight time than the peak corresponding to the parent B_{10} are daughters of B_{10}; others are daughters of higher mass ions. The peaks at a longer flight

time than B_{10} are the B_{10} daughters of higher mass parent ions; the heavier parent ion has daughter B_{10} ions at a longer flight time than the lighter parent does (e.g. $[M+H]^+$ vs B_{13}).

2.6 Decay In The Acceleration Region

In the simplest case, a parent ion P^+ is produced at the target and is accelerated across a potential difference V applied between the target and a grounded grid at a distance L from the target, reaching a kinetic energy $T_p = 1/2(m_p v_p^2) = q_p V$. The parent ion P^+ then decays in free flight between the grid and the ion mirror to give charged and neutral daughters ($P^+ \rightarrow D^+ + N$). For simplicity assume zero energy release in the disintegration; then both daughters retain the velocity of the parent ion, and the time of arrival of the neutral daughter at detector 1 defines the parent ion mass m_p.

If the decay occurs in the acceleration region instead of in free flight, the neutral daughter will have a velocity different from the reference value above, so it will simply produce background between the peaks corresponding to various parent ions. However, these peaks have an appreciable breadth resulting from the energy release in the decay (and from the effect considered here), so some neutral daughters from decays in the acceleration region will still be included. Two cases are of particular interest:

1. Where the decay of P^+ occurs just inside the grid i.e. at distance x from the target where $(L-x)/L \ll 1$.

In this case, $T_p = mv_p^2/2 = q_p Vx/L$

$$\Delta T_p/T_p = (T_p - T_p)/T_p = x/L - 1$$

$$\text{Time spread } \Delta t/t = -\Delta T_p/2T_p = (1-x/L)/2$$

2. Where the parent ion P^+ is itself produced by the decay of a predecessor α^+ close to the target, i.e. at distance x, where $x/L \ll 1$.

In this case, $T_p = mv_p^2/2 = q_pV\,[(L-x)/L + x\,m_p/(Lm_\alpha)]$

$$\Delta T_p/T_p = -\,x\,(1 - m_p/m_\alpha)/L$$

Time spread $\Delta t/t = x\,(1 - m_p/m_\alpha)/2L$

In the present experimental configuration the acceleration distance L is 0.9 cm, the distance between grid and mirror is 50 cm, and the acceleration voltage V is 10 kV. The flight time of the $(M+H)^+$ ion is then ≈ 16 μs between grid and mirror, and ≈ 570 ns in the acceleration region.

For case 1 if we assume an acceptable time spread $\Delta t/t = .01$, decays in the distance from x/L=.98 to x/L=1 will give neutrals in the defining peak. This corresponds to a time interval for the decay of only 6 ns (time interval = $570 - 570(.98)^{1/2} \approx 6$ ns), so the contribution of this process to the peak is unlikely to be significant.

Case 2 gives a much larger effect. Again assuming $\Delta t/t = .01$, neutrals appear in the defining peak if the first decay takes place within a distance x from the target, where $x/L = .02 / [1-m_p/m_\alpha]$, which is larger than the value for case 1. More important, the ion is just starting its motion, so the corresponding time interval for the decay (if the neutrals are to appear in the defining peak) is much longer. Also, any ion which decays close to the target has a very high decay rate (assuming exponential decay) so many ions are involved and the effect is magnified.

e.g. for $\alpha^+ = [M+H]^+$ and $P^+ = B_{13}$

$x/L \approx .02/[1-12/20] = .05$

Time interval = $570(.05)^{1/2} \approx 127$ ns

e.g. for $\alpha^+ = [M+H]^+$ and $P^+ = Y_7+2$

$x/L \approx .02/[1-7/20] = .4/13 \approx .03$

Time interval = $570(.4/13)^{1/2} \approx 100$ ns

Although these times are small compared to the overall flight time, the contribution from this process (case 2) may be large when the precursor ion α^+ has a short lifetime, as appears to be the situation in alamethicin . The resulting peak is broadened towards longer

flight time, giving a possible systematic error in mass determination, i.e. a mass larger than it should be.

There will be corresponding changes in the energy of the charged fragment also, but these will be corrected by the mirror, at least partially, so normally they are less significant.

3.1 Sources of Uncertainty in Monolayer Preparation

Uncertainties in the pressure determination:

-reading tensiometer (± .10 to ± .20 divisions)

-thickness of filter paper (.18 ± .03 mm)

-contact angle value (± 0°; this is because clean filter paper cannot have a different contact angle, as verified by hundreds of hours of measurements)

-tensiometer calibration, linear regression coefficient = 0.99994, very low uncertainties

-π (± .9 to ± 1.4 mN/m, depending on the width of the filter paper, the actual reading of the tensiometer and the direction of the barrier movement)

-the value of π considered adequate to indicate a clean surface (determining γ_o from the barrier far position and γ from the barrier near position) was 0 ± ~.5 mN/m. (The error is less than normal largely because the film is stationary, allowing the reading to be taken several times without time constraints.)

-fundamental problem:

-the pressure at the barrier and at the tensiometer slide are not necessarily identical due to film viscosity and pressure gradients

-there is also barrier feedback time lag (not present if a piston oil is used)

-therefore the pressure at the dipping slide is not expected to be the same as that set by the feedback system; the magnitude of this effect is not known

-however, all experiments suffer from this problem so if the trough design, dipping ratios and counter ion concentrations are not unusual the effect, though unknown, is accounted for in the procedures reported in the literature

Uncertainties in the total area determination:

-shape of the meniscus (affected by the surface pressure)

-barrier may not be perpendicular to the trough sides

-for manual recording of barrier position:

-parallax error in the reading of the barrier position (usually small)

-the time lag between reading the barrier and the tensiometer (approximately constant)

-this leads to an total uncertainty of ± .3 mm (but see below)

- for automated recording of the barrier position:

-nonlinearity in the barrier system which gives an average error compared to the manual system of .25 mm; this is an overestimation because the magnitudes of the deviations follow a wave pattern

-thus the difference in the deviations from the manual readings for nearby barrier positions (such as those used in the calculations of τ) are much less, averaging around .08 mm for a double layer LB film deposition. (This also indicates that the actual error in the manual recording of the barrier position <.3 mm)

- (planimeter area determinations had an error of ~2%, not including the parallax error and the tracing errors involved in determining and drawing the thread's position)

Uncertainties in τ:

-uncertainties in the area of the slide covered

-difficulties in determining the value of h (the distance between the top of the meniscus and the top of the slide -- ± .5 mm)

-uncertainties in the area of monolayer removed from the subphase

-the uncertainties are similar to those for the total area determination

-some uncertainty in the base slope of the barrier position versus time graph (see Appendix 3.5 and Fig. 3.6)

- uncertainties in the barrier position at the time the slide entered the water and exact time at which this occurred

- the values of τ average ~.93 ± .10; perhaps they are low because of a systematic underestimation of h, which would lead to an overestimation of the slide

area coated

-the errors in τ were considerable. Note that "...transfer ratios significantly outside the range 0.95 to 1.05 are in fact usually indicative of poor film homogeneity..." [Peterson '90] which again brings the quality of some of our LB films into question (§3.5). (For our decay pattern studies and for determining general trends in yield versus film thickness, the quality is not crucial. On the other hand, in LB film studies purporting to determine information about the film structure, it is of the utmost importance. Compare to commercial instruments that give errors as low as $\pm$ .01.)

Other uncertainties:

The amplitude and frequency of the water vibrations were difficult to quantitate because they were too small to be measured by eye, especially if a compressed monolayer was present. Because it seemed adequate to know that during dipping such values were not large, no attempt was made to measure these carefully.

The glass microscope slides (12 mm diameter) used were small and might have exhibited edge effects [Peterson '83, Hasmonay '80]. Others have used similar slides [Galera '91].

The transfer rate of the monolayer from the subphase to the substrate was ~ 4 mm/min. There is some disagreement as to what rate is suitable for coating (e.g. at velocities less than 24 mm/min, others have observed horizontal striations on the ML surface, related to instability of the meniscus [Peterson '83], but at velocities as high as 10 mm/min, nonequilibrium deposition was noticed [Hasmonay '80]); many workers use velocities around 1-5 mm/min and others have used values ranging from less than 1 to 60 mm/min [Roberts '85, Kuhn '72]. We very occasionally noticed mensicus instabilities during coating.

The pH value was very difficult to determine, but was usually ~ 5 after 1 min, and ~ 5.6 after 20 min, with the change being due to the electrode itself (see §3.3.3.3). Note

that the electrode was soaked in nanopure water for after calibrating with the buffers to prevent buffer effects on the pH readings (§3.3.3.3). Because the film character does not change in this pH range [Hasmonay '80], the uncertainty is not very serious. In fact, even the very act of coating causes pH fluctuations in the meniscus due to the CO_2 in the air [Riegler '88]. The pH was not adjusted except by CO_2 in the air, which gave the desired value of ~5.5.

The amount of solution deposited is also difficult to record exactly using our micrometer syringe. This is important for the pressure-area measurements where it shifts the horizontal zero position. The actual amount of solution deposited was determined solely by the behavior of the stearic acid / hexane droplets on the subphase.

Subphase cleanliness and contamination throughout the experiment are so difficult to measure that they represent unknowns in any result in which there is no obvious contamination; the difference between the two pressure area curves shown in Fig. 3.1 and Fig. A3.1 is probably due to these effects [Peterson '90]. The surface cleanliness at the beginning of the experiments is easy to verify by checking the tensiometer settings with the barrier far from and close to the tensiometer; if the difference is 0, the surface is clean.

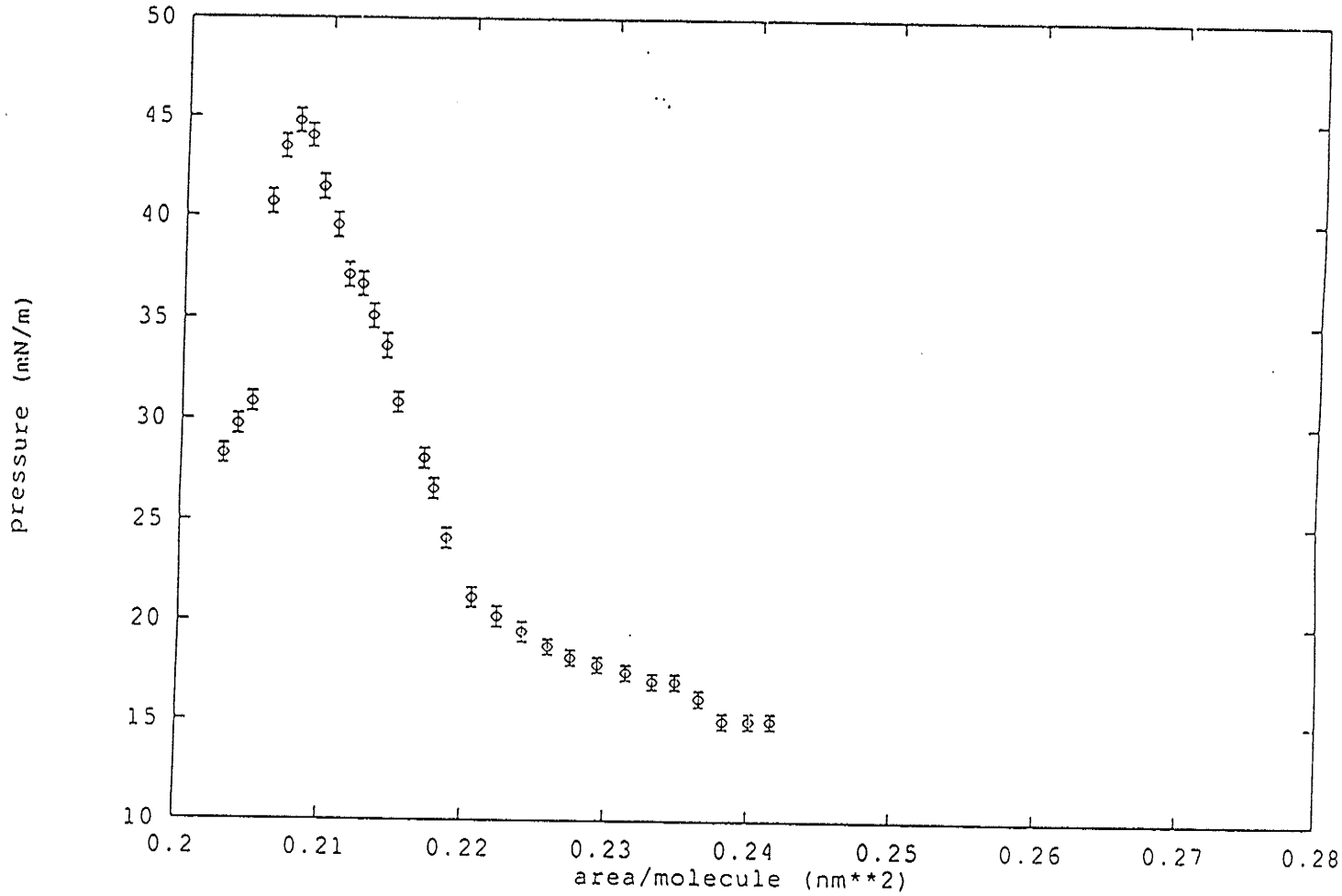

Fig. A3.1 Pressure area diagram of stearic acid on a subphase containing 5 x 10^{-4} M $CdCl_2$. (Errors in the area / molecule may be considerable, but do not affect the shape of the curve. See Appendix 3.1.)

3.2 Cleaning Glass Slides

In this procedure as in all others involving monolayers, clean and washed gloves must be worn. (To see how much contamination is on even a freshly washed finger, sweep a surface clean (Appendix 3.4), coat it with clean talcum powder, blow on it to verify cleanliness (§3.3.3.1), and dip in a "clean" finger. The oils will spread from the finger immediately and push the talcum powder back.)

1) put slides into holder (see Fig. A3.2)
2) sonicate in a boiling water/detergent mixture (~10%) for about 7 minutes
3) rinse with nanopure water:
    a) pour some water over the whole slide-holder assembly
    b) put holder assembly into a beaker full of water
    c) rinse it with this water and dip it into another beakerful of water(this step may be omitted for the rinsing after step 2 and 4, but in that case fresh cleaning solutions may need to be prepared more often)
    d) use a Pasteur pipette to rinse each slide with copious amounts of nanopure water
4) sonicate in concentrated HNO_3 solution for 5 min at room temperature, and rinse as above
5) sonicate in $5x10^{-3}$ M NaOH for 7 minutes at room temperature, and rinse as above
6) shake excess water off gently and put back into an empty beaker for air drying and storage. Protect from dust.
7) use within the next day or two if coating monolayers directly onto glass and within up to ten days (preferably less) if evaporating silver directly onto slides.

Note:
After this treatment the slides should exhibit nice hydrophilic behavior; if not, contamination is still present and they must be cleaned again, probably with fresh solutions.
The extravagant rinsing after steps 2 and 4 allow the HNO_3 and NaOH solutions to be reused. (This procedure is similar to one reported by Sagiv.)

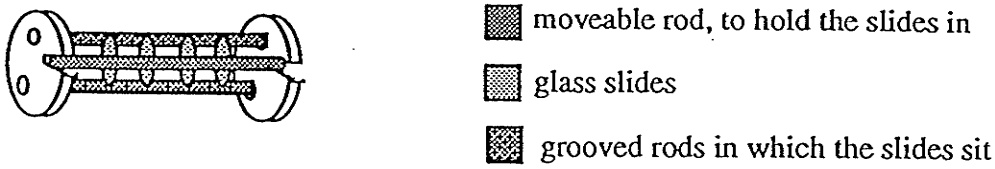

Fig. A3.2 Slide cleaning holder (teflon).

3.3 Preparing Wilhelmy Filter Paper Slides

To prepare the slides, Schleicher and Schuell filter paper (589 black) was put between clean sheets of office paper (from the middle of a fresh package) in preparation for cutting into ~2.5 by 5 cm rectangles. Each filter paper piece was removed from the protecting paper and stored in the original plastic bag. Pieces were removed from the bag using a freshly washed (10% detergent, tap water rinse and nanopure water rinse) and air-dried pair of tweezers. They were then put onto a freshly cleaned block of teflon with a small hole in it. The filter paper holder, a stainless steel rod bent at 90 degrees, was inserted through the paper into the hole in the teflon. The paper could then be lifted off the block and rinsed well with nanopure water. The holder was then inserted into the tensiometer, and any water droplets remaining on the holder were drained off using the edge of a clean kimwipe. If the filter paper rotated slightly and hung at an angle, it was adjusted by tapping its edge with a freshly cleaned piece of teflon. After each experiment, the width of the wet filter paper was measured.

This elaborate attention to cleanliness was found to be important. Any substance on the filter paper will contaminate the subphase and / or the monolayer (depending on whether the contamination is a surfactant or not). For example, several pressure area measurements showed anomalous results; closer inspection showed that, upon drying, the upper corners of the paper used were yellowed; clean filter paper dries white. The source of contamination was not determined.

The thickness of the wet filter paper was measured with calipers and the filter paper did not seem to compress. The same thickness value was used for an entire set of filter paper plates cut from one large sheet of filter paper.

3.4 Detailed Monolayer Spreading and Dipping Procedures, Used in Our Work

(D at the beginning of a line denotes an instruction that pertains only to dipping slides)

D -plan and prepare for SIMS experiments immediately after dipping (reserve and optimize spectrometer)

-ensure that the barrier position is back far enough in the trough; if not, set the drive to run the barrier backwards (turn the feedback light on and let the light reach the photoresistor) and continue, checking on the barrier periodically to make sure it does not run into the end of the drive shaft

-ensure have enough $CdCl_2$, stearic acid solution, deuterated stearic acid solution, fresh nanopure water, gloves and good filter paper pieces

D -set up temporary storage for dipped slides, if necessary

D -clean slides (Appendix 3.2)

D -vapor coat with Ag and do glow discharge

D -ensure dipping system is ready to set up

- dust-free, pulleys freely turning
- position on dipping cylinder is suitable for dipping [so don't run out of cylinder when the slide is half in the water]

D -ensure that it will be possible to obtain meniscus information for *both* sides of the dipping slide [we put a mirror behind the trough]

-check that the Atari-driveshaft connection is OK

-set trough antivibration mounts up properly so that the spacing and alignment of trough, barrier drive and tensiometer will be appropriate

D -ensure that the feedback zero point and the tensiometer visual zero point coincide

-check apparatus voltages (V_{motor}, V_{light} and $V_{dipping}$)

-record the temperature

-put on a new pair of gloves and wash hands

-clean trough, water containers, filter paper holder, tweezer and teflon block with soap and water, rinse with tap water and then with nanopure water

-let trough drip dry a bit and wipe the bottom and the sides so that it cannot drip on the barrier electronics

-put the trough in place and add 500 ml nanopure water

-add 270 µl $CdCl_2$ (3.6×10^{-4} M) using a 5 to 40 µl digital pipette

-add 850 ml water

* -prepare the tensiometer filter paper (Appendix 3.3), making sure to rinse it well, and put onto tensiometer

-close plexiglass box after ensuring everything is within reach of the sliding doors

-sweep the surface 4 times with 4 clean barriers (freshly washed with soap, rinsed with tap water and then with nanopure water)

-position the tensiometer and insert the tensiometer slide

-sweep again, and read the tensiometer with the barrier far and the barrier close; record values

-if these values are not the same, repeat the sweeping with a freshly cleaned barrier each time, until the values are the same

-put the compression barrier into place and sweep it toward the filter paper slide; if the reading changes, remove and reclean the compression barrier and repeat

-record the compression barrier position

-adjust the tensiometer setting so that spreading the monolayer will allow it to leave the water

-add stearic acid and hexane, estimating the amount from the relationship between film area and the amount of stearic acid that will spread [after many experiments we made a plot]

- stop adding stearic acid when the drops no longer spread and vanish quickly (this

takes some experience)

-begin the stopwatch

D -set tensiometer to the 30mN/m value (γ_o - 15.3 tensiometer divisions, in our case)

-let the hexane evaporate and the monolayer stabilize ~ 20 min

-while waiting:

-set up the automatic barrier position recording program

D -set up the dipping system, avoiding vibrations:

D -make sure drive, pulleys and string are arranged correctly

(*i.e.* two pulleys are in line and parallel -- system 1, Fig. 3.5)

D -double check the dipping area of the monolayer for dust and other problems

D -put the slide on the string and position it 0.5 to 1 cm above the monolayer

D -to adjust slide height (system 1, Fig. 3.5)

i) move the rod for pulley A, either vertically or horizontally, very carefully after the slide is in position above the water

ii) for very fine adjustments, pulley B's holder may be moved slightly

D -to adjust slide height (system 2, Fig. 3.5)

i) loop or unloop string around dipping drive pulley (large adjustments)

ii) move dipping drive itself close to or away from pulleys at the box's end (fine adjustments)

-set up data table in logbook, and record the clock time (in case something happens to the stopwatch or computer)

D -switch V_{light} on and check that the light works

-switch V_{motor} on

D -record V_{motor}, V_{light} and $V_{dipping}$ approximately every 10 min

D -record feedback barrier position with respect to time using either the automatic or the manual system; and record the time at which the film reaches equilibrium compression

-if performing a pressure-area run, record tensiometer values every minute until the readings begin to change significantly; then record at least twice a minute and continue until after collapse

-keep an eye on the filter paper meniscus

D -proceed to dipping IF THE MONOLAYER IS FREE FROM OBVIOUS DEFECTS

D** -record which way the slide is facing, and ensure that the meniscus will be visible on both sides

D*** -dip the slide and record time, barrier position, meniscus information, any information on wet spots, and the distance of the meniscus from the top of the slide

D -record the times the slide enters, begins to exit and exits the water

D -make sure that the clip does not enter the water; be prepared for the meniscus to "jump" up if it gets too close

D -let the slide dry; the time may be quite long after the coating the first monolayer; in other cases allow at least 2 or 10 min (for the automatic or manual system respectively), while still recording the barrier position and time, to be able to determine τ (Eqn. 3.1, and Fig 3.6)

D -repeat from *** for as many coats as needed

D -set up the next slide (either system 1 or 2, Fig 3.5)

D -open sliding door of box, move slide away from trough, remove from dipping system and store for later dipping or analysis

D -put second slide on dipping system and carefully position it over the trough

D -repeat from ** for as many slides as desired

-turn off motor power supply, finalize computerized barrier position recording

-remove tensiometer, measure and record the filter paper width

D -if making alternating film layers, turn motor supply back on and turn feedback

light on so that the barrier runs backwards

D -repeat from * using a different fatty acid (e.g. deuterated stearic acid), keeping the box closed

D -note that sweeping away an old film is tricky because the water may go onto the trough wall; if it does, move the sweeping barrier back a bit and try again; this may take several tries

D -lifting a barrier from the end of the trough in the presence of an old collapsed film causes large ripples and care must be taken that the water does not slop out of the trough onto the feedback system electronics

-turn off all power supplies

-record the temperature

-check the pH (optional unless coating LB films)

REFERENCES

V. K.Agarwal, Physics Today, p. 40, June 1988.

G. Allen, Sequencing of Peptides and Proteins, Second Revised Edition, Vol. 9 in Laboratory Techniques in Biochemistry and Molecular Biology, Ed. R.H. Burdon and P. H. van Knippenberg, Elsevier (1989).

M.H.Allen and I.A.S.Lewis, Rapid Commun. Mass Spectrom. 3, 255 (1989); B.S.Larsen and C.N.McEwen, J. Am. Soc. Mass Spectrom. , 2, 199 (1991).

R.S.Annan, H.J. Kochling, J.A. Hill, and K.Biemann, Rapid Commun. Mass Spectrom. 6, 298 (1993).

T.Armen, K.Halperin, P.Dutta, J.B. Ketterson, Rev. Sci. Instrum. 58, 822 (1987).

T.M.Balasubramanian, N.C.E. Kendrick, M.Taylor, G.R.Marshall, J.E. Hall, I.Vodayanoy, and F.Reusser, J.Am. Chem. Soc. 103, 6127 (1981).

M. Barber, R.J. Bordoli, R.D. Sedgwick, A. N. Tyler, J.C.S. Chem Comm. 325 (1981a).

M. Barber, R.J. Bordoli, R.D. Sedgwick, A. N. Tyler, Nature 293, 325 (1981b).

J.A.Barker and J.P.McTague in R.G.Lerner and G.L.Trigg (Eds.), Encyclopedia of Physics, 2nd Edition, VCH Publishers, Inc., New York, 1991, p.544.

R. C. Beavis and B. T. Chait, Proc. Natl. Acad. Sci. USA 87, 6873 (1990).

R.C. Beavis and B. T. Chait, Chem. Phys. Lett. 181, 479 (1991).

A.Benninghoven, D. Jaspers and W. Sichtermann, Appl. Phys. 11, 36 (1976).

A. Benninghoven ,in A. Benninghoven, (Ed.), Ion Formation from Organic Solids, Springer-Verlag, New York, 1983, p.64.

A. Benninghoven, F.G. Rudenauer and H.W.Werner, Secondary Ion Mass Spectrometry: Basic Concepts , Instrumental Aspects, Applications and Trends, John Wiley and Sons, Inc., New York, (1987).

S.C.Beu, M.W.Senko, J.P.Quinn, F.M.WamplerIII, and F.W.McLafferty, J. Am. Soc. Mass Spectrom. 4, 557 (1993).

K.Biemann, Mass Spectometry, Organic Chemical Applications, McGraw-Hill, New York (1962), as referred to in M. Przybylski, I. Dietrich, I. Manz and H. Bruckner, Biomed. Mass Spectrom, 11, 569 (1984).

K. Biemann and S. A. Martin, Mass Spectrom. Rev. 6, 1 (1987).

K. Biemann in Protein Sequencing: A Practical Approach in The Practical Approach Series, ed. by J.B.C. Findlay and M.J. Geisow, IRL Press, New York, 1989, p. 102.

K. Biemann, Annu. Rev. Biochem. 61, 977 (1992).

L.M.Blinov, Sov Phys. Usp. 31, 623 (1988).

K.B.Blodgett, J. Am. Chem. Soc. 56, 495 (1934).

K.B.Blodgett, J. Am. Chem. Soc., 57, 1007 (1935).

K.B.Blodgett and I. Langmuir, Phys. Rev., 51, 964 (1937a).

K.B.Blodgett, J. Phys. Chem., 41, 975 (1937b).

B.Bodo, S. Rebuffat, M.E. Hajji, and D. Davous, J. Am. Chem. Soc., 107, 6011 (1985).

T.T.M.Bohanon, J.M.Mikrut, B.M.Abraham, J.B.Ketterson, S.Jacobson, L.S.Flosenzier, J.M.Torkelson, and P.Dutta, Rev. Sci. Instrum., 63, 1822 (1992).

G. Bolbach, R. Beavis, W.Ens, D.E.Main, B. Schueler, and K.G.Standing, 33rd ASMS San Diego, CA May 1985, p. 945.

G. Bolbach, R.Beavis, S.Della Negra, C Deprun, W.Ens, Y. Lebeyec, D.E.Main, B. Schueler and K.G.Standing, Nucl. Instr. Meth. Phys. Res B30, 74 (1988).

G.Bolbach and J.C.Blais, in A.Benninghoven, A.M.Huber, H.H.Werner (Eds.), Secondary Ion Mass Spectrometry SIMS VI, John Wiley and Sons, Chichester, 1988a, p. 655.

G. Bolbach, R. Galera, and J.C.Blais, J. Physique, Colloque C2, 50, C2-69 (1989).

G.Bolbach, M.Plissonnier, R. Galera, J.C.Blais, G. Dufour and H.Roulet, by mail from G. Bolbach, Sept. 1989; journal unknown.

G. Bolbach, experimental notes.

L. Bourdieu, P. Silberzan and D.Chatenay, Phys. Rev. Lett. 57, 2029 (1991).

L.Bourdieu, O.Ronsin and D.Chatenay, Science, 259, 798 (1993).

L.Bourdieu, O.Ronsin, and D.Chatenay, Science, 263, 1158 (1994a).

L. Bourdieu, J.Daillant, D.Chatenay, A. Braslau and D.Colson, Phys. Rev. Lett., 72, 1502 (1994b).

C.V.Bradley, D.H.Williams, and M.R.Hanley, Biochem. Biophys. Res. Commun. 104, 1223 (1982).

D. Brewer, F.G. Mason and A. Taylor, Can J. Microbiol. 33, 619 (1987).

C.A. Browne, H.P.J. Bennett and S. Soloman, Anal. Biochem. 124, 201 (1982).

H. Bruckner and M. Przybilski, J. Chromatog. 296, 263 (1984).

A. Brunelle, Ph.D. Thesis, Universite Paris - Sud, 1990.

A.M. Buko, V.K. Sarin, Rapid Commun. Mass Spectrom. 4, 541 (1990).

D. M. Bunk and R. D. Macfarlane, Int. J. Mass Spectrom. Ion Processes, 111, 55 (1991).

D. M. Bunk and R. D. Macfarlane, Proc. Nat. Acad. Sci. USA 89, 6215 (1992).

N.A.Burnham, D.D.Dominguez, RL.Mowrey and F.J.Colton, Phys. Rev. Lett. 64, 1931 (1990).

K. L. Busch, G. L. Glish, S. A. McLuckey, Mass Spectrometry / Mass Spectrometry: Techniques and Applications of Tandem Mass Spectrometry, VCH Publishers, Inc., 1988, New York.

R. M. Caprioli, Mass Spectrom. Rev. 6 (1987) 237.

R. M. Caprioli, in Seminar on Chemistry of Biologically Active Compounds and Modern Analytical Methods (1988: Interlaken, Switzerland), Ed. U. P. Schlunegger, Springer-Verlag, (1989) p.39; [p.67,68,and 73].

R. M. Caprioli and M. J. F. Suter, Int. J. Mass Spectrom. Ion Physics 118/119, 449 (1992).

S. A. Carr, Proc. 38th ASMS Conf. on Mass Spectrom. and Allied Topics, Tucson, Ariz., June 1990, p. 1575.

B. T. Chait and F. H. Field, Int. J. Mass Spectrom. Ion Processes 41, 17 (1981).

B. T. Chait, B. F. Gisin, F. H. Field, J. Am. Chem. Soc. 104, 5157 (1982).

B. T. Chait and F. H. Field, J. Am. Chem. Soc. 107, 6743 (1985).

B. T. Chait and F. H. Field, Biochem. Biophys. Research Commun. 134, 420 (1986).

B.T. Chait, T.Chaudhury and F.H.Field, in K.A.Walsh (Ed.), Methods of Protein Sequence Analysis 1986, Humana Press, Clifton, NJ, 1987, p.483.

B.T. Chait, Int. J. Mass Spectrom. Ion Processes 78, 237 (1987).

B. T. Chait, T. Chaudhury and F. H. Field, in Methods of Protein Sequence Analysis 1986, Ed. K. A. Walsh (Humana Press, Clifton, NJ, 1987a), p. 483.

B. T. Chait and S. B. H. Kent, Science 257, 1885 (1992).

B.T. Chait, R. Wang, R.C. Beavis, S.B.H.Kent, Science 262, 89 (1993).

B.T.Chait, R.Wang, R.C.Beavis, and S.B.H.Kent, Science, 262, 89 (1993).

B. T. Chait, private communication to K. G. Standing, 1993a.

W.S.Champney, J. Chromatography, 522, 163 (1990).

I.Chernushevich, A. Verentchikov, K.G.Standing and W.Ens, Proceedings of the 42nd ASMS Conference on Mass Spectrometry and Allied Topics, Chicago, Illinois, May 29-June 3, 1994.

I. Chernushevich, A.Verentchikov, J. Zhou et al, manuscript in preparation about work by our group and H. Duckworth's group on the iclR protein; also presented at the Annual Meeting of the Chemical Institute of Canada, 1994.

J.Z.Chou, M.J. Kreek, B.T.Chait, J. Am Soc. Mass Spectrom., 5, 10 (1994).

S. K. Chowdhury and B. T. Chait, Anal. Biochem. 180 (1989) 387.

R. G. Cooks, J. H. Beynon, R. M. Caprioli and G. R. Lester, Metastable Ions, Elsevier, New York, 1973.

R.G.Cooks and K.L.Busch, Int. J. Mass Spectrom. and Ion Physics 53, 111 (1983).

P.A.Cornelio and J.A.Gardella, Jr. J. Vac. Sci. Technol. A, 8, 2283 (1990).

P.A.Cornelio-Clark and J.A.Gardella, Jr., Langmuir, 7, 2279 (1991).

T.Cornish and R.J.Cotter Rapid Commun. Mass Spectrom. 6, 242 (1992).

T.J.Cornish and R.J.Cotter, Rapid Commun. Mass Spectrom. 7, 1037 (1993).

T.J.Cornish and R.J.Cotter, Org. Mass Spectrom. 28 (1993) 1129.

A. G. Craig, ≈. Engstr^m, H. Bennich and I. Kaminsky, Biomed. Environment. Mass Spectrom. 14 (1987) 669.

W. J. Craigen and C.T. Caskey, Nature 322, 273 (1986).

J. M. Curtis, P. Thibault, R. K. Boyd, S. Chen, P. J. Derrick, B. A. Thomson, Proceedings of the 41st ASMS Conference on Mass Spectrometry and Allied Topics, San Francisco, CA, May 30- June 4, 1993, p. 921a.

C. Dass and D. M. Desiderio, Proceedings of the 40th ASMS Conference on Mass Spectrometry and Allied Topics, Washington, DC, May 31-June 5, 1992, p. 1937.

P.H.Dawson, Ed., Quadrupole Mass Spectrometry and its Applications, Elsevier, New York, 1976.

P.H. Dawson and D.J. Douglas in Tandem Mass Spectrometry, Ed. F.W. McLafferty, John Wiley and Sons, Inc., New York (1983), p. 127;

P.H. Dawson, Mass Spectrom. Rev. 5,1 (1986).

S.Della-Negra and Y.LeBeyec, Int. J. Mass Spectrom. Ion Processes, 61, 21 (1984).

S.Della-Negra and Y.LeBeyec, Anal.Chem., 57, 2035 (1985).

S.Della-Negra and Y.LeBeyec, Springer Proc. Phys., 9, 42 (1986).

E. De Pauw, Mass Spectrom. Rev. 5, 191 (1986).

D. Despeyroux, A.D. Wright, K.R. Jennings, Int. J. Mass Spectrom. Ion Processes 126, 95 (1993).

V.M. Doroshenko, R.J.Cotter Rapid Commun. Mass Spectrom. 7, 822 (1993).

H.E.Duckworth , R.C. Barber, and V.S. Venkatasubramanian, Mass Spectroscopy, Second Edition, Cambridge University Press, New York (1986).

P.Dutta, J.B.Peng, B.Lin, J.B.Ketterson, M.Prakash, P.Georgopoulos, S.Ehrlich, Phys. Rev. Lett., 58, 2228 (1987).

M.Eisenberg, J.E.Hall, and C.A. Mead, J. Membr. Biol. , 14, 143 (1973).

W.Ens, Ph.D. Thesis, University of Manitoba, 1984.

W. Ens, D. E. Main, K. G. Standing and B. T. Chait, Anal. Chem. 60, 1494 (1988).

W.Ens, P.Hakansson, B.U.R. Sundqvist, in A.M.Huber, A.Benninghoven, H.W.Werner and G.Slodzian, (Eds.), Seconary Ion Mass SPectrometry SIMS VI, Wiley, Chichester 1988a, p 623.

W. Ens, Y. Mao, X. Tang and K.G. Standing, Proc. 37th ASMS Conference on Mass Spectrometry and Allied Topics, Miami Beach, Florida, 21-26 May, 1989, p.1059.

W.Ens, K.G.Standing and A. Verentchikov, in G.J.Blanar and R.J.Cotter (Eds.), Proc. Int. Conference on Instrumentation for Time-of-Flight Mass Spectrometery, LeCroy Corp., Chestnut Ridge, NY, 1993, p.137.

W. Ens,in P.Sigmund (Ed.), Fundamental Processes in Sputtering of Atoms and Molecules, Symposium on the Occasion of the 250th Anniversary of the Royal Danish Academy of Sciences and Letters, Copenhagen, 30 August- 4 September, 1992, Mat. Fys. Medd. Dan. Vid. Selsk., 43, 155 (1993a).

D. Fabris, M. Kelly, C. Murphy, Z. Wu and C. Fenselau, J. Am. Soc. Mass Spectrom. 4, 652 (1993).

J.B. Fenn, M.Mann, C.K.Meng, S.F. Wong, and C. M. Whitehouse, Mass Spectrom. Rev. 9,37 (1990).

S.Ferestehkhou, R.D.Neuman, R.Ovalle, J.Coll. Interface Sci., 109, 385 (1986).

Fisher Scientific technical staff, May 31, 1991.

Florsheimer, A.J.Steinfort and P. Gunter, Surface Sci. Lett. 297, L39 (1993).

W. Forst, Theory of Unimolecular Reactions, Academic Press, New York, 1973.

R.O. Fox and F.M.Richards, Nature, 300, 325 (1982).

T. D. Fox, Annu. Rev. Genet. 21, 67 (1987).

A. Fraefel and J. Seibl, Mass Spectrom. Rev. 4, 151 (1985).

T.Fujita,Y. Takaishi, K. Matsuura, Y. Takeda, Y. Yoshioka and H. Bruckner, Chem. Pharm. Bull. 32, 2870 (1984).

G.L.Gaines, Jr., J. Colloid Sci. 15, 321 (1960).

G.L.Gaines, Jr., General Electric Research Laboratory, Technical Infromation Series, #63-RL-3206 C, Schenectady, N.Y., 1963.

G.L.Gaines,Jr., Insoluble Monolayers at Liquid-Gas Interfaces, Interscience Publishers, John Wiley and Sons, Inc., New York, (1966).

R. Galera, Ph.D. Thesis, University of Paris 7, 1990.

R. Galera, J.C.Blais and G.Bolbach, Int. J. Mass Spectrom. Ion Processes, 107, 531 (1991).

General Electric Company, Schenectady, New York.

G.S.Gorman, J.P. Speir, C.A.Turner and I.J. Amster, J. Am. Chem. Soc. 114, 3986 (1992).

R. P. Grese, R. L. Cerny and M. L. Gross, J. Am. Chem. Soc. 111 (1989) 2835.

F. Grunfeld, Rev. Sci. Instrum., 64, 548 (1993).

D. Guo, C.T.Mant, A.K.Taneja, J.M.R.Parker and R.S.Hodges, J. Chromatography, 359, 499 (1986).

W.F. Haddon, F.W. McLafferty, Anal. Chem. 41, 31 (1969).

C. Hafok-Peters, I. Maurer-Fogy and E. R. Schmid, Biomed. Environment. Mass Spectrom. 19 (1990) 159.

B. Hagenhoff, M.Diemel, A. Benninghoven, H-U Siegmund and D. Holtkamp, J. Phys. D: Appl. Phys. 25, 818 (1992).

R.A.Hann, Phil. Trans. R. Soc. Lond. A, 330, 141 (1990).

A. G. Harrison and R. J. Cotter, in Methods in Enzymology 193, Ed. J. A. McClosky (Academic Press, San Diego, CA, 1990).

H.Hasmonay, M.Vincent, M.Dupeyrat, Thin Solid Films 68, 21 (1980).

R.A. Henderson, H. Michel, K. Sakaguchi, J. Shabanowitz, E. Appella, D.F. Hunt, and V. J. Engelhard, Science 255, 1264 (1992).

S.Henon, J.Meunier, Rev. Sci. Instrum., 62, 936 (1991).

M.A. Hermodson in Laboratory Methodology in Biochemistry: Amino Acid Analysis and

Protein Sequencing, ed. by C. Fini, A. Floridi, V. N. Finelli and B. Wittman-Liebold, CRC Press, Inc. , Boca Raton, Florida, 1990, p. 1.

W.Hickel, D.Kamp, W.Knoll, Nature, 339, 186 (1989).

F. Hillenkamp, in Secondary Ion Mass Spectrometry SIMS V, Ed., A. Benninghoven, R. J. Colton, D.S. Simons, and H. W. Werner, Springer-Verlag, New York , 1986.

K. Hiraoka, K. Murata, I. Kudaka, Rapid Commun. Mass Spectrom. 7, 363 (1993).

Y.Hong, T.Takao, S.Aimoto, Y. Shimonishi, Biomed. Mass Spectrom. 10, 450 (1983).

E.P.Honig, J.H.T.Hengst and D.den Engelsen, J. Coll. Interface Sci., 45, 92 (1974).

R. E. Honig, in Secondary Ion Mass Spectrometry SIMS V, Ed., A. Benninghoven, R. J. Colton, D.S. Simons, and H. W. Werner, Springer-Verlag, New York , 1986.

J.Hoyes, S. Curbishely, P.Doorbar, P.Tatterton, R.H.Bateman, B.Beer and J.Lockett, 42nd ASMS Conf. on Mass Spectrom., Chicago, Ill, May/June 1994, paper WP9.

R. J. Hughes and R. E. March, Int. J. Mass Spectrom. Ion Processes 127, 27 (1993).

D.F.Hunt, J.R.YeatsIII, J. Shabanowitz, S.Winston and C.R.Hauer, Proc. Natl. Acad. Sci. USA, 83, 6233 (1986).

D.F. Hunt , J. Shabanowitz, J. R. Yates III, J. Chem. Soc. Chem. Commun. Iss. 8, 548, 1987.

D. F. Hunt, R. A. Henderson, J. Shabanowitz, K. Sakaguchi, H. Michel, N. Sevilir, A. L. Cox, E. Appella, and V. H. Engelhard, Science 255, 1261 (1992); the amount of sample was calculated from information given in the paper.

T.W. Hutchins and T-T. Yip, Rapid Commun. Mass Spectrom. 7, 576 (1993).

A. Iida, M. Okuda, S. Uesato, Y. Takaishi, T. Shigu, M. Morita and T. Fujita, J. Chem. Soc. Perkin Trans. 1(1990), 3249.

C.F. Ijames and C.C.Wilkins, J. Am. Chem. Soc.110, 2687 (1988).

JASMS: Special ESMS issues of J.Am. Soc. Mass Spectrom. 4, 523-686 (1993).

K.R.Jennings, R.S. Mason in *Tandem Mass Spectrometry*, Ed. F.W. McLafferty, John Wiley and Sons, Inc., New York (1983) , p.197.

K. R. Jennings and G. G. Dolnikowski, in Methods in Enzymology, Vol. 193, Mass Spectrometry, Ed. J. McCloskey, Academic Press, 1990, Toronto.

C.L. Johlman, R.L. White, and C.L. Wilkins, Mass Spectrom. Rev. 2,389 (1983).

R. S. Johnson and K. Biemann, Biochem. 26, 1209 (1987).

R.S. Johnson, S.A.Martin, K.Biemann, Int. J. Mass Spectrom. Ion Proc., 86, 137 (1988).

R. S. Johnson and K. Biemann, Biomed. Environ. Mass Spectrom. 18, 945 (1989).

R.W.Johnson, Jr., P.A.Cornelio-Clark, and J.A.Gardella, Jr., in P. Stroeve and A.C. Balazs, (Eds.), Macromoleuclar Assemblies in Polymeric Systems, 1992, p. 113.

G. P. Jonsson, A.B.Hedin, P.L.Hakansson, B.U.R. Sundqvist, B.G.S. Save, P.F. Nielsen, P.Roepstorff, K.E. Johansson, I. Kamensky, M.S.L. Lindberg, Anal. Chem. 58, 1084 (1986).

G. Jonsson, A.Hedin, P. Hakansson, B.U.R. Sundqvist, H.Bennick, and P. Roepstorff, Rapid Commun. Mass Spectrom. 3, 190 (1989).

K.Jonscher, G.Currie, A.L. McCormack, J.R. YatesIII, Rapid Commun. Mass Spectrom. 7, 20 (1993).

M. Karas, D. Bachmann, U. Bahr, F. Hillenkamp, Int. J. Mass Spectrom. Ion Processes 78, 53 (1987).

M. Karas and F. Hillenkamp, Anal. Chem. 60, 2299 (1988).

V. Katta, B. T. Chait, Rapid Commun. Mass Spectrom. 5, 214 (1991).

R.Kaufmann, D.Kirsch, H-A.Rood, B.Spengler Rapid Commun. Mass Spectrom. 6, 98 (1992).

R.Kaufmann, B.Spengler and F. Lutzenkirchen, Rapid Commun. Mass Spectrom. 7, 902 (1993).

R. Kaufmann, D. Kirsch, and B. Spengler, Int. J. Mass Spectrom. Ion Processes, in press.

J.Keesey, Ed. Biochemica Information, (Boehringer Mannheim Pharmaceuticals, Indianapolis, IN, 1987).

P.T.M.Kenny, K.Nomoto and R.Orlando, Rapid Commun. Mass Spectrom., 6, 95 (1992).

M. Kinzler, A.Schertel, G.Hahner, Ch.Woll, M.Grunze, H.Albrecht, G.Holzhuter and Th.Gerber, J.Chem Phys. 100, 7722 (1994).

K. Klarskov, K. Breddam and P. Roepstorff, Anal. Biochem. 180 (1989) 28.

W.A.Konig and M.Ayden in K.Brunfeldt, (Ed.), Peptides, Proc. 16th European Peptide Symposium, Scriptor, Copenhagen (1980), p. 711.

C. Koster, M. S. Kahr, J.A. Castoro and C. L. Wilkins, Mass Spectrom. Rev. 11, 495 (1992).

H. Kuhn and D.Mobius, Angew. Chem. Int. Ed., 10, 620 (1971).

H.Kuhn, D.Mobius and H.Bucher, Physical Methods in Chemistry Vol 1, Part 3b, Wiley, New York, 1972, p. 577.

W. Kulik, W.Heerma, J.Terlouw, Rapid Commun. Mass Spectrom., 3, 276 (1989).

F. Lafortune, R. Beavis, X. Tang, K.G. Standing and B. T. Chait Rapid Commun. Mass Spectrom. 1,114 (1987).

D.A. Laude, Jr., C. L. Johlman, R.S. Brown, D.A. Weil and C.L. Wilkins , Mass Spectrom. Rev. 5,107 (1986).

L.Laxhuber, H.Mohwald and M.Hashmi, Int. J. Mass Spectrom. Ion Phys., 51, 93

(1983).

L. Laxhuber, H. Mohwald, M.Hashmi, Colloids and Surf., 10, 225 (1984).

J.A.Leary, T.D.Williams, G.Bott, Rapid Commun. Mass Spectrom. 3, 192 (1989).

T. D. Lee and J. Shively, in Methods in Enzymology 193, Ed. J. A. McClosky (Academic Press, San Diego, CA, 1990), p. 361.

Y. Li and R.T.McIver, Jr., Rapid Commun. Mass Spectrom., 8, 743 (1994).

B. Lin, M.C.Shih , T.M.Bohanaon, G.E.Ice and P.Dutta, Phys. Rev. Lett. 65, 191 (1990).

J.A. Loo, E.R. Willimas, J.J.P. Furlong, B.H.Wang, F.W. McLafferty, B.T.Chait and F.H.Field, Int. J. Mass Spectrom. Ion Processes, 78, 305 (1987).

J.A. Loo, C.G.Edmonds and R.D.Smith, Anal. Chem., 65 (1993) 425.

R.D. Macfarlane and D. F. Torgerson, Science, 191, 920 (1976).

B.A.Mamyrin, V.I.Karataev, D.V.Schmikk and V.A. Zagulin, Sov. Phys. -JETP 37, 45 (1973).

M. Mann and J.B. Fenn in Mass Spectrometry: Clinical and Biomedical Applications, Vol. 1, Ed. by D. M. Desiderio,Plenum Press, New York (1992) p. 26.

D.R.Martin and R.J.P. Williams, Biochem. J. 153, 181 (1976).

J. Martens, W.Ens, K.G.Standing, A.Verentchikov, Rapid Commun. Mass Spectrom. 6, 147 (1992).

S.A. Martin and K. Biemann, Int. J. Mass Spectrom. Ion Processes, 78, 213 (1987).

J.A.McCloskey,Mass Spectrometry, in Methods of Enzymology, Vol. 193, Academic Press, Inc., Toronto (1990).

H.M.McConnell, Ann. Rev. Phys. Chem. 42, 171 (1991).

A.L.McCormack, A. Somogyi, A.R.Dongre, V.H.Wysocki, Anal. Chem. 65, 2859 (1993).

F.W. McLafferty, Tandem Mass Spectrometry, John Wiley and Sons, Inc., New York (1983).

P.Meller, Rev. Sci. Instrum. 59, 2225 (1988).

Millipore Continental Water Systems, Ultrapure Ion-Free/Organic-Free Water for the Trace Analysis, year unknown, p. 19.

K.Miyano, T. Maeda, Rev. Sci. Instrum, 58, 428 (1987).

H.Mohwald, Ann. Rev. Phys. Chem., 41, 441 (1990).

H.R.Morris, A. Dell, M.Panico, R.McDowell and A. Chatterjee, in U.P.Schlunegger (Ed.), Biologically Active Molecules, Springer Verlag, 1989.

D.R.Mueller, M.Eckersley, and W.J.Richter, Org. Mass Spectrom., 11, 601 (1984).

R.D.Neuman, S. Fereshtehkhou and R. Ovalle, J. Coll. Interface Sci., 101, 309 (1984).

P. F. Nielsen, K. Klarskov, P. Hojrup, and P. Roepstorff, Biomed. Environ. Mass Spectrom. 17, 355 (1988).

P.F.Nielsen, B.Landis, M.Svoboda, K. Schneider, M. Przybylski, Analyt. Biochem.191,

302 (1990).

P. F. Nielsen, P. Roepstorff, I. G. Clausen, A. B. Jensen, I. Jonasson, A. Svendsen, P. Balschmidt and F. B. Hansen, Protein Eng. 2, 449 (1989).

P.F.Nielsen and P.Roepstorff Biomed. Env. Mass Spectrom. 18, 131-137 (1989a).

R.C.Pandey, H.Meng, J.C.Cook,Jr. and K.L.Rinehart, Jr., J. Am. Chem. Soc., 99 (1977b) 8469.

I. A. Papayannopoulos and K. Biemann, J. Am. Soc. Mass Spectrom. 2, 174 (1991).

S. M. Partridge and H. F. Davis, Nature 165, 62 (1950).

J. R. Perkins, B. Smith, R. T. Gallagher, D. S. Jones, S. C. Davis, A. D. Hoffman, K. B. Tomer, J. Am. Soc. Mass Spectrom. 4, 670 (1993).

I.R.Peterson, G.J.Russell, and G.G.Roberts, Thin Solid Films, 109, 371 (1983).

I.R.Peterson, G.Veale and C.M.Montgomery, J. Coll. Interface Sci., 109, 527 (1986).

I.R.Peterson, J. Phys. D: Appl. Phys. 23, 379 (1990).

C.W.Pitt and L.M.Walpita, Electrocomponent Sci. and Technol., 3, 191 (1977).

R. Popovitz-Biro, K.Hill, E.M. Landau, E.M.Landau, M.Lahav, L.Leiserowitz, J.Sagiv, H.Hsiung, G.R.Meredith and H.Vanherzeele J. Am. Chem. Soc. 110, 2672 (1988).

N. Poppe-Schriemer, D.R. Binding, W.Ens, F. Mayer, K.G. Standing, X. Tang, and J.B. Westmore, Int. J. Mass Spectrom. Ion Proc. 111, 301 (1991).

N. Poppe-Schriemer and J. Zhou, unpublished results, 1991a.

N.Poppe-Schriemer, W.Ens, K.G.Standing, J.B.Westmore, J.Zhou,Proceedings of the 40th ASMS Conference on Mass Spectrometry and Allied Topics, Washington, DC, May 31-June 5, 1992, p.456.

N. Poppe-Schriemer, W.Ens, J.O'Neil, K.G.Standing, V. Spicer, J.B. Westmore and A.Yee, Proceedings of the 41st ASMS Conference on Mass Spectrometry and Allied Topics, San Francisco, CA, May 30- June 4, 1993, p.955a.

N. Poppe-Schriemer, W.Ens, J.D.O'Neil,V. Spicer, K.G.Standing, J.B. Westmore and A.A.Yee, to be published in Int. J. Mass Spectrom.

M. Przybylski, I. Dietrich, I. Manz, and H. Bruckner, Biomed. Mass Spectrom. 11, 569 (1984).

M.Przybylski, I. Manz, P. Fonrobert, I.Dietrich and H.Bruckner, Adv. Mass Spectrom. Vol. B, 1519 (1985).

X. Qiu, J. Ruiz-Garcia, K.J.Stine, C. M. Knobler and J. V Selinger, Phys. Rev. Lett. 67, 703 (1991).

K.L.Rinehart, Jr., J.C.Cook, Jr., H.Meng, K.L.Olson and R.C.Pandey, Nature, 269, 833 (1977).

J.E.Riegler and J.D.LeGrange, Phys. Rev. Lett., 61, 2492 (1988).

H.E. Ries and W.A.Kimball, J. Phys. Chem., 59, 94 (1955).

P. Roepstorff and J. Fohlman, Biomed. Mass Spectrom. 11, 601 (1984) .

P.Roepstorff, P. Hojrup and J. Moller, Biomed. Mass Spectrom. 12, 181 (1985).

P.Roepstorff, P.F. Nielsen, B.U.R. Sundqvist, P Hakansson and G. Jonsson, Int. J. Mass Spectrom. Ion Processes 78, 229 (1987).

P. Roepstorff, P. F. Nielsen, K. Klarskov and P. H¯jrup, Biomed. Environment. Mass Spectrom. 16 (1988) 9.

P. Roepstorff, P. F. Nielsen, K. Klarskov and P. H¯jrup, in The Analysis of Peptides and Proteins by Mass Spectrometry, Ed. C. J. McNeal (John Wiley & Sons, Chichester, England, 1988a), p. 55.

P. Roepstorff, K. Klarskov, J. Anderson, M. Mann, O. Vorm, G. Etienne, and J. Parello, Int. J. Mass Spectrom Ion Phys. 111,151 (1991).

K.J. Rosnack, J.G. Stroh, Rapid Commun. Mass Spectrom. 6, 637 (1992).

J.Ruiz-Garcia, X.Qiu, M.W.Tsao, G.Marshall C.M.Knobler, G.A.Overbeck and D.Mobius, J.Phys Chem., 97, 6955 (1993).

D. H. Russell, Mass Spectrom. Rev. 5,170 (1986).

G.Save, Ph.D. Thesis, Uppsala University, 1987.

M.L.Schlossman, D.K.Schwartz, P.S.Pershan, E.H.Kawamoto, G.J.Kellog and S.Lee, Phys. Rev. Lett. 66, 1599 (1991).

D.K.Schwartz, R.Viswanathan, J.Garnaes and J.A.Zasadzinski, J.Am. Chem. Soc., 115, 7374 (1993a).

D.K.Schwartz, R.Viswanathan and J.A.N.Zasadzinski, Phys. Rev. Lett., 70, 1267 (1993b).

D.K.Schwartz, J.Ruiz-Garcia, X. Qiu, J.V.Selinger and C.M.Knobler, Physica A, 204, 606 (1994a).

D.K.Schwartz, R.Viswanathan, J.A.Zasadzinski, Science, 263, 1158 (1994b).

J.C. Schwartz and M.E.Bier, Rapid Commun. Mass Spectrom. 7, 27 (1993).

H. A. Scoble and S. A. Martin, Mass Spectrometry, Volume 193 in Methods in Enzymology, Ed. J. A. McClosky, p. 519.

M.A.Seeterlin, P.R.Vlasck, D.J.Beussman, R.D.McLane and C.G.Enke, J. Am. Soc. Mass Spectrom., 4 (1993) 751.

S. Seki, H. Kambara, H, Naoki, Org. Mass Spectrom 20, 18 (1985).

N.F.Sepetov, O.L.Issakova, M.Lebl, K. Swiderek, D.C.Stahl, T.D. Lee, Rapid Commun. Mass Spectrom 7, 58 (1993).

M. Seul and M.J.Sammon, Phys. Rev. Lett. 64, 1903, (1990).

D.J.Shaw, Introduction to Colloid and Surface Chemistry, Second Edition, Butterworths, London, 1970.

E. Sheppard, R.P.Bronson, and N.Tcheurekdjian, J. Coll. Sci. 19, 833 (1964).

Y. Shimonishi, T. Takao in Laboratory Methodology in Biochemistry: Amino Acid Analysis and Protein Sequencing, ed. by C. Fini, A. Floridi, V. N. Finelli and B. Wittman-Liebold, CRC Press, Inc. , Boca Raton, Florida, 1990, p. 239.

P. Sigmund, Rev. Roum. Phys, 17, 823 (1972).

P. Sigmund, in N.H.Tolk, J.C.Tully, W.Heiland, and C.W.White (Eds.), Inelastic Ion-Surface Collisions, Academic Press, Inc., New York, (1977), p.121.

P. Sigmund in R. Behrisch, Sputtering by Particle Bombardment I, Springer, Heidelberg (1981), p. 9.

B. Spengler, D. Kirsch and R. Kaufmann, Rapid Commun. Mass Spectrom. 5, 198 (1991).

B. Spengler, D. Kirsch, R. Kaufmann, and E. Jaeger, Rapid Commun. Mass Spectrom. 6, 105 (1992).

J.A.Spink, J. Colloid Interface Sci. 23, 9 (1967).

K.G. Standing, W.Ens, R. Beavis, G.Bolbach, D.Main, B.Schueler and J.B.Westmore, Springer Proc. Phys., 9, 37 (1986).

K.G.Standing, R. Beavis, W.Ens, X. Tang and J.B.Westmore, in C. J. McNeal (Ed.), The Analysis of Peptides and Proteins by Mass Spectrometry, Wiley, Chichester, 1988, p.267.

K. G. Standing, W.Ens, Y. Mao, F. Lafortune, F. Mayer, N. Poppe-Schriemer, B. Scheuler, X. Tang, and J. B. Westmore, J. Physique, colloque C2 50, C2-163 (1989).

K.G.Standing, W. Ens, F. Mayer, X. Tang and J.B.Westmore, in A. Hedin, B.U.R. Sunquist and A.B. Benninghoven (Eds.), Ion Formation from Organic Solids-IFOS V. Wiley, Chechester, 1990a, p.93.

K.G. Standing, W. Ens, F. Mayer, X. Tang and J.B.Westmore, in E.R. Hilf and W. Tuszynski (Eds.), Mass Spectometry of Large Non-Volatile Molecules for Marine Organic Chemistry, World Scientific, Singapore, 1990b, p.186.

K.G. Standing, W.Ens, X. Tang and J.B.Westmore, in D. Desiderio (Ed.), Mass Spectrometry of Peptides, CRC Press, Boca Raton, FL, 1990c, p.159.

B. Sundqvist and R.D. MacFarlane, Mass Spectrom. Rev. 4, 421 (1985).

D.J. Surman and J. C. Vickerman, J.C.S. Chem Comm. 324 (1981).

G.Talbo, P.Roepstorff, Rapid Commun. Mass Spectrom. 7, 201 (1993).

K.Tanaka, H.Waki, Y.Ido, S.Akita, Y.Yoshida and T.Yoshida, Rapid Commun. Mass Spectrom. 2, 151 (1988).

X.Tang, R. Beavis, W. Ens, F. Lafortune, B. Schueler, K.G. Standing, Int. J. Mass Spectrom Ion Processes, 85, 43 (1988).

X. Tang, W.Ens, K.G. Standing and J.B.Westmore, Anal. Chem. 60, 1791 (1988a).

X. Tang, W. Ens, F. Mayer, K.G. Standing, and J.B. Westmore, Rapid Commun. Mass Spectrom. 3, 443 (1989).

X. Tang, W.Ens and K.G.Standing, Proceedings of the 38th ASMS Conference on Mass Spectrometry and Allied Topics, Tucson, AZ, p. 542 (1990).

X. Tang, Ph.D. Thesis, University of Manitoba, 1991.

X. Tang, W.Ens, N.Poppe-Schriemer and K.G.Standing in K.G.Standing and W.Ens (Eds.), Methods and Mechanisms for Producing Ions from Large Molecules, in the NATO ASI Series, Plenum Press, New York, NY,

1991a, p. 139.

X.J.Tang, P.Thibault and R.K.Boyd, Proceedings of the 40th ASMS Conference on Mass Spectrometry and Allied Topics, Washington, DC, May 31-June 5, 1992, p. 1819.

X. Tang and R. K. Boyd, Rapid Commun. Mass Spectrom. 6, 651 (1993).

Texas '92: Proceedings of the 6th Texas Synposium on Mass Spectrometry, 1992 reported in Int. J. Mass Spectrom. Ion Processes, 126 (1993).

H.T.Tien, Bilayer Lipid Membranes (BLM): Theory and Practice, Marcel Dekker, Inc., New York, 1974; D.S.Cafiso, Annu. Rev. Biophys. Biomol. Struct. 23, 141 (1994).

P.J. Todd, M.A. Baldwin, and F.W. McLafferty, Tandem Mass Spectrometry, Ed. F.W. McLafferty, John Wiley and Sons, Inc., New York (1983, p.271.

K.B.Tomer, F.W.Crow and M.L.Gross, J. Am. Chem. Soc., 105, 5488 (1983).

D.F. Torgerson, R.P. Skowronski and R.D. Macfarlane, Biochem. Biophys. Res. Commum. 60, 616 (1974).

R.H.Tredgold, Rep. Prog. Phys., 50, 1609 (1987).

A.Ulman, An Introduction to Ultrathin Organic Films from Langmuir Blodgett to Self-Assembly, Academic Press, Inc., Toronto, 1991.

The Upjohn Company. 1966. U.K. Patent 1152659.

P.A.Van Veelen, U.R.Tjaden and J.van der Greef, Int. J. Mass Spectrom. Ion Proc., 110, 92 (1991).

J. E. Vath and K. Biemann, Int. J. Mass Spectrom. Ion Processes 100 (1990) 287.

G.Veale and I.R.Peterson, J. Coll. Interface Sci., 103, 178 (1985).

A.Verentchikov, W.Ens, J.Martens, K.G.Standing, Int. J. Mass Spectrom. Ion Processes 126, 75 (1993).

A. N. Verentchikov, W. Ens, and K. G. Standing, Anal. Chem. 66, 126 (1994)

D. Voet and J.G. Voet, Biochemistry, John Wiley and Sons, New York, 1990.

J.H.Wandass and J.A.Gardella, Jr., J. Am. Chem. Soc., 107, 6192 (1985).

J.H.Wandass, III, Ph. D. Thesis, University of New York at Buffalo, 1986.

R.J.Waugh, J.H. Bowie, M.L.Gross, Rapid Commun. Mass Spectrom. 7, 623 (1993).

J. B. Westmore, W. Ens, and K. G. Standing, Biomed. Mass Spectrom. 9, 119 (1982).

C.L. Wilkins, A.K. Chowdhury, L.M. Nuwaysir, M.L. Coates,Mass Spectrom. Rev. 8, 67 (1989).

D.H. Williams, C.V. Bradley, S. Santikarn, and G. Bojesen, Biochem. J. 201, 105 (1982).

B.E.Winger, S.A. Hofstadler, J.E.Bruce, H.R.Udseth and R.D.Smith,J. Am. Soc. Mass Spectrom. 4, 566 (1993).

K. Wittmaack, L. Laxhuber and H. Mohwald, Nucl. Instrum. Meth. Phys. Res. B18, 639

(1987).

B. Wolf, R.D.Macfarlane, J. Am. Chem. Soc.2, 29 (1991).

A.S. Woods, private communication.

Z. Wu and C. Fenselau, Rapid Commun. Mass Spectrom., 6, 403 (1992).

V.H.Wysocki, M.E.Bier and R.G.Cooks, Org. Mass Spectrom., 23, 627 (1988).

V.H.Wysocki and M.M.Ross, Int. J. Mass Spectrom. Ion Proc, 104, 179 (1991).

J.R. Yates III, PhD. Thesis, University of Virginia, 1987.

A. Yee and J.O'Neil, Biochemistry, 31, 3135 (1992).

R.A. Yost and C.G. Enke, J. Am. Chem. Soc. 100, 2274 (1978).

R.A. Yost and C. Enke in Tandem Mass Spectrometry, Ed. F.W. McLafferty, John Wiley and Sons, Inc., New York (1983a), p. 175.

R.A. Yost and D.D. Fetterolf, Mass Spectrom. Rev. 2,1 (1983b), p.31.

J.A.Zasadzinski, R.Viswanathan, L. Madesen, J.Garnaes and D.K.Schwartz, Science, 263, 1726 (1994).

S. Zhao, K. V. Somayajula, A.G. Sharkey, D. Hercules, F. Hillenkamp, M. Karas, A. Ingendoh, Anal. Chem. 63, 450 (1991).

J. Zhou, W. Ens, K.G. Standing, and A. Verentchikov, Rapid Commun. Mass Spectrom. 6, 671 (1992).

J. Zhou, Ph.D. Thesis, University of Manitoba, 1993.

J. Zhou, W. Ens, N. Poppe-Schriemer, K. G. Standing, J. B. Westmore, Int. J. Mass Spectrom. Ion Processes 126, 115 (1993a).

J. Zhou et al, in preparation.